UNIVERSITY OF CALIFORNIA, MERCED

Impacts of climate change and agricultural water demand on groundwater in the Greater Kern County Region

A dissertation submitted in partial satisfaction of the requirements for the degree Doctor of Philosophy

in

Environmental Systems

by

Jorge Alberto Valero Fandiño

Committee in charge:

Dr. Thomas Harmon, Chair

Dr. Jay Lund

Dr. Joshua Viers

Dr. Alvar Escriva Bou

Dr. Josué Medellín Azuara, Advisor

2023

The dissertation of Jorge Alberto Valero Fandiño is approved, and it is acceptable in quality and form for publication on microfilm and electronically:

Dr. Josué Medellín Azuara (Advisor)

Dr. Jay Lund

Dr. Joshua Viers

Dr. Alvar Escriva Bou

Dr. Thomas Harmon, Chair

University of California, Merced

2023

ACKNOWLEDGEMENTS

I express my heartfelt gratitude to Josue Medellin-Azuara for his invaluable collaboration since my arrival in Merced in 2018. Achieving my academic goals would not have been possible without his guidance, exemplary support, and patience. Josue stands as a remarkable example, demonstrating that dreams can be realized through dedication and hard work.

I am grateful to my entire family, including my wife, children, parents, and other relatives. A heartfelt acknowledgment goes to my wife, Martha Viviana Arteaga Oviedo, for her unwavering love, support, and understanding. Words can never adequately convey my appreciation for her infectious joy and wisdom, which served as a soothing presence during the most challenging moments of this journey. I also thank my children, Juan Camilo and José Daniel, whom I couldn't accompany frequently due to the demands of this research. I recognize that the hours we missed together are irretrievable. I hope witnessing my dedicated work's countless hours inspires you to become better individuals. A sincere thank you goes to my parents, Jose Antonio Valero Jerez and Carmen Fandiño, who have motivated me since childhood and offered numerous prayers on my behalf. I appreciate my brother Juan Carlos, his wife Sandra Pardo, my niece Laura, and my nephew Diego for their care and support in caring for my parents in my absence over these years.

I sincerely thank German and Yolanda, who generously shared their friendship and wisdom without any expectations. German and Yolanda possess outstanding academic and personal qualities, and their beautiful family is a testament to their character. I want to particularly acknowledge German, my professor of Applied Hydraulics in the Spring of 2001, who became a commendable example to emulate.

I thank my friends and colleagues, Jose Manuel Rodriguez Flores and Angel Santiago Fernandez Bou, with whom I've shared numerous experiences and moments of joy. Jose and Angel generously devoted their free time to addressing my academic and personal concerns.

Over these five years, I was privileged to meet esteemed researchers, each possessing remarkable personal qualities. Jairo Viola, Felber Arroyave, Stefano Casirati, Spencer Cole, and Liying Li stand out. It was indeed a pleasure to share time and experiences with them.

I want to express my gratitude to my friends, Rick Worden, Grace Hunter, Arturo and Cindy Fernandez, Gabriel and Maria Olivares, Jany Zaugg, Ralph Becker, Tania Silva, Ariel Silva, Edward Tovar, and the members of the WME. In each of them, I discovered the warmth and support reminiscent of the friends and family I left in my home country.

I extend my gratitude all other members of my dissertation committee, Professors Thomas Harmon, Jay Lund, Joshua Viers, and Alvar Escriva Bou, for their valuable insights throughout the development of this research. Additionally, I appreciate the guidance and responsiveness of Nelson Obregón Neira, Can Dogrul, and Tariq Kadir in providing advice, sharing enthusiasm, and addressing my inquiries related to Artificial Neural Networks and C2VSim.

I want to express special gratitude to the taxpayers of the United States of America, whose contributions funded my doctoral studies. Additionally, I thank the Universidad Francisco Jose de Caldas of Colombia for enabling me to pursue my academic development abroad.

Lastly, I express my gratitude to all those who supported me during this phase of my life, although I do not mention them all.

FUNDING ACKNOWLEDGMENTS

Research under this dissertation funded by the NSF INFEWS program grant number 1639268 INFEWS/T2: The sustainability-productivity tradeoff: Water supply vulnerabilities and adaptation opportunities in California's coupled agricultural and energy sectors. Additional funding from the NOAA grant NA22OAR4310546 allowed the completion of the research in the case study areas.

VITA

2023	Ph.D. in Environmental Systems, University of California, Merced
2008	M.Sc. in Hydro Systems. Pontificia Universidad Javeriana, Colombia
2004	B.S. in Civil Engineering. Universidad Industrial de Santander, Colombia.

PUBLICATIONS

Fernandez-Bou, A. S., Rodríguez-Flores, J. M., Guzman, A., Ortiz-Partida, J. P., Classen-Rodriguez, L. M., Sánchez-Pérez, P. A., **Valero-Fandiño, J**., Pells, C., Flores-Landeros, H., Sandoval-Solís, S., Charaklis, G. W., Harmon, T. C., McCullough, M., & Medellín-Azuara, J. (2022). Water, environment, and socioeconomic justice in California: A multi-benefit framework. Science of The Total Environment, 858(February 2022), 159963. https://doi.org/10.1016/j.scitotenv.2022.159963

Rodríguez-Flores, J. M., **Valero-Fandino, J. A.**, Cole, S. A., Malek, K., Karimi, T., Zeff, H. B., Reed, P. M., Escriva-Bou, A., & Medellín-Azuara, J. (2022). Global Sensitivity Analysis of a Coupled Hydro - Economic Model and Groundwater Restriction Assessment. Water Resources Management, 0123456789. https://doi.org/10.1007/s11269-022-03344-5

Fernandez-Bou, A. S., Ortiz-Partida, J. P., Pells, C., Classen-Rodriguez, L., Espinoza, V., Rodríguez-Flores, J., Booth, L., Burmistrova, J., Cai, A., Cairo, A., Capitman, J. A., Cole, S., Flores-Landeros, H., Guzman, A., Maskey, M., Martínez-Escobar, D., Sanchez-Perez, P., **Valero-Fandiño, J**., Viers, J., … Medellín-Azuara, J. (2021). Regional Report for the San Joaquin Valley Region on Impacts of Climate Change.

Tovar Romero, E. L., **Valero-Fandiño, J. A**., & Cepeda Ariza, L. (2021). Methodology for the Selection of Trenchless Sewer Rehabilitation Technologies in Bogotá, Colombia. Tecnura, 25(68), 105–124. https://doi.org/10.14483/22487638.15570

Bernacchi, L. A., Fernandez-Bou, A. S., Viers, J. H., **Valero-Fandino, J**., & Medellín-Azuara, J. (2020). A glass half empty: Limited voices, limited groundwater security for California. Science of the Total Environment, 738, 139529. https://doi.org/10.1016/j.scitotenv.2020.139529

Martínez Tobón, C. D., Aunta Duarte, J. E., & **Valero-Fandiño, J. A**. (2013). Aplicación de datos LiDAR en la estimación del volumen forestal en el parque metropolitano bosque San Carlos. Ciencia e Ingeniería Neogranadina, 23(1), 7. https://doi.org/10.18359/rcin.229

ABSTRACT

Impacts of climate change and agricultural water demand on groundwater in the Greater Kern County Region

by

Jorge Alberto Valero Fandiño

Doctor of Philosophy in Environmental Systems

University of California Merced, 2023

Dr. Thomas Harmon, Chair

This research analyzes the potential effects of climate change and land use dynamics on groundwater in highly productive agricultural regions dependent on water imports and groundwater regulation. Before focusing on the research topic, solving a series of conceptual, operational, and computational challenges, such as having reliable, integrable, and fast models, was necessary. So, in the first part of the research, we evaluate the performance of three emulators of the sophisticated hydrology model known as the Fine Grid California Central Valley Groundwater-Surface Water Simulation Model (C2VSimFG) to estimate how climate and agriculture affect groundwater levels. Once the best emulator was identified, we assessed the hypothesis that groundwater levels in the Greater Kern County Region would exhibit a more rapid decline with projected climate change scenarios compared to a historical climate resembling 1995 and 2015. Finally, we focus on determining economically and environmentally optimal operational policies for the Shafter-Wasco irrigation district by considering the conjunctive water use approach and identifying the best policies through Bayesian Optimization Programming. The findings suggest groundwater levels are likely to decline unless agricultural water demand is reduced and recharge is increased, with climate scenarios exacerbating this decline compared to historical conditions. Our findings underscore the balance between profit and aquifer recovery, indicating farmers' need to curtail profits to achieve groundwater sustainability. Ultimately, our method can potentially integrate water and agricultural systems facing various uncertainties, providing valuable insights into optimal operational policies and tradeoffs.

Table of Contents

List of Tables

List of Figures

Chapter 1 Introduction

Water is a precious and limited resource on Earth, and its responsible use is essential for the survival of all living things. While it may seem that the planet is plentiful in water resources, a closer examination shows from all supplies that only 2.5% is freshwater, of which 68.7% is trapped in glaciers and ice caps, 30.1% is groundwater, and a mere 0.25% is in lakes and streams (Shiklomanov's, 1993). Despite lakes and rivers containing a small fraction of all water (about 1/156 of one percent), they are the primary water sources for most of the world's population (USGS, 2018). Groundwater plays a more prominent role in regions where access to surface water supply is inaccessible, scarce, or too costly to obtain. However, challenges arise due to population growth and climate fluctuations. Over the past 50 years, the global population has doubled from 3.9 billion in 1973 to 8.0 billion in 2022 (United Nations, 2022). This growth intensifies the demand for various resources, including water, food, technology, and recreational spaces. Also, climate change shifted in rainfall distribution across the planet, a trend expected to continue with rising global temperatures (Fawzy et al., 2020). Groundwater often serves as a buffer to alleviate precipitation deficits, particularly in places with highly variable surface water supplies. As a result, planning and designing infrastructure based on assumptions of a stable climate must be reevaluated to address emerging challenges. Therefore, adaptations are necessary to ensure sustainable water use and preservation in evolving environmental conditions.

A reliable water supply is indispensable in agricultural areas, supporting various stages of the production chain, from preparing the land for planting to harvesting. However, farmers face multiple challenges when water becomes scarce due to droughts. They may resort to importing water from alternative sources, utilizing groundwater, engaging in water exchanges, constructing infrastructure for water storage, and, in extreme cases, reducing crop areas. As scarcity cost can be high, the optimal portfolio of sources ant their selected reliability for a region often involves economic, technological, and political considerations. For instance, during California's 2012-216 drought, agricultural economic losses to agriculture were approximately 3.8 billion dollars (Lund et al., 2018). Contributing factors to the strain on water resources include the misconception that groundwater is nearly limitless (Khair et al., 2019), recurrent droughts, inadequate legislation, lax control over water extractions, prioritization of economic goals over environmental concerns, advancements in pumping technology, and reduced energy costs associated with pumping (Closas & Rap, 2017; Perrone & Jasechko, 2019; Wada et al., 2010). Droughts may exacerbate the overuse of resources, particularly groundwater. Excessive groundwater withdrawal can lead to reduced underground reserves and the deterioration of water quality, land subsidence, changes in the interactions between aquifers and surface waters, and adverse impacts on ecosystems (Jakeman et al., 2016).

This merits an improved understanding of how climate change, land use, and environmental legislation may affect water availability for agriculture. However, assessing the potential impacts varies in complexity depending on the specific water source to study. Analyzing historical records is a viable method for estimating the effects of climate change on stream flows. In contrast, evaluating the impact on groundwater necessitates the use of models to overcome the scarcity of information (Foster et al., 2020; Taylor, 2013) and to trace the connections between the atmosphere and aquifers, which in many cases are weak or obscured due to the intermediate processes that separate them (Cuthbert et al., 2019).

Studying the connections between the atmosphere and aquifers poses several operational challenges since climate and groundwater models typically operate independently. They function under different spatial and temporal scales, have distinct information requirements, and are often developed using other programming languages. As a result, most studies primarily focus on how climate change impacts the visible aspects of the water cycle, such as precipitation, flows, and snowmelt (Amanambu et al., 2020). These conflicting modeling approaches have led to a fragmented understanding of the complex interactions between climate and groundwater. Recognizing this, numerous scholars have underscored the importance of addressing the operational challenges to enhance our comprehension of the effects of climate change on groundwater (Blöschl et al., 2019; Larocque et al., 2019; Meixner et al., 2016; Ouhamdouch et al., 2019).

This research seeks to enhance our understanding of the interplay among the atmospheric water cycle, water demand, and groundwater levels within the context of climate change. Despite the seemingly straightforward question—how do climate change and agricultural water demand impact groundwater reserves?—we encounter various conceptual, operational, and computational challenges in addressing it. To answer this question, the initial step involved defining key parameters, including the study area, the timeframe for analysis, computational methods, and statistical tests. We identified the models to be employed, specifying their information requirements and establishing how these models would be integrated. Subsequently, we gathered the necessary data to run the models, conducting numerous simulations. The resulting information was then scrutinized using statistical indices and graphical representations to draw meaningful insights.

This study focuses on groundwater behavior in the Greater Kern County Region (GKCR) at the water district level across different time intervals. Various Global Climate Models (GCMs) are employed under diverse Representative Concentration Pathways (RCPs) to assess the impact of climate change on precipitation, surface water deliveries, agricultural water demand, and depth to groundwater. We define the GKCR as a region located south of the Central Valley in Kern and Tulare counties in California, United States. The GKCR comprises a selectin of 15 water districts namely: Semitropic WSD, Wheeler Ridge-Maricopa WSD, Rosedale-Rio Bravo WSD, Southern San Joaquin MUD, Arvin- Edison WSD, Kern Delta WD, Cawelo WD, Shafter-Wasco ID, Buena Vista WSD, Henry Miller WD, North Kern WSD, Tulare ID, Saucelito ID, Delano Earlimart ID, Kern Tulare WD. The agricultural production value of Kern and Tulare counties in 2021 was $8.34 and $8.09 billion, respectively (Kern County Department of Agriculture and Measurement Standards, 2021; Tulare County, 2021). The GKCR has low average precipitation and runoff levels, substantial evaporative demands, and a heavy dependence on groundwater for irrigation (Ghasemizade et al., 2019).

Our interest in this region lies in its history of groundwater overexploitation, attributed to droughts over the past few decades (Jasperse & Pairis, 2020) and the expansion of irrigated agriculture, particularly permanent crops. The groundwater overexploitation has led to the depletion of shallow wells and caused subsidence (Faunt et al., 2016) and dry wells (R. Pauloo et al., 2020). Additionally, climate projections for the Central Valley suggest an increase in temperatures and more precipitation variability (CDWR (California Department of Water Resources), 2017; Fernandez-Bou et al., 2021). As a result, the region is likely to face more frequent and severe droughts and floods (Smerdon, 2017). The repercussions of recent droughts and the shift from annual to perennial crops have further intensified groundwater challenges. In response to these issues, the state of California implemented the 2014 Sustainable Groundwater Management Act (SGMA) to prevent excessive groundwater extraction and improve water

supply resilience. SGMA targets six undesirable outcomes resulting from unsustainable groundwater management: lowering groundwater levels, reduction in storage, seawater intrusion, degraded quality, land subsidence, and surface water depletion (California State Legislature, 2014).

While the GKCR draws groundwater from various aquifer layers, our research concentrates on the contribution from the uppermost confined aquifer because this layer supplies approximately 80% of the agricultural wells, as detailed in Chapter 2. Although the unconfined aquifer supplies 15.1% of agricultural wells, many farmers prefer deeper wells because they are less susceptible to low water levels and contamination and have greater pumping capacities (R. Pauloo et al., 2020).

Before assessing the potential impacts of climate change on aquifers in the study area and formulating operational policies for irrigation districts, there is a significant operational modeling challenge. This challenge involved creating a versatile and efficient model for incorporating climatic and hydrological characteristics to facilitate modeling of thousands of scenarios. After evaluating various groundwater models, we decided to use the Fine Grid California Central Valley Groundwater-Surface Water Simulation Model (C2VSimFG) (DWR, 2020). As part of a collaborative project for simulating surface and groundwater hydrology, the California Food-Energy-Water System (CALFEWS) (Zeff et al., 2021) was selected for water allocation to irrigated areas in the GKCR. Integrating these models presented operational challenges since climatic, hydrologic, and groundwater models typically function independently and are designed more from a scientific perspective than an operational one. Also, they differ in spatial and temporal scales, information requirements, and programming languages.

To overcome these challenges, we devised the use of a C2VSimFG emulator. This emulator streamlines the integration of C2VSimFG, CALFEWES, and the GCMs, simultaneously reducing computation times. Chapter 2 assesses of three C2VSimFG emulators: Multiple Linear Regression (MLR), Multilayer Perceptron (MLP), and Long Short-Term Memory (LSTM). We aimed to address the scarcity of reliable, integrable, and swift hydrological models. Our goal was to overcome the lack of reliable, integrable, and fast hydrological models, mainly when scientists, planners, and decision-makers only accept highly complex Process-Based Models (PBMs) (Castelletti, Galelli, Restelli, et al., 2012). Therefore, Chapter 2, focuses on How changes in depth to groundwaters can be reproduced using emulators in agricultural regions dependent on water imports and pumping? This question is related to one of the 23 unsolved problems in the field of hydrology: "*What are the synergies and tradeoffs between societal goals related to water management (e.g., water–environment–energy–food–health)*" (Blöschl et al., 2019). This study is innovative in developing an emulator for a widely used yet computationally expensive groundwater model like C2VSimFG, a common problem with comprehensive models (Simpson et al., 2008). The assessment of the three pilot emulators through the metrics Root Mean Squared Error (RMSE), Nash–Sutcliffe Efficiency coefficient (NSE), and the Kling-Gupta Efficiency coefficient (KGE) demonstrated that the LSTM exhibited the best performance.

The third chapter tested the hypothesis that groundwater levels would decline more rapidly under climate change scenarios compared to climate within the recent historical period (between 1995 and 2015). This evaluation relied on climate projections from six GCMs under two RCPs (4.5 and 8.5) for nine water districts in the GKCR. The selected GCMs, included CanESM2, CCSM4, CNRM-CM5, HadGCM2-CC, HadGCM2-ES, and MIROC5. The GCMs were chosen based on their ability to represent California's climate accurately (Pierce et al., 2018). The downscaled and bias-corrected models were sourced from the California Climate Adaptation Planning Tool (Cal-Adapt) webpage (*Cal-Adapt*, 2022). We also employed CALFEWS, to estimate surface water deliveries (SWD) to agriculture. Agricultural water demands (AWD) were calculated, accounting

for carbon dioxide (CO2) emissions adjustments. Three sets of scenarios—Business as Usual (BU), Influence of climate change on two dynamic variables (IC2D), and Influence of climate change on three dynamic variables (IC3D)—were examined to understand the implications of climate change on groundwater levels. The findings suggest groundwater levels are likely to decline unless agricultural water demand is reduced or recharge is increased, with climate change scenarios exacerbating this decline compared to historical conditions.

Chapter 4, identifies optimal operational policies for the Shafter-Wasco Irrigation District (SWID), considering the impact of climate change and groundwater regulation. We defined an operational policy as maximizing profits and minimizing depth to the groundwater based on the areas of annual and perennial crops and expected climatic conditions from 2020 to 2040, the time horizon of groundwater regulation. We pursued a sustainable and strategic approach by simultaneously employing surface and groundwater resources, a method referred to as conjunctive water use (CWU). Our goal was to address social, economic, and environmental objectives effectively. We used the CanESM2 GCM under RCP 4.5 to estimate precipitation and surface water deliveries. The selection of the CanESM2 model was based on its ability to accurately represent California's average climate (Pierce et al., 2018). Bayesian Optimization was used to derive the Pareto front and optimal operational policies. Utilizing the k-means clustering method, we categorized points on the Pareto front into three groups: lowest, medium, and highest net revenue and depth to groundwater. Our findings underscore the balance between profit and aquifer recovery, indicating farmers' need to rethink the intertemporal choice of cropping decisions to maximize profits while attaining groundwater sustainability. Ultimately, our method can potentially integrate water and agricultural systems facing various uncertainties, providing valuable insights into optimal operational policies and associated tradeoffs.

In Chapter 5, the research culminates in presenting the overall conclusions. This section underscores the significance of integrating climate, hydrology, water allocation, and optimization within a unified framework. This approach reveals comprehensive insights on a broader scale into the intricate interplay among these concepts. Without integrated research efforts, valuable knowledge would remain disjointed, limiting our understanding of the world. In this study, our focus wasn't solely on generating new fragments of knowledge but rather on interconnecting existing elements to attain a more comprehensive and reliable perspective on sustained water resource management. Furthermore, this research demonstrated that coupling these knowledge pieces is not feasible for individuals; it requires collaboration and interdisciplinary expertise.

1.1 References

Alam, S., Gebremichael, M., Li, R., Dozier, J., & Lettenmaier, D. P. (2019). Climate change impacts on groundwater storage in the Central Valley, California. *Climatic Change*, *157*(3–4), 387–406. https://doi.org/10.1007/s10584-019-02585-5

Allen, R. G., Pereira, L. S., Raes, D., & Smith, M. (1998). *FAO irrigation and Drainage paper No. 56. Crop Evapotranspiration* (Vol. 56).

Amanambu, A. C., Obarein, O. A., Mossa, J., Li, L., Ayeni, S. S., Balogun, O., Oyebamiji, A., & Ochege, F. U. (2020). Groundwater system and climate change: Present status and future considerations. *Journal of Hydrology*, *589*(December 2019), 125163. https://doi.org/10.1016/j.jhydrol.2020.125163

Asher, M. J., Croke, B. F. W., Jakeman, A. J., & Peeters, L. J. M. (2015). A review of surrogate models and their application to groundwater modeling. *Water Resources Managment*, *51*(8), 5957–5973. https://doi.org/https://doi.org/10.1002/2015WR016967

Benjamin, P., Erraguntla, M., Delen, D., & Mayer, R. (1998). Simulation modeling at multiple levels of abstraction. *Winter Simulation Conference Proceedings*, *1*, 391–398. https://doi.org/10.1109/wsc.1998.745013

Blöschl, G., Bierkens, M. F. P., Chambel, A., Cudennec, C., Destouni, G., Fiori, A., Kirchner, J. W., McDonnell, J. J., Savenije, H. H. G., Sivapalan, M., Stumpp, C., Toth, E., Volpi, E., Carr, G., Lupton, C., Salinas, J., Széles, B., Viglione, A., Aksoy, H., … Zhang, Y. (2019). Twenty-three unsolved problems in hydrology (UPH)–a community perspective. *Hydrological Sciences Journal*, *64*(10), 1141–1158. https://doi.org/10.1080/02626667.2019.1620507

Bowes, B., Sadler, J., Morsy, M., Behl, M., & Goodall, J. (2019). Forecasting Groundwater Table in a Flood Prone Coastal City with Long Short-term Memory and Recurrent Neural Networks. *Water*, *11*(1098). https://doi.org/10.3390/w11051098

Box, G., Jenkins, G., Reinsel, G., & Ljung, G. (2016). *Time series analysis: Forecasting and control* (Fifth). John Wiley & Sons.

Branke, J., Deb, K., Miettinen, K., & Slowinski, R. (Eds.). (2008). *Introduction to Multiobjective Optimization: Interactive Approaches*.

Bras, R., & Rodriguez-Iturbe, I. (1993). Generalized univariate time-series analysis in hydrology. In *Random functions and hydrology*. Dover Publications, Inc.

Brunner, P., & Simmons, C. T. (2012). HydroGeoSphere: A Fully Integrated, Physically Based Hydrological Model. *Groundwater*, *50*(2), 170–176. https://doi.org/https://doi.org/10.1111/j.1745-6584.2011.00882.x

Cal-Adapt. (2022). https://cal-adapt.org/

California State Legislature. (2014). *Sustainable groundwater management act*. https://water.ca.gov/programs/groundwater-management/sgma-groundwater-management

Castelletti, A., Galelli, S., Ratto, M., Soncini-Sessa, R., & Young, P. C. (2012). A general framework

for Dynamic Emulation Modelling in environmental problems. *Environmental Modelling and Software*, *34*, 5–18. https://doi.org/10.1016/j.envsoft.2012.01.002

Castelletti, A., Galelli, S., Restelli, M., & Soncini-Sessa, R. (2012). Data-driven dynamic emulation modelling for the optimal management of environmental systems. *Environmental Modelling and Software*, *34*, 30–43. https://doi.org/10.1016/j.envsoft.2011.09.003

CDWR. (2021a). *California's Groundwater Update 2020 highlights. Bulletin 118*. https://water.ca.gov/programs/groundwater-management/bulletin-118

CDWR (California Department of Water Resources). (2017). *Central Valley Flood Protection Plan 2017 Update* (Issue August).

CDWR, (California Department of Water Resources). (2020). *Well Completion Reports*. https://data.cnra.ca.gov/dataset/well-completion-reports

CDWR, (California Department of Water Resources). (2021b). *GIS*. https://gis.water.ca.gov/arcgis/rest/services/Boundaries/i03_WaterDistricts/FeatureServer/0

Chen, C., He, W., Zhou, H., Xue, Y., & Zhu, M. (2020). A comparative study among machine learning and numerical models for simulating groundwater dynamics in the Heihe River Basin, northwestern China. *Scientific Reports*, *10*(1), 1–13. https://doi.org/10.1038/s41598-020-60698-9

Chen, L., Roy, S. B., & Hutton, P. H. (2018). Emulation of a process-based estuarine hydrodynamic model. *Hydrological Sciences Journal*, *63*(5), 783–802. https://doi.org/10.1080/02626667.2018.1447112

Cheng, F., & Zhao, J. (2019). A novel process monitoring approach based on Feature Points Distance Dynamic Autoencoder. In *Computer Aided Chemical Engineering* (Vol. 46). Elsevier Masson SAS. https://doi.org/10.1016/B978-0-12-818634-3.50127-2

Cohen, J. S., & Herman, J. D. (2021). Dynamic Adaptation of Water Resources Systems Under Uncertainty by Learning Policy Structure and Indicators. *Water Resources Research*, *57*(11), 1–24. https://doi.org/10.1029/2021WR030433

Cui, T., Peeters, L., Pagendam, D., Pickett, T., Jin, H., Crosbie, R. S., Raiber, M., Rassam, D. W., & Gilfedder, M. (2018). Emulator-enabled approximate Bayesian computation (ABC) and uncertainty analysis for computationally expensive groundwater models. *Journal of Hydrology*, *564*(December 2017), 191–207. https://doi.org/10.1016/j.jhydrol.2018.07.005

Cuthbert, M. O., Gleeson, T., Moosdorf, N., Befus, K. M., Schneider, A., Hartmann, J., & Lehner, B. (2019). Global patterns and dynamics of climate–groundwater interactions. *Nature Climate Change*, *9*(2), 137–141. https://doi.org/10.1038/s41558-018-0386-4

D'Agostino, D., Borg, M., Hallett, S. H., Sakrabani, R. S., Thompson, A., Papadimitriou, L., & Knox, J. W. (2020). Multi-stakeholder analysis to improve agricultural water management policy and practice in Malta. *Agricultural Water Management*, *229*, 105920. https://doi.org/https://doi.org/10.1016/j.agwat.2019.105920

Dale, L. L., Dogrul, E. C., Brush, C. F., Kadir, T. N., Chung, F. I., Miller, N. L., & Vicuna, S. D. (2013).

Simulating the Impact of Drought on California's Central Valley Hydrology, Groundwater and Cropping. *British Journal of Environment & Climate Change*, *3*(3), 271–291.

Deb, K., Pratap, A., Agarwal, S., & Meyarivan, T. (2002). A fast and elitist multiobjective genetic algorithm: NSGA-II. *IEEE Transactions on Evolutionary Computation*, *6*(2), 182–197. https://doi.org/10.1109/4235.996017

Delano Earlimart Irrigation District GSA. (2022). *Groundwater Sustainability Plan. Delano-Earlimart Irrigation District*. https://www.deid.org/wp-content/uploads/2022/07/deid_gsp_draft_final_20220720.pdf

Diaz-Granados, M. (2023). *Hidrologia, una sintesis probabilistica* (1st ed.).

Dogrul, E. C., Brush, C. F., & Kadir, T. N. (2016). Groundwater modeling in support of water resources management and planning under complex climate, regulatory, and economic stresses. *Water (Switzerland)*, *8*(12). https://doi.org/10.3390/w8120592

Dogrul, E. C., & Kadir, T. N. (2020a). *DWR Technical Memorandum: Theoretical Documentation and User's Manual for IWFM Demand Calculator (IDC-2015), Revision 88* (Issue August). https://data.cnra.ca.gov/dataset/idc-version-2015-0-88/resource/9d2890d5-52ed-4158-bdb5-4440f9030d12

Dogrul, E. C., & Kadir, T. N. (2020b). *DWR Technical Memorandum: Theoretical Documentation for the Integrated Water Flow Model (IWFM-2015), Revision 1045* (Issue August). https://data.cnra.ca.gov/dataset/iwfm-version-2015-0-1045

Duffy, C., Shi, Y., Davis, K., Slingerland, R., Li, L., Sullivan, P. L., Goddéris, Y., & Brantley, S. L. (2014). Designing a Suite of Models to Explore Critical Zone Function. *Procedia Earth and Planetary Science*, *10*, 7–15. https://doi.org/https://doi.org/10.1016/j.proeps.2014.08.003

DWR. (2019). *C2VSim: California Central Valley Groundwater-Surface Water Simulation Model*. https://water.ca.gov/Library/Modeling-and-Analysis/Central-Valley-models-and-tools/C2VSim

DWR, C. D. of W. R. (2020). *California Central Valley Groundwater-Surface Water Simulation Model – Fine Grid (C2VSimFG) Development and Calibration Version 1.0* (Issue December). https://data.cnra.ca.gov/dataset/c2vsimfg-version-1-0

Escriva-bou, A., Hui, R., Maples, S., Medellín-azuara, J., Harter, T., & Lund, J. R. (2020). Planning for groundwater sustainability accounting for uncertainty and costs : An application to California ' s Central Valley. *Journal of Environmental Management*, *264*(March), 110426. https://doi.org/10.1016/j.jenvman.2020.110426

Faunt, C. C., Sneed, M., Traum, J., & Brandt, J. T. (2016). Water availability and land subsidence in the Central Valley, California, USA. *Hydrogeology Journal*, *24*(3), 675–684. https://doi.org/10.1007/s10040-015-1339-x

Fawzy, S., Osman, A. I., Doran, J., & Rooney, D. W. (2020). Strategies for mitigation of climate change: a review. *Environmental Chemistry Letters*, *18*(6), 2069–2094. https://doi.org/10.1007/s10311-020-01059-w

Fernandez-Bou, A. S., Ortiz-Partida, J. P., Pells, C., Classen-Rodriguez, L., Espinoza, V., Rodríguez-

Flores, J., Booth, L., Burmistrova, J., Cai, A., Cairo, A., Capitman, J. A., Cole, S., Flores-Landeros, H., Guzman, A., Maskey, M., Martínez-Escobar, D., Sanchez-Perez, P., Valero-Fandiño, J., Viers, J., … Medellín-Azuara, J. (2021). *Regional Report for the San Joaquin Valley Region on Impacts of Climate Change*.

Fetter, C. (2001). *Applied Hydrogeology* (P. Lynch (Ed.); Fourth). Prentice Hall.

Fiering, M., & Jackson, B. (1971). *Synthetic streamflows*. https://doi.org/10.1029/WM001

Foster, T., Mieno, T., & Brozović, N. (2020). Satellite-Based Monitoring of Irrigation Water Use: Assessing Measurement Errors and Their Implications for Agricultural Water Management Policy. *Water Resources Research*, *56*(11), e2020WR028378. https://doi.org/https://doi.org/10.1029/2020WR028378

GEI Consultants Inc. (2020). *Groundwater Sustainability Plan. Kern County, CA*. https://kerngwa.com/wp-content/uploads/2022/07/kga-umbrella-gsp_final.pdf

Gers, F. A., Eck, D., & Schmidhuber, J. (2002). Applying LSTM to Time Series Predictable Through Time-Window Approaches. In R. Tagliaferri & M. Marinaro (Eds.), *Neural Nets WIRN Vietri-01* (pp. 193–200). Springer London.

Ghaseminejad, A., & Uddameri, V. (2020). Physics-inspired integrated space-time artificial neural networks for regional groundwater flow modeling. *Hydrology and Earth System Sciences*, *24*(12), 5759–5779. https://doi.org/10.5194/hess-24-5759-2020

Ghasemizade, M., Asante, K. O., Petersen, C., Kocis, T., Dahlke, H. E., & Harter, T. (2019). An Integrated Approach Toward Sustainability via Groundwater Banking in the Southern Central Valley, California. *Water Resources Research*, *55*(4), 2742–2759. https://doi.org/10.1029/2018WR024069

Goharian, E., & Burian, S. J. (2018). Developing an integrated framework to build a decision support tool for urban water management. *Journal of Hydroinformatics*, 708–727. https://doi.org/10.2166/hydro.2018.088

Haasnoot, M., Kwakkel, J. H., Walker, W. E., & ter Maat, J. (2013). Dynamic adaptive policy pathways: A method for crafting robust decisions for a deeply uncertain world. *Global Environmental Change*, *23*(2), 485–498. https://doi.org/10.1016/j.gloenvcha.2012.12.006

Hallegatte, S., Shah, A., Lempert, R., Brown, C., & Gill, S. (2012). *Investment Decision Making under Deep Uncertainty* (Issue September). https://elibrary.worldbank.org/doi/epdf/10.1596/1813-9450-6193

Hanak, E., Escriva-Bou, A., Gray, B., Green, S., Harter, T., Jezdimirovic, J., Lund, J., Medellín-Azuara, J., Moyle, P., & Seavy, N. (2019). *Water and the Future of the San Joaquin Valley* (Issue February). https://www.ppic.org/wp-content/uploads/water-and-the-future-of-the-san-joaquin-valley-february-2019.pdf

Hipel, K. W., & McLeod, A. I. (Eds.). (1994). Chapter 2 Basic Statistical Concepts. In *Time Series Modelling of Water Resources and Environmental Systems* (Vol. 45, pp. 63–86). Elsevier. https://doi.org/https://doi.org/10.1016/S0167-5648(08)70658-0

Hochreiter, S., & Schmidhuber, J. (1997). Long Short-Term Memory. *Neural Computation*, *9*(8),

1735–1780. https://doi.org/10.1162/neco.1997.9.8.1735

Huang, D., Zhang, C., Li, Q., Han, H., Huang, D., Li, T., & Wang, C. (2020). Prediction of Solar Photovoltaic Power Generation Based on MLP and LSTM neural networks. *2020 IEEE 4th Conference on Energy Internet and Energy System Integration (EI2)*, 2744–2748. https://doi.org/10.1109/EI250167.2020.9347223

Jakeman, A. J., Barreteau, O., Hunt, R. J., Rinaudo, J.-D., Ross, A., Arshad, M., & Hamilton, S. (2016). Integrated Groundwater Management: An Overview of Concepts and Challenges. In A. J. Jakeman, O. Barreteau, R. J. Hunt, J.-D. Rinaudo, & A. Ross (Eds.), *Integrated Groundwater Management: Concepts, Approaches and Challenges* (pp. 3–20). Springer International Publishing. https://doi.org/10.1007/978-3-319-23576-9_1

Jasperse, L., & Pairis, A. (2020). *Climate Change Consortium for Specialty Crops: Southern California Region*. www.climatesciencealliance.org/resilient-roots-resources

Karpatne, A., Atluri, G., Faghmous, J. H., Steinbach, M., Banerjee, A., Ganguly, A., Shekhar, S., Samatova, N., & Kumar, V. (2017). Theory-guided data science: A new paradigm for scientific discovery from data. *IEEE Transactions on Knowledge and Data Engineering*, *29*(10), 2318–2331. https://doi.org/10.1109/TKDE.2017.2720168

Kern-Tulare Water District. (2022). *Kern-Tulare Water District. Description of District*. https://drive.google.com/file/d/1sDPYGnB8wPS26GdwypfHtCd_rQHBPd9R/view

Kern County Department of Agriculture and Measurement Standards. (2015). *Kernag*. http://www.kernag.com/gis/gis-data.asp

Kern County Department of Agriculture and Measurement Standards. (2021). *Kern County Agricultural Crop Report*. http://www.kernag.com/caap/crop-reports/crop20_29/crop2021.pdf

Khair, S. M., Mushtaq, S., Reardon-Smith, K., & Ostini, J. (2019). Diverse drivers of unsustainable groundwater extraction behaviour operate in an unregulated water scarce region. *Journal of Environmental Management*, *236*, 340–350. https://doi.org/https://doi.org/10.1016/j.jenvman.2018.12.077

Khan, A., Najmus, S., Hillaire, T., Qian, F., Hass, J., Van Lienden, B., Shipman, P., Namvar, R., & Sogge, C. (2020). *Handbook for Water Budget Development with or without models. DRAFT.* https://water.ca.gov/-/media/DWR-Website/Web-Pages/Programs/Groundwater-Management/Data-and-Tools/Files/Water-Budget-Handbook.pdf

Knoben, W. J. M., Freer, J. E., & Woods, R. A. (2019). Technical note: Inherent benchmark or not? Comparing Nash-Sutcliffe and Kling-Gupta efficiency scores. *Hydrology and Earth System Sciences*, *23*(10), 4323–4331. https://doi.org/10.5194/hess-23-4323-2019

Kratzert, F., Klotz, D., Shalev, G., Klambauer, G., Hochreiter, S., & Nearing, G. (2019). Towards learning universal, regional, and local hydrological behaviors via machine learning applied to large-sample datasets. *Hydrology and Earth System Sciences*, *23*(12), 5089–5110. https://doi.org/10.5194/hess-23-5089-2019

Krogh, A. (2008). What are artificial neural networks? *Nature Biotechnology*, *26*(2), 195–197.

https://doi.org/10.1038/nbt1386

Kumaraswamy, B. (2021). 6 - Neural networks for data classification. In D. Binu & B. R. Rajakumar (Eds.), *Artificial Intelligence in Data Mining* (pp. 109–131). Academic Press. https://doi.org/https://doi.org/10.1016/B978-0-12-820601-0.00011-2

Larocque, M., Levison, J., Martin, A., & Chaumont, D. (2019). A review of simulated climate change impacts on groundwater resources in Eastern Canada. *Canadian Water Resources Journal*, *44*(1), 22–41. https://doi.org/10.1080/07011784.2018.1503066

Lavers, D. A., Ralph, F. M., Waliser, D. E., Gershunov, A., & Dettinger, M. D. (2015). Climate change intensification of horizontal water vapor transport in CMIP5. *Geophysical Research Letters*, *42*(13), 5617–5625. https://doi.org/10.1002/2015GL064672

Lazer, D., Kennedy, R., King, G., & Vespignani, A. (2014). The parable of google flu: Traps in big data analysis. *Science*, *343*(6176), 1203–1205. https://doi.org/10.1126/science.1248506

Loucks, D. P., & Beek, E. van. (2017). Water Resource Systems Planning and Management: An Introduction to Methods, Models, and Applications. In *Advances in Water Resources* (1st ed.). Springer Cham. https://doi.org/https://doi.org/10.1007/978-3-319-44234-1

Lund, J., Medellin-Azuara, J., Durand, J., & Stone, K. (2018). Lessons from California's 2012-2016 drought. *Journal of Water Resources Planning and Management*, *144*(10), 1–13. https://doi.org/10.1061/(ASCE)WR.1943-5452.0000984

MacEwan, D., Cayar, M., Taghavi, A., Mitchell, D., Hatchett, S., & Howitt, R. (2017). Hydroeconomic modeling of sustainable groundwater management. *Water Resources Research*, *53*(3), 2384–2403. https://doi.org/10.1002/2016WR019639

Majedi, H., Fathian, H., Nikbakht-shahbazi, A., Zohrabi, N., & Hassani, F. (2021). Multi-Objective Optimization of Integrated Surface and Groundwater Resources Under the Clean Development Mechanism. *Water Resources Management*, 2685–2704. https://doi.org/10.1007/s11269-021-02860-0

Mall, N. K., & Herman, J. D. (2019). Water shortage risks from perennial crop expansion in California's Central Valley. *Environmental Research Letters*, *14*(10). https://doi.org/10.1088/1748-9326/ab4035

Massoud, E. C., Purdy, A. J., Miro, M. E., & Famiglietti, J. S. (2018). Projecting groundwater storage changes in California's Central Valley. *Scientific Reports*, *8*(1), 1–9. https://doi.org/10.1038/s41598-018-31210-1

Meixner, T., Manning, A. H., Stonestrom, D. A., Allen, D. M., Ajami, H., Blasch, K. W., Brookfield, A. E., Castro, C. L., Clark, J. F., Gochis, D. J., Flint, A. L., Neff, K. L., Niraula, R., Rodell, M., Scanlon, B. R., Singha, K., & Walvoord, M. A. (2016). Implications of projected climate change for groundwater recharge in the western United States. *Journal of Hydrology*, *534*, 124–138. https://doi.org/10.1016/j.jhydrol.2015.12.027

Molina-Navarro, E., Bailey, R. T., Andersen, H. E., Thodsen, H., Nielsen, A., Park, S., Jensen, J. S., Jensen, J. B., & Trolle, D. (2019). Comparison of abstraction scenarios simulated by SWAT and SWAT-MODFLOW. *Hydrological Sciences Journal*, *64*(4), 434–454.

https://doi.org/10.1080/02626667.2019.1590583

Murray, K. D., & Lohman, R. B. (2018). Short-lived pause in Central California subsidence after heavy winter precipitation of 2017. *Science Advances*, *4*(8), 1–9. https://doi.org/10.1126/sciadv.aar8144

NASA. (2018). *SRTM 90m Digital Elevation Data from the CGIAR-CSI Consortium for Spatial Information*. http://srtm.csi.cgiar.org/

Nguyen, Q. (2023). *Bayesian Optimization in Action*. Manning.

Nouiri, I., Yitayew, M., Maßmann, J., & Tarhouni, J. (2015). Multi-objective Optimization Tool for Integrated Groundwater Management. *Water Resources Management*, *29*(14), 5353–5375. https://doi.org/10.1007/s11269-015-1122-8

Nourani, V., & Mousavi, S. (2016). Spatiotemporal groundwater level modeling using hybrid artificial intelligence-meshless method. *Journal of Hydrology*, *536*, 10–25. https://doi.org/10.1016/j.jhydrol.2016.02.030

Østergård, T., Jensen, R. L., & Maagaard, S. E. (2018). A comparison of six metamodeling techniques applied to building performance simulations. *Applied Energy*, *211*(August 2017), 89–103. https://doi.org/10.1016/j.apenergy.2017.10.102

Ouhamdouch, S., Bahir, M., Ouazar, D., Maria, P., & Kamel, C. (2019). Evaluation of climate change impact on groundwater from semi-arid environment (Essaouira Basin, Morocco) using integrated approaches. *Environmental Earth Sciences*, *78*(15), 1–14. https://doi.org/10.1007/s12665-019-8470-2

Pauloo, R. A., Escriva-Bou, A., Dahlke, H., Fencl, A., Guillon, H., & Fogg, G. E. (2020). Domestic well vulnerability to drought duration and unsustainable groundwater management in California's Central Valley. *Environmental Research Letters*, *15*(4). https://doi.org/10.1088/1748-9326/ab6f10

Pauloo, R., Escriva-Bou, A., Dahlke, H., Fencl, A., Guillon, H., & Fogg, G. (2020). Domestic well vulnerability to drought duration and unsustainable groundwater management in California's Central Valley. *Environmental Research Letters*. http://iopscience.iop.org/10.1088/1748-9326/ab6f10

Perrone, D., & Rohde, M. (2016). Benefits and economic costs of managed aquifer recharge in California. *San Francisco Estuary and Watershed Science*, *14*(2), 1–13. https://doi.org/10.15447/sfews.2016v14iss2art4

Pierce, D. W., Kalansky, J. F., & Cayan, D. R. (2018). *Climate, Drought, and Sea Level Rise Scenarios for California's Fourth Climate Change Assessment* (Issue CNRA-CEC-2018-006). https://www.energy.ca.gov/sites/default/files/2019-11/Projections_CCCA4-CEC-2018-006_ADA.pdf

Ratto, M., Castelletti, A., & Pagano, A. (2012). Emulation techniques for the reduction and sensitivity analysis of complex environmental models. *Environmental Modelling and Software*, *34*, 1–4. https://doi.org/10.1016/j.envsoft.2011.11.003

Ray, P. A., Bonzanigo, L., Wi, S., Yang, Y. C. E., Karki, P., García, L. E., Rodriguez, D. J., & Brown, C.

M. (2018). Multidimensional stress test for hydropower investments facing climate, geophysical and financial uncertainty. *Global Environmental Change*, *48*(December 2017), 168–181. https://doi.org/10.1016/j.gloenvcha.2017.11.013

Razavi, S., Tolson, B. A., & Burn, D. H. (2012). Review of surrogate modeling in water resources. *Water Resources Research*, *48*(7). https://doi.org/10.1029/2011WR011527

Read, J. S., Jia, X., Willard, J., Appling, A. P., Zwart, J. A., Oliver, S. K., Karpatne, A., Hansen, G. J. A., Hanson, P. C., Watkins, W., Steinbach, M., & Kumar, V. (2019). Process-Guided Deep Learning Predictions of Lake Water Temperature. *Water Resources Research*, *55*(11), 9173–9190. https://doi.org/10.1029/2019WR024922

Sabale, R., Venkatesh, B., & Jose, M. (2023). Sustainable water resource management through conjunctive use of groundwater and surface water: a review. *Innovative Infrastructure Solutions*, *8*(1), 1–12. https://doi.org/10.1007/s41062-022-00992-9

Safavi, H. R., Darzi, F., & Mariño, M. A. (2010). Simulation-Optimization Modeling of Conjunctive Use of Surface Water and Groundwater. *Water Resour Manage*, *24*, 1965–1988. https://doi.org/10.1007/s11269-009-9533-z

Sahoo, S., Russo, T. A., Elliot, J., & Foster, I. (2017). Machine learning algorithms for modeling groundwater level changes in agricultural regions of the U.S. *Journal of the American Water Resources Association*, *53*(5). https://doi.org/10.1002/2016WR019933

Sepahvand, R., Safavi, H. R., & Rezaei, F. (2019). Multi-Objective Planning for Conjunctive Use of Surface and Ground Water Resources Using Genetic Programming. *Water Resources Management*, *33*(6), 2123–2137. https://doi.org/10.1007/s11269-019-02229-4

Shen, C. (2018). A Transdisciplinary Review of Deep Learning Research and Its Relevance for Water Resources Scientists. *Water Resources Research*, *54*(11), 8558–8593. https://doi.org/10.1029/2018WR022643

Shi, H., Xu, M., & Li, R. (2018). Deep Learning for Household Load Forecasting—A Novel Pooling Deep RNN. *IEEE Transactions on Smart Grid*, *9*(5), 5271–5280. https://doi.org/10.1109/TSG.2017.2686012

Shiklomanov's, I. (1993). World fresh water resources. In P. H. Gleick (Ed.), *Water in crisis: A Guide to the World's Fresh Water Resources*. Oxford University Press.

Simpson, T., Toropov, V., Balabanov, V., & Viana, F. (2008). Design and Analysis of Computer Experiments in Multidisciplinary Design Optimization: A Review of How Far We Have Come - Or Not. In *12th AIAA/ISSMO Multidisciplinary Analysis and Optimization Conference*. American Institute of Aeronautics and Astronautics (AIAA). https://doi.org/https://doi.org/10.2514/6.2008-5802

Smerdon, B. D. (2017). A synopsis of climate change effects on groundwater recharge. *Journal of Hydrology*, *555*, 125–128. https://doi.org/10.1016/j.jhydrol.2017.09.047

Struye, J., & Latré, S. (2020). Hierarchical temporal memory and recurrent neural networks for time series prediction: An empirical validation and reduction to multilayer perceptrons. *Neurocomputing*, *396*, 291–301.

https://doi.org/https://doi.org/10.1016/j.neucom.2018.09.098

Taylor, R. G. (2013). Ground water and climate change. *Nature Climate Change*, *3*(November 2012). https://doi.org/10.1038/NCLIMATE1744

Tracy, J., Chang, W., St George Freeman, S., Brown, C., Palma Nava, A., & Ray, P. (2022). Enabling dynamic emulation of high-dimensional model outputs: Demonstration for Mexico City groundwater management. *Environmental Modelling and Software*, *147*(October 2021), 105238. https://doi.org/10.1016/j.envsoft.2021.105238

Tran, H., Leonarduzzi, E., De la Fuente, L., Hull, R. B., Bansal, V., Chennault, C., Gentine, P., Melchior, P., Condon, L. E., & Maxwell, R. M. (2021). Development of a deep learning emulator for a distributed groundwater–surface water model: Parflow-ml. *Water (Switzerland)*, *13*(23). https://doi.org/10.3390/w13233393

Tulare County. (2021). *Tulare county crop and livestock report*. https://agcomm.co.tulare.ca.us/pest-exclusion-standardization/crop-reports1/crop-reports-2021-2030/crop-and-livestock-report-2021/

United Nations. (2022). *UN*. https://www.un.org/en/global-issues/population

USGS. (2018). *USGS*. Where Is Earth's Water? https://www.usgs.gov/special-topics/water-science-school/science/where-earths-water

USGS. (2019). *MODFLOW and Related Programs*. https://www.usgs.gov/mission-areas/water-resources/science/modflow-and-related-programs

Weber de Melo, W., da Silva Pinho, J., & Iglesias, I. (2022). Emulating the estuarine morphology evolution using a deep convolutional neural network emulator based on hydrodynamic results of a numerical model. *Journal of Hydroinformatics*, *00*(0), 1–15. https://doi.org/10.2166/hydro.2022.068

Wunsch, A., Liesch, T., & Broda, S. (2020). Groundwater Level Forecasting with Artificial Neural Networks: A Comparison of LSTM, CNN and NARX. *Hydrology and Earth System Sciences Discussions*, 1–23. https://doi.org/10.5194/hess-2020-552

Yu, X., Cui, T., Sreekanth, J., Mangeon, S., Doble, R., Xin, P., Rassam, D., & Gilfedder, M. (2020). Deep learning emulators for groundwater contaminant transport modelling. *Journal of Hydrology*, *590*(July), 125351. https://doi.org/10.1016/j.jhydrol.2020.125351

Zeff, H. B., Hamilton, A. L., Malek, K., Herman, J. D., Cohen, J. S., Medellin-Azuara, J., Reed, P. M., & Characklis, G. W. (2021). California's food-energy-water system: An open source simulation model of adaptive surface and groundwater management in the Central Valley. *Environmental Modelling and Software*, *141*(April), 105052. https://doi.org/10.1016/j.envsoft.2021.105052

Zhang, C., Gao, L., Li, X., Shen, W., Zhou, J., & Tan, K. C. (2022). Resetting Weight Vectors in MOEA/D for Multiobjective Optimization Problems with Discontinuous Pareto Front. *IEEE Transactions on Cybernetics*, *52*(9), 9770–9783. https://doi.org/10.1109/TCYB.2021.3062949

Zhang, J., Zhu, Y., Zhang, X., Ye, M., & Yang, J. (2018). Developing a Long Short-Term Memory

(LSTM) based model for predicting water table depth in agricultural areas. *Journal of Hydrology*, *561*(January), 918–929. https://doi.org/10.1016/j.jhydrol.2018.04.065

Chapter 2 Change in depth to groundwater through deep learning models in agricultural regions.

Abstract

Thanks to the development of science and computers, the Process-Based Models (PBMs) used in water resources can accurately represent individual processes. However, the integration challenges and computational demands of the PBMs often result in significant simplifications or, even worse, the exclusion of the hydrological component in complex studies. This research addresses this issue by developing reliable, integrable, fast hydrological emulators of the sophisticated hydrological model known as the Fine Grid California Central Valley Groundwater-Surface Water Simulation Model (C2VSimFG). The evaluated emulators were Multiple Linear Regression (MLR), Multilayer Perceptron (MLP), and Long Short-Term Memory (LSTM). The emulators calculate the change in the groundwater levels as a function of precipitation, surface water deliveries, and agricultural demand, variables whose selection was inspired by the law of conservation of mass. The case study focuses on the Great Kern County Region (GKCR), one of the highest agricultural production regions in the United States and the world, highly dependent on water imports and groundwater pumping. The most relevant results of this research are: First, developing a method to emulate highly complex mechanistic models dependent on space and time. Second, the studied emulators are characterized by their simplicity, run time speed and quality of results. With these tools, decision-makers can evaluate multiple scenarios more efficiently without compromising the quality of the results.

2.1 Introduction

Thanks to the development of science and computers, the Process-Based Models (PBMs) used in water resources can accurately represent individual processes (Razavi et al., 2012). However, running PBMs can be computationally demanding since these models are conceived more from a scientific point of view (to facilitate the understanding of the processes) than from an operational point of view (to facilitate the simulation of possible scenarios) (Castelletti, Galelli, Restelli, et al., 2012). In other words, although current supercomputers have notably reduced model run time, they have also promoted the development of more realistic and complex models, keeping run times and other limitations almost unchanged (Castelletti, Galelli, Restelli, et al., 2012).

In many studies, the PBM's integration challenges and computational demands lead to massive simplifications or, even worst, the absence of the hydrological component. A possible solution is to develop computationally efficient simplified models called emulators (Castelletti, Galelli, Restelli, et al., 2012). The goal of an emulator is to represent the most relevant attributes of a PBM without drastically reducing the accuracy of the estimates so that a computationally-demanding model is replaced by a computationally-efficient model (Cui et al., 2018). Also, according to Ray et al. (2018), in coupled systems, the uncertainty associated with hydrology is usually tiny compared to other sources of uncertainty. For this reason, with hydrological emulators, a large portion of the computational load can be alleviated to dedicate more resources to modeling anthropogenic uncertainties and improve the understanding of the water systems (demographic or financial) (Tracy et al., 2022).

In groundwater systems, PBMs can be classified into two categories: Pure Groundwater Models (PGM) and Integrated Hydrology Models (IHM) (Dogrul et al., 2016). PGMs are exclusively dedicated to modeling the aquifer, leaving aside its interactions with other systems. Conversely,

IHMs incorporate most or all of the hydrological cycle components, water demands, and environmental regulations. Although IHMs seem more attractive, as happens with PBMs, they require highly specialized knowledge, large volumes of information, numerous parameters, and often unknown boundary conditions (Bowes et al., 2019; L. Chen et al., 2018; Nourani & Mousavi, 2016). Hence, many parameters are assumed, the calibration processes are computationally demanding (Bowes et al., 2019), and the run times are expensive (Cui et al., 2018; Tran et al., 2021). Nonlinear interactions, spatial heterogeneity, and time delays between the occurrence of a phenomenon and the arrival of its effects (for example, rainfall and aquifer recharge) pose additional challenges (Sahoo et al., 2017).

This research seeks to overcome the lack of reliable, integrable, and fast hydrological models; mainly when scientists, planners, and decision-makers only accept highly complex Process-Based Models (PBMs) (Castelletti, Galelli, Restelli, et al., 2012). Hence, we evaluate the performance of three emulators of a highly complex hydrological model to facilitate its integration with other models and promote a run times reduction. The emulated model was the Fine Grid California Central Valley Groundwater-Surface Water Simulation Model (C2VSimFG). The three evaluated emulators were Multiple Linear Regression (MLR), Multilayer Perceptron (MLP), and Long Short-Term Memory (LSTM). The three analyzed emulators allow calculating the change in the groundwater level as a function of precipitation, surface water deliveries, and agricultural demand, variables whose selection was inspired by the law of conservation of mass. In addition, we propose a novel approach that simultaneously considers space and time to simulate groundwater's complex spatiotemporal dynamics.

We were interested in answering the question: How can changes in depth to groundwater be reproduced using emulators in agricultural regions dependent on water imports and pumping? This question is closely related to one of the 23 unsolved problems in the field of hydrology: "*What are the synergies and tradeoffs between societal goals related to water management (e.g., water–environment–energy–food–health)*" (Blöschl et al., 2019). Also, this study is timely as no other research is devoted to IWFM emulation. Research like this is essential since the high cost of simulations is a common topic in the most cited review articles on emulation (Simpson et al., 2008). Finally, the case study focuses on the Great Kern County Region (GKCR), one of the highest agricultural production regions in the United States and the world, highly dependent on water imports and groundwater pumping.

This document is organized as follows: Section two describes the theoretical framework focusing on the most widely used groundwater models, the emulators discussed here, and the metrics selected to assess their performance. Section three describes the study area, particularly the evaluated aquifer. Section four describes the structure of analyzed emulators, focusing on variable selection, training, validation, and testing. Section five presents the results and discussion. Finally, the conclusions are shown in section 6.

2.2 Theoretical framework

2.2.1 Groundwater models

Some of the most widely used IHMs at present are HydroGeoSphere (HGS), the Penn State Integrated Hydrologic Model (PIHM), the Modular Groundwater Flow (MODFLOW), and the Integrated Water Flow Model (IWFM). First, HGS couples processes such as precipitation, streamflow, evapotranspiration, snowmelt, soil freeze/thaw, groundwater recharge, and subsurface discharge into surface water bodies such as rivers or lakes. Using finite elements, HGS

simultaneously solves the 2D diffusive wave equation for overland flow and the 3D form of the Richards equation for saturated groundwater flow (Brunner & Simmons, 2012). Likewise, PIHM simulates the major hydrological processes at a catchment scale. PIHM considers processes such as channel routing, surface overland flow, subsurface flow, interception, snowmelt, and evapotranspiration. The model uses kinematic and diffusion wave approximations for channel routing and overland flow modeling. For saturated groundwater flow, PIHM considers the 2-D Dupuit approximation. The unsaturated flow is simulated through the 1-D Richards equation (Duffy et al., 2014).

On the other hand, MODFLOW is a fully distributed, three-dimensional PBM developed by the U.S. Geological Survey (Molina-Navarro et al., 2019). MODFLOW simulates groundwater management, coupled groundwater/surface-water systems, aquifer parameter estimation, aquifer-system compaction, land subsidence, variable-density flow (including saltwater), and solute transport (USGS, 2019). On the other hand, the State of California Department of Water Resources (CDWR) has been developing IWFM. This widely accepted model is oriented to the planning of groundwater resources, capable of simulating not only the groundwater flow in complex multi-layered aquifers; but also essential components of the hydrological cycle; agricultural and urban water demands; water supply in terms of pumping and surface water diversions; and the effect of water supply on surface and groundwater resources (Dogrul et al., 2016).

The IWFM's application to the Central Valley is known as the California Central Valley Groundwater–Surface Water Simulation Model (C2VSim), and depending on the finite element mesh resolution, the model can be called coarse grid (C2VSimCG) or fine grid (C2VSimFG). For the coarse grid model, the average area of the grid cells is 37.17 km^2, whereas for the fine grid model, it is 1.65 km^2 (Dogrul et al., 2016; DWR, 2020). Indeed, in C2VSimFG, the Central Valley is represented by more than 32,000 grid cells, 110 stream reaches, four aquifer layers, and 1,024 small watersheds that supply surface and subsurface boundary flows to the Central Valley (DWR, 2019). C2VSimFG inputs include historical precipitation, stream inflows, surface water diversions, and land use. According to Dale et al. (2013), C2VSim simulates at a monthly level rainfall-runoff; stream flow diversions; irrigation return flows; stream-aquifer interaction; infiltration and recharge to the groundwater due to precipitation and irrigation; tile drainage; subsidence; and land surface and root zone flow processes at urban and native vegetation lands. Also, for each grid cell, C2VSim dynamically calculates the available surface water (irrigation, precipitation, and soil moisture) and the water demand (agricultural and urban). Pumping is obtained as the difference between surface water supply and demand. C2VSimFG was calibrated considering surface water flows, groundwater heads, groundwater head differences between well pairs, and stream-groundwater flows (DWR, 2020). However, the C2VSimFG's computational requirements are remarkable due to its ability to model high-resolution areas. For example, run time can be in the order of hours to model California's Central Valley monthly from 1,974 to 2,015, considering four aquifer layers and a fine grid resolution. Like other IHMs, using C2VSimFG for water management and planning could be challenging. Besides, modifying or adding new modules is an arduous task (Goharian & Burian, 2018).

In this research, we use the C2VSimFG version 1.01 model as the basis for the development of the emulators after considering its widespread use in studies of planning and operation of water resources (Escriva-bou et al., 2020), climate change studies (Alam et al., 2019), groundwater storage investigations (Dale et al., 2013), as well as its possible future applications in ecosystem and infrastructure improvements.

2.2.2 Analyzed emulators

Emulation is the second level of modeling abstraction (Benjamin et al., 1998; Razavi et al., 2012) oriented to developing a PBM approximation to replace the latter in computationally intensive applications (Castelletti, Galelli, Ratto, et al., 2012). Emulation can receive different names such as meta-modelling, surrogate modeling, response surface modelling, response landscape modeling, model approximation, reduced models, proxy models, lower fidelity modeling, or model of a model (L. Chen et al., 2018; Cui et al., 2018; Razavi et al., 2012). According to Ratto, Castelletti, and Pagano (2012), since its beginnings in the 1970s, emulation has evolved considerably to the point where today it is considered an important area of research and one of the most significant advances in the study of complex mathematical models.

The running times' reduction in emulation is explained by how PBMs and emulators perform their calculations (Weber de Melo et al., 2022). For instance, while the IWFM's computational resources are dedicated to solving the conservation equation for the multilayer aquifer system using the Galerkin finite element method (Dogrul & Kadir, 2020b), emulators perform operations more straightforwardly, such as simple matrix operations. In the latter case, the computational demand is dedicated to the emulator's calibration rather than its execution (Weber de Melo et al., 2022).

Emulators can be classified into hierarchical-based, projection-based, and data-driven models (Asher et al., 2015). On the one hand, in hierarchical-base models (also known as multi-fidelity models), the physical system representation is simplified by reducing the resolution (spatial, temporal, or numerical) or by suppressing specific components (Asher et al., 2015). On the other hand, in projection-based models (also called structural-based models), the main equations of the original model are projected onto a reduced-dimensional subspace characterized by a base of orthonormal vectors (Asher et al., 2015; Tracy et al., 2022). Finally, the data-driven models are dedicated to capturing relationships between the inputs and outputs of the original model (Asher et al., 2015). According to Castelletti, Galelli, Restelli, et al. (2012), data-driven models have been the most explored emulators in the environmental literature.

An emulator must guarantee three conditions: credibility, efficacy, and efficiency. The essential emulator's feature is credibility, or what is the same, reflecting the transparency and interpretability of the emulated PBM. (Castelletti, Galelli, Ratto, et al., 2012). Efficacy refers to reproducing the original model's results, especially when the emulator faces scenarios different than those used during its conception or training (Cui et al., 2018). Finally, efficiency means that the emulator's demand for resources (processing capacity, storage, run time) should be much lower than those used by the original model (L. Chen et al., 2018). Some examples of groundwater model emulators are described by Asher et al. (2015) and Cui et al. (2018).

2.2.2.1 Multiple Linear Regression

An MLR is a model that follows the form of Equation 3-11 where y is the dependent variable, β_0 is the intercept of the hyperplane, and β_i is the coefficient of the i-th explanatory variable x_i. The MLR is used here as a reference model because it is less expensive regarding the number of parameters and calibration requirements. According to Østergård, Jensen, and Maagaard (2018), these models are simple, fast, easy to interpret, and valuable when dealing with scarce data and high noise.

$$y = \beta_0 + \sum_{i=1}^{n} \beta_i * x_i$$ Equation 2-1

Aware of the highly nonlinear relationships between the variables that characterize environmental phenomena, we implemented two of the most widely used Artificial Neural Networks (ANNs) in time series analysis: an MLP and an LSTM. According to Krogh (2008), an ANN is a mathematical model inspired by sensory processing models of the brain, made up of interconnected artificial neurons, which receive information from external resources or other neurons. After adding the weights of their inputs and passing the results through activation functions, they can solve classification or regression problems.

2.2.2.2 Multilayer Perceptron

An MLP is a network consisting of an input layer, an output layer, and two or more hidden layers (Struye & Latré, 2020), where information flows in only one direction: from input to output. On the one hand, the numbers of neurons in the input and output layers coincide with the numbers of input and output variables, respectively. Through an optimization process known as hyper parameterization, the numbers of hidden layers and their corresponding neurons are calculated. Additionally, the training of an MLP is carried out through a process known as backpropagation (Shen, 2018), where the MLP receives inputs and generates outputs that are compared with the observed values. The differences between the estimated and observed values are distributed among the neuron weights, starting with those located in the output layer and continuing to the preceding layers. In this way, the error distribution, by derivation, indicates the direction in which the neurons' weights should be adjusted to improve the accuracy of the results (Struye & Latré, 2020).

Although MLPs have produced good results working with time series (Gers et al., 2002; Huang et al., 2020; Struye & Latré, 2020), their main disadvantage is that the temporal structure of the data does not play any role. For example, two MLPs that use the same input variables might produce similar results when the order of the input variables is different. That situation violates the definition that a time series is a set of data ordered sequentially or chronologically, where the order of the observations is decisive (Box et al., 2016; Hipel & McLeod, 1994).

2.2.2.3 Long short-term memory artificial neural network

To remedy the order independence suffered by MLPs, recurrent neural networks (RNN) were developed in the 1980s (J. Zhang et al., 2018). Since then, this type of ANN has been used to consider the effect of time on speech recognition, language processing, automatic image captioning, machine translation, and multiple scientific applications (Karpatne et al., 2017; J. Zhang et al., 2018). An RNN has two inputs, two outputs, and two ANNs (see Figure 2-1a). After each ANN, there are sigmoidal or logistic activation functions (black semicircles). The RNN inputs include the input vector at time *t* (x_t) and the hidden state at time *t-1* (h_{t-1}). The outputs are h_t and the vector of outputs (y_t). Although this type of network is capable of handling variable-length sequences (Cheng & Zhao, 2019), modeling long-term dependencies (Kumaraswamy, 2021), and sharing parameters across all time steps (Shi et al., 2018), it may face vanishing or exploding gradient problems by using the backpropagation algorithm over time. The

vanishing gradient problem prevents the network from remembering past events (J. Zhang et al., 2018). The exploding gradient problem can lead to wrong solutions or high computational times.

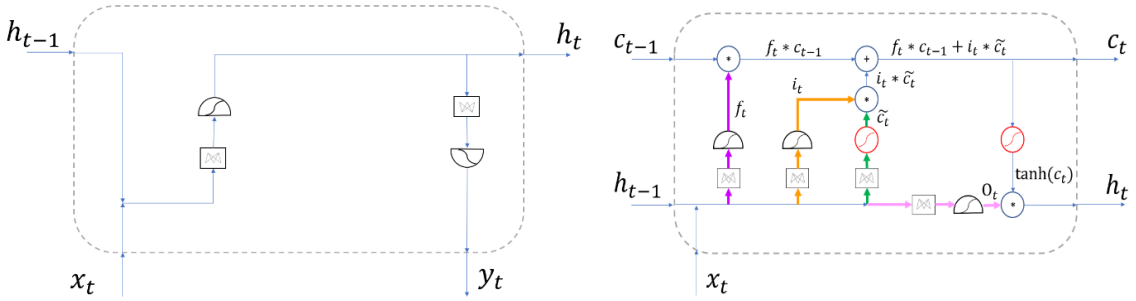

a) b)

Figure 2-1. Visualization of a) RNN. b) LSTM.

One way to overcome the difficulties mentioned above is through a type of RNN known as Long Short-Term Memory (LSTM) (Wunsch et al., 2020). An LSTM has three input and two output variables (see Figure 2-1b). The input variables are x_t, h_{t-1}, and the cell memory (or cell state) of the previous time (c_{t-1}). The output variables c_t and h_t are the two-state vectors used to store the long-term memory and the short-term memory, respectively (Yu et al., 2020). In this way, the straight horizontal path that connects the variables c_{t-1} and c_t acts as a conveyor belt that preserves the system's long-term memory (Huang et al., 2020). Since there is no ANN on the conveyor belt, the gradient does not degrade as quickly as in the case of RNN. For this reason, LSTMs can capture long-term relationships, and the information can remain in memory for many steps (Hochreiter & Schmidhuber, 1997).

A LSTMs have four ANNs fed by h_{t-1} and x_t. Three of the ANNs act as logic gates, while the fourth ANN is responsible for generating candidate vectors ($\tilde{c}_t$) to be included in memory (green path Figure 2-1b and Equation 2-3). Gates (forget, input, and output) are symbolized in Figure 2-1b by purple, orange, and pink paths, respectively. Finally, the activation function at the end of each gate can be sigmoidal or logistic (black semicircles). Thanks to these activation functions, the results are scaled between zero and one to restrict or allow the information flow.

Once the four ANNs have been trained, the information flows as follows: First, the forget gate (Equation 2-2) decides what information from the previous state c_{t-1} should be forgotten (first term on the right-hand side of Equation 2-5). Second, the input gate (Equation 2-4) decides which components of $\tilde{c}_t$ will be included in memory (second term on the right-hand side of Equation 2-5). Third, once the irrelevant information has been ignored and the network memory has been updated, the new c_t is obtained (Equation 2-5). Subsequently, with the help of a hyperbolic tangent function (red circle in Figure 2-1b), the values of c_t are scaled between negative one and one. Finally, the output gate (Equation 2-6) is responsible for choosing the scald elements that will be shown as output at time t (h_t) (Equation 2-7) (Wunsch et al., 2020).

$$f_t = \sigma\left(\boldsymbol{w_f} x_t + \boldsymbol{u_f} h_{t-1} + \boldsymbol{b_f}\right)$$ Equation 2-2

$$\widetilde{c_t} = tanh(\boldsymbol{w_c} x_t + \boldsymbol{u_c} h_{t-1} + \boldsymbol{b_c})$$ Equation 2-3

$$i_t = \sigma(\boldsymbol{w_i} x_t + \boldsymbol{u_i} h_{t-1} + \boldsymbol{b_i})$$ Equation 2-4

$$c_t = f_t \otimes c_{t-1} + i_t \otimes \widetilde{c_t}$$ Equation 2-5

$$o_t = \sigma(\boldsymbol{w_o} x_t + \boldsymbol{u_o} h_{t-1} + \boldsymbol{b_o})$$ Equation 2-6

$$h_t = o_t \otimes tanh(c_t)$$ Equation 2-7

In the previous equations, $\boldsymbol{w}$ and $\boldsymbol{u}$ represent the weight matrices for x_t and h_{t-1} respectively, while $\boldsymbol{b}$ represents the bias vectors. The subscripts *f*, *i*, and *o* refer to the forget, input, and output gates, while the subindex *c* refers to the candidate vector. The symbol ⊗ represents element-wise multiplication. Finally, for the first time step, the hidden and cell states are initialized with a vector of zeros ($h_0 = 0, c_0 = 0$) (J. Zhang et al., 2018).

2.2.3 Performance metrics

Emulators' performance was analyzed considering three metrics: the Root Mean Squared Error (RMSE), Nash–Sutcliffe Efficiency coefficient (NSE), and the Kling-Gupta Efficiency coefficient (KGE) (see equations from Equation 2-8 to Equation 2-12) (Gupta et al. 2009; Clark et al. 2021; Ghaseminejad and Uddameri 2020).

$$RMSE = \left(\frac{1}{n} * \sum_{i=1}^{n} (O_i - S_i)^2\right)^{0.5}$$ Equation 2-8

$$NSE = 1 - \frac{RMSE^2}{\sigma_O^2}$$ Equation 2-9

$$KGE = 1 - \sqrt{(r-1)^2 + (\alpha - 1)^2 + (\beta - 1)^2}$$ Equation 2-10

$$\alpha = \frac{\sigma_s}{\sigma_o}$$ Equation 2-11

$$\beta = \frac{\mu_s}{\mu_o}$$ Equation 2-12

Where O and S represent the observed and emulated values, respectively. Furthermore, the means of these variables are μ_o and μ_s, while their deviations are σ_o and σ_s. Additionally, r is the linear correlation coefficient between O and S. We used the RMSE to measure the average difference between observations and emulations in the same units of the analyzed variables (meters) so that values close to zero reflect an excellent emulator. The NSE criteria was used for its straightforward interpretation since as its value approaches one, the quality of the emulator increases. On the other hand, an NSE close to zero indicates that the emulator estimates are as good as the mean of the observations. In contrast, a negative value reveals that the mean of the observations is better than the emulator estimates. Finally, the KGE criteria was chosen because it integrates several statistical parameters. A KGE close to one represents a good model because the means, deviations, and correlation between O and S are similar. Also, the model's performance is considered reasonable when KGE exceeds -0.41, and the mean is used as its benchmark (Knoben et al., 2019).

2.3 Model application area

This research focuses on the Greater Kern County Region (GKCR), comprised of 15 water districts whose areas add up to 4,496 km^2. The GKCR is located south of the Central Valley in Kern and Tulare counties in California, United States. The region borders Fresno County to the north, the Tehachapi Mountains to the south, the Sierra Nevada to the east, and the South Coast Range to the west (Figure 2-2). As in California's Central Valley, agriculture is part of the GKCR's identity since it constitutes a significant gross revenue source, net income, and employment (Hanak et al., 2019). For instance, the agricultural production value of Kern and Tulare counties in 2021 were $8.34 and $8.09 billion, respectively, the highest in the state (Kern County Department of Agriculture and Measurement Standards, 2021; Tulare County, 2021).

Agriculture is the largest water user in California and consumes 80% of the water in a typical year (Lund et al., 2018), of which groundwater supplies about 30, 40 and 60% of the water demand on average dry and drought years, respectively (Perrone & Rohde, 2016). However, the GKCR lacks enough natural surface water, relying on groundwater pumping, and imported water to meet demand. Thanks to a sophisticated network of canals and pipes, water is distributed from groundwater wells, reservoirs, and the Sacramento-San Joaquin Delta to different users (cities, irrigation districts, industries, etc.).

Drought is the greatest threat to agriculture in this region, leading to groundwater overexploitation that causes aquifer depletion, dries shallow wells, and promotes subsidence (Faunt et al., 2016). Additionally, according to the climatic projections for California's Central Valley, an increase in temperature and more significant precipitation variability are expected for the next decades (CDWR (California Department of Water Resources), 2017; Fernandez-Bou et al., 2021); therefore, frequent and severe droughts and flood events are expected (Smerdon, 2017). Moreover, the droughts of recent decades have promoted the transition from annual to perennial crops, whose irrigation has exacerbated the persistent groundwater overexploitation. To prevent such overdrafts and other undesirable effects, the State of California enacted the 2014 Sustainable Groundwater Management Act (SGMA), which will further reduce groundwater availability. The studied emulators were selected to support decision-making in the study region, which may be affected by climate change and environmental regulations such as SGMA.

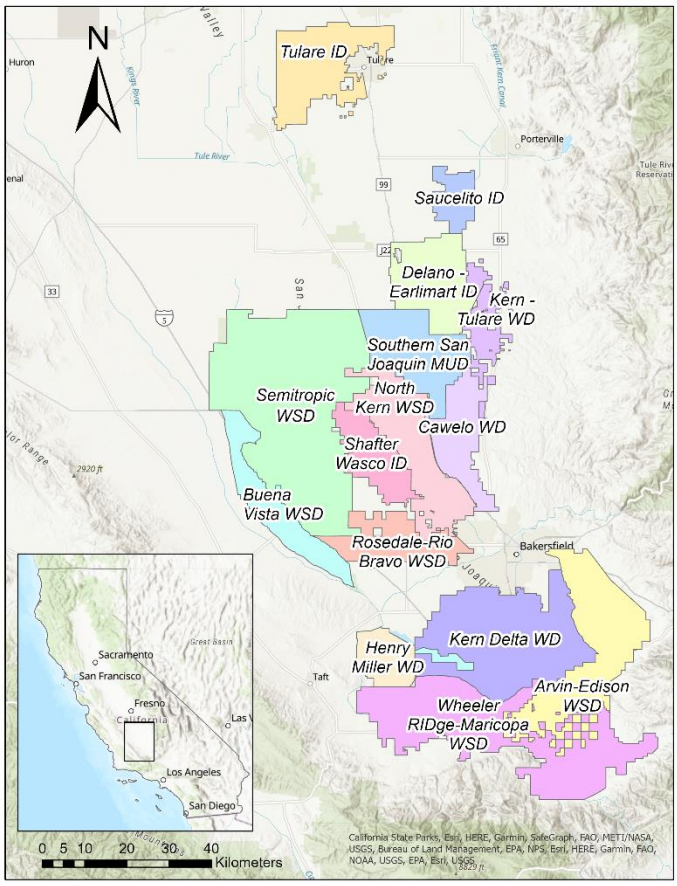

Figure 2-2. Fifteen water districts in the Greater Kern County Region (GKCR).

2.3.1 Analyzed aquifer

Two sources of information were analyzed to identify the aquifers that feed the agricultural wells in the study area. The sources were the stratigraphy of the study area and the vertical wells' screen location. Data related to the stratigraphy was reported in the C2VSimFG. In that model, the Central Valley aquifer is represented by four layers of variable thickness, where the unconfined aquifer, or layer 1, sits over three confined aquifers numbered from top to bottom as layers 2 through 4. On the other hand, the vertical location of the well screens was obtained from the California groundwater wells database known as Well Completion Report (WCR) (CDWR, 2020). The WCR database has more than one million wells of different uses. That information was filtered to guarantee that wells had agricultural use, belonged to the studied districts, were in operation, and the depth to the top and bottom of the well screen were congruent.

In the GKCR, 62.5% of the wells are fed by a single layer, while the remaining wells receive water from two or more layers (Figure 2-3). A single aquifer layer feeds a well if the top and bottom of the well screen belong to the same layer. The bars in Figure 2-3 have different colors to show the layers that feed the wells in the most unfavorable scenario: when the water level decreases until it approaches the bottom of the screen. For example, if the top of a well screen is in layer 1 and its base is in layer 2, the well will receive water from both layers under normal

operating conditions. However, the worst operating condition occurs when the water level drops below layer 1, and the well can only be supplied by layer 2. Our research focuses on modeling the depths to groundwater of layer 2 because, under the most unfavorable condition, this layer is fed by around 80% of the wells. In addition, layer 2 was also selected because although the number of agricultural wells supplied by layer 1 was 15.1%, most farmers tend to invest in deeper wells, which are less susceptible to lower water levels and contamination and have higher pumping capacities (R. A. Pauloo et al., 2020).

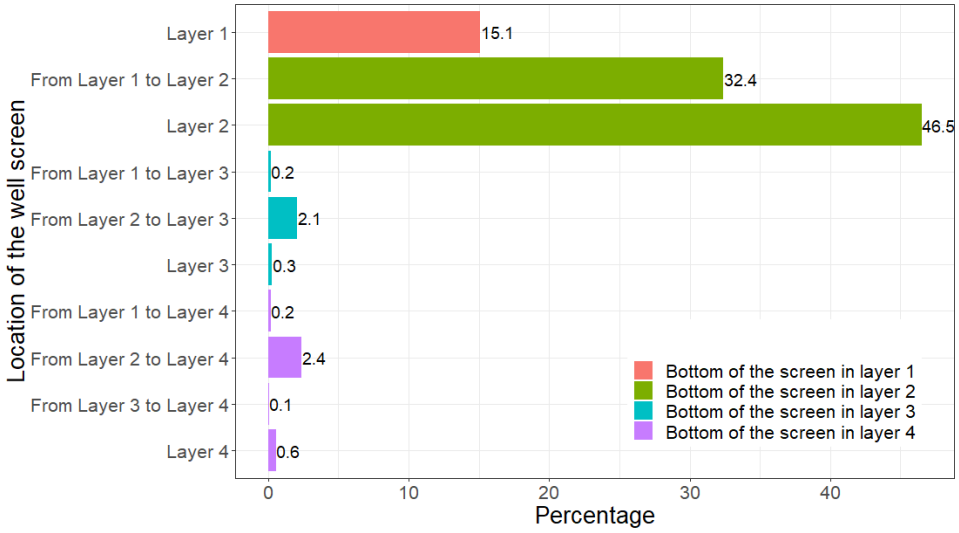

Figure 2-3. Aquifers that feed the study area's wells

2.4 Emulators' structure

Commonly, emulators consider time and space independently. Some models can make local estimates, in which time varies, while others are useful for making spatial predictions independent of time. For example, MacEwan et al. (2017) used independent MLRs to estimate changes in depth to groundwater for three hydrological regions in Central Valley, California. On the other hand, when time is left aside, the emulators focus on recreating similar surfaces to those generated by the reference PBMs. This approach includes spatial interpolation methods such as kriging (Razavi et al., 2012). Some researchers follow a multi-step algorithm for simultaneous consideration of time and space. First, an independent model is trained for each observation point, and then the model's outputs are interpolated using geostatistical methods. Although this approach has many advantages, groundwater systems are tightly integrated in time and space (Ghaseminejad & Uddameri, 2020) and require consistency with the law of conservation of mass.

The emulators we present in this study integrate time and space simultaneously to estimate the change in depth to groundwater (ΔGWD). As these emulators aim to support future planning processes, the spatial resolution was set at the water district level. In contrast, the temporal resolution of the original model (monthly basis) was maintained. Hence, the proposed emulators can be classified as hierarchical-based and data-driven models. Additionally, we used static and dynamic variables to model the combined effects of space and time, as Kratzert et al. (2019) proposed. We used static variables to consider space patterns and dynamic variables to model time dependencies. The static variables refer to water districts' average characteristics. They can

be classified into geometric features (surface area and ground surface slope), soil characteristics (field capacity, saturated hydraulic conductivity, and total porosity), and aquifer characteristics (hydraulic conductivity, aquifer vertical hydraulic conductivity, specific yield, and specific storage). Precipitation (P), surface water deliveries (SWD), and agricultural water demands (AWD) constitute the dynamic components of the model. Ranges of the static and dynamic variables for the 15 analyzed water districts are shown in Table 2-1. A detailed analysis of the dynamic variables selection is made in section 2.4.1. All variables, except geometric features, were extracted from C2VSimFG databases. Water district areas were obtained from the California Department of Water Resources Geographical Information System (CDWR, 2021b). The ground surface slope was derived from the Digital Elevation Model from the National Aeronautics and Space Administration web page (NASA, 2018). General emulators' structure is shown in Figure 2-4.

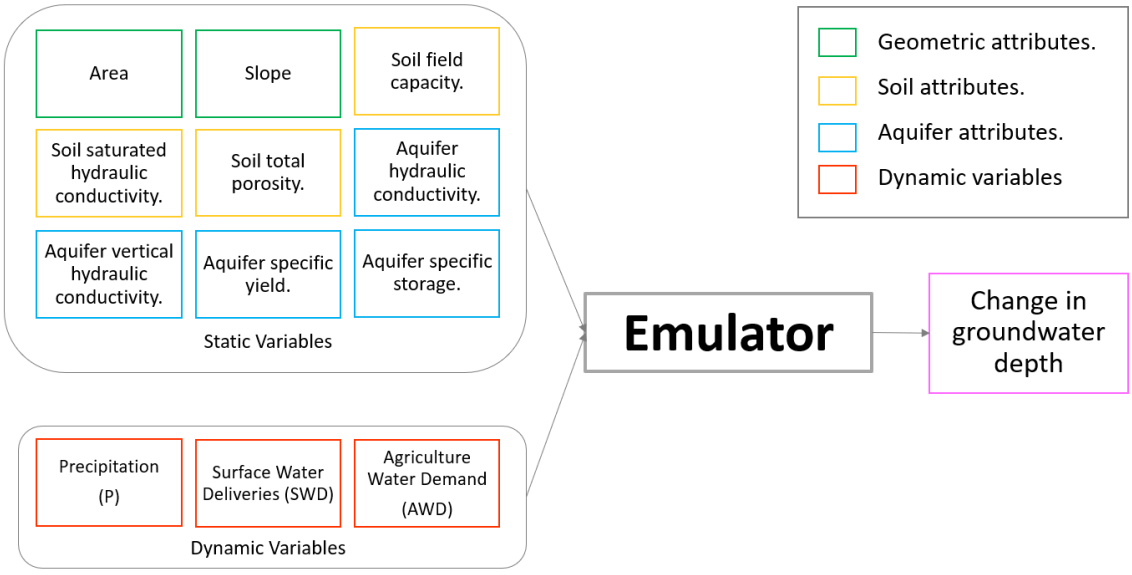

Figure 2-4. General emulators' structure.

Table 2-1. Ranges of the static and dynamic variables for the 15 water districts analyzed

Category		Input variables	Units	Range
Static Variables	Geometric features	Surface area	Hectares	7,963 ~ 90,451
		Ground surface slope	Percentage	0.11 ~ 2.25
	Soil Properties	Field capacity	Dimensionless	0.18 ~ 0.37
		Saturated hydraulic conductivity	m/s	$7.23*10^{-9}$ ~ $6.34*10^{-8}$
		Total porosity	Dimensionless	0.37 ~ 0.50
	Aquifer properties	Hydraulic conductivity	m/s	$8.6*10^{-7}$ ~ $4.33*10^{-6}$
		Vertical hydraulic conductivity	m/s	$7.14*10^{-9}$ ~ $3.02*10^{-8}$
		Specific yield	Dimensionless	0.08 ~ 0.14
		Specific storage	1/m	$7.97*10^{-5}$ ~ $2.52*10^{-4}$
Dynamic variables		Precipitation (P)	km3/month	0 ~ 0.13
		Surface water deliveries to agriculture (SWD)	km3/month	0 ~ 0.07
		Agricultural water demands (AWD)	km3/month	0 ~ 0.14

2.4.1 Dynamic variables' selection

Dynamic variables were selected following the principle of conservation of mass to guarantee the emulators' consistency with the physical processes. Although ANNs can reproduce complex interactions between input and output, ignorance of the physical laws or principles that govern such relationships can lead to inaccurate or false predictions (Read et al., 2019). In 2008, Google Flu Trends (GTF) was presented as a successful model for predicting influenza incidence. However, GTF received widespread criticism for overestimating the proportion of doctor visits for influenza-like illnesses compared to the widely accepted models developed by the Centers for Disease Control and Prevention (CDC). GTF failed due to using an exploratory variable highly correlated to influenza susceptibility but structurally unrelated (Lazer et al., 2014). Similar problems have been observed across different fields.

To avoid the shortcomings of the GTF approach, we identified the variables structurally most related to the depth to groundwater for the second aquifer layer yet preserving the principle of conservation of mass. According to Khan et al. (2020), the groundwater system in a region extends vertically from the unsaturated zone (water table) to the bottom of the groundwater basin, which may include several aquifer layers in between. Water inflows to the groundwater system are recharge due to precipitation, recharge due to applied water, managed aquifer recharge, seepage from conveyance infrastructure, groundwater gain from streams and lakes, subsurface inflows, and water release caused by land subsidence (Khan et al., 2020). Water outflows include pumping, groundwater loss to streams and lakes, and subsurface outflows. The difference between inputs and outputs is the change in groundwater storage (ΔGWS) per time step.

After comparing the contributions of input and output variables to the groundwater system reported by C2VSimFG, we found that precipitation (*P*), surface water deliveries (*SWD*), and pumping (*PG*) were the variables that affected the *ΔGWS* estimation the most. However, C2VSimFG estimates pumping as the difference between Applied Water (*AW*) and the *SWD* (Dogrul & Kadir, 2020a; DWR, 2020) because pumping records are scarce in the Central Valley, as well as in other parts of the world (Massoud et al., 2018). If AW is assumed to be equal to the Agricultural Water Demand (*AWD*), the most relevant variables to estimate *ΔGWS* are *P*, *SWD*, and *AWD*. Figure 2-5 shows that these variables have a consistent seasonal behavior of 12 months for the Semitropic Water District (similar charts are in Appendix A.1).

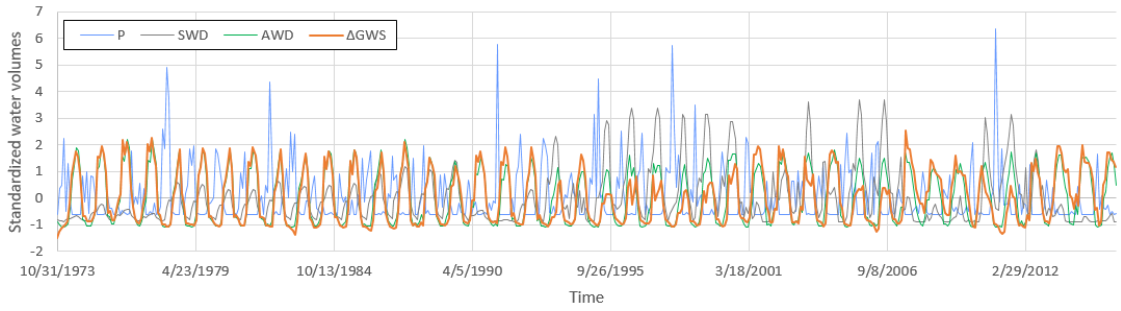

Figure 2-5. Standardized water volumes for Semitropic Water District.

Figure 2-6 compares each dynamic variable with the *ΔGWS* for the Semitropic Water District. The time series were de-seasonalized and standardized to facilitate their comparisons. The deseasonalization was made by the difference between the observed values in months *t* and *t-12*. Standardization consisted of transforming the deseasonalized variables into values with zero mean and one standard deviation. According to Figure 2-6a, *SWD* and *ΔGWS* have a positive correlation so that when deliveries increase, the change in groundwater storage also increases, which implies an increase in aquifer recharge. Figure 2-6b shows the relationship between *P* and *ΔGWS.* From that figure, we can see a lag between *P* and *ΔGWS*, so minimum and maximum values of change in storage follow the minimum and maximum values of precipitation. The lag refers to the time between the rainfall and the aquifer recharge. Finally, *AWD* and *ΔGWS* have a negative correlation since when *AWD* decreases (high values in the chart due to the effect of the sign change), the *ΔGWS* increases (Figure 2-6c). Similar graphs for the other districts can be found in Appendix A.2.

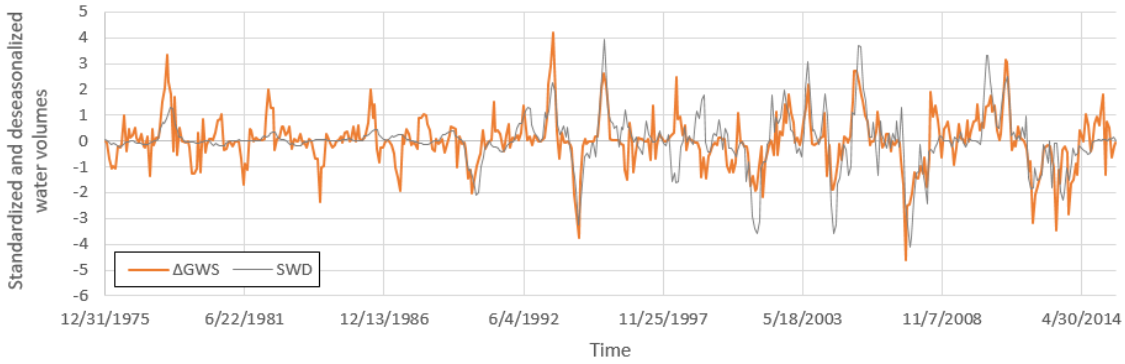

a)

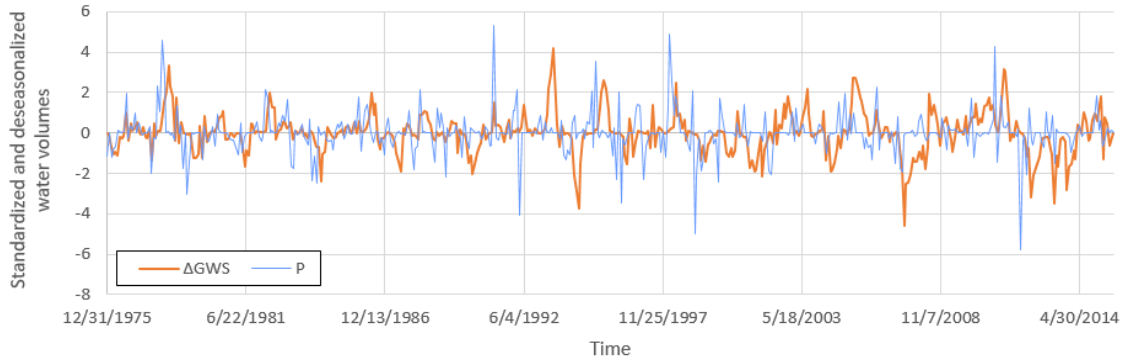

b)

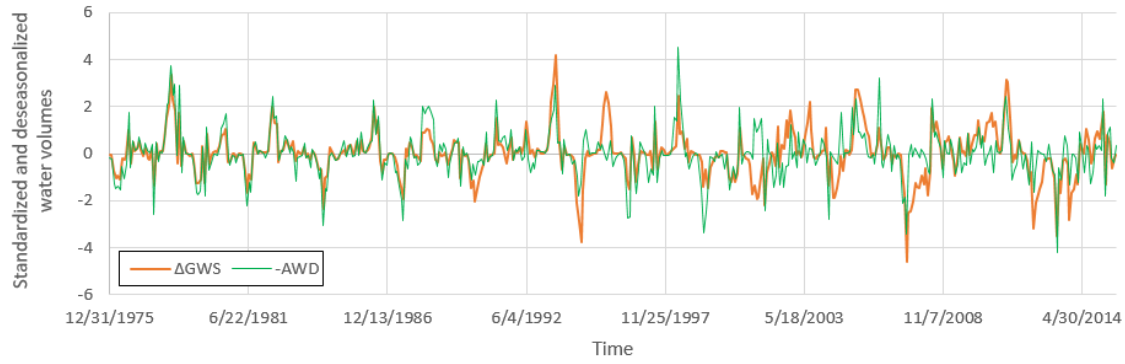

c)

Figure 2-6. Standardized and deseasonalized water volumes for Semitropic Water District. a) Change in groundwater storage (ΔGWS) versus surface water deliveries (SWD). b) ΔGWS versus precipitation (P). c) ΔGWS versus agricultural water demand (AWD). AWD's signs were reversed to facilitate data comparisons.

Figure 2-7 shows the standardized moving average values for depth to groundwater (*GWD*) and groundwater storage (*GWS*) for the Semitropic Water District, considering the C2VsimFG data. Note that the vertical axis has been reversed to facilitate variable interpretation. The decrease in the brown and black lines represents the increase in depth and the decrease in storage, respectively. Similar images are in the supplementary material for the other districts. Here, the *GWS* refers to the sum of the groundwater storage of the four aquifers. On the other hand, GWD

refers to the average depth of the mesh nodes that belong to the second aquifer layer. Although the *GWS* does not refer exclusively to the second aquifer layer, GWS can be used to estimate GWD because most of the wells belong to the second aquifer layer (see Figure 2-3). Considering that the two-time series (GWD and GWS) have similar behaviors (Figure 2-7), *GWS* can be used to estimate *GWD*, or even better, the dynamic variables (*P*, *SWD*, and *AWD*) can be used to estimate *ΔGWD*.

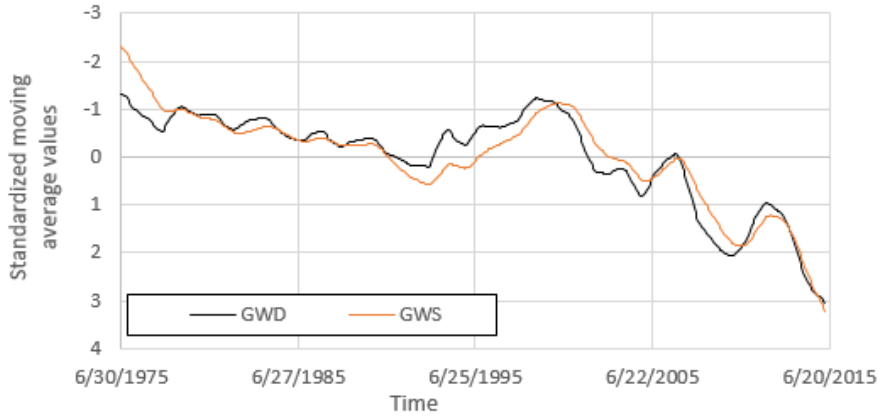

Figure 2-7. Standardized moving average values for depth to groundwater (GWD) and groundwater storage (GWS) for Semitropic Water District. The vertical axis was reversed to facilitate interpretation. The decrease in the brown and black lines represents the increase in depth and the decrease in storage, respectively.

The dynamic variables selected here are similar to those in other studies. For example, Massoud et al. (2018) developed an aggregate model to estimate the *ΔGWS* in Central Valley California, considering the relationships between precipitation, supply, and demand. Murray and Lohman (2018) showed that the seasonal cycles of precipitation, land use, and water use had a close relationship with the elastic deformation of the aquifer/aquitard system during the storm events between 2016 and 2017 in the Tulare Basin. Finally, C. Chen, He, Zhou, Xue, & Zhu (2020) estimated groundwater levels in the Heihe River Basin, northwestern China, as a function of two inflows: recharge and stream flow, and one outflow: pumping. In this study, our inflows *P* and *SWD* contribute to recharge, and the stream flow role is represented by the surface water delivered to districts. Finally, here pumping is expressed as the difference between *AWD* and *SWD*.

2.4.2 Models' architecture

During the LSTM training, fragments of the time series must be shown to the emulator. The time series fragments length (FL) refers to the time until past events could affect current events. For instance, if FL is three, the emulator will receive the present and the three previous dynamic values for the *ΔGWD* estimates. Considering that *FL* plays a significant role in the model results, researchers like Kratzert et al. (2019) have proposed to use optimization methods for its definition (hyperparameter tuning). Here, the *FL* was estimated by analyzing a graph that we called Multiple Squared Correlation Function (MSCF), equivalent to the autocorrelation function used in time series analysis. To draw the MSCF, first, we remove the seasonal effect of the dynamic variables and *ΔGWD* by subtracting its values in the months *t* and *t-12*. Subsequently, we calculated the square of the multiple correlation coefficient (R^2) for the deseasonalized variables

for different lags using Equation 2-13 and Equation 2-14. In these equations, x_i refers to *i-th* dynamic variable or predictor; *y* is the output variable (*ΔGWD*); ***Rxx*** is the correlation matrix between predictors; and ***C*** is the vector that storages the correlations between predictors and the output variable ($r_{xi,y}$).

$$R^2 = \boldsymbol{C}^T * \boldsymbol{R}_{xx}^{-1} * \boldsymbol{C} \quad \text{Equation 2-13}$$

$$\boldsymbol{C}^T = (r_{x1,y}, r_{x2,y}, \dots, r_{xn,y}) \quad \text{Equation 2-14}$$

According to the MSCF for Semitropic Water District (Figure 2-8), the relationship between the dynamic variables and *ΔGWD* is relevant for up to 12 months. Until that lag, most R^2 values are above the limit defined by a 0.95 confidence level (see red line). Since similar behaviors were identified in the other water districts, a 12-month FL was assumed (see Appendix A.4).

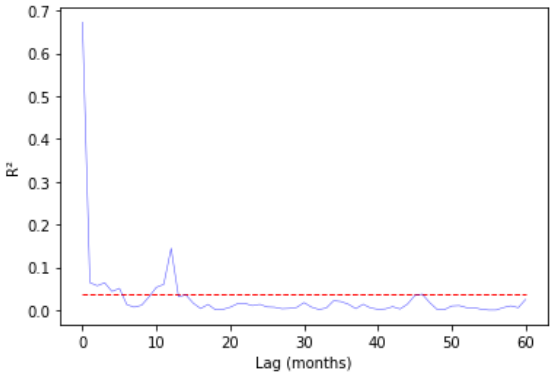

Figure 2-8. Multiple Squared Correlation Function (MSCF) between the dynamic variables and ΔGWD for the Semitropic Water District after removing seasonal effects.

For the analyzed emulators, the number of input variables (*NIV*) was calculated using Equation 2-15. In that equation, *NSV* is the number of static variables, and number three refers to the number of dynamic variables. Note that one is added to *FL* to indicate that *ΔGWD* in the current month depends on the dynamic variables in the same month and the previous months defined by *FL*. Therefore, the *NIV* for each emulator is 48, that is, nine static input variables plus 39 dynamic variables. In sum, the studied emulators preserve the temporal resolution of the original model (monthly basis) and consider the effect of dynamic variables' previous observations (12 months) in estimating *ΔGWD*.

$$NIV = NSV + 3 * (FL + 1) \quad \text{Equation 2-15}$$

The architecture of each emulator implies different numbers of parameters. For example, the number of parameters for the MLR is 49, equal to the *NIV* plus one additional parameter to represent the intercept (see Equation 3-11). MLP architecture was defined by contemplating the LSTM because the last one is more complex since it consists of four gates, each with an ANN. After performing the hyper-parametrization process, we found that an LSTM with a hidden layer of 20 neurons (which means 2,661 parameters) could emulate the relationship between inputs and outputs the best. Finally, given the large number of possible architectures for the MLP, we decided to train a model with four hidden layers (alluding to the total number of hidden layers of the LSTM) with the same number of neurons in each layer. To guarantee that the total number of parameters of the MLP and the LSTM were equal, the theoretical number of neurons in each hidden layer of the MLP should be around 7.18. Given the infeasibility of using a non-integer number of neurons, we selected eight neurons per hidden layer. As a result, the MLP has four hidden layers, each with eight neurons, which means 3,296 parameters.

2.4.3 Training, validation, and testing

Many studies recommend running the Physical Based Models under different conditions to generate a significant number of training patterns for the emulator (Castelletti, Galelli, Ratto, et al., 2012; L. Chen et al., 2018; Weber de Melo et al., 2022). However, the C2VSimFG historical scenario provides enough patterns to train the three emulators because each emulator receives patterns from all the districts, guaranteeing that the models are trained under different conditions. The validity of this hypothesis was corroborated by the good estimates made by the emulators during testing (see section 2.5). The idea implemented here agrees with Cui et al. (2018), who affirm that the training samples can also correspond to historical scenarios. For the MLP and LSTM, we divided the number of patterns into three categories: 70 % for training, 15 % for validation, and 15 % for testing. The training data set was used to fit the model parameters (neuron weights). The validation dataset was defined to unbiased evaluate the models while adjusting for their hyperparameters: learning rate and the number of neurons. A testing data set was used to assess the quality of the final models using an independent data set. Training, validation, and test samples were randomly selected from the entire time series length to improve the emulators‘ generalizability. Therefore, thanks to the samples‘ random selection, we abandoned the common practice of choosing the training samples from the oldest portion of the time series and selecting the test samples from its most recent periods.

Before and after training, validation, and testing, input and output data were normalized to reduce the influence of the *variables'* ranges on the results. Thanks to *Equation 2-16*, the variables were normalized in the range *[*0, 1*], w*here *x* is the original data; *x** represents the normalized ones; x_{min} and x_{max} are the minimum and maximum values of *x*. Finally, *t*he MLP and LSTM were trained to minimize the output layer's mean square error (MSE) using the Adaptive Moment Estimation (ADAM) optimizer.

$$x^* = \frac{(x - x_{min})}{x_{max} - x_{min}} \qquad \text{Equation 2-16}$$

2.5 Results and discussion

Table 2-2 summarizes the emulators' ability to replicate ΔGWD during the testing phase for the 15 water districts. MLR results appear in columns two to four (from left to right). The MLR-RMSE ranges between 0.11 m and 1.39 m. Although 0.11 m reflects a good model, an RMSE of

1.39 m is relatively high. When the RMSE is large, the ΔGWS errors are magnified by the effect of the water district surface area due to ΔGWS can be expressed as the product of the ΔGWD, the water district surface area, and the storage coefficient or storativity (S) (Fetter, 2001). As mentioned in section 2.2.3, an emulator is attractive when the RMSE is close to zero. The positive skewness of the MLR-RMSE indicates that most of the RMSEs were small. On the other hand, MLR-NSE values vary between 0.09 and 0.93. As marked above, an NSE value close to zero indicates that the emulator cannot capture the time series details but only their mean, whereas values close to one reflect a good model. The negative skewness of the MLR-NSE means that high NSE values are abundant. Finally, the MLR-KGE fluctuates between -0.46 and 0.88. From the KGE's point of view, a model is acceptable when values are close to one. The negative skewness of the MLR-KGE reveals the model's good qualities.

MLP summary results are shown in Table 2-2 in columns five to seven (from left to right). The MLP-RMSE oscillates between 0.08 m and 0.52 m. There is an upgrade concerning the MLR-RMSE because the maximum MLP-RMSE was reduced by 0.87 m. In addition, MLP- NSE values also improved substantially, now ranging between 0.85 and 0.97. Finally, the MLP-KGE ranges from -2.02 to 0.97. The negative MLP-KGE skewness and positive MLP-KGE kurtosis mean that MLP is a good model.

Columns eight to ten (from left to right) in Table 2-2 shows the LSTM summary results. The LSTM-RMSE varies between 0.06 m and 0.39 m. There is a significant improvement in relation to the MLR-RMSE because the maximum MLP-RMSE was reduced by 1.0 m. The LSTM- NSE values also improved substantially, now ranging between 0.90 and 0.99. However, the LSTM-KGE ranges from -5.52 to 0.94. The negative LSTM-KGE skewness and positive LSTM-KGE kurtosis mean that higher KGE values were abundant.

Table 2-2. Summary metrics for the emulators: MLR, MLP, and LSTM.

Summary metric	MLR			MLP			LSTM		
	RMSE (m)	NSE	KGE	RMSE (m)	NSE	KGE	RMSE (m)	NSE	KGE
Minimum	0.11	0.09	-0.46	0.08	0.85	-2.02	0.06	0.9	-5.52
Mean	0.62	0.63	0.29	0.25	0.93	0.52	0.21	0.95	-0.19
Standard dev.	0.43	0.25	0.33	0.12	0.04	0.76	0.1	0.03	1.71
Skewness	1.00	-0.95	-0.31	0.57	-0.72	-3.05	0.32	-0.56	-2.52
Kurtosis	-0.37	0.15	1.09	0.12	-0.77	10.19	-0.87	-1.27	6.86
Maximum	1.39	0.93	0.88	0.52	0.97	0.97	0.39	0.99	0.94

Figure 2-9 shows the Cumulative Distribution Functions (CDF) for each metric. Considering the curves shown in Figure 2-9a and that a model has good quality when the RMSE is close to zero, the best model from the RMSE's point of view is the LSTM. Regarding the NSE and KGE metrics (Figure 2-9 b and c, respectively), the models are suitable to the extent that these indices are close to one. According to the NSE, the LSTM is the best model, and from the KGE's perspective, the MLP is the best. The LSTM has the best performance in terms of RMSE and NSE from the three analyzed models. A deeper analysis indicates that lower LSTM-KGE values echo differences between the observed and emulated means (μ_o and μ_s). However, the maximum means difference was 0.16 m.

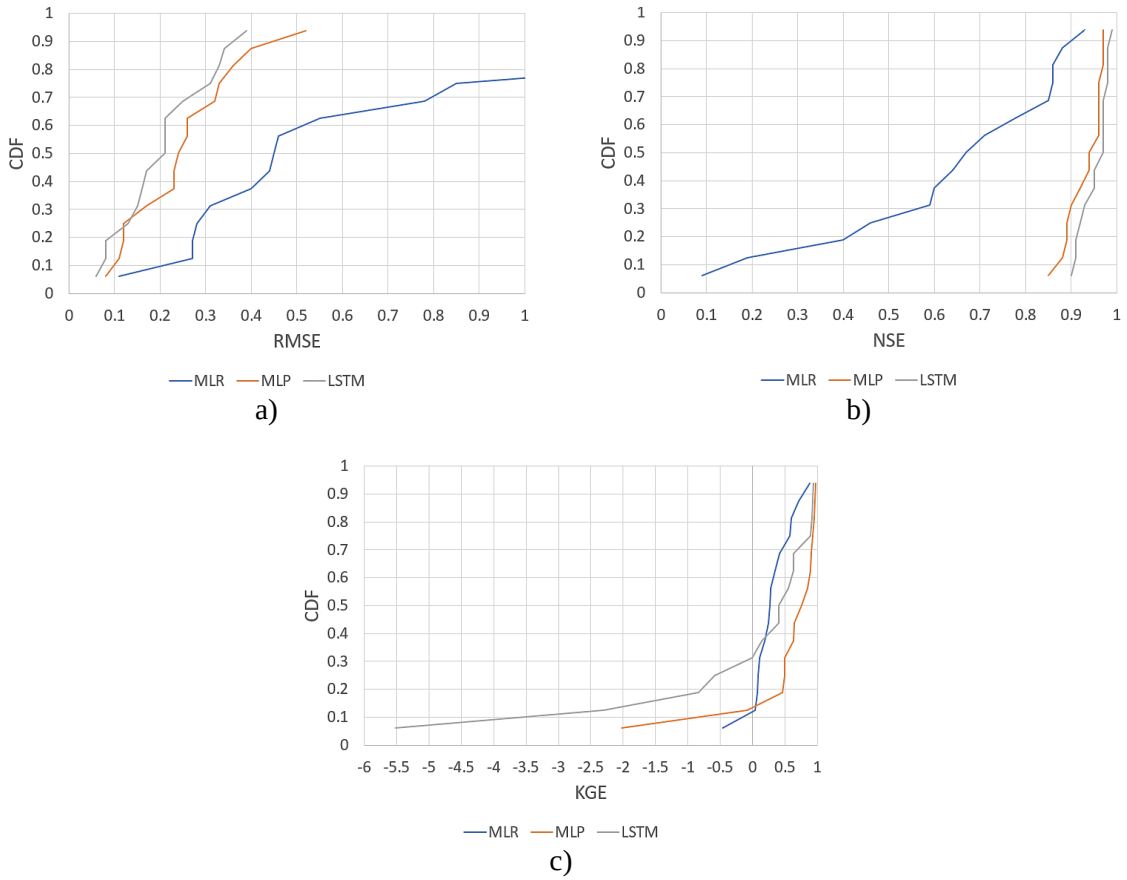

Figure 2-9. Cumulative Distribution Functions (CDF) for emulators' metrics during the testing phase. a) CDF for the RMSE. b) CDF for NSE. c) CDF for KGE.

Figure 2-10 shows the *ΔGWD* estimates for the Semitropic Water District using the emulators. The red and blue lines represent the observed and emulated values, respectively. Figure 2-10a shows that the MLR can reproduce the trend and seasonality but not the minimum and maximum values. On the other hand, Figure 2-10b and Figure 2-10c show a notable improvement in emulating extreme values using an MLP and an LSTM, respectively. Similar figures for the other water districts are in the Appendix A.5.

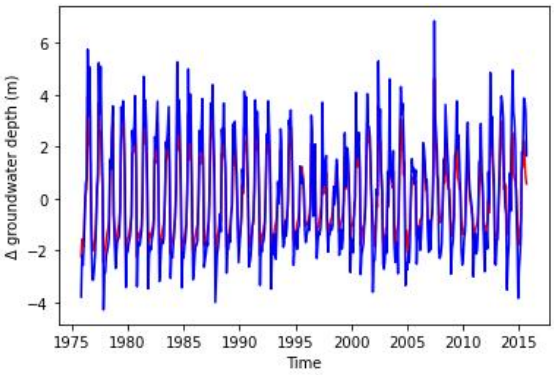

a)

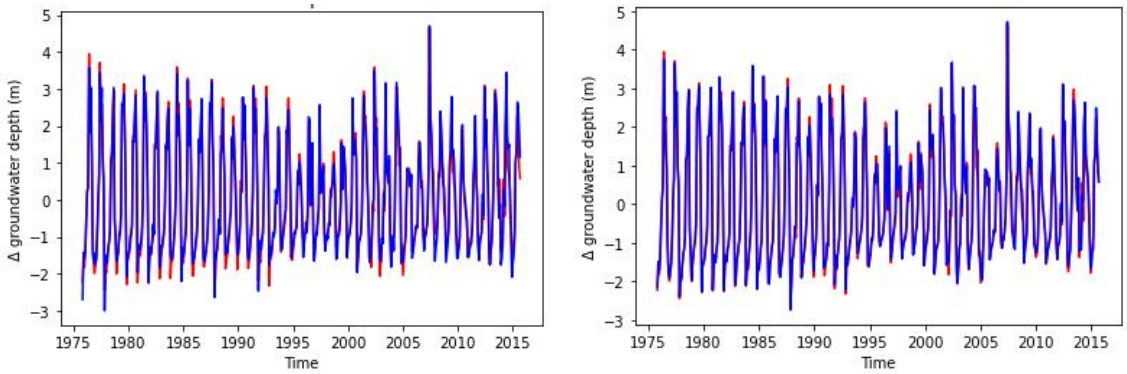

b) c)

Figure 2-10. Emulators' ΔGWD estimations for the Semitropic Water District. a) MLR, b) MLP, and c) LSTM. Observed values are in red, and emulated values are in blue.

The metrics' spatial distribution is shown in Figure 2-11, where brown and yellow colors represent a continuum between poor and good performances, respectively. In this figure, each row represents the same metric, while the columns refer to the same emulator. In addition, the intervals for the same metric (row) are similar to facilitate comparisons.

The *RMSE* (first row of Figure 11) shows a noticeable improvement from the *MLR* to the *LSTM*. The *MLP* and *LSTM* emulators have lower *RMSE* values regardless of the location of the water district. According to the *RMSE* metric, the best model is the *LSTM*, and its maximum values occurred in Buena Vista WSD (*RMSE = 0.39 m*) and Henry Miller WD (*RMSE = 0.34 m*). However, those values are low compared to the standard deviations of the *ΔGWD* values simulated by C2VSimFG, 2.12 m, and 1.55 m, respectively.

The middle row of Figure 11 shows that the *NSE* metric also upgraded from *MLR* to *LSTM*. For the *LSTM-NSE* image, some water districts look brown for the use of a common scale for the three emulators. However, for those brown areas, their LSTM range between 0.90 and 0.92.

Finally, according to the KGE (last row of Figure 11), the MLP was the best model, with good results (*KGE > -0.41*) for 14 of the 15 water districts, especially for those located in the middle of the analyzed area. The minimum MLP-*KGE* was -2.01 and occurred in Henry Miller WD (located in the bottom center of the study area). However, for the same district and emulator, the RMSE was 0.51 m. LSTM-*KGE* values were better than those for the MLR, but with some negative values distributed across the entire area. Nonetheless, a more exhaustive analysis showed that the worst LSTM-*KGE* (-5.52) occurred again in Henry Miller WD. However, in this case, the LSTM-RMSE was 0.34 m (a low value compared to the standard deviations of its ΔGWD, 1.55 m).

On the other hand, several experiments were carried out to compare the C2VSimFG and the emulators' run times. Those experiments were done on a computer with the following characteristics. Processor Intel(R) Core(TM) i7-9700 3.00GHz CPU, 16GB of RAM, with 1 TB NVMe Solid State Drive. While C2VSimFG's runtime was 4.2 hours, the emulators' run times were 3.8 s, 4.2 s, and 9.1 s for the MLR, MLP, and LSTM, respectively. Although a noticeable reduction in time is observed at first glance, it is necessary to remember that C2VSimFG simulates most (if not all) of the Central Valley hydrologic cycle components. Besides, C2VSimFG considers four aquifer layers and has an average horizontal grid resolution of 1.65 km^2. Instead, the studied emulators focus on estimating the second aquifer's ΔGWD as a function of three variables (*P*, *SWD*, and *AWD*) and offer aggregated results for 15 water districts with an average area of 299.75 km^2. However, for both C2VSimFG and the emulators, the time window (from 1974 to 2015) and the temporal resolution (monthly) were the same. In short, time decreases due to spatial aggregation, variables reduction, and focus on the second aquifer layer.

In some cases, the C2VSimFG's ability to model Central Valley's hydrology with high resolution (spatial and temporal) becomes a disadvantage when looking for its coupling with other models due to run time and complexity. Consequently, simplifying the model and reducing the spatial or temporal resolutions is a suitable alternative that does not compromise model output accuracy. Without the emulators studied here, running C2VSimFG for the entire area and performing the desired aggregations later is necessary. Thanks to the developed emulators, it is possible to quickly know the response of the second aquifer under different conditions.

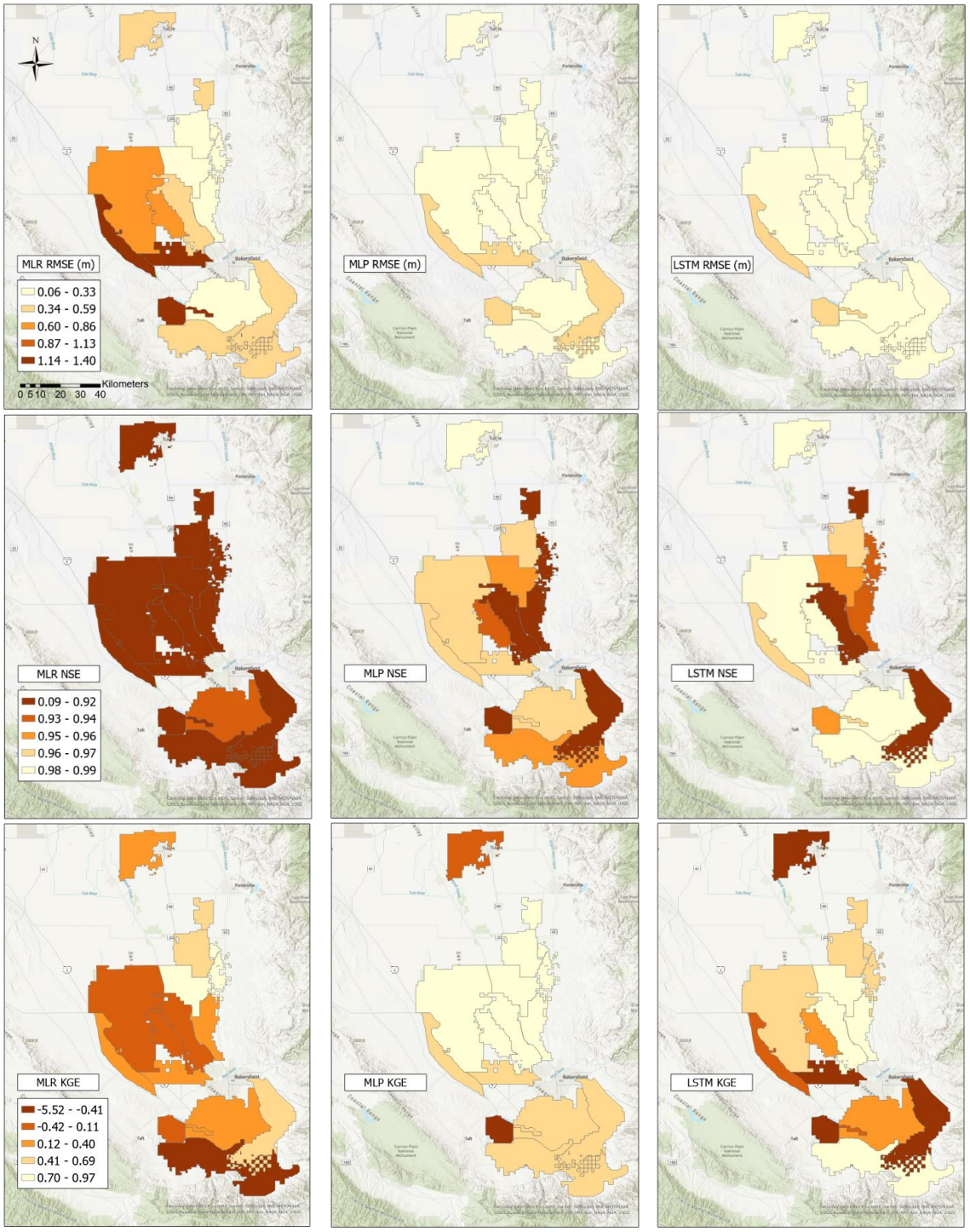

Figure 2-11. Spatial distribution of metrics for each emulator. Analyzed emulators: Multiple Linear Regression (MLR), Multilayer Perceptron (MLP), and Long Short-Term Memory (LSTM). Metrics: Root Mean Squared Error (RMSE), Nash–Sutcliffe Efficiency coefficient (NSE), and the Kling-Gupta Efficiency coefficient (KGE).

2.6 Conclusions

This study presents three emulators to reproduce groundwater patterns in California's Kern and Tulare counties. Our analyses show that the emulators adequately replicate the *ΔGWD* as a function of precipitation, surface water deliveries, and applied water demand. Some important results arise from this work. First, we identified variables more structurally related to the depth to groundwater for the second aquifer layer within the conservation of mass. The methodology includes comparing the input and output variables after removing the trend and seasonality effects. Second, developing a method to emulate highly complex mechanistic models dependent on space and time. Third, this research proposes a simple way to estimate the fragment length of the time series presented to the emulators during their training phase using the Multiple Squared Correlation Function (MSCF) graphs. Fourth, the studied emulators are characterized by their credibility, efficacy, and efficiency, facilitating groundwater integration in broader modeling frameworks. Hence, decision-makers will be able to evaluate multiple scenarios relatively simply and accurately without compromising the quality of the results.

Emulators like the ones proposed here can be used in regions lacking detailed information on the groundwater system but with rainfall records, aquifer levels, water deliveries, agricultural demands, and easily acquired hydrogeological parameters. Emulators' input variables were classified into static and dynamic. The first focused on modeling the spatial patterns, and the second on the temporal component. Whereas the static variables include the geometry of the districts, the characteristics of the soil and the aquifer, the dynamic variables include the most relevant variables of the groundwater balance: water inflows (precipitation and *SWD*), outflows (*AWD*), and change in storage (*ΔGWS*). The latter is highly related to the depth to groundwater of the uppermost confined aquifer (*ΔGWD*).

Results indicate that the LSTM is the best emulation alternative because it meets the desired attributes, such as conservation of mass, quality of the results, and reduction of computation times. First, from the credibility point of view, this model considers the effects of previous events on future estimates. In addition, using static variables, we sought to address the spatial component. Therefore, LSTMs are one of the best alternatives to represent environmental phenomena. Second, all metrics (except the KGE index) show that the LSTM performs best. On the other hand, the MLP has the second-best performance. However, the fact that the temporary structure of variables does not play any role detracts from emulation credibility. Finally, the MLR, with its reduced number of parameters, can also simulate the trend and seasonality of the observations. However, the MLR cannot represent the maximum and minimum values, which is reflected in the quality of the metrics.

Commonly, LSTM models consider the effect of preceding observations of the output variable. However, a novel approach is proposed here, in which the output variable does not depend on its previous values but on the static variables and earlier observations of the dynamic variables. This approach was adopted to prevent error propagation when calculating depth to groundwater. In addition, thanks to the analysis of fragments of the time series of 13 months of extension (12 lagged months and the current month), the LSTM can learn the aquifer's behavior hidden in the data. For future studies, evaluating the performance of LSTM in diverse districts within the Central Valley distinct from those constituting the GKCR is recommended to assess the LSTM generalization ability. Finally, this work is expected to contribute to the hydrological process modeling literature.

2.7 References

Alam, S., Gebremichael, M., Li, R., Dozier, J., & Lettenmaier, D. P. (2019). Climate change impacts on groundwater storage in the Central Valley, California. *Climatic Change*, *157*(3–4), 387–406. https://doi.org/10.1007/s10584-019-02585-5

Allen, R. G., Pereira, L. S., Raes, D., & Smith, M. (1998). *FAO irrigation and Drainage paper No. 56. Crop Evapotranspiration* (Vol. 56).

Amanambu, A. C., Obarein, O. A., Mossa, J., Li, L., Ayeni, S. S., Balogun, O., Oyebamiji, A., & Ochege, F. U. (2020). Groundwater system and climate change: Present status and future considerations. *Journal of Hydrology*, *589*(December 2019), 125163. https://doi.org/10.1016/j.jhydrol.2020.125163

Asher, M. J., Croke, B. F. W., Jakeman, A. J., & Peeters, L. J. M. (2015). A review of surrogate models and their application to groundwater modeling. *Water Resources Managment*, *51*(8), 5957–5973. https://doi.org/https://doi.org/10.1002/2015WR016967

Benjamin, P., Erraguntla, M., Delen, D., & Mayer, R. (1998). Simulation modeling at multiple levels of abstraction. *Winter Simulation Conference Proceedings*, *1*, 391–398. https://doi.org/10.1109/wsc.1998.745013

Blöschl, G., Bierkens, M. F. P., Chambel, A., Cudennec, C., Destouni, G., Fiori, A., Kirchner, J. W., McDonnell, J. J., Savenije, H. H. G., Sivapalan, M., Stumpp, C., Toth, E., Volpi, E., Carr, G., Lupton, C., Salinas, J., Széles, B., Viglione, A., Aksoy, H., … Zhang, Y. (2019). Twenty-three unsolved problems in hydrology (UPH)–a community perspective. *Hydrological Sciences Journal*, *64*(10), 1141–1158. https://doi.org/10.1080/02626667.2019.1620507

Bowes, B., Sadler, J., Morsy, M., Behl, M., & Goodall, J. (2019). Forecasting Groundwater Table in a Flood Prone Coastal City with Long Short-term Memory and Recurrent Neural Networks. *Water*, *11*(1098). https://doi.org/10.3390/w11051098

Box, G., Jenkins, G., Reinsel, G., & Ljung, G. (2016). *Time series analysis: Forecasting and control* (Fifth). John Wiley & Sons.

Branke, J., Deb, K., Miettinen, K., & Slowinski, R. (Eds.). (2008). *Introduction to Multiobjective Optimization: Interactive Approaches*.

Bras, R., & Rodriguez-Iturbe, I. (1993). Generalized univariate time-series analysis in hydrology. In *Random functions and hydrology*. Dover Publications, Inc.

Brunner, P., & Simmons, C. T. (2012). HydroGeoSphere: A Fully Integrated, Physically Based Hydrological Model. *Groundwater*, *50*(2), 170–176. https://doi.org/https://doi.org/10.1111/j.1745-6584.2011.00882.x

Cal-Adapt. (2022). https://cal-adapt.org/

California State Legislature. (2014). *Sustainable groundwater management act*. https://water.ca.gov/programs/groundwater-management/sgma-groundwater-management

Castelletti, A., Galelli, S., Ratto, M., Soncini-Sessa, R., & Young, P. C. (2012). A general framework

for Dynamic Emulation Modelling in environmental problems. *Environmental Modelling and Software*, *34*, 5–18. https://doi.org/10.1016/j.envsoft.2012.01.002

Castelletti, A., Galelli, S., Restelli, M., & Soncini-Sessa, R. (2012). Data-driven dynamic emulation modelling for the optimal management of environmental systems. *Environmental Modelling and Software*, *34*, 30–43. https://doi.org/10.1016/j.envsoft.2011.09.003

CDWR. (2021a). *California's Groundwater Update 2020 highlights. Bulletin 118*. https://water.ca.gov/programs/groundwater-management/bulletin-118

CDWR (California Department of Water Resources). (2017). *Central Valley Flood Protection Plan 2017 Update* (Issue August).

CDWR, (California Department of Water Resources). (2020). *Well Completion Reports*. https://data.cnra.ca.gov/dataset/well-completion-reports

CDWR, (California Department of Water Resources). (2021b). *GIS*. https://gis.water.ca.gov/arcgis/rest/services/Boundaries/i03_WaterDistricts/FeatureServer/0

Chen, C., He, W., Zhou, H., Xue, Y., & Zhu, M. (2020). A comparative study among machine learning and numerical models for simulating groundwater dynamics in the Heihe River Basin, northwestern China. *Scientific Reports*, *10*(1), 1–13. https://doi.org/10.1038/s41598-020-60698-9

Chen, L., Roy, S. B., & Hutton, P. H. (2018). Emulation of a process-based estuarine hydrodynamic model. *Hydrological Sciences Journal*, *63*(5), 783–802. https://doi.org/10.1080/02626667.2018.1447112

Cheng, F., & Zhao, J. (2019). A novel process monitoring approach based on Feature Points Distance Dynamic Autoencoder. In *Computer Aided Chemical Engineering* (Vol. 46). Elsevier Masson SAS. https://doi.org/10.1016/B978-0-12-818634-3.50127-2

Cohen, J. S., & Herman, J. D. (2021). Dynamic Adaptation of Water Resources Systems Under Uncertainty by Learning Policy Structure and Indicators. *Water Resources Research*, *57*(11), 1–24. https://doi.org/10.1029/2021WR030433

Cui, T., Peeters, L., Pagendam, D., Pickett, T., Jin, H., Crosbie, R. S., Raiber, M., Rassam, D. W., & Gilfedder, M. (2018). Emulator-enabled approximate Bayesian computation (ABC) and uncertainty analysis for computationally expensive groundwater models. *Journal of Hydrology*, *564*(December 2017), 191–207. https://doi.org/10.1016/j.jhydrol.2018.07.005

Cuthbert, M. O., Gleeson, T., Moosdorf, N., Befus, K. M., Schneider, A., Hartmann, J., & Lehner, B. (2019). Global patterns and dynamics of climate–groundwater interactions. *Nature Climate Change*, *9*(2), 137–141. https://doi.org/10.1038/s41558-018-0386-4

D'Agostino, D., Borg, M., Hallett, S. H., Sakrabani, R. S., Thompson, A., Papadimitriou, L., & Knox, J. W. (2020). Multi-stakeholder analysis to improve agricultural water management policy and practice in Malta. *Agricultural Water Management*, *229*, 105920. https://doi.org/https://doi.org/10.1016/j.agwat.2019.105920

Dale, L. L., Dogrul, E. C., Brush, C. F., Kadir, T. N., Chung, F. I., Miller, N. L., & Vicuna, S. D. (2013).

Simulating the Impact of Drought on California's Central Valley Hydrology, Groundwater and Cropping. *British Journal of Environment & Climate Change*, *3*(3), 271–291.

Deb, K., Pratap, A., Agarwal, S., & Meyarivan, T. (2002). A fast and elitist multiobjective genetic algorithm: NSGA-II. *IEEE Transactions on Evolutionary Computation*, *6*(2), 182–197. https://doi.org/10.1109/4235.996017

Delano Earlimart Irrigation District GSA. (2022). *Groundwater Sustainability Plan. Delano-Earlimart Irrigation District*. https://www.deid.org/wp-content/uploads/2022/07/deid_gsp_draft_final_20220720.pdf

Diaz-Granados, M. (2023). *Hidrologia, una sintesis probabilistica* (1st ed.).

Dogrul, E. C., Brush, C. F., & Kadir, T. N. (2016). Groundwater modeling in support of water resources management and planning under complex climate, regulatory, and economic stresses. *Water (Switzerland)*, *8*(12). https://doi.org/10.3390/w8120592

Dogrul, E. C., & Kadir, T. N. (2020a). *DWR Technical Memorandum: Theoretical Documentation and User's Manual for IWFM Demand Calculator (IDC-2015), Revision 88* (Issue August). https://data.cnra.ca.gov/dataset/idc-version-2015-0-88/resource/9d2890d5-52ed-4158-bdb5-4440f9030d12

Dogrul, E. C., & Kadir, T. N. (2020b). *DWR Technical Memorandum: Theoretical Documentation for the Integrated Water Flow Model (IWFM-2015), Revision 1045* (Issue August). https://data.cnra.ca.gov/dataset/iwfm-version-2015-0-1045

Duffy, C., Shi, Y., Davis, K., Slingerland, R., Li, L., Sullivan, P. L., Goddéris, Y., & Brantley, S. L. (2014). Designing a Suite of Models to Explore Critical Zone Function. *Procedia Earth and Planetary Science*, *10*, 7–15. https://doi.org/https://doi.org/10.1016/j.proeps.2014.08.003

DWR. (2019). *C2VSim: California Central Valley Groundwater-Surface Water Simulation Model*. https://water.ca.gov/Library/Modeling-and-Analysis/Central-Valley-models-and-tools/C2VSim

DWR, C. D. of W. R. (2020). *California Central Valley Groundwater-Surface Water Simulation Model – Fine Grid (C2VSimFG) Development and Calibration Version 1.0* (Issue December). https://data.cnra.ca.gov/dataset/c2vsimfg-version-1-0

Escriva-bou, A., Hui, R., Maples, S., Medellín-azuara, J., Harter, T., & Lund, J. R. (2020). Planning for groundwater sustainability accounting for uncertainty and costs : An application to California ' s Central Valley. *Journal of Environmental Management*, *264*(March), 110426. https://doi.org/10.1016/j.jenvman.2020.110426

Faunt, C. C., Sneed, M., Traum, J., & Brandt, J. T. (2016). Water availability and land subsidence in the Central Valley, California, USA. *Hydrogeology Journal*, *24*(3), 675–684. https://doi.org/10.1007/s10040-015-1339-x

Fawzy, S., Osman, A. I., Doran, J., & Rooney, D. W. (2020). Strategies for mitigation of climate change: a review. *Environmental Chemistry Letters*, *18*(6), 2069–2094. https://doi.org/10.1007/s10311-020-01059-w

Fernandez-Bou, A. S., Ortiz-Partida, J. P., Pells, C., Classen-Rodriguez, L., Espinoza, V., Rodríguez-

Flores, J., Booth, L., Burmistrova, J., Cai, A., Cairo, A., Capitman, J. A., Cole, S., Flores-Landeros, H., Guzman, A., Maskey, M., Martínez-Escobar, D., Sanchez-Perez, P., Valero-Fandiño, J., Viers, J., … Medellín-Azuara, J. (2021). *Regional Report for the San Joaquin Valley Region on Impacts of Climate Change*.

Fetter, C. (2001). *Applied Hydrogeology* (P. Lynch (Ed.); Fourth). Prentice Hall.

Fiering, M., & Jackson, B. (1971). *Synthetic streamflows*. https://doi.org/10.1029/WM001

Foster, T., Mieno, T., & Brozović, N. (2020). Satellite-Based Monitoring of Irrigation Water Use: Assessing Measurement Errors and Their Implications for Agricultural Water Management Policy. *Water Resources Research*, *56*(11), e2020WR028378. https://doi.org/https://doi.org/10.1029/2020WR028378

GEI Consultants Inc. (2020). *Groundwater Sustainability Plan. Kern County, CA*. https://kerngwa.com/wp-content/uploads/2022/07/kga-umbrella-gsp_final.pdf

Gers, F. A., Eck, D., & Schmidhuber, J. (2002). Applying LSTM to Time Series Predictable Through Time-Window Approaches. In R. Tagliaferri & M. Marinaro (Eds.), *Neural Nets WIRN Vietri-01* (pp. 193–200). Springer London.

Ghaseminejad, A., & Uddameri, V. (2020). Physics-inspired integrated space-time artificial neural networks for regional groundwater flow modeling. *Hydrology and Earth System Sciences*, *24*(12), 5759–5779. https://doi.org/10.5194/hess-24-5759-2020

Ghasemizade, M., Asante, K. O., Petersen, C., Kocis, T., Dahlke, H. E., & Harter, T. (2019). An Integrated Approach Toward Sustainability via Groundwater Banking in the Southern Central Valley, California. *Water Resources Research*, *55*(4), 2742–2759. https://doi.org/10.1029/2018WR024069

Goharian, E., & Burian, S. J. (2018). Developing an integrated framework to build a decision support tool for urban water management. *Journal of Hydroinformatics*, 708–727. https://doi.org/10.2166/hydro.2018.088

Haasnoot, M., Kwakkel, J. H., Walker, W. E., & ter Maat, J. (2013). Dynamic adaptive policy pathways: A method for crafting robust decisions for a deeply uncertain world. *Global Environmental Change*, *23*(2), 485–498. https://doi.org/10.1016/j.gloenvcha.2012.12.006

Hallegatte, S., Shah, A., Lempert, R., Brown, C., & Gill, S. (2012). *Investment Decision Making under Deep Uncertainty* (Issue September). https://elibrary.worldbank.org/doi/epdf/10.1596/1813-9450-6193

Hanak, E., Escriva-Bou, A., Gray, B., Green, S., Harter, T., Jezdimirovic, J., Lund, J., Medellín-Azuara, J., Moyle, P., & Seavy, N. (2019). *Water and the Future of the San Joaquin Valley* (Issue February). https://www.ppic.org/wp-content/uploads/water-and-the-future-of-the-san-joaquin-valley-february-2019.pdf

Hipel, K. W., & McLeod, A. I. (Eds.). (1994). Chapter 2 Basic Statistical Concepts. In *Time Series Modelling of Water Resources and Environmental Systems* (Vol. 45, pp. 63–86). Elsevier. https://doi.org/https://doi.org/10.1016/S0167-5648(08)70658-0

Hochreiter, S., & Schmidhuber, J. (1997). Long Short-Term Memory. *Neural Computation*, *9*(8),

1735–1780. https://doi.org/10.1162/neco.1997.9.8.1735

Huang, D., Zhang, C., Li, Q., Han, H., Huang, D., Li, T., & Wang, C. (2020). Prediction of Solar Photovoltaic Power Generation Based on MLP and LSTM neural networks. *2020 IEEE 4th Conference on Energy Internet and Energy System Integration (EI2)*, 2744–2748. https://doi.org/10.1109/EI250167.2020.9347223

Jakeman, A. J., Barreteau, O., Hunt, R. J., Rinaudo, J.-D., Ross, A., Arshad, M., & Hamilton, S. (2016). Integrated Groundwater Management: An Overview of Concepts and Challenges. In A. J. Jakeman, O. Barreteau, R. J. Hunt, J.-D. Rinaudo, & A. Ross (Eds.), *Integrated Groundwater Management: Concepts, Approaches and Challenges* (pp. 3–20). Springer International Publishing. https://doi.org/10.1007/978-3-319-23576-9_1

Jasperse, L., & Pairis, A. (2020). *Climate Change Consortium for Specialty Crops: Southern California Region*. www.climatesciencealliance.org/resilient-roots-resources

Karpatne, A., Atluri, G., Faghmous, J. H., Steinbach, M., Banerjee, A., Ganguly, A., Shekhar, S., Samatova, N., & Kumar, V. (2017). Theory-guided data science: A new paradigm for scientific discovery from data. *IEEE Transactions on Knowledge and Data Engineering*, *29*(10), 2318–2331. https://doi.org/10.1109/TKDE.2017.2720168

Kern-Tulare Water District. (2022). *Kern-Tulare Water District. Description of District*. https://drive.google.com/file/d/1sDPYGnB8wPS26GdwypfHtCd_rQHBPd9R/view

Kern County Department of Agriculture and Measurement Standards. (2015). *Kernag*. http://www.kernag.com/gis/gis-data.asp

Kern County Department of Agriculture and Measurement Standards. (2021). *Kern County Agricultural Crop Report*. http://www.kernag.com/caap/crop-reports/crop20_29/crop2021.pdf

Khair, S. M., Mushtaq, S., Reardon-Smith, K., & Ostini, J. (2019). Diverse drivers of unsustainable groundwater extraction behaviour operate in an unregulated water scarce region. *Journal of Environmental Management*, *236*, 340–350. https://doi.org/https://doi.org/10.1016/j.jenvman.2018.12.077

Khan, A., Najmus, S., Hillaire, T., Qian, F., Hass, J., Van Lienden, B., Shipman, P., Namvar, R., & Sogge, C. (2020). *Handbook for Water Budget Development with or without models. DRAFT.* https://water.ca.gov/-/media/DWR-Website/Web-Pages/Programs/Groundwater-Management/Data-and-Tools/Files/Water-Budget-Handbook.pdf

Knoben, W. J. M., Freer, J. E., & Woods, R. A. (2019). Technical note: Inherent benchmark or not? Comparing Nash-Sutcliffe and Kling-Gupta efficiency scores. *Hydrology and Earth System Sciences*, *23*(10), 4323–4331. https://doi.org/10.5194/hess-23-4323-2019

Kratzert, F., Klotz, D., Shalev, G., Klambauer, G., Hochreiter, S., & Nearing, G. (2019). Towards learning universal, regional, and local hydrological behaviors via machine learning applied to large-sample datasets. *Hydrology and Earth System Sciences*, *23*(12), 5089–5110. https://doi.org/10.5194/hess-23-5089-2019

Krogh, A. (2008). What are artificial neural networks? *Nature Biotechnology*, *26*(2), 195–197.

https://doi.org/10.1038/nbt1386

Kumaraswamy, B. (2021). 6 - Neural networks for data classification. In D. Binu & B. R. Rajakumar (Eds.), *Artificial Intelligence in Data Mining* (pp. 109–131). Academic Press. https://doi.org/https://doi.org/10.1016/B978-0-12-820601-0.00011-2

Larocque, M., Levison, J., Martin, A., & Chaumont, D. (2019). A review of simulated climate change impacts on groundwater resources in Eastern Canada. *Canadian Water Resources Journal*, *44*(1), 22–41. https://doi.org/10.1080/07011784.2018.1503066

Lavers, D. A., Ralph, F. M., Waliser, D. E., Gershunov, A., & Dettinger, M. D. (2015). Climate change intensification of horizontal water vapor transport in CMIP5. *Geophysical Research Letters*, *42*(13), 5617–5625. https://doi.org/10.1002/2015GL064672

Lazer, D., Kennedy, R., King, G., & Vespignani, A. (2014). The parable of google flu: Traps in big data analysis. *Science*, *343*(6176), 1203–1205. https://doi.org/10.1126/science.1248506

Loucks, D. P., & Beek, E. van. (2017). Water Resource Systems Planning and Management: An Introduction to Methods, Models, and Applications. In *Advances in Water Resources* (1st ed.). Springer Cham. https://doi.org/https://doi.org/10.1007/978-3-319-44234-1

Lund, J., Medellin-Azuara, J., Durand, J., & Stone, K. (2018). Lessons from California's 2012-2016 drought. *Journal of Water Resources Planning and Management*, *144*(10), 1–13. https://doi.org/10.1061/(ASCE)WR.1943-5452.0000984

MacEwan, D., Cayar, M., Taghavi, A., Mitchell, D., Hatchett, S., & Howitt, R. (2017). Hydroeconomic modeling of sustainable groundwater management. *Water Resources Research*, *53*(3), 2384–2403. https://doi.org/10.1002/2016WR019639

Majedi, H., Fathian, H., Nikbakht-shahbazi, A., Zohrabi, N., & Hassani, F. (2021). Multi-Objective Optimization of Integrated Surface and Groundwater Resources Under the Clean Development Mechanism. *Water Resources Management*, 2685–2704. https://doi.org/10.1007/s11269-021-02860-0

Mall, N. K., & Herman, J. D. (2019). Water shortage risks from perennial crop expansion in California's Central Valley. *Environmental Research Letters*, *14*(10). https://doi.org/10.1088/1748-9326/ab4035

Massoud, E. C., Purdy, A. J., Miro, M. E., & Famiglietti, J. S. (2018). Projecting groundwater storage changes in California's Central Valley. *Scientific Reports*, *8*(1), 1–9. https://doi.org/10.1038/s41598-018-31210-1

Meixner, T., Manning, A. H., Stonestrom, D. A., Allen, D. M., Ajami, H., Blasch, K. W., Brookfield, A. E., Castro, C. L., Clark, J. F., Gochis, D. J., Flint, A. L., Neff, K. L., Niraula, R., Rodell, M., Scanlon, B. R., Singha, K., & Walvoord, M. A. (2016). Implications of projected climate change for groundwater recharge in the western United States. *Journal of Hydrology*, *534*, 124–138. https://doi.org/10.1016/j.jhydrol.2015.12.027

Molina-Navarro, E., Bailey, R. T., Andersen, H. E., Thodsen, H., Nielsen, A., Park, S., Jensen, J. S., Jensen, J. B., & Trolle, D. (2019). Comparison of abstraction scenarios simulated by SWAT and SWAT-MODFLOW. *Hydrological Sciences Journal*, *64*(4), 434–454.

https://doi.org/10.1080/02626667.2019.1590583

Murray, K. D., & Lohman, R. B. (2018). Short-lived pause in Central California subsidence after heavy winter precipitation of 2017. *Science Advances*, *4*(8), 1–9. https://doi.org/10.1126/sciadv.aar8144

NASA. (2018). *SRTM 90m Digital Elevation Data from the CGIAR-CSI Consortium for Spatial Information*. http://srtm.csi.cgiar.org/

Nguyen, Q. (2023). *Bayesian Optimization in Action*. Manning.

Nouiri, I., Yitayew, M., Maßmann, J., & Tarhouni, J. (2015). Multi-objective Optimization Tool for Integrated Groundwater Management. *Water Resources Management*, *29*(14), 5353–5375. https://doi.org/10.1007/s11269-015-1122-8

Nourani, V., & Mousavi, S. (2016). Spatiotemporal groundwater level modeling using hybrid artificial intelligence-meshless method. *Journal of Hydrology*, *536*, 10–25. https://doi.org/10.1016/j.jhydrol.2016.02.030

Østergård, T., Jensen, R. L., & Maagaard, S. E. (2018). A comparison of six metamodeling techniques applied to building performance simulations. *Applied Energy*, *211*(August 2017), 89–103. https://doi.org/10.1016/j.apenergy.2017.10.102

Ouhamdouch, S., Bahir, M., Ouazar, D., Maria, P., & Kamel, C. (2019). Evaluation of climate change impact on groundwater from semi-arid environment (Essaouira Basin, Morocco) using integrated approaches. *Environmental Earth Sciences*, *78*(15), 1–14. https://doi.org/10.1007/s12665-019-8470-2

Pauloo, R. A., Escriva-Bou, A., Dahlke, H., Fencl, A., Guillon, H., & Fogg, G. E. (2020). Domestic well vulnerability to drought duration and unsustainable groundwater management in California's Central Valley. *Environmental Research Letters*, *15*(4). https://doi.org/10.1088/1748-9326/ab6f10

Pauloo, R., Escriva-Bou, A., Dahlke, H., Fencl, A., Guillon, H., & Fogg, G. (2020). Domestic well vulnerability to drought duration and unsustainable groundwater management in California's Central Valley. *Environmental Research Letters*. http://iopscience.iop.org/10.1088/1748-9326/ab6f10

Perrone, D., & Rohde, M. (2016). Benefits and economic costs of managed aquifer recharge in California. *San Francisco Estuary and Watershed Science*, *14*(2), 1–13. https://doi.org/10.15447/sfews.2016v14iss2art4

Pierce, D. W., Kalansky, J. F., & Cayan, D. R. (2018). *Climate, Drought, and Sea Level Rise Scenarios for California's Fourth Climate Change Assessment* (Issue CNRA-CEC-2018-006). https://www.energy.ca.gov/sites/default/files/2019-11/Projections_CCCA4-CEC-2018-006_ADA.pdf

Ratto, M., Castelletti, A., & Pagano, A. (2012). Emulation techniques for the reduction and sensitivity analysis of complex environmental models. *Environmental Modelling and Software*, *34*, 1–4. https://doi.org/10.1016/j.envsoft.2011.11.003

Ray, P. A., Bonzanigo, L., Wi, S., Yang, Y. C. E., Karki, P., García, L. E., Rodriguez, D. J., & Brown, C.

M. (2018). Multidimensional stress test for hydropower investments facing climate, geophysical and financial uncertainty. *Global Environmental Change*, *48*(December 2017), 168–181. https://doi.org/10.1016/j.gloenvcha.2017.11.013

Razavi, S., Tolson, B. A., & Burn, D. H. (2012). Review of surrogate modeling in water resources. *Water Resources Research*, *48*(7). https://doi.org/10.1029/2011WR011527

Read, J. S., Jia, X., Willard, J., Appling, A. P., Zwart, J. A., Oliver, S. K., Karpatne, A., Hansen, G. J. A., Hanson, P. C., Watkins, W., Steinbach, M., & Kumar, V. (2019). Process-Guided Deep Learning Predictions of Lake Water Temperature. *Water Resources Research*, *55*(11), 9173–9190. https://doi.org/10.1029/2019WR024922

Sabale, R., Venkatesh, B., & Jose, M. (2023). Sustainable water resource management through conjunctive use of groundwater and surface water: a review. *Innovative Infrastructure Solutions*, *8*(1), 1–12. https://doi.org/10.1007/s41062-022-00992-9

Safavi, H. R., Darzi, F., & Mariño, M. A. (2010). Simulation-Optimization Modeling of Conjunctive Use of Surface Water and Groundwater. *Water Resour Manage*, *24*, 1965–1988. https://doi.org/10.1007/s11269-009-9533-z

Sahoo, S., Russo, T. A., Elliot, J., & Foster, I. (2017). Machine learning algorithms for modeling groundwater level changes in agricultural regions of the U.S. *Journal of the American Water Resources Association*, *53*(5). https://doi.org/10.1002/2016WR019933

Sepahvand, R., Safavi, H. R., & Rezaei, F. (2019). Multi-Objective Planning for Conjunctive Use of Surface and Ground Water Resources Using Genetic Programming. *Water Resources Management*, *33*(6), 2123–2137. https://doi.org/10.1007/s11269-019-02229-4

Shen, C. (2018). A Transdisciplinary Review of Deep Learning Research and Its Relevance for Water Resources Scientists. *Water Resources Research*, *54*(11), 8558–8593. https://doi.org/10.1029/2018WR022643

Shi, H., Xu, M., & Li, R. (2018). Deep Learning for Household Load Forecasting—A Novel Pooling Deep RNN. *IEEE Transactions on Smart Grid*, *9*(5), 5271–5280. https://doi.org/10.1109/TSG.2017.2686012

Shiklomanov's, I. (1993). World fresh water resources. In P. H. Gleick (Ed.), *Water in crisis: A Guide to the World's Fresh Water Resources*. Oxford University Press.

Simpson, T., Toropov, V., Balabanov, V., & Viana, F. (2008). Design and Analysis of Computer Experiments in Multidisciplinary Design Optimization: A Review of How Far We Have Come - Or Not. In *12th AIAA/ISSMO Multidisciplinary Analysis and Optimization Conference*. American Institute of Aeronautics and Astronautics (AIAA). https://doi.org/https://doi.org/10.2514/6.2008-5802

Smerdon, B. D. (2017). A synopsis of climate change effects on groundwater recharge. *Journal of Hydrology*, *555*, 125–128. https://doi.org/10.1016/j.jhydrol.2017.09.047

Struye, J., & Latré, S. (2020). Hierarchical temporal memory and recurrent neural networks for time series prediction: An empirical validation and reduction to multilayer perceptrons. *Neurocomputing*, *396*, 291–301.

https://doi.org/https://doi.org/10.1016/j.neucom.2018.09.098

Taylor, R. G. (2013). Ground water and climate change. *Nature Climate Change*, *3*(November 2012). https://doi.org/10.1038/NCLIMATE1744

Tracy, J., Chang, W., St George Freeman, S., Brown, C., Palma Nava, A., & Ray, P. (2022). Enabling dynamic emulation of high-dimensional model outputs: Demonstration for Mexico City groundwater management. *Environmental Modelling and Software*, *147*(October 2021), 105238. https://doi.org/10.1016/j.envsoft.2021.105238

Tran, H., Leonarduzzi, E., De la Fuente, L., Hull, R. B., Bansal, V., Chennault, C., Gentine, P., Melchior, P., Condon, L. E., & Maxwell, R. M. (2021). Development of a deep learning emulator for a distributed groundwater–surface water model: Parflow-ml. *Water (Switzerland)*, *13*(23). https://doi.org/10.3390/w13233393

Tulare County. (2021). *Tulare county crop and livestock report*. https://agcomm.co.tulare.ca.us/pest-exclusion-standardization/crop-reports1/crop-reports-2021-2030/crop-and-livestock-report-2021/

United Nations. (2022). *UN*. https://www.un.org/en/global-issues/population

USGS. (2018). *USGS*. Where Is Earth's Water? https://www.usgs.gov/special-topics/water-science-school/science/where-earths-water

USGS. (2019). *MODFLOW and Related Programs*. https://www.usgs.gov/mission-areas/water-resources/science/modflow-and-related-programs

Weber de Melo, W., da Silva Pinho, J., & Iglesias, I. (2022). Emulating the estuarine morphology evolution using a deep convolutional neural network emulator based on hydrodynamic results of a numerical model. *Journal of Hydroinformatics*, *00*(0), 1–15. https://doi.org/10.2166/hydro.2022.068

Wunsch, A., Liesch, T., & Broda, S. (2020). Groundwater Level Forecasting with Artificial Neural Networks: A Comparison of LSTM, CNN and NARX. *Hydrology and Earth System Sciences Discussions*, 1–23. https://doi.org/10.5194/hess-2020-552

Yu, X., Cui, T., Sreekanth, J., Mangeon, S., Doble, R., Xin, P., Rassam, D., & Gilfedder, M. (2020). Deep learning emulators for groundwater contaminant transport modelling. *Journal of Hydrology*, *590*(July), 125351. https://doi.org/10.1016/j.jhydrol.2020.125351

Zeff, H. B., Hamilton, A. L., Malek, K., Herman, J. D., Cohen, J. S., Medellin-Azuara, J., Reed, P. M., & Characklis, G. W. (2021). California's food-energy-water system: An open source simulation model of adaptive surface and groundwater management in the Central Valley. *Environmental Modelling and Software*, *141*(April), 105052. https://doi.org/10.1016/j.envsoft.2021.105052

Zhang, C., Gao, L., Li, X., Shen, W., Zhou, J., & Tan, K. C. (2022). Resetting Weight Vectors in MOEA/D for Multiobjective Optimization Problems with Discontinuous Pareto Front. *IEEE Transactions on Cybernetics*, *52*(9), 9770–9783. https://doi.org/10.1109/TCYB.2021.3062949

Zhang, J., Zhu, Y., Zhang, X., Ye, M., & Yang, J. (2018). Developing a Long Short-Term Memory

(LSTM) based model for predicting water table depth in agricultural areas. *Journal of Hydrology*, *561*(January), 918–929. https://doi.org/10.1016/j.jhydrol.2018.04.065

Chapter 3 Climate change impacts on groundwater levels for irrigated agriculture in the greater Kern County region

Abstract

Understanding the complex interplay among climate, environment, and society is crucial for preserving ecosystems, communities, and production systems. While most studies focus on how climate change affects the visible elements of the water cycle (precipitation, streamflow, snowmelt, etc.), this research aims to improve our understanding of how the atmospheric water cycle and groundwater levels interact under changing climate conditions. This study assesses the hypothesis that groundwater levels in nine water districts of the Great Kern County Region (GKCR) will exhibit a more rapid decline under projected climate change scenarios compared to a historical climate resembling the period between 1995 and 2015. We are interested in the GKCR due to its history of groundwater overexploitation, linked to recent droughts, increased irrigated agriculture, and the region's ability to handle water shortages thanks to a complex water system. To test this hypothesis, we analyzed the climate projections from six Global Climate Models (GCMs) under two scenarios: the intermediate (RCP 4.5) and high (RCP 8.5) greenhouse gas and aerosol emissions. Using the water allocation model California Food-Energy-Water System (CALFEWS), we estimate surface water deliveries (SWD) to agriculture. Besides, we estimate agricultural water demands (AWD) considering adjustments for carbon dioxide (CO2) emissions. Also, we employed the Long Short-Term Memory Emulator (LSTME), developed in the preceding chapter, to effectively integrate direct and indirect climate change effects on groundwater levels within the studied water districts. Three scenario groups, Business as usual (BU), Influence of Climate Change in Two Dynamic Variables (IC2D), and Influence of Climate Change in Three Dynamic Variables (IC3D), are examined to test the research hypothesis. Findings indicate that groundwater levels will mainly decline unless agricultural water demand is reduced and/or recharge augmented. Moreover, results show that groundwater levels would experience a more rapid decline under climate change scenarios compared to historical conditions.

3.1 Introduction

Understanding the complex interplay among climate, environment, and society is crucial for preserving ecosystems, communities, and production systems. By thoroughly examining these interrelationships, it becomes possible to devise feasible and practical approaches to mitigate the potential negative consequences of climate change. However, merely understanding the climatic and hydrological processes is insufficient. Identifying the most effective ways to couple these processes (Schneider et al., 2022) and recognizing that the uncertainties associated with climate change can cloud those relationships are also necessary (Hallegatte et al., 2012).

While most studies focus on how climate change affects the visible elements of the water cycle (precipitation, streamflow, snowmelt, etc.) (Amanambu et al., 2020), this research aims to improve our understanding of how the atmospheric water cycle and groundwater levels interact under changing climate conditions. The limited number of studies examining the interrelations between climate change and groundwater levels can be attributed to three key factors. The first is the scarcity of groundwater information (Foster et al., 2020; Taylor, 2013). Second, since the

atmosphere and groundwater stand in extremes within the hydrological cycle, their interconnections are weakened or obscured by intermediate processes separating them (Cuthbert et al., 2019). These processes include snowmelt, surface runoff, river flow, infiltration, percolation, and aquifer-river interactions. Third, there are several operational challenges to integrating these processes because climate and groundwater models typically operate independently. Also, these models exhibit distinct spatial and temporal scales, possess differing information requirements, and generally are developed using dissimilar programming languages.

The absence of direct monitoring and analysis of climate effects on groundwater (Kurylyk & MacQuarrie, 2013) and the substantial reliance on groundwater for freshwater withdrawals (Taylor, 2013) have led to the misconception that groundwater is near limitless (Khair et al., 2019). However, heightened water demand, more frequent and prolonged droughts, advancements in pumping technology, and reduced energy costs associated with pumping have led to decreased aquifer levels worldwide (Closas & Rap, 2017; Perrone & Jasechko, 2019; Wada et al., 2010). Therefore, numerous scholars have emphasized that improving our understanding of the climate change effects on groundwater represents one of the main challenges in hydrology (Blöschl et al., 2019; Larocque et al., 2019; Meixner et al., 2016; Ouhamdouch et al., 2019).

This study assesses the hypothesis that groundwater levels in nine water districts of the Great Kern County Region (GKCR) will exhibit a more rapid decline under projected climate change scenarios compared to a historical climate resembling the period between 1995 and 2015. In this context, the term "groundwater level" refers to the potentiometric level of the uppermost confined aquifer. As previously defined in Chapter 2, the GKCR is in southern California's Central Valley. This region is marked by distinctive features, including notably low average precipitation and runoff levels, substantial evaporative demands, and a heavy dependence on groundwater for irrigation (Ghasemizade et al., 2019). Our interest in this region lies in its history of groundwater overexploitation, which can be attributed to the droughts over the past few decades (Jasperse & Pairis, 2020) and the expansion of irrigated agriculture, particularly permanent crops. The resilience of the GKCR region in mitigating water shortages hinges on an intricate water system comprising reservoirs, aquifers, canals, pipelines, pumping stations, irrigation districts, and urban aqueducts.

To test this hypothesis, we analyzed the climate projections from six Global Climate Models (GCMs) under two scenarios: the intermediate (RCP 4.5) and high (RCP 8.5) greenhouse gas and aerosol emissions (Moss et al., 2010). Using the water allocation model California Food-Energy-Water System (CALFEWS) (Zeff et al., 2021), we estimate surface water deliveries (SWD) to agriculture. Besides, we estimate agricultural water demands (AWD) considering adjustments for carbon dioxide (CO2) emissions. Also, we employed the Long Short-Term Memory Emulator (LSTME), developed in the preceding chapter, to effectively integrate direct and indirect climate change effects on groundwater levels within the studied water districts. Three scenario groups, Business as usual (BU), Influence of Climate Change in Two Dynamic Variables (IC2D), and Influence of Climate Change in Three Dynamic Variables (IC3D), are examined to test the research hypothesis. For these scenarios, the climate change effects are gradually included. For the BU scenario, precipitation (*P*), surface water deliveries (*SWD*), and agricultural water demands (*AWD*) - retain their 1995-2015 historical patterns. In the IC2D scenario, climate change impacts are incorporated into *P* and *SWD*. In contrast, in the IC3D scenario, climate change influences all three variables (*P*, *SWD*, and *AWD*). We test the hypothesis on the influence of climate on groundwater levels in nine water districts of the Great Kern County Region (GKCR) defined in Chapter 2.

This chapter is organized as follows. Section two presents the theoretical foundation for the study. Section three provides an overview of the study area, followed by section four, which outlines the modeling scenarios and the techniques used to estimate dynamic variables essential for the emulator. In section five, we examine the behavior of input and output dynamic variables to identify potential impacts of climate change on groundwater. Lastly, section six summarizes the key findings derived from this research.

3.2 Theoretical framework

3.2.1 Climate change impacts on groundwater

It is crucial to incorporate various elements of the hydrological cycle to enhance our understanding of the impacts of climate change on groundwater resources. However, this endeavor faces challenges due to scarce observational and measuring data on groundwater processes (Green, 2016), leading to the use of groundwater models to infer the aquifers' behavior. Hence, the challenges of investigating the influence of climate on groundwater are more formidable compared to examining surface water resources. As a result, many studies prioritize assessing the impacts of climate on surface water resources (Amanambu et al., 2020), leading to research gaps.

The impacts of climate change on the groundwater system can be direct or indirect. Direct effects refer to the immediate consequences of climate change on recharge, discharge, storage, flow, water quality, and subsidence, among others (Amanambu et al., 2020; Murray & Lohman, 2018). The indirect impacts arise through a series of interconnected processes affecting the groundwater system. The indirect effects include changes in land use, surface water, water demand, saltwater intrusion, and vegetation (Amanambu et al., 2020; Taylor, 2013). Although climate change's direct and indirect impacts on the groundwater system are not yet fully understood (Amanambu et al., 2020), some researchers suggest that indirect effects may have more significant consequences than direct ones (Taylor, 2013). This research incorporated precipitation to evaluate the direct impacts of climate change projections on the groundwater system. At the same time, surface water deliveries to agriculture and agricultural water demand were considered to simulate indirect effects.

3.2.2 Climate models

A Global Climate Model, or General Circulation Model (GCM), is a mathematical representation of the Earth's climate capable of simulating physical processes in the atmosphere, ocean, land surface, and cryosphere (IPCC, 2014). These models are supported by physics, chemistry, thermodynamics, and fluid dynamics to describe the conservation principles of mass, energy, and momentum (Kashinath et al., 2021). GCMs divide the Earth into a three-dimensional grid, for which mathematical equations are solved for each element and time step (NOAA, 2022). Typically, GCMs use a horizontal resolution ranging from 250 to 600 km, a vertical resolution of 1 km, and a temporal resolution of 30 minutes. GCMs usually employ between 10 and 20 layers to represent the atmosphere and about 30 layers for the ocean (Curry, 2017; IPCC, 2022). GCMs help comprehend past and current climate conditions and estimate future climate scenarios to assess the potential adverse effects of climate change and create policies to lessen them (Cubasch et al., 2013).

The climate modeling community has developed a set of standardized emission scenarios called Representative Concentration Pathways (RCPs) to consider the effect of greenhouse gases (GHG), aerosols, active chemical gases, and land/use cover on climate (van Vuuren et al., 2011). The term "representative concentration" indicates that each RCP represents just one among numerous possible scenarios that could lead to a particular radiative forcing level (Moss et al., 2010). At the same time, the term "pathway" signifies that the trajectory taken to attain the final concentration is equally significant as the GHG concentrations (Moss et al., 2010). For example, an RCP 8.5 refers to a scenario in which radiative forcing will be at least 8.5 W/m^2 by 2100. In sum, GCMs allow climate simulation at different emission levels, while the RCPs offer a standardized way of referring to those emission scenarios.

When utilizing GCMs for impact studies in specific regions, it is crucial to account for both the spatial resolution and the presence of systematic errors, referred to as biases (D. Pierce et al., 2016). These biases reflect the tendency of GCMs to either underestimate or overestimate specific climatic phenomena (D. Pierce et al., 2016). Corrections and adjustments, known as downscaling, are implemented to enhance GCMs' spatial resolution and minimize their biases. Downscaling techniques can be either dynamic or statistical. In dynamic downscaling, results from a GCM are used like boundary conditions to feed a Regional Climate Model (RCM) to get higher spatial resolution results (Murphy, 1999; Rummukainen, 2010). On the other hand, statistical downscaling refers to using statistical models that capture the relationship between the coarse-resolution predictors derived from a GCM and the fine-scale predictors from historical observations (Walton et al., 2020).

We selected six GCMs from the Climate Model Intercomparison Project version 5 (CMIP5) based on their ability to represent California's climate accurately, according to Pierce et al. (2018). The analyzed models were: CanESM2, CCSM4, CNRM-CM5, HadGCM2-CC, HadGCM2-ES, and MIROC5 (see Table 3-1). We analyzed them under two scenarios: the intermediate greenhouse gas and aerosol emissions (RCP 4.5) and the higher greenhouse gas and aerosol emissions (RCP 8.5). The downscaled and bias-corrected models were downloaded from the California Climate Adaptation Planning Tool (Cal-Adapt) web page (*Cal-Adapt*, 2022). For Cal-Adapt data, the bias correction process aims to prevent false or unrealistic changes in the original climate change signal predicted by GCMs (Pierce et al., 2018). In contrast, the original coarse resolution (about 150 km, 93 miles) is transformed to a finer resolution (about 6 km, or 3.7 miles) using a statistical downscaling method known as Localized Constructed Analogs (LOCA) (D. Pierce et al., 2016).

Table 3-1. Global Climate Models analyzed in this research. Adapted from Pierce et al. (2018).

Model	Model institution	Description
CanESM2	Canadian Centre for Climate Modeling and Analysis. Canada	Average model
CCSM4	National Center for Atmospheric Research. United States	
CNRM-CM5	Centre National de Recherches Meteorologiques / Centre Europeen de Recherche et Formation Avancees en Calcul Scientifique. France	Cool/wet model
HadGCM2-CC	Met Office Hadley Centre. United Kingdom	
HadGCM2-ES	Met Office Hadley Centre. United Kingdom	Warm/dry model
MIROC5	Atmosphere and Ocean Research Institute (The University of Tokyo), National Institute for Environmental Studies, and Japan Agency for Marine-Earth Science and Technology. Japan	Most unlikely model compared to CanESM2, CNRM-CM5, and HadGCM2-ES

3.2.3 Groundwater models

Groundwater hydrology in California's Central Valley has been simulated using models like the Central Valley Hydrologic Model (CVHM) (Faunt, 2009) or the California Central Valley Groundwater–Surface Water Simulation Model (C2VSim) (Brush & Dogrul, 2016). Such models estimate variables that are difficult to measure, like lateral and vertical flows, exchanges between aquifers and surface water bodies (rivers, lakes, reservoirs), and groundwater pumping. To simulate the possible effects of climate change on the GKCR, we decided to use the fine grid version of C2Vsim (C2VSimFG) (DWR, 2020). However, to enhance the integration of C2VSimFG with other models and to minimize computational time, we employed the LSTM emulator (LSTME) developed in the preceding chapter. LSTME focuses on simulating the changes in depth to groundwater (ΔGWD) for the uppermost confined aquifer of the GKCR because that aquifer feeds about 80% of the wells in the study region (see Chapter 2). Besides, LSTME depends on static and dynamic variables to capture spatial patterns and temporal dependencies. The static variables encompass average characteristics of water districts, including geometric features and soil and aquifer properties. Dynamic variables enable the model to account for changes over time. Static and dynamic variables are summarized in Table 3-2. For more details about static and dynamic variables, see section 2.4 of Chapter 2.

Table 3-2. Long Short-Term Memory Emulator (LSTME) input variables. For more details, see Table 2-1in Chapter 2.

Category		Input variables
Static Variables	geometric features	Surface area and ground surface slope
	Soil Properties	field capacity, saturated hydraulic conductivity, and total porosity
	Aquifer properties	Hydraulic conductivity, aquifer vertical hydraulic conductivity, specific yield, and specific storage
Dynamic variables		Precipitation (P), surface water deliveries to agriculture (SWD), and agricultural water demands (AWD)

3.2.4 Surface water allocation models

We employ a water allocation model to estimate surface water deliveries to agriculture under different projected climate scenarios. A water allocation model takes into account various factors, including the water availability (measured by indicators like precipitation, reservoir storage, and snowpack), the demands of agriculture and urban areas, the hydraulic infrastructure used to distribute water, and factors such as environmental flow needs, the hierarchy of water rights, and operational regulations (CWEMF, 2021). Some examples of water allocation models are the California Value Integrated Network (CALVIN) (Draper et al., 2003), the California Water Resources Simulation Model (CalSim) (Draper et al., 2004), the Water Evaluation and Planning (WEAP) model (Forni et al., 2016; Yates et al., 2005), and the California Food-Energy-Water System (CALFEWS) (Zeff et al., 2021). Each of these models is briefly described below.

CALVIN is a comprehensive hydro-economic optimization model of California's water system (Null, 2016). Draper et al. (2003) state that CALVIN allocates surface and groundwater resources to meet urban and agricultural water demand by maximizing the economic values derived from urban and agricultural water usage throughout the state, considering environmental, physical, and carefully chosen policy constraints. CalSim, developed by the California Department of Water Resources (DWR), is a simulation model designed to assess operation alternatives for both the Central Valley Project (CVP) and the California State Water Project (SWP). This comprehensive model includes the management of reservoirs, streams, aqueducts, and water exports to southern California (Jayasundara et al., 2020). The Stockholm Environment Institute developed WEAP for long-term scenario planning and water policy analysis. The WEAP application designed for the Sacramento Valley water system has several key components like reservoirs, alluvial aquifers, rivers, trans-basin diversion from the Trinity River, major irrigation canals, and water demand centers for municipal, agricultural, and industrial uses (Joyce et al., 2005). Finally, CALFEWS, created by Zeff et al. (2021), integrates water storage and conveyance networks, connecting the operations of irrigation districts with the CVP and SWP. This model incorporates a set of decision rules based on the historical regulatory conditions, hydrological data, and system infrastructure. CALFEWS input variables are snowpack, flow, and service area water demands.

3.3 Model application area

This study concentrates on nine water districts of the Great Kern County Region (GKCR). The GKCR is situated south of California's Central Valley and includes water districts spanning Kern and Tulare counties. Figure 3-1 illustrates the nine water districts under examination in this chapter, and Table 3-3 provides information about the major crop groups in each water district and the total irrigated area by district. Crops listed in that table are the ones that cover more than 5% of the district's irrigated area. Whereas four aquifers supply agricultural wells in the GKCR (comprising one unconfined aquifer and three confined aquifers), this research specifically targeted the uppermost confined aquifer because it supplies approximately 80% of the agricultural wells in the region (see section 2.3.1 of the preceding chapter). The GKCR was selected because the groundwater contribution to agriculture is significant, especially during dry years. In the Central Valley of California, groundwater provides approximately 30% of the water demand during average years, 40% during dry years, and 60% during drought years (Perrone & Rohde, 2016). The additional groundwater extractions during dry and drought years have led to aquifers overexploitation, threatening future reserves and water supply infrastructure due to subsidence (Murray & Lohman, 2018).

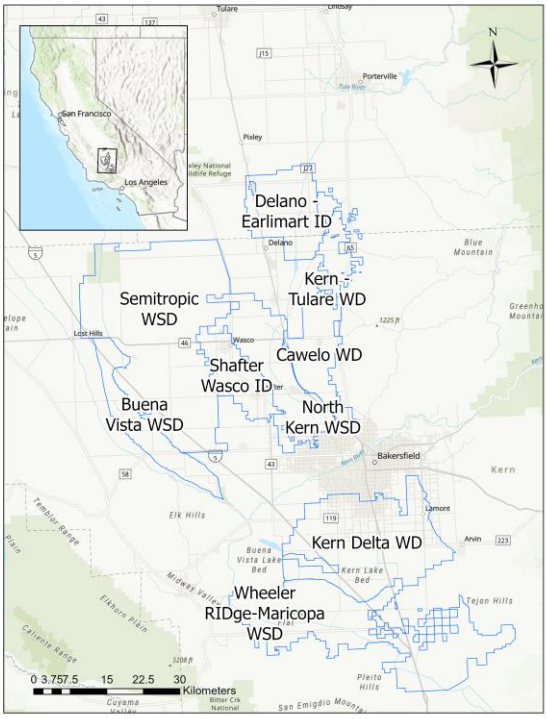

Figure 3-1. Study area. The impact of climate change on groundwater levels in the uppermost confined aquifer is evaluated in nine water districts.

Table 3-3. Major crop groups and irrigated areas by water district. Reference 1: 2021 database from Kern County Department of Agriculture and Measurement Standards (2015). Reference 2: Delano Earlimart Irrigation District GSA (2022). Reference 3: Kern-Tulare Water District (2022)

Water District	Major crops groups	Total irrigated area (hectares)	Reference
Semitropic WSD	Almonds and pistachios, grains, corn, alfalfa	60,249	1
Wheeler Ridge Maricopa WSD	Vineyard, almonds and pistachios, subtropical, other truck	46,007	1
Kern Delta WD	Grains, almonds and pistachios, corn, alfalfa, other truck	52,672	1
Cawelo WD	Almonds and pistachios, subtropical, vineyard	15,196	1
Shafter Wasco ID	Almonds and pistachios, vineyard, other deciduous	12,456	1
Buena Vista WSD	Almonds and pistachios, cotton, vineyard, grains, alfalfa, other deciduous, corn	15,814	1
North Kern WSD	Almonds and pistachios, other truck, vineyard, potatoes	25,327	1
Delano Earlimart ID	Vineyard, pistachios, almonds, citrus, and various tree fruit	22,396	2
Kern - Tulare WD	Almonds and pistachios, oranges, vineyard.	6,677	3

3.4 Modeling future climate change impacts on Groundwater

Three scenario groups were examined to assess the indirect effects of climate change on groundwater in the GKCR from 2015 to 2099. These scenarios cover different behaviors of the dynamic variables that feed the LSTME model (Table 3-2). The three groups are Business as usual (BU), Influence of Climate Change in Two Dynamic Variables (IC2D), and Influence of Climate Change in Three Dynamic Variables (IC3D). The BU groups one thousand scenarios, whereas the IC2D and IC3D group 12 scenarios each, corresponding to the possible combinations between six GCMs and the two RCPs (Table 3-4).

Table 3-4. Analyzed scenarios for the dynamic input variables

Scenario group	Number of scenarios	Precipitation (P)	Surface Water Deliveries (SWD)	Agriculture Water Demand (AWD)
Business as usual (BU)	1,000	Variables generated by the univariate seasonal, lag-one, autoregressive model proposed by Fiering & Jackson (1971)		
Influence of Climate Change in Two Dynamic Variables (IC2D)	12	Six GCMs under two RCPs (4.5 and 8.5) downloaded from Cal-Adapt	Projected by CALFEWS considering six GCMs under two RCP (4.5 and 8.5)	Monthly median values from 1995 to 2015
Influence of Climate Change in Three Dynamic Variables (IC3D)	12	Six GCMs under two RCPs (4.5 and 8.5) downloaded from Cal-Adapt	Projected by CALFEWS considering six GCMs under two RCP (4.5 and 8.5)	Function of the reference evapotranspiration (ET_o) adjusted by the effect of carbon dioxide

BU is the reference scenario against which the other two groups' results are compared. Through BU, we aim to mimic the aquifer's behavior as if P, SWD, and AWD followed a similar trajectory to the historical data between 1974 and 2015. BU scenarios were created as described in section 3.4.1. The IC2D scenario considers climate change's impact in only two variables: P and SWD. For AWD, we use the monthly median values from 1995 to 2015. We use the median instead of the mean because the first is less affected by data asymmetry and outliers (Loucks & van Beek, 2017). For the IC3D scenario group, all variables consider climate change. Also, for the IC2D and IC3D categories, precipitation data (*P*) was downloaded from the Cal-Adapt site, and the SWD values were calculated by CALFEWS (Zeff et al., 2021). Additionally, for the IC3D scenario group, agricultural demand (AWD) was estimated as a function of the reference evapotranspiration (*ETo*) adjusted by the effect of carbon dioxide (CO2) (see section 3.4.3). In summary, the BU scenario group assumes no climate change, whereas the IC3D scenario group is highly influenced by climate change. Table 3-2 shows the static and dynamic variables that feed the LSTME model under the IC3D scenario group.

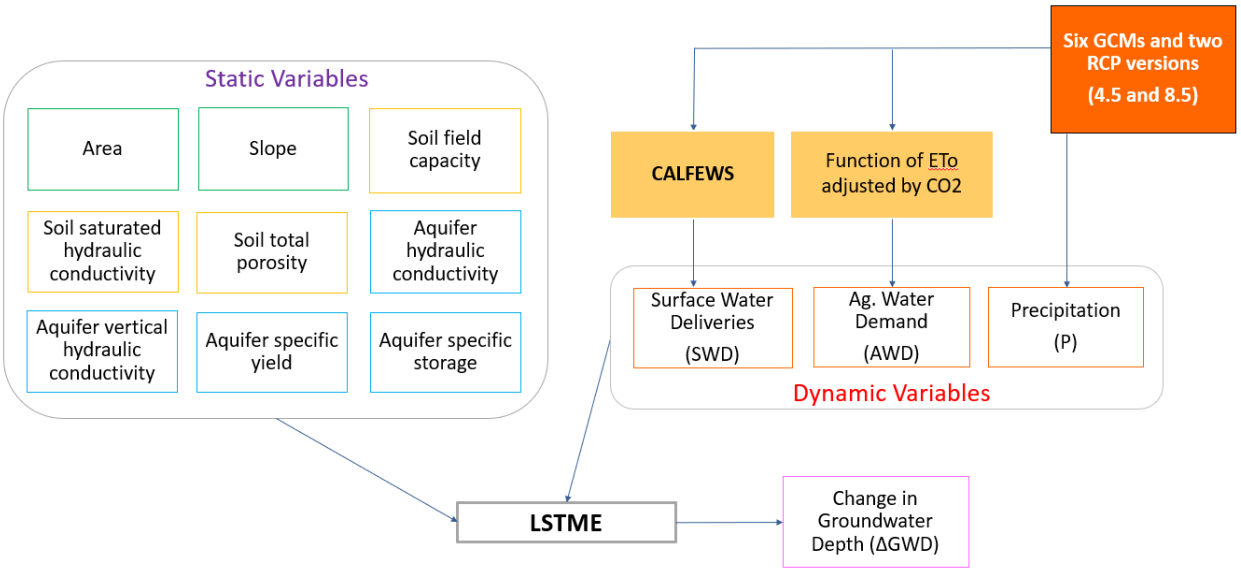

Figure 3-2. Hydroclimatic coupling considering Influence of Climate Change in Three Dynamic Variables (IC3D)

To determine the depth to groundwater ($GWD_{g,t}$) of the uppermost confined aquifer in irrigation district g for a given month (t), we employ the Long Short-Term Memory network (LSTME), which provides the change in depth to groundwater ($\Delta GWD_{g,t}$) or what is the same the difference between the depths to groundwater at month t and the previous month (t-1) (Equation 3-1). Expanding this equation back to the initial time (t=0), we derive Equation 3-2. In essence, the depth to groundwater for irrigation district g at time t depends on the initial groundwater level ($GWD_{g,0}$) in September 2015 and the cumulative changes in depth to groundwater up to the specified month t.

$$GWD_{g,t} = GWD_{g,t-1} + \Delta GWD_{g,t} \qquad \text{Equation 3-1}$$

$$GWD_{g,t} = GWD_{g,0} + \sum_{i=1}^{t} \Delta GWD_{g,i} \qquad \text{Equation 3-2}$$

3.4.1 Synthetic time series for the BU scenario

We generated synthetic time series data for the BU scenario group by applying the univariate seasonal, lag-one, autoregressive model proposed by Fiering & Jackson (1971), an extension of the famous Thomas-Fiering model. Although the Thomas-Fiering model was initially designed as an annual autoregressive Markov model (Diaz-Granados, 2023), we have employed the Fiering &

Jackson model because it can generate monthly data, its use is extensive, and it preserves the mean, variance, skewness, and lag-one correlation coefficient of the original data (Bras & Rodriguez-Iturbe, 1993). For the Fiering & Jackson model, synthetic values can be generated through Equation 3-3, where $X_{t,j}$ represents the value of the random process (P, SWD, or AWD) at year *t* and season *j*. The parameters m_j, σ_j, and γ_j denote the mean, standard deviation, and skewness at season *j*. Besides, ρ_j is the lag-one correlation coefficient between seasons *j* and *j-1*. Equation 3-3 incorporates a random number $\varepsilon_{t,j}$, following a gamma distribution to prevent negative values' generation. According to Equation 3-4, it is possible to generate gamma distributed numbers as a function of the independent normal variable $W_{t,j}$ (with mean zero and variance one) and the adjusted skewness $\gamma_{\varepsilon,j}$ (Equation 3-5).

$$X_{t,j} = m_j + \rho_j * \frac{\sigma_j}{\sigma_{j-1}} * \left(X_{t,j-1} - m_{j-1}\right) + \sigma_j * \varepsilon_{t,j} * \left(1 - \rho_j^2\right)^{1/2} \quad \text{Equation 3-3}$$

$$\varepsilon_{t,j} = \frac{2}{\gamma_{\varepsilon,j}} * \left(1 + \frac{\gamma_{\varepsilon,j} * W_{t,j}}{6} - \frac{\gamma_{\varepsilon,j}^2}{36}\right)^3 - \frac{2}{\gamma_{\varepsilon,j}} \quad \text{Equation 3-4}$$

$$\gamma_{\varepsilon,j} = \frac{\left(\gamma_j - \rho_{j-1}^3 * \gamma_{j-1}\right)}{\left(1 - \rho_j^2\right)^{1.5}} \quad \text{Equation 3-5}$$

3.4.2 Surface Water Deliveries for IC2D and IC3D scenario groups

Before using the water deliveries projected by CALFEWS from 2016 to 2099, we compared the water deliveries generated by CALFEWS and those from C2VSimFG for the historical timeframe from 1974 to 2015. This evaluation was necessary because the LSTME model was trained using historical data from C2VSimFG. After comparing the two models, we found that SWDs from the two models differed in magnitudes. To address this discrepancy, we normalized CALFEWS output so that its mean was one and its deviation zero. Later, we incorporated the mean and standard deviation values of the historical C2VSimFG data, as shown in Equation 3-6. In this equation, subscripts *1* and *2* refer to the C2VSimFG and CALFEWS models, respectively, while the "*hist*" subscript refers to the historical period. $SWD_{2,\,adj}$ represents the adjusted SWDs ready to be used in the emulator, whereas SWD_2 are the original values generated by CALFEWS. Finally, $\overline{SWD_{i,hist}}$ and $SSWD_{i,hist}$ (for *i=[1, 2]*) represent the means and standard deviations of the two models during the historical period, respectively.

$$SWD_{2,adj} = \frac{SSWD_{1,hist}}{SSWD_{2,hist}} * \left(SWD_2 - \overline{SWD_{2,hist}}\right) + \overline{SWD_{1,hist}} \quad \text{Equation 3-6}$$

3.4.3 Agriculture Water Demand for IC3D scenario group

The Agricultural Water Demand (AWD), called in C2VSimFG Agricultural Supply Requirement (ASR), indicates the amount of water farmers need to provide to the soil to reach irrigation demands (DWR, 2020), enabling optimal plant growth and productivity (Wallace, 2000). AWD contributes to plant tissue formation and satisfies evaporation, transpiration, return flow, and percolation demands (Dogrul and Kadir, 2020). These crop water demands can be classified as recoverable and non-recoverable losses. Recoverable losses include return flow (RF) and percolation (PC). Non-recoverable losses, also known as Consumptive Use of Applied Water (CUAW), refer to water that cannot be reused in the same area from which it was extracted (OpenET, 2023; Shaffer and Runkle, 2007). CUAW includes Water in Plant Tissues (WPT) and evapotranspiration (ET) (Cooley, 2015). However, CUAW is generally set equal to ET because, during the growing season, WPT is typically much lower than ET (Bhatt and Hossain, 2019).

For a time step *t*, AWD can be expressed as the sum of return flow (*RF*), percolation (*PC*), and *ET*, where the subscript *i* refers to the crops in the study area (Equation 3-7). In Equation 3-8, the volume of *ET* depends on the crop area (*A*), the water stress coefficient (*Ks*), the crop coefficient (*Kc*), and the reference evapotranspiration (*ETo*). These terms represent the climatic factors, crop characteristics, and agricultural practices that affect ET (Allen et al., 1998). By replacing Equation 3-8 in Equation 3-7, we get Equation 3-9, where *RFT* and *PCT* represent the return flow and percolation of all crops in the study area. After regrouping some terms, Equation 3-9 can be written as shown in Equation 3-10, where $\beta 0_t$ groups recoverable losses and $\beta 1_t$ the factors that transform ET_o into *ET*. Note that all terms in Equation 3-10 change over time, so this equation does not represent a linear regression.

Figure 3-3 illustrates box plots summarizing the R-squared values between *AWD* and ET_o adjusted by the carbon dioxide effect (ETo_{adj}), categorized by GCM and RCP. Box plots were generated considering information from the analyzed water districts. The medians of the box plots in Figure 3-3, represented by the center horizontal lines, exceed 0.84, indicating that ETo_{adj} generally accounts for over 84% of the *AWD* variance. Consequently, we substitute Equation 3-10 with Equation 3-11, where the coefficients $\widetilde{\beta 0}$ and $\widetilde{\beta 1}$ represent the intercept and slope of the linear models established for each water district, GCM, and RCP. By doing so, Equation 3-11 establishes a time-independent relationship between the agricultural water demand and reference evapotranspiration adjusted by the carbon dioxide effect (*AWD* and ETo_{adj}). In summary, our estimation of future *AWD* relies on the ETo_{adj} values between 2016 and 2099.

$$AWD_t = \sum_{i=1}^{n} \left(RF_{t,i} + PC_{t,i} + ET_{t,i} \right) \qquad \text{Equation 3-7}$$

$$ET_{t,i} = A_i * Ks_{t,i} * Kc_{t,i} * ETo_t \qquad \text{Equation 3-8}$$

$$AWD_t = RFT_t + PCT_t + ETo_t * \sum_{i=1}^{n} A_i * Ks_{t,i} * Kc_{t,i} \qquad \text{Equation 3-9}$$

$$AWD_t = \beta 0_t + \beta 1_t * ETo_t$$ Equation 3-10

$$AWD = \widetilde{\beta 0} + \widetilde{\beta 1} * ETo_{adj}$$ Equation 3-11

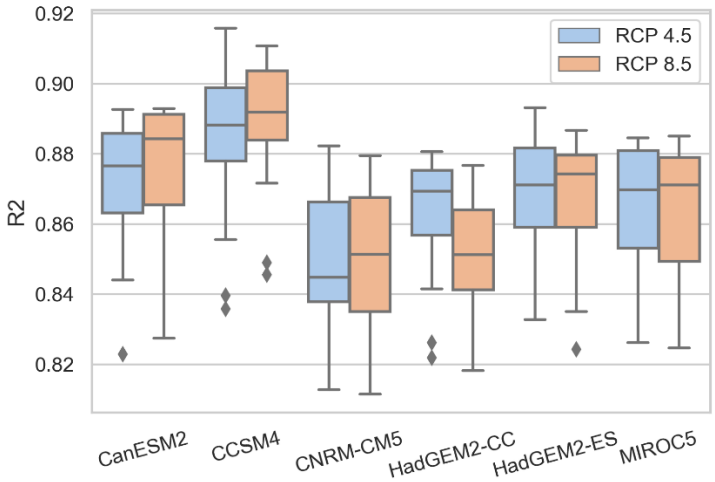

Figure 3-3. R-squared distribution for the variables Agricultural Water Demand (AWD) and Reference Evapotranspiration adjusted by CO2 ($ETo_{adj,t}$) for different Global Climate Models (GCMs) and Representative Concentration Pathways (RCPs).

Climate models without the *ETo* adjustment tend to overestimate *ETo* and provide contradictory results, like projecting dry climates with increased runoff (McEvoy et al., 2020; Yang et al., 2019). Thus the $ETo_{adj,}$ allows us to consider the effect of carbon dioxide (CO2) on vegetation water demand. Here, we consider the approach of Yang et al. (2019), which suggests that imposing a penalty on CO2 values greater than 300 ppm increases the vegetation surface resistance (*rs*), leading to decreased plant transpiration. Where *rs* encompasses the resistance of vapor to flow through stomata openings, total leaf area, and soil surface (Allen et al., 1998).

3.4.4 Comparison between scenarios without and with climate change

The Welch's t-test was used to determine if climate change significantly impacts groundwater levels. Welch's t-test, also known as the unpaired t-test, is commonly used in planned experiments to verify if altering the experimental conditions has a statistically significant impact on the outcome of a process (DeCoursey, 2003; Kanji, 2006). For instance, Lavers et al. (2015) applied Welch's t-test to investigate the similarity of global atmospheric water vapor changes between historical and future scenarios, analyzing data from 22 GCMs. With Welch's t-test, we wanted to

know if the null hypothesis that the depletion or replenishment rate (DRR) under the BU scenario is equal to that of the IC2D and IC3D scenarios at a significance level of 5%. We define DRR as the first derivative of depths to time or, what is the same, the change of depth to groundwater over time. Before applying Welch's t-test, we estimated each scenario group's average DRR from 2015 to 2099 in meters per year. Using the nonparametric Shapiro-Wilk test (Kottegoda & Rosso, 2008) at a significance level of 5%, we tested the normality of the DRRs as a prerequisite before running Welch's t-test.

3.5 Results and discussion

We summarize the intra and inter-annual behavior of the dynamic variables in two seasons and four periods, respectively. The seasons were irrigation (dry months) and non-irrigation (wet months). The time periods were Historical (HIST, 1974-2015), beginning of the century (BOC, 2016-2040), middle of the century (MOC, 2041-2070), and end of the century (EOC, 2071-2099). We set the irrigation period from March 1 to September 30 every year following Kadir (2017), although, for the Central Valley, this interval can be defined in alternative ways (Budd et al., 2009; Medellín-Azuara et al., 2015; Vahmani et al., 2022). The 2040 time horizon was established as the upper limit for the BOC period, given that critically over-drafted groundwater basins, such as those analyzed in this study, are required to achieve balance in recharge and extraction to comply with the California 2014 Sustainable Groundwater Management Act (SGMA) around that time. The remaining period (from 2040 to 2099) was split into two equal-duration categories, MOC and EOC.

Figure 3-4 illustrates the dynamic variables' behavior for the Semitropic Water District under historical records (green box) and two RCPs (blue for RCP 4.5 and orange for RCP 8.5) of the CNRM-CM5 global climate model for the IC3D scenario group. Regarding precipitation (Figure 3-4a), non-irrigation months consistently display higher precipitation than irrigation months. The left-hand side of Figure 3-4a shows no substantial change in precipitation across the four periods (HIST, BOC, MOC, and EOC). However, when comparing future projections to historical data, there is an increase in median precipitation during the non-irrigation season. However, there is no discernible trend from BOC to EOC for the two seasons. On the other hand, future surface water deliveries for agriculture during the irrigation season (left-hand side of Figure 3-4b) show an increase in median and lower dispersion concerning the historical period. During the non-irrigation season (right-hand side of Figure 3-4b), no consistent pattern was found in the median values, but variability increased for projected periods. The differences between historical and future values can be attributed to the normalization process outlined in Equation 3-6. This process encompasses the entire period from 1974 to 2015 without distinguishing between irrigation and non-irrigation seasons. Finally, the agricultural water demand for the irrigation and non-irrigation seasons (Figure 3-4c) exhibits a gradual increase over time (from HIST to EOC). This can be attributed to the fact that AWD was expressed as a function of the ETo_{adj} (Equation 3-11), and that variable is expected to increase over time (from 2015 to 2099) (McEvoy et al., 2020).

Similar patterns to those in Figure 3-4 are shown in Appendix B.1 for other water districts. First, precipitation variability during the non-irrigation months tends to be greater than or equal to historical values, whereas, during the irrigation season, it tends to be constant. Second, the most significant differences between historical and future scenarios were observed in the SWD values. While the historical values are based on records stored in C2VSimFG, the projected values were estimated by CALFEWS and later adjusted to maintain the mean and deviation of the historical values. Since it is difficult to predict a variable highly dependent on human decisions, such as SWD, using CALFEWS is a viable option. Finally, the agricultural water demand (AWD) tends to increase over time due to the projected increase in the reference evapotranspiration (ETo_{adj}).

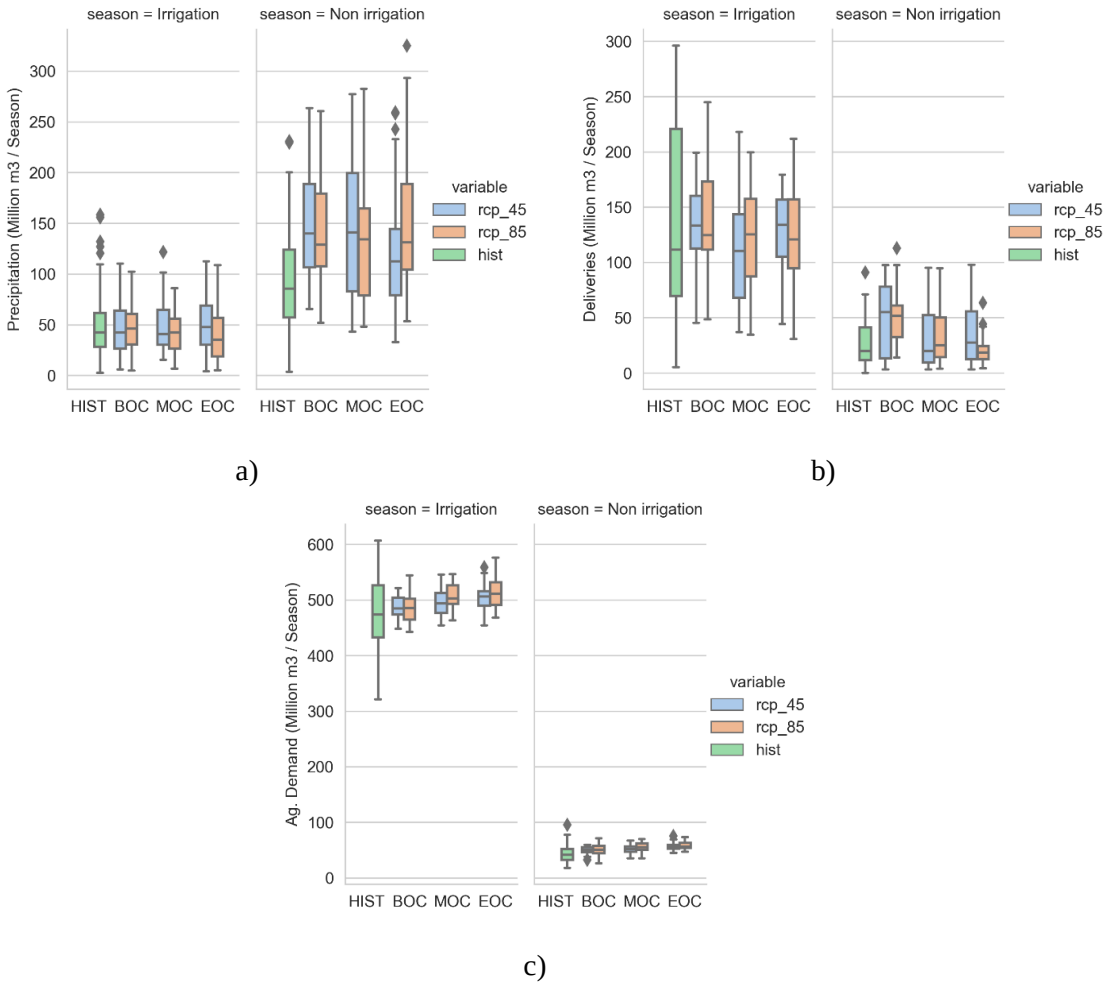

Figure 3-4. Seasonal distribution of precipitation (a), Surface Water Deliveries (b), and Agricultural Water Demand (c) in Semitropic Water District for the historical (green) and future climate considering the CNRM-CM5 GCM under two RCPs (Blue, 4.5; Orange, 8.5). The horizontal axis displays four temporal intervals: Historical (HIST, 1974-2015), beginning of the century (BOC, 2016-2040); middle of the century (MOC,2041-2070), end of the century (EOC, 2071-2099). The irrigation period runs from March 1 to September 30.

3.5.1 Future depths to groundwater

Figure 3-5 shows the projected depths to groundwater for selecting water districts (rows) over the two RCPs (columns). The vertical axis of these figures has been inverted to facilitate their interpretation. Each of the six figures (from a to f) contains the three scenario groups: BU (blue area), IC2D (green area), and IC3D (orange area). The shaded regions comprise the results of the scenarios analyzed for each scenario group (see Table 3-4). Thick lines in the middle of the shaded areas symbolize the median for each scenario group. In addition, each figure has three horizontal lines: measurable objective (MO, yellow), minimum threshold (MT, gray), and bottom of the uppermost confined aquifer (BL, brown). MO refers to the desired depth for 2040 that guarantees sustainable aquifer operation, while MT refers to the depth beyond which undesired results can occur in the groundwater basin (CDWR, 2017). The MO and MT values used in this research correspond to the averages of the projected values for the monitoring sites reported in the Groundwater Sustainability Plans (GSPs) related to each water district (Eastern Tule GSA, 2020; GEI Consultants Inc, 2019, 2020; MID-Kaweah GSA, 2022).

The first two rows of Figure 3-5 represent one of the two possible behaviors for the GWDs in the study area. The first row illustrates districts where the depths estimated by the BU scenario group are greater than those estimated by the other scenarios (IC2D and IC3D). This behavior was noted in eight districts: Semitropic WSD, Wheeler Ridge-Maricopa WSD, Kern Delta WD, Cawelo WD, Shafter Wasco ID, North Kern WSD, Delano-Earlimart ID, and Kern-Tulare WD. The second row of the exact figure exemplifies districts where the depths of the BU scenario fall within the range of depths estimated by the other scenarios as in Buena Vista WSD. The third row separately examines the Wheeler Ridge-Maricopa WSD district based on the aquifer recovery under the BU scenario. Similar images to those in Figure 3-5 are shown in 0 for the other districts.

Figure 3-5 demonstrates the LSTME's ability to replicate historical patterns. When historical data exhibits a downward trajectory, the LSTME foresees a decline in the BU scenario. Conversely, the model predicts an upturn in the BU scenario when historical data reflects an upward trend, as in Wheeler Ridge-Maricopa WSD for both RCPs (Figure 3-5 e and f). This congruence between the model's forecasts and historical trends in the BU scenario stems from the approach detailed in section 3.4.1, where input variables for the BU scenario were tailored to maintain the historical data's behavior. On the other hand, projected depths by the IC2D and IC3D scenarios decrease for all water districts, which mainly depend on the unique conditions within each district concerning AWD and SWD rather than precipitation, whose behavior is similar across districts. SWD plays a pivotal role in replenishing aquifers and consequently boosting groundwater levels. Conversely, the decline in groundwater levels is primarily linked to heightened agricultural water demand.

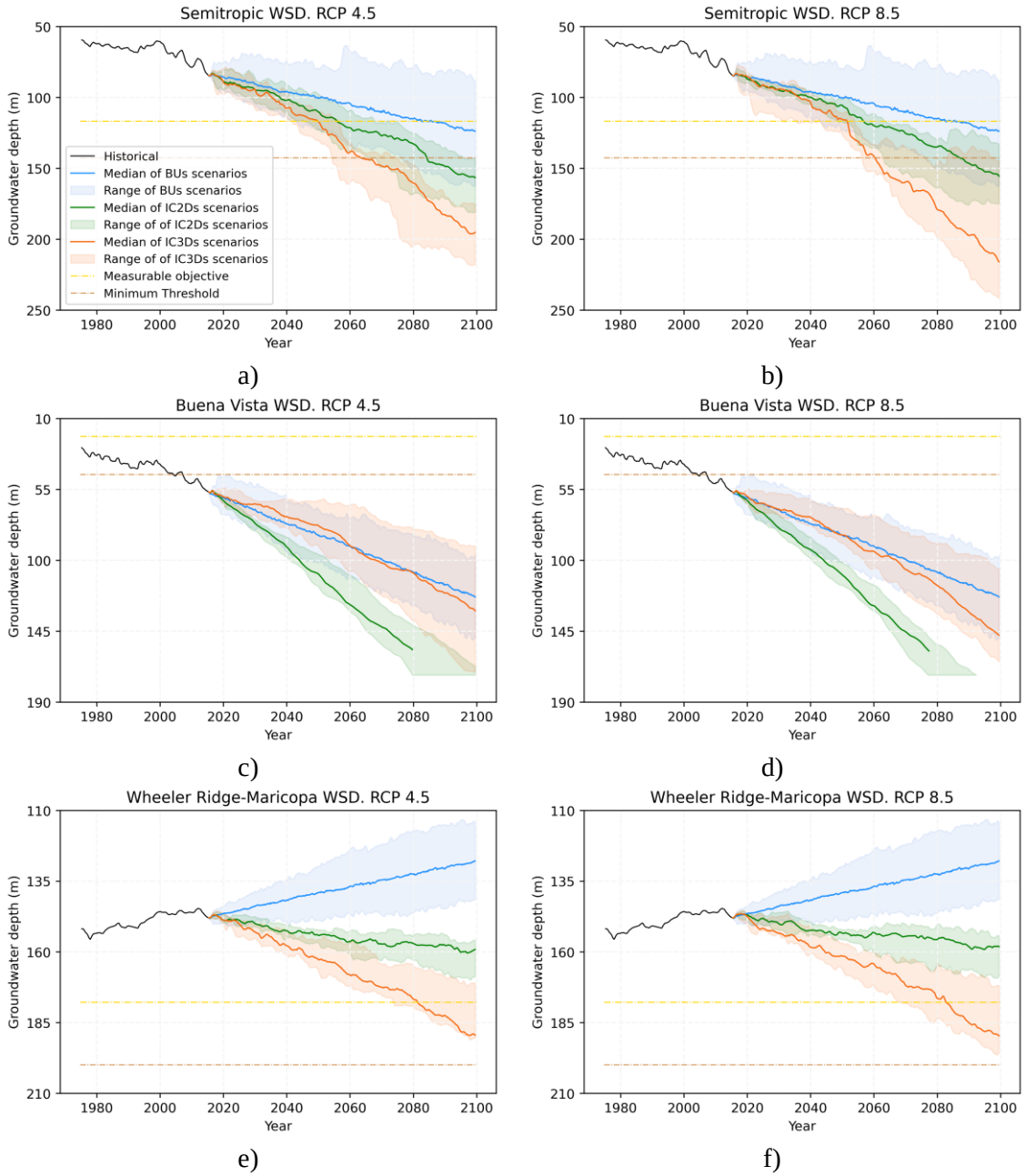

Figure 3-5. Depths to groundwater for different water districts and scenario groups of Precipitation, Agricultural Water Demand, and Surface Water Deliveries. The scenario groups are Business as Usual (BU, blue area), Influence of Climate Change in Two Dynamic Variables (IC2D, green area), and Influence of Climate Change in Three Dynamic Variables (IC3D, orange area). The thick lines in the middle of the shaded regions symbolize the median of the scenario group. The vertical axis has been inverted to facilitate interpretation.

3.5.2 Hypothesis testing

We used Welch's t-test to assess whether the depletion or replenishment rate (DRR) under the BU scenario is equivalent to that of the IC2D and IC3D scenarios at a 5% significance level. To do this, we first needed to confirm the normal distribution of the DRR data. This was achieved by conducting the Shapiro-Wilk test at a 5% significance level. The average DRR and p-values from the Shapiro-Wilk test are presented in Table 3-5 for each scenario group (BU, IC2D, and IC3D) and RCPs (4.5 and 8.5). Table 3-5, on the right-hand side, displays the results of these tests. Notably, all the p-values were greater than or equal to 0.05, suggesting we cannot reject the hypothesis that the populations follow a normal distribution. However, it's worth mentioning that some districts, like Kern Delta WD (IC3D at 8.5), Sharter Wasco ID (for IC2D and IC3D at 4.5), and Delano Earlimart (IC3D at 4.5), exhibited borderline results in the test.

Table 3-5. Groundwater depletion or recharge rate (DRR) and p-values for the Shapiro-Wilk's test for normality for each water district, scenario group (BU, IC2D, and IC3D), and RCP (4.5 and 8.5)

Water District	DRR (m/yr)					P-values				
	BU	RCP 4.5		RCP 8.5		BU	RCP 4.5		RCP 8.5	
		IC2D	IC3D	IC2D	IC3D		IC2D	IC3D	IC2D	IC3D
Semitropic WSD	0.49	0.96	1.43	0.88	1.57	0.94	0.36	0.8	0.8	0.39
Wheeler Ridge Maricopa WSD	-0.24	0.16	0.44	0.14	0.48	0.64	0.74	0.28	0.12	0.4
Kern Delta WD	0.5	2.25	2.07	2.31	2.3	0.21	0.58	0.64	0.15	0.06
Cawelo WD	0.77	1.14	1.31	1.09	1.39	0.37	0.56	0.34	0.64	0.14
Shafter Wasco ID	0.55	1.52	1.49	1.57	1.63	0.68	0.07	0.05	0.82	0.47
Buena Vista WSD	0.77	1.65	0.84	1.76	0.97	0.46	0.97	0.28	0.74	0.45
North Kern WSD	0.63	1.13	1.21	1.18	1.3	0.36	0.39	0.22	0.75	0.44
Delano Earlimart ID	0.98	1.64	1.78	1.72	1.97	0.43	0.58	0.05	0.8	0.59
Kern - Tulare WD	0.95	1.39	1.45	1.38	1.49	0.85	0.25	0.72	0.24	0.8

The depletion or replenishment rates for each scenario group (BU, IC2D, and IC3D) and RCP (4.5 and 8.5) from Table 3-5 are displayed in Figure 3-6. Positive values indicate depletion, whereas negative values mean replenishment (blue area). Figure 3-6a shows DRRs for the BU scenario group under historical conditions that do not consider projected climate change. In Figure 3-6a, the highest depletion rates are between 0.58 and 1.16 m/yr located in Buena Vista WSD, North Kern WSD, Cawelo WD, Kern – Tulare WD, and Delano – Earlimart ID. At the same time, the aquifer in the Wheeler Ridge-Maricopa WSD experiences recovery (Figure 3-6a and Table 3-5). Figure 3-6b to e show the DRRs for different combinations of scenario groups and RCPs, while the hatched areas indicate the rejection of the null hypothesis for Welch's t-test. For example, for Semitropic WSD, when comparing the BU and the IC3D scenario for RCP 8.5 (Figure 3-6 a and e), the district is hatched, indicating that the two scenario groups (BU and IC3D, RCP 8.5) are different for a significance level of 5%. Figure 3-6 b to e show that the null hypothesis is rejected in all cases except for both RCPs of the IC3D scenario group of Buena Vista WSD.

We assess the impact of the RCP on the DRR by comparing images within the same row in Figure 3-6. On the other hand, when comparing images by column, we investigate the influence of AWD because the distinction between the IC2D and IC3D scenarios arises from the different approaches used to estimate AWD, as outlined in Table 3-4. Elevating the RCP correlates with an amplified depletion rate, particularly in the IC2D scenario (Figure 3-6 b and c). When we examine Figure 3-6 d and e, the RCP seems not to influence the DRRs. Nevertheless, upon examining the IC3D columns for both RCPs in Table 3-5, it becomes apparent that as the RCP increases, the depletion also increases. On the other hand, when we analyze images by columns, it can be seen that in most cases, the IC3D scenario leads to greater than or equal DRRs than those generated by the IC2D scenario (see Table 3-5).

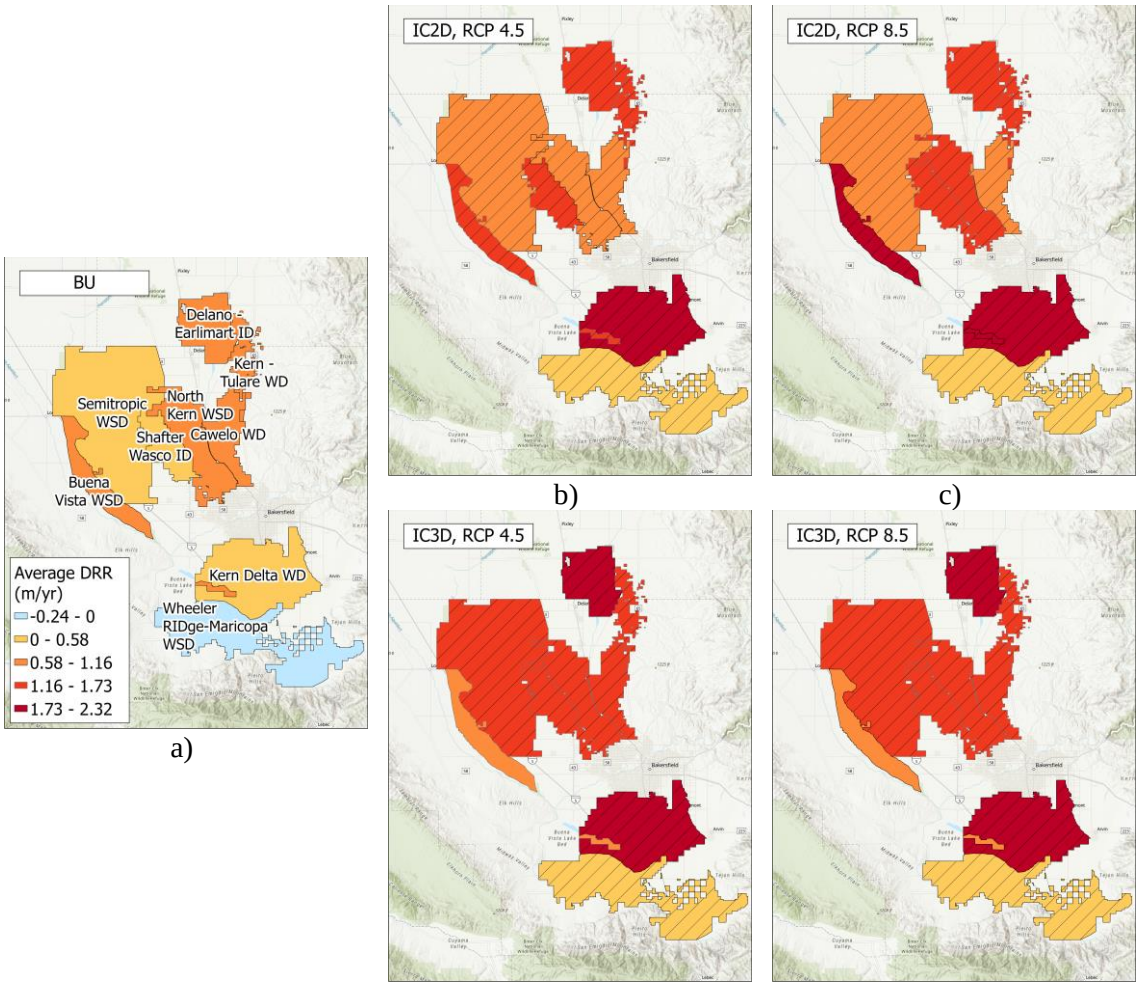

Figure 3-6. Average depletion or replenishment rates (DRR) in meters per year for different water districts, scenarios, and RCPs. a) Business as usual (BU) scenario. b) Influence of Climate Change in Two Dynamic Variables under RCP 4.5. c) Influence of Climate Change in Two Dynamic Variables under RCP 8.5. d) Influence of Climate Change in Three Dynamic Variables under RCP 4.5. e) Influence of Climate Change in Three Dynamic Variables under RCP 8.5. Hatched areas in Figure 3-6 b-e represent districts where Welch's t-test null hypothesis for equal means between the BU scenario and other scenarios (IC2D and IC3D under RCPs 4.5 and 8.5) is rejected at a 5% significance level.

3.5.3 Groundwater depletion or replenishment rates (DRR)

We analyzed the relationship between the projected DRRs for each time frame (BOC, MOC, and EOC) and scenario group (BU, IC2D, and IC3D), as illustrated in Figure 3-7 and 0. This figure denotes different climate conditions by distinct color-coded areas (historical: green, RCP 4.5: blue, RCP 8.5: orange). The border color of the circles indicates whether depletion (red) or replenishment (black) is anticipated. Additionally, the numerical values inside the circles on the right-hand side indicate the magnitude of DRR in meters per year. The circles and semicircles in Figure 3-7 of a given water district can be read either row-wise or column-wise. When read row-

wise, it allows observing DRR evolution over time within the same scenario group. When the figure is read column-wise, it provides insights into how the DRR changes between climate scenario groups for a specific time period. In general, the projected DRRs under the BU scenario remain relatively constant for all water districts (depicted in green circles in Figure 3-7 and blue lines in Figure 3-5) since the dynamic input variables were synthetically generated to preserve the mean, deviation, skew, and lag-one correlation coefficient (between seasons *t* and *t-1)* of historical data (P, SWD, and AWD). Also, groundwater levels are expected to keep decreasing until the end of the century for all scenario groups and RCPs except for Wheeler Ridge-Maricopa WSD under the BU scenario, reflecting that the aquifer shows signs of recovery under future conditions similar to historic conditions.

We compared time frames and scenario groups to know if the groundwater levels in the Kern region would experience a more accelerated decline from 2016 to 2099 under scenarios without climate change and with climate change. However, this postulate holds only for seven water districts: Semitropic WSD, Kern Delta WD, Cawelo WD, Shafter Wasco ID, North Kern WSD, Delano-Earlimart ID, and Kern - Tulare WD. For instance, in Figure 3-7a, when comparing the scenario groups (rows) of Semitropic WSD, it is observed that the depletion rate increases (indicated by larger circles) when transitioning from a scenario group without projected climate change (BU) to a scenario incorporating climate change in two variables (IC2D), and to the more climate change influenced scenario (IC3D). Furthermore, for the Semitropic WSD, it seems the DRR increases over time (from left to right) for the IC2D and IC3D groups. However, for Semitropic WSD, the RCP effect is not as relevant.

For the other districts shown in Figure 7 (Wheeler Ridge-Maricopa WSD and Buena Vista WSD), the DRR does not exhibit a general change pattern between scenario groups and time periods. For Wheeler Ridge-Maricopa WSD (Figure 3-7b), the DRRs of the IC3D group increase in time from BOC to EOC and are higher than those of the other scenario groups. However, when comparing the DRRs of the BU and IC2D group scenarios, it is observed that the latter are lower. Also, in the IC2D scenario group, the DRRs do not increase over time. Finally, in the case of Buena Vista WSD (Figure 3-7c), the DRRs increase over time, and the results of IC2D are greater than those of the IC3D scenario group.

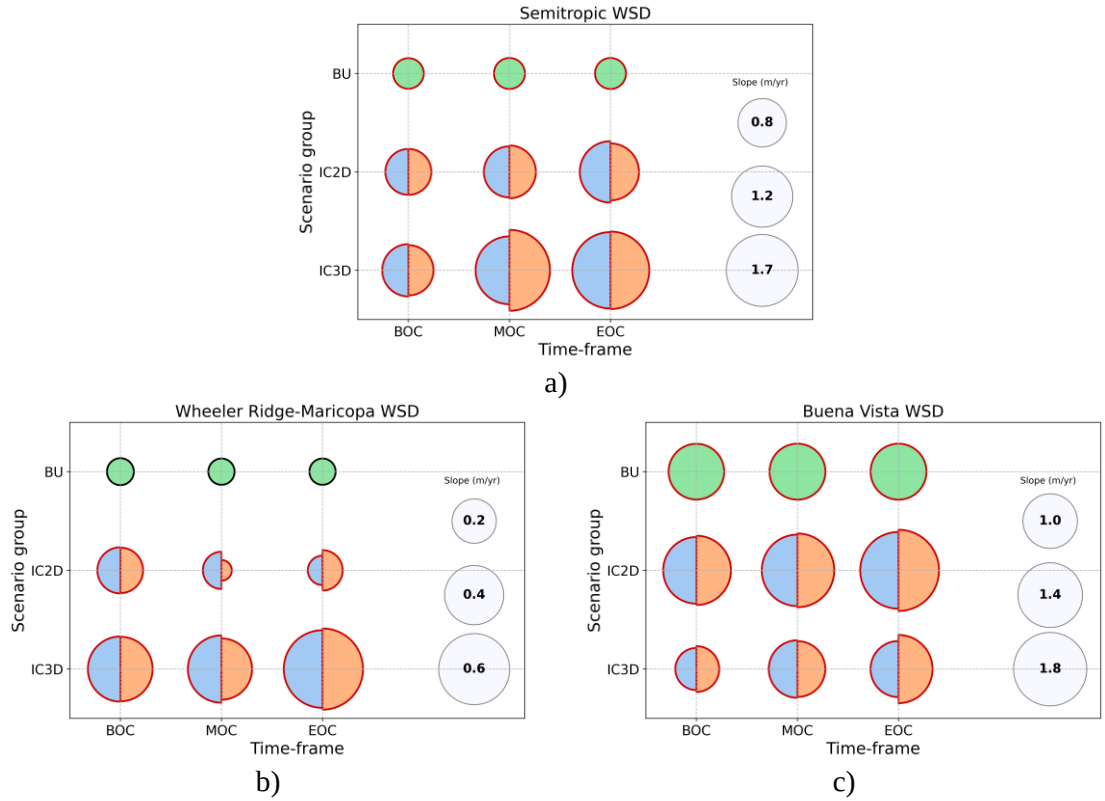

Figure 3-7. Groundwater depletion or recharge rate (DRR) by timeframe (columns) and scenario group (rows). Different colors represent different RCPs: Historical (green), 4.5 (blue), and 8.5 (orange). The circle's border color indicates whether the depth increases (red) or decreases (black) over time. The number inside the circles on the right shows the yearly DRR magnitude in meters.

3.6 Conclusions

This research examines the projected impact of climate change on groundwater levels for the uppermost confined aquifer for a selection of nine water districts of the Great Kern County Region (GKCR). Findings indicate that under a six-GCM ensemble of climate change scenarios, groundwater levels will mainly continue to decline unless agricultural water demand is reduced and/or recharge augmented. Moreover, results show that groundwater levels would experience a more rapid decline under climate change scenarios compared to historical conditions.

Precipitation was considered in the analysis to assess the direct effects of climate change on the groundwater system. Surface Water Deliveries to agriculture (SWD) and Agricultural Water Demand (AWD), on the other hand, were considered to account for the indirect effects of climate change. Besides, we employed an innovative approach characterized by the following: first, the AWDs change over time based on the ETo adjusted by the influence of carbon dioxide projections ($ETo_{adj,t}$). Second, the Long Short-Term Memory Emulator (LSTME) was the framework to integrate the water allocation model CALFEWS, precipitation, and agricultural water demands under the six-GCM ensemble for two Representative Concentration Pathways (RCPs 4.5 and 8.5). Third, the selected water districts overlay an area where aquifers have been critically overdrafted (CDWR, 2021a).

Three scenario groups (BU, IC2D, and IC3D) were proposed to test the hypothesis that climate change may increase aquifer drawdown rates. Such scenarios incept climate change gradually;

thus, the BU scenario assumes climate conditions similar to those from 1974 to 2015. For the IC2D scenario, the effect of climate change was included in two dynamic variables: precipitation and surface water deliveries. Lastly, for the IC3D scenario, a third adjustment was introduced for the agricultural water demand by adjusting the reference evapotranspiration to account for higher temperatures and carbon dioxide concentrations. Also, the GCMs used here correspond to six of the GCMs that best describe California's climate following the state's Fourth Climate Assessment" (D. Pierce et al., 2016). Finally, the water allocation model used here (CALFEWS) was selected for its ability to resemble historical deliveries in the southern California Central Valley.

Here, we utilized an ensemble of six GCMs and two RCPs to study projected climate impacts on groundwater. However, we only used a hydrological model (C2VSimFG) and a water allocation model (CALFEWS). For future research, we recommend a more comprehensive approach employing ensembles of hydrological models, such as HydroGeoSphere (HGS), the Penn State Integrated Hydrologic Model (PIHM), Modular Groundwater Flow (MODFLOW), and ensembles of water allocation models like CALVIN or CALSIM. This broader approach will provide a more holistic perspective on future groundwater levels. Furthermore, we advise considering the dynamic changes in land use over time. By incorporating this aspect, we can conduct more realistic simulations to reflect the intricate relationship between climate change and groundwater dynamics. Lastly, it is imperative to consider the regulatory constraints on groundwater pumping. Doing so can mitigate undesirable consequences for the aquifers' structure. Nonetheless, our current analysis does offer valuable insights into the potential impact of various climate scenarios on groundwater levels over time.

3.7 References

Allen, Richard. G., Pereira, Luis. S., Raes, D., & Smith, M. (1998). *FAO irrigation and Drainage paper No. 56. Crop Evapotranspiration* (Vol. 56).

Amanambu, A. C., Obarein, O. A., Mossa, J., Li, L., Ayeni, S. S., Balogun, O., Oyebamiji, A., & Ochege, F. U. (2020). Groundwater system and climate change: Present status and future considerations. *Journal of Hydrology*, *589*(December 2019), 125163. https://doi.org/10.1016/j.jhydrol.2020.125163

Bhatt, R., & Hossain, A. (2019). Concept and consequence of evapotranspiration for sustainable crop production in the era of climate change. In D. Bucur (Ed.), *Advanced evapotranspiration methods and applications* (First).

Blöschl, G., Bierkens, M. F. P., Chambel, A., Cudennec, C., Destouni, G., Fiori, A., Kirchner, J. W., McDonnell, J. J., Savenije, H. H. G., Sivapalan, M., Stumpp, C., Toth, E., Volpi, E., Carr, G., Lupton, C., Salinas, J., Széles, B., Viglione, A., Aksoy, H., … Zhang, Y. (2019). Twenty-three unsolved problems in hydrology (UPH)–a community perspective. *Hydrological Sciences Journal*, *64*(10), 1141–1158. https://doi.org/10.1080/02626667.2019.1620507

Brush, C., & Dogrul, E. (2016). *DWR Technical Memorandum: User's Manual for the California Central Valley Groundwater-Surface Water Simulation Model (C2VSim), Version 3.02-CG*.

Budd, R., O'Geen, A., Goh, K. S., Bondarenko, S., & Gan, J. (2009). Efficacy of Constructed Wetlands in Pesticide Removal from Tailwaters in the Central Valley, California. *Environmental Science & Technology*, *43*(8), 2925–2930. https://doi.org/10.1021/es802958q

CDWR. (2017). *Best management practices for the sustainable management of groundwater. Sustainable Management Criteria (draft)*.

(CEC) California Energy Commission, & (GIF) Geospatial Innovation Facility. (2011). *Cal-Adapt*. https://cal-adapt.org/

Closas, A., & Rap, E. (2017). Solar-based groundwater pumping for irrigation: Sustainability, policies, and limitations. *Energy Policy*, *104*, 33–37. https://doi.org/https://doi.org/10.1016/j.enpol.2017.01.035

Cooley, H. (2015). *Need To Know. California Agricultural Water Use: Key background information* (Issue April). https://doi.org/978-1-893790-65-0

Cubasch, U., Wuebbles, D., Chen, D., Facchini, M. C., Frame, D., Mahowald, N., & Winthe, J.-G. (2013). Introduction. In *Climate Change 2013: The Physical Science Basis. Contribution of Working Group I to the Fifth Assessment Report of the Intergovernmental Panel on Climate Change*. Cambridge University Press.

Curry, J. (2017). *Climate models for the layman*.

CWEMF. (2021). *Protocols for Water and Environmental Modeling*. https://cwemf.org/wp/wp-content/uploads/2021/11/Modeling-Protocols-Report-Final-11-19-2021.pdf

DeCoursey, W. J. (2003). *Statistics and Probability for Engineering Applications with Microsoft Excel*. Newnes.

Diaz-Granados, M. (2023). *Hidrologia, una sintesis probabilistica* (1st ed.).

Dogrul, E. C., & Kadir, T. N. (2020). *DWR Technical Memorandum: Theoretical Documentation and User's Manual for IWFM Demand Calculator (IDC-2015), Revision 88* (Issue August).

Draper, A. J., Jenkins, M. W., Kirby, K. W., Lund, J. R., & Howitt, R. E. (2003). Economic-Engineering Optimization for California Water Management. *Journal of Water Resources Planning and Management*, *129*(3), 155–164. https://doi.org/10.1061/(asce)0733-9496(2003)129:3(155)

Draper, A. J., Munévar, A., Arora, S. K., Reyes, E., Parker, N. L., Chung, F. I., & Peterson, L. E. (2004). CalSim: Generalized Model for Reservoir System Analysis. *Journal of Water Resources Planning and Management*, *130*(6), 480–489. https://doi.org/10.1061/(ASCE)0733-9496(2004)130:6(480)

Eastern Tule GSA. (2020). *Sustainable Groundwater Management Act. Groundwater Sustainability Plan*.

Ekstrom, J., Gautam, M., Anderson, J., & Andrew, J. (2019). *DWR Contributes to California's Fourth Climate Change Assessment* (Issue July).

Faunt, C. C. (2009). *Groundwater Availability of the Central Valley Aquifer , California*.

Fiering, M., & Jackson, B. (1971). *Synthetic streamflows*. https://doi.org/10.1029/WM001

Forni, L. G., Medellín-Azuara, J., Tansey, M., Young, C., Purkey, D., & Howitt, R. (2016). Integrating complex economic and hydrologic planning models: An application for drought under climate change analysis. *Water Resources and Economics*, *16*(May 2015), 15–27. https://doi.org/10.1016/j.wre.2016.10.002

Foster, T., Mieno, T., & Brozović, N. (2020). Satellite-Based Monitoring of Irrigation Water Use: Assessing Measurement Errors and Their Implications for Agricultural Water Management Policy. *Water Resources Research*, *56*(11), e2020WR028378. https://doi.org/https://doi.org/10.1029/2020WR028378

GEI Consultants Inc. (2019). *Buena Vista GSA. Groundwater Sustainability Plan: Public Review Draft. Kern County Groundwater Subbasin* (Issue September).

GEI Consultants Inc. (2020). *Groundwater Sustainability Plan. Kern County, CA*.

Ghasemizade, M., Asante, K. O., Petersen, C., Kocis, T., Dahlke, H. E., & Harter, T. (2019). An Integrated Approach Toward Sustainability via Groundwater Banking in the Southern Central Valley, California. *Water Resources Research*, *55*(4), 2742–2759. https://doi.org/10.1029/2018WR024069

Green, T. R. (2016). Linking Climate Change and Groundwater. In A. J. Jakeman, O. Barreteau, R. J. Hunt, J.-D. Rinaudo, & A. Ross (Eds.), *Integrated Groundwater Management: Concepts, Approaches and Challenges* (pp. 97–141). Springer International Publishing. https://doi.org/10.1007/978-3-319-23576-9_5

Hallegatte, S., Shah, A., Lempert, R., Brown, C., & Gill, S. (2012). *Investment Decision Making under Deep Uncertainty*. *September*, 1–41.

Hatch, T. (2020). *California Central Valley Groundwater-Surface Water Simulation Model – Fine Grid (C2VSimFG) Development and Calibration Version 1.0* (Issue December). https://data.cnra.ca.gov/dataset/c2vsimfg-version-1-0

IPCC. (2014). *Climate Change 2014: Synthesis Report. Contribution of Working Groups I, II and III to the Fifth Assessment Report of the Intergovernmental Panel on Climate Change*. https://doi.org/10.1016/S0022-0248(00)00575-3

IPCC. (2022). *IPCC. Data Distribution Centre*. https://www.ipcc-data.org/guidelines/pages/gcm_guide.html

Jasperse, L., & Pairis, A. (2020). *Climate Change Consortium for Specialty Crops: Southern California Region*.

Jayasundara, N., Seneviratne, S., Reyes, E., & Chung, F. (2020). Artificial Neural Network for Sacramento–San Joaquin Delta Flow–Salinity Relationship for CalSim 3.0. *Journal of Water Resources Planning and Management*, *146*(4), 4020015. https://doi.org/10.1061/(ASCE)WR.1943-5452.0001192

Joyce, B., Vicuña, S., Dale, L., Dracup, J., Hanemann, M., & Purkey, D. (2005). *Climate Change Impacts on Water for Agriculture in California: A Case Study in the Sacramento Valley*. https://citeseerx.ist.psu.edu/document?repid=rep1&type=pdf&doi=534a99c15b67d637f2191bfede79ed7e79511502

Kadir, T. (2017). *Coupled Reservoir Operation and Integrated Hydrologic Simulation Modeling of the SWP and CVP Systems in California with Dynamic Hydrology Adjustment*. University of California, Davis.

Kanji, G. (2006). *100 statistical tests* (Third).

Kashinath, K., Mustafa, M., Albert, A., Wu, J.-L., Jiang, C., Esmaeilzadeh, S., Azizzadenesheli, K., Wang, R., Chattopadhyay, A., Singh, A., Manepalli, A., Chirila, D., Yu, R., Walters, R., White, B., Xiao, H., Tchelepi, H. A., Marcus, P., Anandkumar, A., … Prabhat, null. (2021). Physics-informed machine learning: case studies for weather and climate modelling. *Philosophical Transactions of the Royal Society A: Mathematical, Physical and Engineering Sciences*, *379*(2194), 20200093. https://doi.org/10.1098/rsta.2020.0093

Khair, S. M., Mushtaq, S., Reardon-Smith, K., & Ostini, J. (2019). Diverse drivers of unsustainable groundwater extraction behaviour operate in an unregulated water scarce region. *Journal of Environmental Management*, *236*, 340–350. https://doi.org/https://doi.org/10.1016/j.jenvman.2018.12.077

Kottegoda, N., & Rosso, R. (2008). *Applied statistics for civil and environmental engineers* (Second). Blackwell Publishing.

Kurylyk, B. L., & MacQuarrie, K. T. B. (2013). The uncertainty associated with estimating future groundwater recharge: A summary of recent research and an example from a small unconfined aquifer in a northern humid-continental climate. *Journal of Hydrology*, *492*, 244–253. https://doi.org/https://doi.org/10.1016/j.jhydrol.2013.03.043

Larocque, M., Levison, J., Martin, A., & Chaumont, D. (2019). A review of simulated climate change impacts on groundwater resources in Eastern Canada. *Canadian Water Resources Journal*, *44*(1), 22–41. https://doi.org/10.1080/07011784.2018.1503066

Loucks, D. P., & van Beek, E. (2017). An Introduction to Probability, Statistics, and Uncertainty. In *Water Resource Systems Planning and Management: An Introduction to Methods, Models, and Applications* (pp. 213–300). Springer International Publishing. https://doi.org/10.1007/978-3-319-44234-1_6

McEvoy, D. J., Pierce, D. W., Kalansky, J. F., Cayan, D. R., & Abatzoglou, J. T. (2020). Projected Changes in Reference Evapotranspiration in California and Nevada: Implications for Drought and Wildland Fire Danger. *Earth's Future*, *8*(11), 1–17. https://doi.org/10.1029/2020EF001736

Medellín-Azuara, J., MacEwan, D., Howitt, R. E., Koruakos, G., Dogrul, E. C., Brush, C. F., Kadir, T. N., Harter, T., Melton, F., & Lund, J. R. (2015). Hydro-economic analysis of groundwater pumping for irrigated agriculture in California's Central Valley, USA. *Hydrogeology Journal*, *23*(6), 1205–1216. https://doi.org/10.1007/s10040-015-1283-9

Meixner, T., Manning, A. H., Stonestrom, D. A., Allen, D. M., Ajami, H., Blasch, K. W., Brookfield, A. E., Castro, C. L., Clark, J. F., Gochis, D. J., Flint, A. L., Neff, K. L., Niraula, R., Rodell, M., Scanlon, B. R., Singha, K., & Walvoord, M. A. (2016). Implications of projected climate change for groundwater recharge in the western United States. *Journal of Hydrology*, *534*, 124–138. https://doi.org/10.1016/j.jhydrol.2015.12.027

MID-Kaweah GSA. (2022). *2022 First Amended Groundwater Sustainability Plan*.

Moss, R. H., Edmonds, J. A., Hibbard, K. A., Manning, M. R., Rose, S. K., van Vuuren, D. P., Carter, T. R., Emori, S., Kainuma, M., Kram, T., Meehl, G. A., Mitchell, J. F. B., Nakicenovic, N., Riahi, K., Smith, S. J., Stouffer, R. J., Thomson, A. M., Weyant, J. P., & Wilbanks, T. J. (2010). The next generation of scenarios for climate change research and assessment. *Nature*, *463*(7282), 747–756. https://doi.org/10.1038/nature08823

Murphy, J. (1999). An Evaluation of Statistical and Dynamical Techniques for Downscaling Local Climate. *Journal of Climate*, *12*(8), 2256–2284. https://doi.org/https://doi.org/10.1175/1520-0442(1999)012<2256:AEOSAD>2.0.CO;2

Murray, K. D., & Lohman, R. B. (2018). Short-lived pause in Central California subsidence after heavy winter precipitation of 2017. *Science Advances*, *4*(8), 1–9. https://doi.org/10.1126/sciadv.aar8144

NOAA. (2022). *Climate.gov*. https://www.climate.gov/maps-data/climate-data-primer/predicting-climate/climate-models

Null, S. E. (2016). Water Supply Reliability Tradeoffs between Removing Reservoir Storage and Improving Water Conveyance in California. *JAWRA Journal of the American Water Resources Association*, *52*(2), 350–366. https://doi.org/https://doi.org/10.1111/1752-1688.12391

OpenET. (2023). *OpenET*. https://openetdata.org/what-is-evapotranspiration/

Ouhamdouch, S., Bahir, M., Ouazar, D., Maria, P., & Kamel, C. (2019). Evaluation of climate change impact on groundwater from semi-arid environment (Essaouira Basin, Morocco) using integrated approaches. *Environmental Earth Sciences*, *78*(15), 1–14. https://doi.org/10.1007/s12665-019-8470-2

Perrone, D., & Jasechko, S. (2019). Deeper well drilling an unsustainable stopgap to groundwater depletion. *Nature Sustainability*, *2*(8), 773–782. https://doi.org/10.1038/s41893-019-0325-z

Perrone, D., & Rohde, M. (2016). Benefits and economic costs of managed aquifer recharge in California. *San Francisco Estuary and Watershed Science*, *14*(2), 1–13. https://doi.org/10.15447/sfews.2016v14iss2art4

Pierce, D., Cayan, D., & Dehann, L. (2016). *Creating Climate projections to support the 4th California Climate Assessment*.

Pierce, D. W., Kalansky, J. F., & Cayan, D. R. (2018). *Climate, Drought, and Sea Level Rise Scenarios for California's Fourth Climate Change Assessment* (Issue CNRA-CEC-2018-006).

Rummukainen, M. (2010). State-of-the-art with regional climate models. *WIREs Climate Change*, *1*(1), 82–96. https://doi.org/https://doi.org/10.1002/wcc.8

Schneider, R., Koch, J., Troldborg, L., Henriksen, H. J., & Stisen, S. (2022). Machine learning-based downscaling of modelled climate change impacts on groundwater table depth. *Hydrology and Earth System Sciences Discussions*, *May*.

Shaffer, K. H., & Runkle, D. L. (2007). *Consumptive Water-Use Coefficients for the Great Lakes basin and Climatically Similar Areas*.

Taylor, R. G. (2013). Ground water and climate change. *Nature Climate Change*, *3*(November 2012). https://doi.org/10.1038/NCLIMATE1744

Vahmani, P., Jones, A. D., & Li, D. (2022). Will Anthropogenic Warming Increase Evapotranspiration? Examining Irrigation Water Demand Implications of Climate Change in California. *Earth's Future*, *10*(1), 1–13. https://doi.org/10.1029/2021EF002221

van Vuuren, D. P., Edmonds, J., Kainuma, M., Riahi, K., Thomson, A., Hibbard, K., Hurtt, G. C., Kram, T., Krey, V., Lamarque, J. F., Masui, T., Meinshausen, M., Nakicenovic, N., Smith, S. J., & Rose, S. K. (2011). The representative concentration pathways: An overview. *Climatic Change*, *109*(1), 5–31. https://doi.org/10.1007/s10584-011-0148-z

Wada, Y., van Beek, L. P. H., van Kempen, C. M., Reckman, J. W. T. M., Vasak, S., & Bierkens, M. F. P. (2010). Global depletion of groundwater resources. *Geophysical Research Letters*, *37*(20). https://doi.org/https://doi.org/10.1029/2010GL044571

Wallace, J. S. (2000). Increasing agricultural water use efficiency to meet future food production. *Agriculture, Ecosystems & Environment*, *82*(1), 105–119. https://doi.org/https://doi.org/10.1016/S0167-8809(00)00220-6

Walton, D., Berg, N., Pierce, D., Maurer, E., Hall, A., Lin, Y. H., Rahimi, S., & Cayan, D. (2020). Understanding Differences in California Climate Projections Produced by Dynamical and Statistical Downscaling. *Journal of Geophysical Research : Atmospheres*, 1–16. https://doi.org/10.1029/2020JD032812

Yang, Y., Roderick, M. L., Zhang, S., McVicar, T. R., & Donohue, R. J. (2019). Hydrologic implications of vegetation response to elevated CO2 in climate projections. *Nature Climate Change*, *9*(1), 44–48. https://doi.org/10.1038/s41558-018-0361-0

Yates, D., Sieber, J., Purkey, D., & Huber-Lee, A. (2005). WEAP21—A Demand-, Priority-, and Preference-Driven Water Planning Model. *Water International*, *30*(4), 487–500. https://doi.org/10.1080/02508060508691893

Zeff, H. B., Hamilton, A. L., Malek, K., Herman, J. D., Cohen, J. S., Medellin-Azuara, J., Reed, P. M., & Characklis, G. W. (2021). California's food-energy-water system: An open source simulation model of adaptive surface and groundwater management in the Central Valley. *Environmental Modelling and Software*, *141*(April), 105052. https://doi.org/10.1016/j.envsoft.2021.105052

Chapter 4 An application of conjunctive water use under climate change and groundwater regulation in a semiarid region of California

Abstract

Growing water demand, overexploitation of rivers and aquifers, declining water quality, and the impact of climate change highlight the need for innovative water planning and management methods. The coordinated use of surface and groundwater, known as conjunctive water use (CWU), offers a strategic approach to sustainably meeting social, economic, and environmental objectives. This research focuses on finding optimal operational policies for the Shafter-Wasco irrigation district (SWID) using CWU while considering the influence of climate change and groundwater regulation. We employ Bayesian Optimization Programming (BOP), a comprehensive water management method that combines simulation and optimization. BOP encourages simultaneous decision-making, collective performance evaluation, and guided decision search through multiobjective optimization. We formulate a multiobjective optimization problem that maximizes average net revenue in farming and minimizes average depth to groundwater between 2020 and 2040. We use the Global Climate Model, CanESM2, under the RCP 4.5 emissions scenario to estimate precipitation and surface water deliveries. To derive the Pareto front and optimal operation policies, we use Bayesian Optimization with 5,000 objective function evaluations. By employing the k-means clustering method, we categorized points on the Pareto front into three groups: lowest, medium, and highest net revenue and depth to groundwater. Our findings highlight the balance of profit and aquifer recovery, supporting prior research indicating farmers need to curtail pumping and profits to promote groundwater sustainability. Finally, our method can be applied to integrate water and agricultural systems facing various uncertainties, providing insights into optimal policies and associated tradeoffs.

4.1 Introduction

In light of escalating water demand, the overexploitation of rivers and aquifers, deterioration in water quality, and visible manifestations of climate change, it is imperative to incorporate innovative methods in water planning and management (Gorelick & Zheng, 2015; Sabale et al., 2023). The conventional planning aims to identify the best solution for a problem and implement it incrementally. However, if the conditions deviate from the initial assumptions while executing the solution, it can result in substantial cost overruns (Hallegatte et al., 2012). Recent studies suggest climate change is challenging the notion of a stable climate, with projections of rising temperatures and increased variability in precipitation in the forthcoming decades (Fawzy et al., 2020). That situation threatens the effectiveness of various planning methodologies. Consequently, farmers will likely need to shift towards groundwater as a buffer for droughts. Unfortunately, on a global scale, the absence of groundwater regulation and insufficient oversight in groundwater pumping have led to diminishing aquifer levels and various environmental and socioeconomic challenges like reduced agricultural yields, job losses, declining quality of life in rural areas, heightened energy expenses associated with accessing deeper wells, and decreased land values (Famiglietti, 2014). On the other hand, stakeholders typically negotiate and decide operation policies based on their expertise. However, implementing those policies without a simulation and optimization framework could lead to high costs, especially when the decision space is not fully sampled.

The conjunctive use of surface and groundwater, known as conjunctive water use (CWU), presents a strategic approach to achieving social, economic, and environmental goals by optimally using all the region's water resources (Sepahvand et al., 2019). We can effectively address water scarcity by integrating CWU with a managed aquifer recharge (MAR) program. In this manner, surface water sources can be used during wet years for irrigation and replenishing groundwater. In contrast, we can withdraw water from the reserves during dry years through pumping (Faunt et al., 2016). The CWU-MAR approach contributes significantly to agricultural production by providing stable access to water and aiding in compliance with groundwater regulations (Sabale et al., 2023; Safavi et al., 2010; Sepahvand et al., 2019). However, it is crucial to employ simulation and optimization techniques to implement the CWU-MAR approach (Nematollahi et al., 2023; Rafipour-Langeroudi et al., 2014). In this way, simulation is a cost-effective means of understanding system behavior under various conditions, while optimization identifies the most efficient ways to operate these systems.

This research seeks operational policies that ensure a CWU strategy maximizing farmers' net revenue while avoiding groundwater overdrafts. We examine optimal operating policies for the Shafter-Wasco irrigation district (SWID) employing the CWU approach, considering the influence of climate change and groundwater regulation. We consider a multiobjective optimization framework instead of the conventional stakeholder water negotiation mechanism. In agricultural regions, that mechanism is a cooperative process where farmers, local communities, governmental agencies, and environmental groups discuss, plan, and establish agreements to strike a balance that addresses the interests, sustainability, and concerns of the involved parties (D'Agostino et al., 2020; Loucks & Beek, 2017). Here, we allow the policies to change every two years, depending on climate conditions and water availability. Our study sets forth two objectives: maximizing farmers' net revenue while preserving groundwater levels. The Pareto front is drawn to identify the best solutions for the multiobjective optimization problem solved using Bayesian Optimization.

The optimization problem solutions are expected to provide valuable insights into a seemingly conflicting situation, maximizing farmers' net revenue while avoiding groundwater overdrafts. Although the two goals might appear at odds initially, further analysis reveals that they complement and reinforce each other because effectively managing and maintaining the groundwater system is essential for achieving sustainable economic growth. The proposed methodology allows the identification of optimal policies and their associated tradeoffs in integrating water and agricultural systems characterized by abundant economic, institutional, hydrological, and biological uncertainties. This framework is significant in agricultural regions experiencing high water stress and heavy reliance on groundwater.

This chapter is organized as follows. Section two overviews the research's fundamental concepts, including adaptive pathways and multiobjective optimization methods. In section three, the study area is described. The fourth section addresses our optimization problem and the underlying assumptions. Lastly, sections 5 and 6 present the results and conclusions drawn from the research, respectively.

4.2 Theoretical framework

4.2.1 Adaptative pathways

Traditional planning aims to identify and systematically apply the most effective solution to a problem. Yet, if circumstances deviate from the initial assumptions while implementing the solution, it may cause substantial cost overruns (Hallegatte et al., 2012). Here is when the adaptative pathways (AP) approach becomes relevant. AP offers an analytical method for examining and arranging a series of potential actions in response to different external developments over time (Haasnoot et al., 2013). AP method suggests flexible strategies that can be modified over time in response to changing conditions or the availability of new information. Also, AP enables decision-makers to navigate a dynamic and uncertain environment effectively (Haasnoot et al., 2011). Here, we propose identifying APs by solving a multiobjective optimization problem in which decisions about fractions of perennial and annual crops change every two years for SWID.

4.2.2 Multiobjective optimization

Optimization consists of finding the best possible solution to a problem from a set of alternatives. In mathematical terms, optimization seeks to maximize or minimize a function, considering constraints to the input variables (Nocedal & Wright, 2000). With a single objective, the solution is generally unique and is called the optimal solution. However, when two or more competing objectives exist, this problem is known as multiobjective optimization (MO). Typically, the MO problem does not have a single solution but rather a set of Pareto optimal or non-dominated solutions located on the Pareto front (Branke et al., 2008). Consequently, solutions in the Pareto front can only improve on one objective by deteriorating at least one of the other (Rachmawati & Srinivasan, 2006). Also, MO problems in water resources need diverse observations of climate, hydrology, and water demand to guide the actions required to enhance the proposed objectives (Cohen & Herman, 2021). Some popular methods to solve MO problems are Weighted Sum, Non-Dominated Sorting Genetic Algorithm (NSGA-II), and Bayesian Optimization.

4.2.2.1 Weighted Sum

The weighted sum method consolidates all objectives in a unique objective function, the weighted sum of them (Loucks & Beek, 2017). As an example, Nouiri et al. (2015) developed the ALL_WATER_gw groundwater management tool, which addresses four objectives: i) meeting demand, ii) minimizing drawdown, iii) reducing costs, and iv) satisfying salinity requirements. To tackle this, researchers employed the weighted sum method to consolidate the initial objectives into two groups. Thus, objectives i) and ii) were consolidated into one group, while objectives iii) and iv) were grouped into another group. Subsequently, a multiobjective genetic algorithm was used to identify the Pareto front for the consolidated objectives. However, the weighted sum method has some issues: difficulty selecting each objective weight without bias, normalizing objectives without knowing their limits, and finding Pareto-optimal solutions when the feasible objective space is non-convex.

4.2.2.2 Non-Dominated Sorting Algorithm Version II

The Non-dominated Sorting Algorithm Version II (NSGA-II) offers an alternative to the weighted sum by generating a set of non-dominated solutions using an elitist principle (Branke et al., 2008; Majedi et al., 2021) without additional parameters such as the weights mentioned above. The elitist principle is a strategy designed to preserve diversity among solutions, ensuring

that the best solutions are kept once they are found (Deb et al., 2002). NSGA-II is a multiobjective evolutionary algorithm (MOEA) based on genetic algorithms that has provided optimal solutions for multiple problems (Majedi et al., 2021).

According to (Deb et al., 2002), the NSGA-II algorithm involves creating an initial parent population (P_t) consisting of N individuals, representing potential candidates for the Pareto front. A new offspring (Q_t) population is generated with the same P_t size through tournament selection, crossover, and mutation applied to the P_t genes. Subsequently, P_t and Q_t are combined into a single population called *Rt*, where objectives are evaluated, and dominance fronts are established. If the stopping criteria (convergence or a specified number of iterations) are not met, a new population P_{t+1} is formed by selecting individuals from each front, starting with the best-nondominated set (*F1*), progressing to the second-best front (*F2*), until reaching the *FL* front. The aim is to choose enough individuals to get *N* elements. However, when the number of selected elements exceeds N, it must be decided which elements of the FL front will be incorporated. For this task, crowding distance criteria or a comparable approach could be used, ensuring a well-distributed space sampling and preventing overemphasis on local optimal points. This iterative process continues until the stopping criteria are met. Notably, NSGA-II necessitates numerous evaluations of objective functions, which can be limited in time, money, or other resources (Manoj et al., 2022). Examples of costly objective function evaluations include conducting physical experiments or running complex computer simulations (Nguyen, 2023). In our research, we abstain from employing the NSGA-II algorithm to identify solutions for our optimization problem (see section 4.4) due to the computationally demanding nature of the functions used here.

4.2.2.3 Bayesian Optimization

Bayesian Optimization uncovers comparable or superior solutions to NSGA-II, requiring fewer objective function evaluations (Manoj et al., 2022; Saad et al., 2022). Bayesian optimization's main idea consists of replacing objectives and constraints with surrogate functions described by Gaussian Processes (GP) (see section 4.2.2.4) that gradually increase their ability to emulate the original functions and locate optimal solutions. According to (Mathern et al., 2021), the original objective functions and constraints are initially evaluated on randomly selected points that satisfy the search space (*S*) constraints. GPs are trained to replace original objectives and constraints thanks to the initial points and their evaluations. Considering the mean and covariance functions of the GPs, a new sampling point is identified. This new point is added to the initial sample set, and the GPs are retrained. The process is repeated until the stopping criterion is met. Identifying the Pareto front with a limited number of evaluations of expensive objective functions has led to the wide adoption of the Bayesian optimization method in fields such as materials research, power plant production, computer games engagements, and neuroscience (Manoj et al., 2022). Although Bayesian Optimization has proven to be appropriate to solve most multiobjective optimization problems, it requires specialized knowledge in mathematics and programming, contributing to its lack of spread.

Unlike deterministic interpolation models, GP provides the mean and the covariance function, which help quantify uncertainty in unsampled areas of *S*. These functions can be used to explore and exploit *the* search space (Manoj et al., 2022). We pinpoint the function's minimum by minimizing the mean function, exhibiting space exploitation. On the other hand, minimizing the covariance function helps locate regions where adding a new point reduces uncertainty, revealing space exploration (Manoj et al., 2022). However, using the mean and covariance functions separately is not recommended. Instead, combining these two functions into an *acquisition function* to balance exploration and exploitation is advisable (Manoj et al., 2022). Some

acquisition functions for a single objective are Expected Improvement, Probability of Improvement, and Lower Confidence Bound (Nguyen, 2023). In multiobjective optimization, a famous acquisition function is the *Expected Hypervolume Improvement* (EHVI), which guides the selection of points that extend the Pareto frontier (Nguyen, 2023). The larger the volume under the Pareto frontier (i.e., the hypervolume of the dominated region), the better the set of optimal solutions. In this research, we used the EHVI acquisition function and 5,000 evaluations of the objective functions as stopping criteria.

4.2.2.4 Gaussian process

Gaussian processes support Bayesian Optimization. According to (Rasmussen, 2004), a Gaussian process is a collection of random variables such that any finite collection of these variables follows a multivariate normal distribution. In other words, a Gaussian process is the generalization of multivariate normal distributions to infinite dimensions (Sun et al., 2014). While conventional regression models aim to find the function that best fits the input and output data, with a Gaussian Process, it is possible to obtain the probability distribution of all the functions that fit the input and output variables. The GPs heart is the covariance function (also called similarity function or kernel function), which captures the similarities between pairs of points in space (Østergård et al., 2018). Some examples of covariance functions are the Gaussian Kernel, the Matern Kernel, and the periodic Kernel (Saad et al., 2022). However, when choosing a covariance function, it's important to fine-tune its hyperparameters for optimal performance. For instance, Equation 4-1 shows that the Gaussian kernel (k), also known as the squared exponential kernel, has hyperparameters (θ) comprising the variance (σ_f^2), the Euclidean distance (r), and the characteristic length-scale (l). On the one hand, r represents the Euclidean distance between pairs of points x_i and x_j. In the same equation, l means the average length at which pairs of points cease to impact each other.

$$k(x_i, x_j|\theta) = \sigma_f^2 * \exp\left(-\frac{1}{2} * \frac{r^2}{l^2}\right) \qquad \text{Equation 4-1}$$

By applying Bayes' theorem in conjunction with the Gaussian Processes properties, we can determine the probability of the latent function $f(x)$, given a specific set of observed values for the output variable y, as is shown in Equation 4-2 (Bradford et al., 2018; Frazier, 2018; Rasmussen, 2004). Thanks to the Bayes theorem, we can update probability estimates based on new information or evidence (Box et al., 2016). Also, a latent function is a hidden function that captures underlying relationships between inputs (x) and outputs (y). In Equation 4-2, $m_p(x)$ and k_p (x) are the posterior mean and posterior covariance, respectively. According to Equation 4-3, $m_p(x)$ represents the weighted mean of prior outcomes (y), considering the covariance matrix between the observed values $\boldsymbol{\Sigma}(x,x)$ (commonly referred to as prior covariance) and the covariance matrix between the observed values and the interest points $\boldsymbol{\Sigma}(x,x^*)$. $k_p(x)$ equals the prior covariance minus a term that reflects the improvement by considering the point x^* (Equation 4-4). Elements from the covariance matrices could be estimated by a covariance function, as described by Equation 4-1.

$$f(x)|y \sim GP\left(m_p(x), k_p(x)\right)$$ Equation 4-2

$$m_p(x) = \boldsymbol{\Sigma}(x, x^*)^T \boldsymbol{\Sigma}(x, x)^{-1} \boldsymbol{y}$$ Equation 4-3

$$k_p(x) = \boldsymbol{\Sigma}(x, x) - \boldsymbol{\Sigma}(x, x^*)^T \boldsymbol{\Sigma}(x, x)^{-1} \boldsymbol{\Sigma}(x, x^*)$$ Equation 4-4

4.3 Model application area

Shafter-Wasco Irrigation District (SWID) is in southern California's Central Valley (CCV) near the lower Sierra Nevada mountains (Figure 4-3). The SWID is neighbored by the Semitropic Water Storage District, North Kern Water Storage District, and Rosedale-Rio Bravo Water Storage District. Even though the cities of Shafter and Wasco are in the district, they don't get water directly from it. Nevertheless, such cities gain advantages from SWID's groundwater recharge efforts because the recharge initiatives benefit the wells that supply water to those municipalities (GEI Consultants. Inc, 2022). SWID has an area of 157.2 km^2, with elevations ranging from 114.3 m on the east to 91.44 m on the west side, which can be broadly described as flat terrain. Also, SWID's soil is made up of sandy loam and clay loam, which is not challenged by issues like salinity, high water table, or high or low infiltration rates, making it suitable for numerous crops (GEI Consultants. Inc, 2022). In 2020, 75% of the SWID's area was cultivated. The crop distribution for the same period was 78.6% almond trees, 3.9% grapes, 3.7% alfalfa, 1.6% wheat, and the remaining percentage with other crops (Figure 4-1).

SWID considers the combined use of surface water and groundwater resources (CWU). SWID lacks surface water streams within its boundaries or adjacent to them. In 2020, the SWID received 65.9 million cubic meters of surface water. The majority, 93.1%, came from the Central Valley Project through the Friant-Kern Canal, followed by 4.7% from recycled water, 2.1% from transferred water from the North Kern Water Storage District, and 0.1% from banked water (Figure 4-2). Regarding groundwater, farmers extract water from wells, typically located in the uppermost confined aquifer. In contrast, most domestic wells draw water from the unconfined aquifer. These aquifers are separated by layers of Corcoran E-clay or similar materials (GEI Consultants. Inc, 2022) and are prone to compaction (Faunt, 2009).

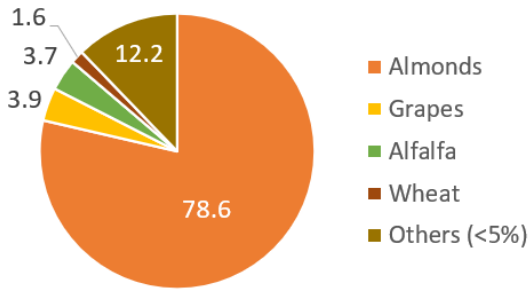

Figure 4-1. Percentage of crop areas for Shafter-Wasco Irrigation District (SWID) during 2020 (GEI Consultants. Inc, 2022).

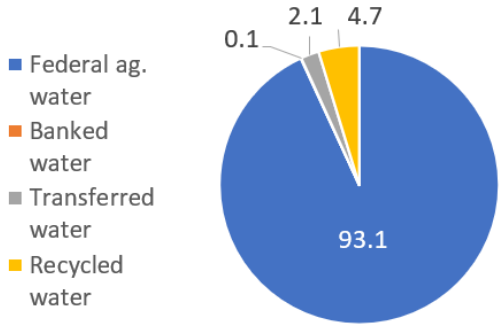

Figure 4-2. Percentage of water supplies during the calendar year 2020 for Shafter-Wasco Irrigation District (SWID) (GEI Consultants. Inc, 2022).

The climate of the study area can be classified as Mediterranean, from warm to hot, with dry summers and mild wet winters. The average monthly temperature ranges from 6.6 Celsius in December to 27.2 Celsius in July. The average monthly precipitation ranges from 0 mm in July and August to 27.4 mm in March. The reference evapotranspiration ranges from 38.1 mm in January to 214.12 mm in July (GEI Consultants. Inc, 2022). Droughts have affected SWID and other irrigation districts in CCV, leading farmers to increase groundwater pumping due to water scarcity, causing significant groundwater depletion. For instance, during the 2006-2009 drought, CCV's groundwater reserves decreased between 24 to 31 km^2 (Taylor, 2013). Alam et al. (2019) reported that from 1950 to 2009, the depletion rate of CCV's aquifer was 3 km^3/yr. Furthermore, the same study projects that these depletion rates will rise in the future under climate change scenarios if no mitigation measures are implemented. As highlighted in the previous chapter and reiterated by Taylor (2013), the impact of climate change on both water demand and surface water deliveries can have a more pronounced indirect effect on groundwater, surpassing the direct consequences of climate change on aquifer recharge.

SWID was legally established in 1937, and from its inception, its mission went beyond merely supplying water to users; it also included preventing aquifer depletion (GEI Consultants. Inc, 2022). Protecting underground resources became more significant after the Sustainable Groundwater Management Act (SGMA) was passed. SGMA mandates that by 2040, all critically over-drafted groundwater basins, including the one supplying SWID, must attain sustainability (Sustainable Groundwater Management Act (SGMA), 2014; CDWR, 2017). Currently, SWID operates under the purview of the Kern Groundwater Authority (KGA), a designated Groundwater Sustainability Agency (GSA) responsible for formulating and executing the Groundwater Sustainability Plans (GSPs) to achieve basin sustainability and avoid undesirable results (CDWR, 2017). To complete sustainable groundwater management, SWID initiated the operation of the Kimberlina Recharge Facility in 2017, covering an initial area of 0.89 km^2, with a projected expansion to encompass 2.5 km^2 by the year 2030. Furthermore, in 2022, the US Department of the Interior invested more than 1.8 million dollars in two projects to reduce the drought's effect. The approved projects encompassed the Southeast Recharge Facility and Conveyance Improvements ($500,000) and the Kimberlina Pipeline Conveyance Improvement Project ($1,315,083) (Bureau of Reclamation, 2022).

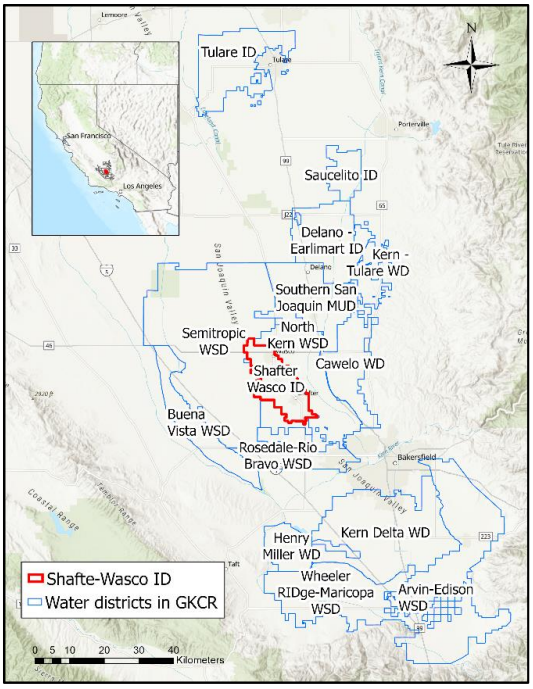

Figure 4-3. Study area. Shafter-Wasco Irrigation District is a Great Kern County Region (GKCR) member.

4.4 Optimization problem

To identify the optimal water operating policies in SWID under climate change and groundwater regulation, the central objective of this research, a multiobjective optimization problem, was formulated with two goals, two decision variables, and four constraints. The two objectives are 1) maximizing the average farmers' Net revenue (Equation 4-5) and 2) minimizing the average depth to groundwater (Equation 4-6) from 2020 to 2040. This timeframe was chosen to align with the critical period for achieving sustainability goals in overdrafted groundwater basins like the one studied. The two decision variables, $x_{1,}$ and $x_{2,}$ correspond to two time-series of coefficients ($x_{1,t,}$ and $x_{2,t}$) that reflect the fractions of annual and perennial crops for the year t relative to their average values from 1996 to 2015. When the fractions take a value of one, the reference areas remain unchanged. In contrast, fractions less than one represent area reductions, and values greater than one indicate area increases. Annual crops include grain, cotton, corn, dry beans, alfalfa, pasture, tomato, cucurbits, onions, garlic, potatoes, and other trucks. In contrast, perennial crops include almonds, pistachios, citrus, subtropical crops, vineyards, and other deciduous. Constraints (from Equation 4-13 to Equation 4-16) limit groundwater levels and fraction values $x_{1,t,}$ and $x_{2,t}$. The multiobjective optimization problem posed here is solved using Bayesian Optimization. So, we will indistinctly employ the terms "decision variable" or "time series" to denote x_1 and x_2. The values within these variables, represented as $x_{1,t,}$ and $x_{2,t,}$ will be called "fractions." In summary, a "decision variable" or "time series" is a collection of fractions.

For the first objective, the net revenue for annual and perennial crops was calculated as the product of their crop areas (AA_t and PA_t) and their corresponding average net revenues expressed in dollars per area ($\overline{NRA}$ and $\overline{NRP}$) (Equation 4-7). For the second objective, Equation 4-8 shows that depth to groundwater for time t (GWD_t) depends on the initial depth to groundwater (GWD_0: September 2015) and the cumulative changes in depth to groundwater (ΔGWD) up to month T.

We estimate ΔGWD by the Long Short-Term Memory (LSTM) artificial neural network, developed in Chapter 2, that emulates the C2VSimFG hydrologic model (Equation 4-9). As in Chapter 3, the emulator is also called LSTME. As mentioned in Chapter 2, LSTME requires static and dynamic variables. Static variables include surface area, ground surface slope, field capacity, saturated hydraulic conductivity, total porosity, hydraulic conductivity, aquifer vertical hydraulic conductivity, specific yield, and specific storage. Dynamic variables consist of Precipitation (*P*), Surface Water Deliveries (*SWD*), and Agricultural Water Demand (*AWD*). The subindex *t-12 ~ t* indicates that the LSTME considers the influence of the current and the 12 preceding observations to make a prediction.

To estimate the dynamic input variables, *P* and *SWD*, for the hydrological model (Equation 4-9) from 2015 to 2040, we resort to the CanESM2 Global Climate Model (GCM) developed by the Canadian Center for Climate Modeling and Analysis under the intermediate greenhouse gas and aerosol emissions, RCP 4.5. We selected the CanESM2 model based on its ability to represent California's average climate accurately, according to (Pierce et al., 2018). The downscaled and bias-corrected precipitation for CanESM2-RCP 4.5 was downloaded from the California Climate Adaptation Planning Tool (*Cal-Adapt*, 2022). On the other hand, the Surface water deliveries (*SWD*) for the same period were obtained from the California Food-Energy-Water System model, CALFEWS (Zeff et al., 2021), considering CanESM2-RCP 4.5. The remaining dynamic variable, Agricultural Water Demand (*AWD*), was determined by multiplying the areas of annual (AA_t) and perennial crops (PA_t) with their respective average water demands per unit area ($\overline{WDA}$ and $\overline{WDP}$) using Equation 4-10. Areas of annual and perennial crops are determined as the product of the fractions $x_{1,t}$ and $x_{2,t}$, and the average area of annual and perennial crops ($\overline{AA}$ and $\overline{PA}$) between 1996 and 2015 (as per Equation 4-11 and Equation 4-12).

Constraints are described from Equation 4-13 to Equation 4-16. Equation 4-13 allows GWD to oscillate between root depth (RD) and the minimum threshold (MT). RD selection aims to avoid rising groundwater levels that impede root respiration. We adopted an RD of 1.82 m (6 ft) considering the crops in the study area and the root depth guidelines provided by NRCS (2016). The MT was set to avoid undesired effects on the aquifer (CDWR, 2017). We adopted an MT of 160 m after analyzing the MT values for the SWID documented in the Groundwater Sustainability Plan for Kern County (GEI Consultants Inc, 2020). The specified bounds for RD and MT imply that there could be situations where GWD_t assumes these extreme values. Nevertheless, it is unlikely for GWD_t to sustain such extremes over an extended period because maintaining constant extreme values would counter one of the established objectives (Equation 4-5 or Equation 4-6).

Equation 4-14 to Equation 4-16 delineate the constraints governing the fractions ($x_{1,t}$ and $x_{2,t}$). According to these equations, the model considers a finite amount of land and crop areas that can oscillate within established limits. The bounds for $x_{1,t}$ and $x_{2,t}$ stem from the analysis of historical records on annual and perennial crop areas, which were sourced from the C2VSimFG1.01 and the Kern County databases (Kern County Department of Agriculture and Measurement Standards, 2015). Equation 4-16 places restrictions on the fluctuations of perennial crops, ensuring they do not deviate by more than 30% from their values at the preceding time step. We used the same databases to define this limit. In essence, the fractions for annual crops can change independently over time, but the fractions associated with perennial crops are temporally interconnected to prevent abrupt changes in cultivated areas.

$$Max\ NR = \frac{1}{T} * \sum_{t=1}^{T} NR_t$$ Equation 4-5

$$Min\ GWD = \frac{1}{T} * \sum_{t=1}^{T} GWD_t$$ Equation 4-6

Where:

$$NR_t = AA_t * \overline{NRA} + PA_t * \overline{NRP}$$ Equation 4-7

$$GWD_t = GWD_o + \sum_{t=1}^{T} \Delta GWD_t$$ Equation 4-8

$$\Delta GWD_t = LSTME\ (static\ parameters, P_{t-12\sim t}, SWD_{t-12\sim t}, AWD_{t-12\sim t})$$ Equation 4-9

$$AWD_t = AA_t * \overline{WDA_t} + PA_t * \overline{WDP_t}$$ Equation 4-10

$$AA_t = x_{1,t} * \overline{AA}$$ Equation 4-11

$$PA_t = x_{2,t} * \overline{PA}$$ Equation 4-12

Subject to:

$$RD \leq GWD_t \leq MT$$ Equation 4-13

$$0.45 \leq x_{1,t} \leq 1.4$$ Equation 4-14

$$0.65 \leq x_{2,t} \leq 1.6$$ Equation 4-15

$$0.7 * x_{2,t-1} \leq x_{2,t} \leq 1.3 * x_{2,t-1}$$ Equation 4-16

In this research, an operational policy is a way to operate SWID under forecasted climatic conditions from 2020 to 2040 as a function of annual and perennial crop areas. In practical terms, it is a matrix that combines the two-time series, x1 and x2. Also, an operating policy is feasible if all fractions $x_{1,t}$ and $x_{2,t}$ adhere to the specified constraints. Nonetheless, the feasibility of a policy does not necessarily imply its optimality. Therefore, a policy is deemed optimal when it successfully achieves the stated objectives and satisfies the constraints. In this study, rather than employing Dynamic Programming (DP) to identify policies, we formulated an optimization problem that simultaneously addresses all fractions that make up the time series, x1 and x2. In other words, while DP involves decision-making stage-wise (Feng et al., 2023; Yakowitz, 1982), our approach, called Bayesian Optimization Programming (BOP), finds all fractions $x_{1,t,}$ and $x_{2,t}$ at the same time by solving the problem described from Equation 4-5 to Equation 4-16 through Bayesian optimization. Another difference from the DP approach is our use of continuous decision variables. In contrast, DP usually discretizes variables (Herman et al., 2020), limiting the options for choosing the best policies.

The solutions to our optimization problem live in a multidimensional space with *ND* dimensions, encompassing the various components constituting a policy. *ND* can be calculated as the product between the number of time series and the number of time windows. For example, if the fractions that make up the decision variables change every five years, as seen in Figure 4-4, then ND amounts to eight (from $x_{1,2025}$ to $x_{2,2040}$). To calculate fractions within each time window, we use linear interpolation. For the 5-year windows example, fractions $x_{1,2027}$ and $x_{2,2027}$ result from linear interpolation between the 2025 and 2030 fractions.

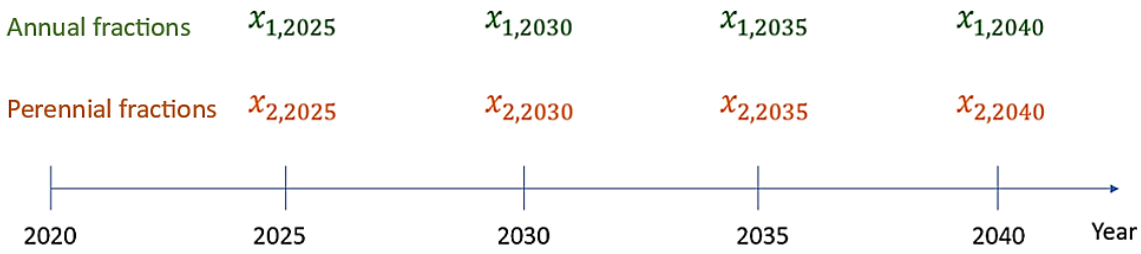

Figure 4-4. Fractions for annual and perennial crops considering a 5-year time window. Each decision variable or time series has four fractions.

Bayesian optimization was used to identify the policies that are part of the Pareto front, called optimal policies, since evaluating all possible combinations of $x_{1,t,}$ and $x_{2,t}$ is impossible, resulting in the well-known curse of dimensionality (Powell, 2007). For example, if the fractions ($x_{1,t,}$ or $x_{2,t}$) adopt the same number of values at each time step, the number of policies (NP) required to define the Pareto front can be calculated using the following equation:

$$NP = (a * b)^{m+1} \quad \text{Equation 4-17}$$

Where *a* and *b* represent the number of values that the fractions $x_{1,t,}$ and $x_{2,t}$ can adopt, respectively, and *m* is the number of time windows. In this way, for the example described in Figure 4-4, if each fraction can take only three values, almost 59,000 policies are needed to evaluate to create the Pareto Front. However, if we allow each variable to take five values ($a=b=5$) and increase the number of windows to ten (changes every two years), $2.38x10^{15}$ policies should be evaluated. Although the number of policies to be assessed is enormous in the latter case, exploring the fractions domain remains limited because we only explore five values per variable by time step. Here, we explore the decision variables x_1 and x_2 in a continuous space every two years from 2020 to 2040. Therefore, the solutions to our optimization problem exist within a 20-dimensional space (ND=20).

4.4.1 Bayesian optimization algorithm

The procedure to identify operational policies through Bayesian optimization consisted of six steps. First, 10,000 operating rules that met the constraints (from Equation 4-13 to Equation 4-16) were randomly generated. For each of these operating rules, the average net revenue and depth to groundwater were calculated during the 20 years of analysis (2020 to 2040). Second, two GPs were trained to emulate each of the stated objectives. Third, from these GPs, the mean and variance values were calculated for a set of auxiliary operating rules to expand the solution space exploration. At this stage, the variances were calculated using Equation 4-1. Fourth, through the EHVI acquisition function, a score was assigned to each operating rule, representing how useful the auxiliary rule is in meeting the objectives and minimizing the variance (Nguyen, 2023). Since the EHVI indicates the contribution of each auxiliary rule in increasing the area under the Pareto front when both objectives are subject to maximization, it was necessary to transform the

objective described by Equation 4-6 from minimization to maximization by a simple multiplication by negative one. Fifth, the rule that contributes the most to the increase in EHVI is added to the set of initial rules, so the number of initial rules is now 10,001. Implementing stages one to five was named New Rule Addition Cycle (NRAC). Here, the NRAC was repeated 5,000 times after observing that the EHVI values did not increase beyond this number of iterations.

4.5 Results and discussion

To obtain the Pareto front and optimal SWID operation policies, we use the BoTorch library developed by the Facebook Artificial Intelligence Research (FAIR) lab (Balandat et al., 2020). With BoTorch, we performed 5,000 evaluations of the objective functions (number of queries), with ten restarts per query to prevent the algorithm from getting stuck in local optima. Furthermore, 10,000 samples were generated to explore the decision space before starting the optimization algorithm. Generating 15,000 samples for a 20-dimensional space is equivalent to randomly sampling each variable 750 times within the ranges defined by Equation 4-14 and Equation 4-15.

Figure 4-5 shows the Pareto front for the two defined objectives: maximization of average farmers' Net revenue and minimization of average depth to groundwater from 2020 to 2040. Regarding Net revenue on the horizontal axis, a favorable decision is preferable when points are situated farther to the right, indicating a higher annual profit for farmers. Alternatively, the average depths to groundwater should be positioned towards the top of the figure due to the vertical axis inversion, ensuring low GWDs. In the same figure, dominated solutions are gray, while the points on the Pareto front are found in other colors. The Pareto front points were classified into three categories using the k-means clustering algorithm. In this way, the points with low net revenue and low depths are in green (upper-left cluster), those with high net revenue and high depths are in blue (lower-right cluster), and those with medium net revenue and depths are in orange (intermediate cluster). Also, numbers from one to seven, close to the Pareto front, identify each cluster's extreme points and midpoints. Finally, for points over the Pareto front, the average GWD ranges between 93.0 and 116.6 m, while the average net revenue is between 49.9 and 70.6 million dollars annually. Observe that the GWDs of the Pareto front correspond to average depths as defined in Equation 4-6. Additionally, these depths consistently adhere to the constraints outlined in Equation 4-13, ensuring that the GWD_t values fall within the range of 1.82 to 160 m. Variations of the optimal decisions for each cluster over time are shown in Figure 4-7 and discussed in the following paragraphs.

The objectives along the Pareto front can be rewritten as stated by Equation 4-18, where GWD is the average depth to groundwater (in meters), and NR is the average net revenue (in millions of dollars per year). The R-squared for that equation is 0.99, and the Root Mean Square Error (RMSE) is 0.68 m. According to Equation 4-18, GWD increases quadratically as a function of NR for points over the Pareto front.

$$GWD = 6.07 * 10^{-2} * NR^2 - 6.19 * NR + 251.03 \quad \text{Equation 4-18}$$

On the other hand, the scarcity of points on the Pareto front (nine points) comes from various factors. The endeavor to reconcile two conflicting objectives limits the number of viable solutions, given that optimizing one objective compromises the other. Tackling a 20-dimensional

optimization problem poses a formidable challenge since identifying the set of 20 values that satisfy the constraints and optimize the objectives is demanding. Finally, our optimization problem constraints significantly limit the solution space since they not only restrict the fraction values (Equation 4-14 and Equation 4-15) but also govern the temporal interactions among the fractions (Equation 4-16) and the possible outcomes for depths (Equation 4-13).

The Bayesian optimization algorithm detailed in section 4.4.1 was run twice for result verification. This procedure was conducted on a computer with the following characteristics: Processor Intel(R) Core(TM) i7-9700 3.00GHz CPU, 16GB of RAM, and 1 TB NVMe Solid State Drive. Each of the two runs of the Bayesian optimization algorithm spanned a week and involved 10,000 initial operating rules and 5,000 NRACs. Despite the random generation of the 10,000 initial operating rules, the Pareto front results remained consistent in both cases, generating only nine points. However, the two runs of the Bayesian optimization algorithm do not provide insights into potential intermediate solutions between the Pareto front points illustrated in Figure 4-5. Consequently, future research should run the Bayesian optimization algorithm multiple times to uncover any intermediate solutions. As highlighted by C. Zhang et al. (2022), the Pareto front in real-world applications may exhibit discontinuities, as seen in Figure 4-5, due to constraints, problem complexity, and discontinuities in the search space.

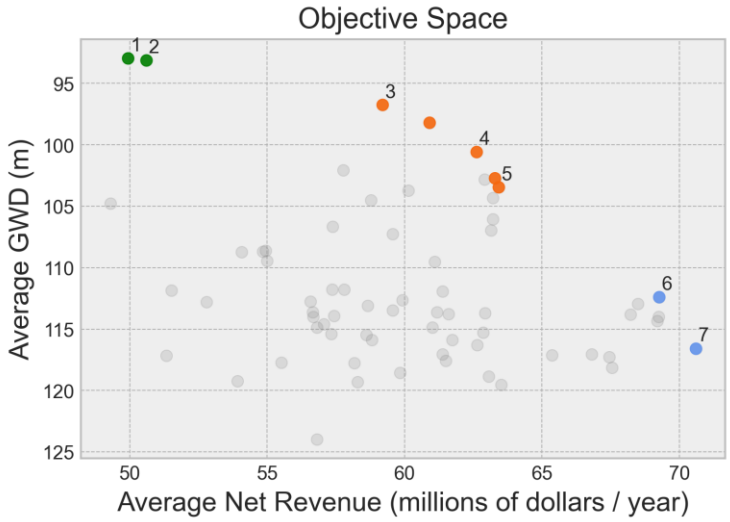

Figure 4-5. Pareto front considering two objectives: maximization of average farmers' net revenue and minimization of average depth to groundwater from 2020 to 2040. The gray dots represent dominated solutions, while the colored dots indicate points on the Pareto front or non-dominated solutions. The numbers near the Pareto front correspond to the extreme and medium points for the three defined clusters.

The Pareto front solution emphasizes the tradeoff between the two objectives. Figure 4-5 depicts an increase in net revenue corresponding to higher depths to groundwater. This correlation implies that farmers must utilize available water resources to maximize profits, resulting in increased groundwater use, as shown in point 7 in Figure 4-5. Moreover, the Pareto front highlights the need for conjunctive water use reductions via reduced irrigated land to contribute to aquifer recovery, as seen in point 1 in Figure 4-5. Transitioning from a scenario where economic

benefits prevail (point 7 in Figure 4-5) to one where aquifer preservation becomes the priority (point 1 in Figure 4-5) entails a $20.7 million reduction in profits and 23.6 m of aquifer recovery regarding point 7.

Figure 4-6 illustrates the Net Revenue Loss (*NRloss*) resulting from aquifer recovery, measured in millions of dollars per meter. These values were computed using Equation 4-19, with point 7 of the Pareto front as a reference due to its highest net revenue and Depth to groundwater (GWD). In that equation, *NR* refers to net revenue, *GWD* to Depth to groundwater, and the subindex *i* to the points shown in Figure 4-5. For instance, reaching point 1 on the Pareto front corresponds to a *NRloss* of 0.87 million dollars per meter of aquifer recovery. Upon careful analysis of Figure 4-6, we opted for point 3 as an intermediate solution between points 1 and 7. Despite the similar *NRloss* values within the central cluster (orange bars in Figure 4-6), point 3 stands out for a superior aquifer recovery (See Figure 4-5). Therefore, for those who find the profit reduction from point 7 to point 1 too drastic, point 3 offers an intermediate alternative. At point 3, net revenue is $59.2 million, with a GWD of 96.7 m. Thus, moving from point 7 to point 3 implies a profit decrease of $11.4 million while simultaneously achieving a 19.9 m aquifer recovery (*NRloss=0.57*). Therefore, point 3 represents a balanced approach, with an intermediate level of profit but substantial aquifer restoration.

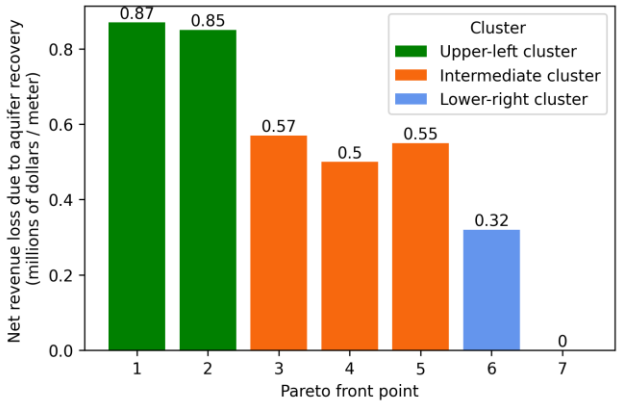

Figure 4-6. Net revenue loss due to aquifer recovery in millions of dollars per meter.

$$NR_{loss} = \frac{NR_7 - NR_i}{GWD_7 - GWD_i} \qquad \text{Equation 4-19}$$

Figure 4-7 illustrates the trajectories taken by x_1, x_2, net revenue, and GWD for the points and clusters identified along the Pareto front, as presented in Figure 4-5. To break it down, the green-shaded regions in the left column of Figure 4-7 correspond to the points of the same color in Figure 4-5. Likewise, the orange-shaded areas in the central column represent the points in the middle cluster, while the blue areas in the right column indicate the lower-right cluster of Figure 4-5. Furthermore, within each panel of Figure 4-7, there are three distinct colored lines: green, orange, and blue. Green lines signify the points within each cluster with the lowest net revenue and GWD, specifically points 1, 3, and 6, as seen in Figure 4-5. The orange lines correspond to

the trajectory nearest to the centroid of each cluster, aligning with point 4 along the Pareto front. Lastly, the blue lines pertain to the points within each cluster with the highest net revenue and GWD: points 2, 5, and 7. For example, the green line in the upper-left panel of Figure 4-7 (annual crops – upper left cluster) represents the temporal changes in the fraction of annual crops for point 1 in Figure 4-5. Similarly, the blue line in the lower-right panel (GWD – lower right cluster) illustrates the GWD for point 7 in Figure 4-5.

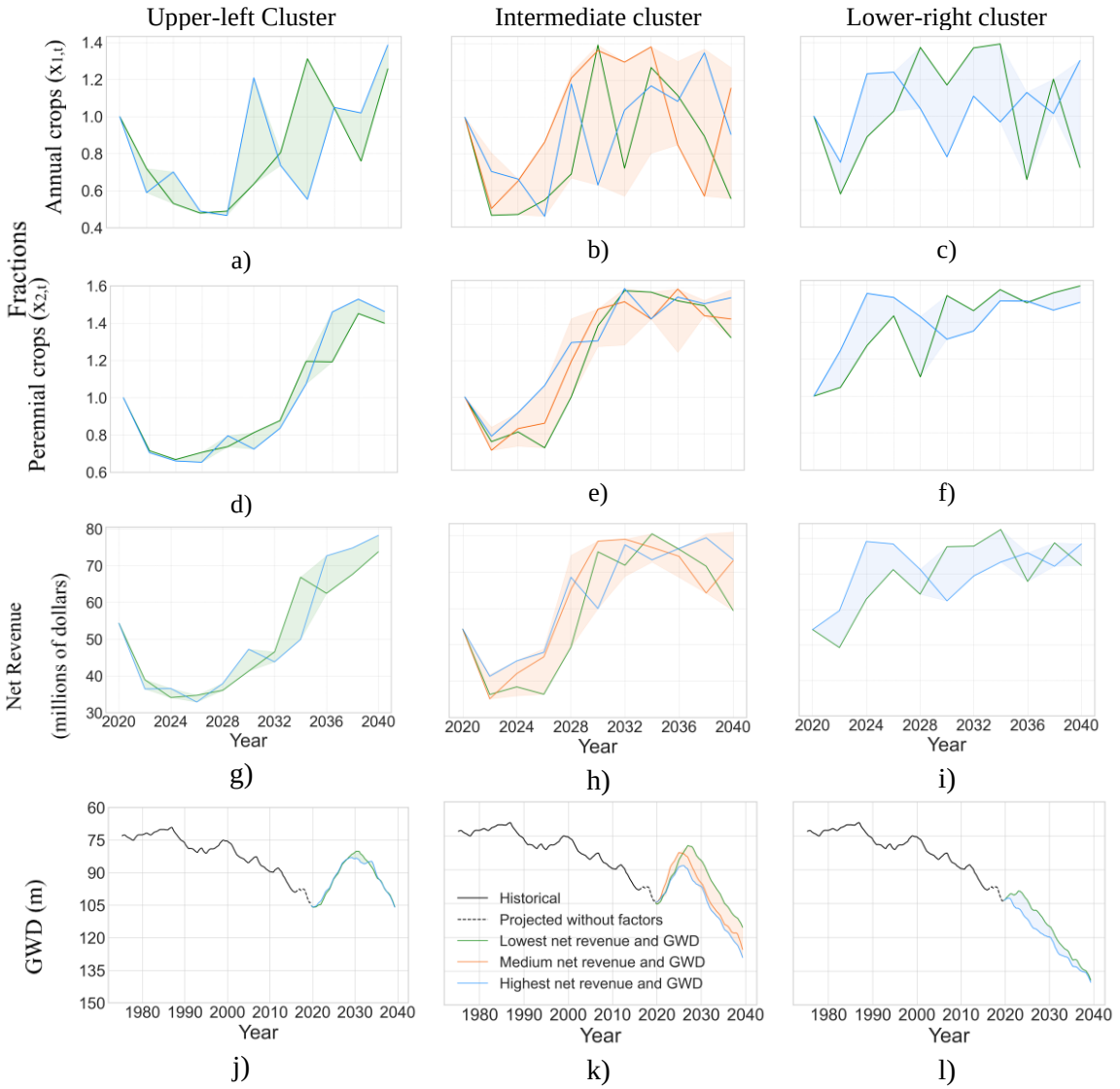

Figure 4-7. Trajectories of the Pareto front points grouped by variable (row) and cluster (column). Shaded areas delimit the minimum and maximum values per variable and cluster. Lines depict the trajectories followed by the cluster's representative points.

In Figure 4-7, trajectories for the same variable and different clusters are conveniently placed alongside each other in the same row. This arrangement allows us to assess the similarities in trajectories and the spatial regions covered by them. First, to evaluate the similarity among trajectories within the same cluster, we examine the size of the shaded areas. Narrow areas

indicate trajectories closely resembling each other, while broader areas suggest significant variability within the same cluster. As depicted in the left column of Figure 4-7, the green areas are notably narrow. This is because the upper-left cluster comprises only two points from the Pareto front close to each other. In contrast, the broader shaded areas belong to the intermediate cluster, encompassing five points from the Pareto front. Lastly, for the lower-right cluster, which includes two points, the shaded regions exhibit a moderate size or level of variability among the trajectories because the points are not close. Secondly, we investigate whether the trajectories of each cluster cover distinct regions of the solution space by analyzing what occurs when we superimpose the shaded areas of the same row. When the superimposed areas overlap, it becomes evident that the compared clusters share some solutions within the decision space. The row-by-row analysis of Figure 4-7 indicates that all clusters share common regions in the solution space, suggesting no discernible relationship between the clusters and the specific areas they occupy within the solution space.

Upon analyzing the panels of Figure 4-7 by columns, a discernible pattern emerges. Initially, there is a reduction in annual and perennial crop areas, contributing to a decline in net revenue and promoting aquifer recovery. Subsequently, the model expands crop areas, increasing profits but decreasing depth to groundwater. If, on the contrary, crop areas follow an opposite trend—larger initially and smaller towards the end—the net revenues would remain constant. However, the average GWD would be higher due to an initial drop followed by a subsequent rise. Therefore, the observed policies ($x_{1,t}$ and $x_{2,t}$ temporal distribution) effectively address groundwater level restrictions, ensuring sustainable water use between 2020 and 2040. A new pattern emerges when comparing fractions of annual and perennial crops within the same cluster (comparing the first two rows of Figure 4-7). The trajectories of annual crops exhibit more abrupt jumps from one year to the next, showcasing the flexibility of this crop type in achieving the proposed objectives. In contrast, the trajectories of permanent crops follow a more consistent pattern, lacking unexpected changes from one year to the next, aligning with the constraints set by Equation 4-16. Hence, the model encourages conjunctive water use by leveraging surface water deliveries in the initial years to recharge the aquifer, subsequently utilizing aquifer water for agricultural production.

However, a limitation in our model is evident—the trends of annual and permanent crops are similar. Thus, when the areas dedicated to annual crops increase, the areas allocated to permanent crops rise, and vice versa. This situation limits the validity of our results because perennial crops have shown an increasing trend over the last three decades, while annual crops have tended to decrease (Mall & Herman, 2019). Another limitation of our model arises when the fractions of permanent crops ($x_{2,t}$) are positive, resulting in a sudden increase in areas filled with fully grown plants. This situation diverges from reality, as the expansion of planting areas typically involves the presence of young plants with lower water demands. Nonetheless, the solutions presented here consistently adhere to the SGMA requirements, preserving the GWD above the specified minimum threshold of 160 m.

As mentioned in section 4.4, an operational policy describes how maximize profits and minimize the depth to groundwater based on the areas of annual and perennial crops and the expected climatic conditions from 2020 to 2040. Here, we focus on the three operational policies described by points 1, 3, and 7 of the Pareto front (Figure 4-5). Points 1 and 7 are our initial selections, as they represent the extremes of the Pareto front. Point 1 underscores the prioritization of groundwater depletion avoidance, while point 7 signifies putting more weight on economic goals. In contrast, point 3 represents the central cluster's upper-left point, which boasts a significant aquifer recovery despite its moderate net revenue. This suggests that allowing a marginal decrease in net revenue may substantially improve depth to groundwater.

Point 1 of the Pareto front is represented by green lines in the left panels of Figure 4-7. In most cases, the fractions $x_{1,t,}$ and $x_{2,t}$ tend to be less than one, reducing crop areas. As anticipated, reducing crop areas leads to declining net revenue, as shown by the green line at the bottom of Figure 4-7 g. Also, the hypothesis that the aquifer recovery depends on crop reduction is verified in Figure 4-7 j, where the groundwater level corresponding to point 1 (green line) generates the lowest GWD.

On the contrary, in the right panels of Figure 4-7, the blue lines represent the trajectories that lead to point 7 of the Pareto front. In terms of annual crops, depicted in Figure 4-7c, the $x_{1,t}$ fractions exhibit oscillations between the maximum and minimum values within the cluster (blue area). These oscillations illustrate the flexibility of annual crops. Meanwhile, Figure 4-7f shows that the fractions of perennial crops, $x_{2,t}$, generally tend to be the largest within the cluster over time. This situation results in net revenues (Figure 4-7 i) that follow a similar trajectory as the perennial crops, with only minor decreases from reductions in the areas allocated to annual crops. However, it's important to note that the high water consumption associated with perennial crops impacts aquifer levels, as shown by the blue line in Figure 4-7 l, where the aquifer levels tend to be the lowest. In sum, the charts in the right panel of Figure 4-7 further emphasize that groundwater levels tend to decrease as crop areas increase.

As mentioned above, point 3 of the Pareto front constitutes a decision balancing farming economic goals and aquifer recovery. Trajectories that give rise to point 3 appear in the central column of Figure 4-7, described by the green lines over orange areas. During the simulation's last ten years, the model tended to increase crop areas, which promoted increased profits and decreased aquifer levels. In the second decade (2030 - 2040), the model increasingly turning to groundwater as their primary water source due to the plentiful availability of groundwater and a decrease in surface water.

The GWD projections from 2020 to 2040 show a noticeable aquifer recovery in the initial years, followed by a subsequent rise in depths (Figure 4-7 j, k, and l). This situation originates from the fact that the highest precipitation and Surface Water Deliveries (SWD) are observed at the beginning of the simulation, as observed in Figure 4-8. After aquifer recovery, the model begins to extract groundwater, considering that the water inputs are insufficient to satisfy the objectives. On the other hand, our projected GWDs range between the levels outlined in the Shafter-Wasco ID Groundwater Sustainability Plan (GSP) between 2020 and 2040 (GEI Consultants Inc, 2020). In that GSP, GWDs fluctuate between 88.1 and 136.9 m, as shown in Figure 4-9, where six monitoring were analyzed. The depths shown in Figure 4-9 reflect the minimum and maximum value projected between 2020 and 2040 considering six models: Baseline, Baseline with projects, 2030 Baseline, 2030 with projects, 2070 Baseline, and 2070 with projects (GEI Consultants Inc, 2020).

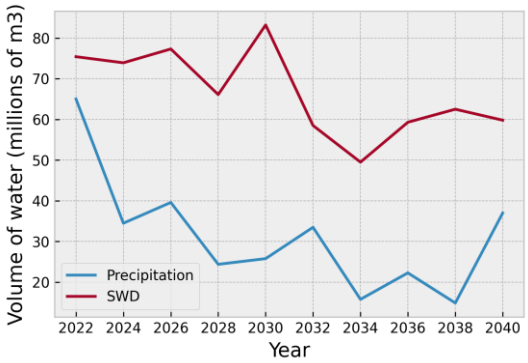

Figure 4-8. Annual variation of precipitation and surface water deliveries (SWD) for Shafter-Wasco Irrigation District.

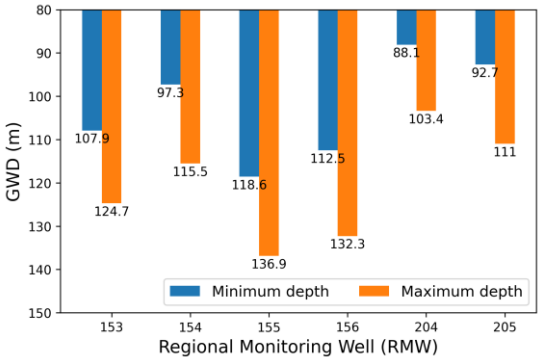

Figure 4-9. Projected GWD from 2020 to 2040 for different C2VSimFG-Kern model scenarios. Adapted from GEI Consultants Inc (2020)

Figure 4-10 describes how the optimal operating policies behave biannually from 2022 to 2040. In this figure, the colored trajectories result from connecting through straight segments the values that the four variables, x_1, x_2, *GWD*, and Net revenue, take for a particular year and a specific point on the Pareto front. The axes of the fractions $x_{1,t}$ and $x_{2,t}$ ascend vertically, with the top representing the highest proportions of crop areas. However, the GWD axis has been reversed to facilitate results interpretation. Thus, the greatest depths are at the bottom of the graph. All variables have been adjusted to have zero mean and one standard deviation. This makes it easier to compare variables and trajectories. The lines' colors depend on the net revenue, so warm colors indicate net revenue (NR) above its average from 2020 to 2040, and cold colors indicate NR below the average. In Figure 4-10, there are 90 trajectories. This number is determined by multiplying the number of points on the Pareto front (nine) by the ten possible values each variable can take from 2022 to 2040 in biannual increments. The results show that net revenues tend to be high (red lines) when the fractions of annual and perennial crops are high, and GWD is low. On the other hand, when the crop areas are low, the net revenues are low (blue lines), and the GWD tends to increase.

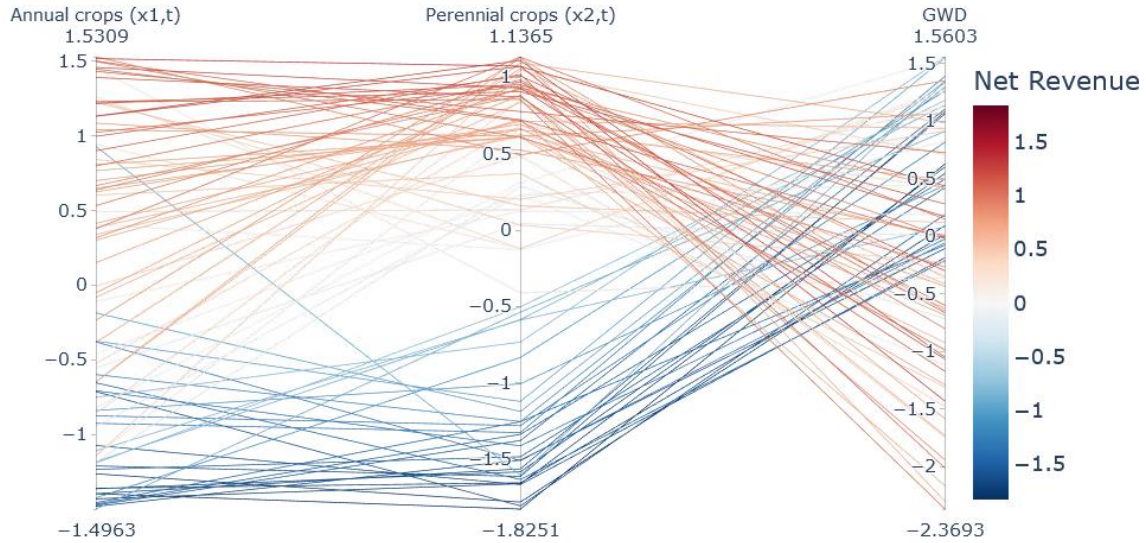

Figure 4-10. Biannual behavior of the operational policies for the Shafter-Wasco Irrigation District. All variables are standardized (mean zero, standard deviation one). The parallel axis includes annual crop fractions ($x_{1,t}$), perennial crop fractions ($x_{2,t}$), and depth to groundwater (GWDt). Warm colors indicate net revenue (NR) above its average from 2020 to 2040, and cold colors indicate NR below the average.

4.6 Conclusions

Our research employed an integrated water management framework comprising surface and groundwater hydrology elements and agricultural production. Through Bayesian Optimization Programming (BOP), simulation and optimization were combined to determine the best policies. The employed BOP uses perfect foresight by simultaneously optimizing all variables for all periods, evaluating their performance collectively, and guiding the decision search process using Bayesian Optimization. Through this approach, we successfully identified operational policies that maximize farmers' net revenue and minimize depth to groundwater. To validate the effectiveness of the BOP approach, we selected the Shafter-Wasco irrigation district (SWID). This district relies on groundwater from one of California's overexploited basins and faces potential impacts on its future water supply due to climate change.

We defined an operational policy as maximizing profits and minimizing the depth to groundwater based on the areas of annual and perennial crops and the expected climatic conditions from 2020 to 2040. Also, a policy was deemed optimal when it successfully met the stated objectives and satisfied the constraints. We formulated an optimization problem with two objectives, two decision variables, and four constraints to determine the optimal policies. The proposed objectives aimed to maximize the average net revenue and minimize the average depth to groundwater between 2020 and 2040. The two decision variables, x_1 and x_2, represent the proportions of annual and perennial crops. The four constraints limit the fractions of annual and perennial crops and groundwater levels to meet SGMA requirements. Also, we employed the Global Climate Model called CanESM2 under the intermediate greenhouse gas and aerosol emissions scenario, RCP 4.5, to simulate future climate conditions. The Long Short-Term Memory Emulator (LSTME), introduced in Chapter 2, facilitated the estimation of depth to groundwater, while CALFEWS was employed for estimating surface water deliveries.

Instead of using the commonly employed NSGA-II algorithm, we utilized Bayesian Optimization for solving the multiobjective optimization problem. This decision was motivated by the fact that while NSGA-II is more straightforward to understand and implement, Bayesian Optimization proves to be more efficient in navigating the solution space with fewer iterations. This efficiency is particularly advantageous in scenarios like the one presented here, where we explore the decision variables x_1 and x_2 in a continuous space every two years from 2020 to 2040, resulting in a 20-dimensional solution space. The enhanced efficiency of Bayesian Optimization translates to significant time and cost savings, especially when dealing with computationally expensive objective functions such as the Long Short-Term Memory Emulator (LSTME) developed in Chapter 2.

The Pareto front highlights tradeoffs between farming profits and aquifer recovery. Shifting from a scenario where economic gains are prioritized (point 7 in Figure 4-7) to one that prioritizes aquifer preservation (point 1) leads to a $20.7 million profit reduction, resulting in a 23.6 m aquifer recovery. However, for those who find the profit reduction from point 7 to point 1 too extreme, point 3 in Figure 4-7 presents an appealing option. It boasts a net revenue of $59.2 million and a depth to groundwater of 96.7 m. Transitioning from point 7 to point 3 involves a profit decrease of $11.4 million while simultaneously achieving a 19.9 m aquifer recovery. Hence, point 3 represents a balanced approach between profit and aquifer restoration. In sum, the Pareto front highlights the need for conjunctive water use reductions via reduced irrigated land to contribute to aquifer recovery.

The method proposed in this study should be viewed more as an academic exercise than as a practical guide for operating the Shafter-Wasco Irrigation District, as certain crucial aspects were not considered. First, the research does not simulate how farmers make decisions regarding economic or climate factors. Additionally, the categorization of crops at the Shafter-Wasco Irrigation District was relatively broad, and it is suggested that more specific categories be included in future research. Also, it is recommended that surface water and groundwater costs be differentiated in future research. Furthermore, it would be worthwhile to use alternative global climate models (GCMs) and representative concentration pathways (RCPs) to identify additional optimal policies. Last, our model could not capture the growth trend of perennial crops and the decline of annual crops over the last decades.

Despite the limitations of the proposed model, it effectively captures the dynamics of depth to groundwater and net revenue in response to changing climatic conditions. The model responds to high surface water deliveries and precipitation by projecting aquifer recharge, while it turns to groundwater use when surface water supply diminishes. Additionally, the model demonstrates flexibility in managing annual crops, allowing for adjustments based on climatic conditions. Another crucial aspect of this research is its insight into the cost of avoiding aquifer depletion, as the metric *NRloss* indicates. Finally, the solutions generated by the model consistently meet the Sustainable Groundwater Management Act (SGMA) requirements, ensuring that the Depth to groundwater (GWD) remains above the specified minimum threshold of 160 meters.

4.7 References

Alam, S., Gebremichael, M., Li, R., Dozier, J., & Lettenmaier, D. P. (2019). Climate change impacts on groundwater storage in the Central Valley, California. *Climatic Change*, *157*(3–4), 387–406. https://doi.org/10.1007/s10584-019-02585-5

Balandat, M., Karrer, B., Jiang, D. R., Daulton, S., Letham, B., Wilson, A. G., & Bakshy, E. (2020). BOTORCH: A framework for efficient Monte-Carlo Bayesian optimization. *Advances in Neural Information Processing Systems*, *2020-Decem*(MC).

Bradford, E., Schweidtmann, A. M., Zhang, D., Jing, K., & del Rio-Chanona, E. A. (2018). Dynamic modeling and Optimization of sustainable algal production with uncertainty using multivariate Gaussian processes. *Computers and Chemical Engineering*, *118*(2018), 143–158. https://doi.org/10.1016/j.compchemeng.2018.07.015

Branke, J., Deb, K., Miettinen, K., & Slowinski, R. (Eds.). (2008). *Introduction to Multiobjective optimization: Interactive Approaches*.

Bureau of Reclamation. (2022). *Biden-Harris Administration Invests More Than $84 million in 36 Drought Resiliency Projects*. 12/22/2022. https://www.usbr.gov/newsroom/news-release/4395

Sustainable Groundwater Management Act (SGMA), (2014).

CDWR. (2017). *Best management practices for the sustainable management of groundwater. Sustainable Management Criteria (draft)*.

CEC, C. E. C., & GIF, G. I. F. (2011). *Cal-Adapt*. https://cal-adapt.org/

Deb, K., & Jain, H. (2014). An evolutionary many-objective optimization algorithm using reference-point-based nondominated sorting approach, Part I: Solving problems with box constraints. *IEEE Transactions on Evolutionary Computation*, *18*(4), 577–601. https://doi.org/10.1109/TEVC.2013.2281535

Deb, K., Pratap, A., Agarwal, S., & Meyarivan, T. (2002). A fast and elitist multiobjective genetic algorithm: NSGA-II. *IEEE Transactions on Evolutionary Computation*, *6*(2), 182–197. https://doi.org/10.1109/4235.996017

Famiglietti, J. S. (2014). The global groundwater crisis. *Nature Climate Change*, *4*(11), 945–948. https://doi.org/10.1038/nclimate2425

Faunt, C. C. (2009). *Groundwater Availability of the Central Valley Aquifer , California*.

Faunt, C. C., Sneed, M., Traum, J., & Brandt, J. T. (2016). Water availability and land subsidence in the Central Valley, California, USA. *Hydrogeology Journal*, *24*(3), 675–684. https://doi.org/10.1007/s10040-015-1339-x

Fawzy, S., Osman, A. I., Doran, J., & Rooney, D. W. (2020). Strategies for mitigation of climate change: a review. *Environmental Chemistry Letters*, *18*(6), 2069–2094. https://doi.org/10.1007/s10311-020-01059-w

Feng, Z., Luo, T., Niu, W., Yang, T., & Wang, W. (2023). A LSTM-based approximate dynamic programming method for hydropower reservoir operation optimization. *Journal of Hydrology*, *625*(PA), 130018. https://doi.org/10.1016/j.jhydrol.2023.130018

Frazier, P. I. (2018). Bayesian Optimization. *INFORMS TutORials in Operations Research*, *October*, 9–11. https://doi.org/https://doi.org/10.1287/educ.2018.0188

GEI Consultants Inc. (2020). *Groundwater Sustainability Plan. Kern County, CA*.

GEI Consultants. Inc. (2022). *North Kern WSD and Shafter-Wasco ID managment area plan* (Issue July). https://kerngwa.com/wp-content/uploads/2022/07/nkwsd-swid-mgmt-area-plan_amended-clean.pdf

Gorelick, S. M., & Zheng, C. (2015). Global change and the groundwater management challenge. *Water Resources Research*, *51*, 3031–3051. https://doi.org/doi:10.1002/ 2014WR016825

Haasnoot, M., Middelkoop, H., Beek, E. Van, & Deursen, W. P. A. Van. (2011). A Method to Develop Sustainable Water Management Strategies for an Uncertain Future. *Sustainable Development*, *19*, 369–381. https://doi.org/10.1002/sd.438

Hallegatte, S., Shah, A., Lempert, R., Brown, C., & Gill, S. (2012). *Investment Decision Making under Deep Uncertainty* (Issue September).

Herman, J. D., Quinn, J. D., Steinschneider, S., Giuliani, M., & Fletcher, S. (2020). Climate Adaptation as a Control Problem: Review and Perspectives on Dynamic Water Resources Planning Under Uncertainty. *Water Resources Research*, *56*(2). https://doi.org/10.1029/2019WR025502

Kern County Department of Agriculture and Measurement Standards. (2015). *Kernag*. http://www.kernag.com/gis/gis-data.asp

Loucks, D. P., & Beek, E. van. (2017). Water Resource Systems Planning and Management: An Introduction to Methods, Models, and Applications. In *Advances in Water Resources* (1st ed.). Springer Cham. https://doi.org/https://doi.org/10.1007/978-3-319-44234-1

Majedi, H., Fathian, H., Nikbakht-shahbazi, A., Zohrabi, N., & Hassani, F. (2021). Multi-Objective Optimization of Integrated Surface and Groundwater Resources Under the Clean Development Mechanism. *Water Resources Management*, 2685–2704. https://doi.org/10.1007/s11269-021-02860-0

Manoj, A., Miriyala, S. S., & Mitra, K. (2022). Multiobjective Bayesian Optimization for Computationally Expensive Reaction Network Models. *2022 8th Indian Control Conference, ICC 2022 - Proceedings*, *Icc*, 428–433. https://doi.org/10.1109/ICC56513.2022.10093513

Mathern, A., Steinholtz, O. S., Sjöberg, A., Önnheim, M., Ek, K., Rempling, R., Gustavsson, E., & Jirstrand, M. (2021). Multiobjective constrained Bayesian optimization for structural design. *Structural and Multidisciplinary Optimization*, *63*(2), 689–701. https://doi.org/10.1007/s00158-020-02720-2

Nematollahi, Z., Reza, H., & Sanayei, Z. (2023). Developing an optimized groundwater exploitation prediction model based on the Harris hawk optimization algorithm for conjunctive use of surface water and groundwater resources. *Environmental Science and Pollution Research*, 16120–16139. https://doi.org/10.1007/s11356-022-23224-0

Nguyen, Q. (2023). *Bayesian Optimization in Action*. Manning.

Nocedal, J., & Wright, S. (2000). *Numerical Optimization* (Second).

NRCS. (2016). Sprinkler Irrigation. In S. Self (Ed.), *National Engineering Handbook* (Issue August). Natural Resources Conservation Service. https://directives.sc.egov.usda.gov/OpenNonWebContent.aspx?content=39754.wba

Østergård, T., Jensen, R. L., & Maagaard, S. E. (2018). A comparison of six metamodeling techniques applied to building performance simulations. *Applied Energy*, *211*(August 2017), 89–103. https://doi.org/10.1016/j.apenergy.2017.10.102

Pierce, D. W., Kalansky, J. F., & Cayan, D. R. (2018). *Climate, Drought, and Sea Level Rise Scenarios for California's Fourth Climate Change Assessment* (Issue CNRA-CEC-2018-006).

Powell, W. (2007). *Approximate dynamic programming: solving the curses of dimensionality*. Wiley & Sons.

Rachmawati, L., & Srinivasan, D. (2006). A Multiobjective Genetic Algorithm with Controllable Convergence on Knee Regions. *2006 IEEE International Conference on Evolutionary Computation*, 1916–1923. https://doi.org/10.1109/CEC.2006.1688541

Rafipour-Langeroudi, M., Kerachian, R., & Bazargan-Lari, M. R. (2014). Developing operating policies for conjunctive use of surface and groundwater considering the water quality issues. *KSCE Journal of Civil Engineering*, *18*(2), 454–461. https://doi.org/10.1007/s12205-014-1193-8

Rasmussen, C. (2004). Advanced lectures on machine learning. In O. Bousquet, U. von Luxburg, & G. Rätsch (Eds.), *Zhurnal mikrobiologii, epidemiologii, i immunobiologii* (pp. 63–71).

Saad, S., Javadi, A. A., Chugh, T., & Farmani, R. (2022). Optimal management of mixed hydraulic barriers in coastal aquifers using multiobjective Bayesian Optimization. *Journal of Hydrology*, *612*(PA), 128021. https://doi.org/10.1016/j.jhydrol.2022.128021

Sabale, R., Venkatesh, B., & Jose, M. (2023). Sustainable water resource management through conjunctive use of groundwater and surface water: a review. *Innovative Infrastructure Solutions*, *8*(1), 1–12. https://doi.org/10.1007/s41062-022-00992-9

Sepahvand, R., Safavi, H. R., & Rezaei, F. (2019). Multiobjective Planning for Conjunctive Use of Surface and Ground Water Resources Using Genetic Programming. *Water Resources Management*, *33*(6), 2123–2137. https://doi.org/10.1007/s11269-019-02229-4

Sun, A. Y., Wang, D., & Xu, X. (2014). Monthly streamflow forecasting using Gaussian process regression. *Journal of Hydrology*, *511*, 72–81. https://doi.org/10.1016/j.jhydrol.2014.01.023

Taylor, R. G. (2013). Ground water and climate change. *Nature Climate Change*, *3*(November 2012). https://doi.org/10.1038/NCLIMATE1744

Yakowitz, S. (1982). Dynamic programming applications in water resources. *Water Resources Research*, *18*(4), 673–696. https://doi.org/10.1029/WR018i004p00673

Zeff, H. B., Hamilton, A. L., Malek, K., Herman, J. D., Cohen, J. S., Medellin-Azuara, J., Reed, P. M., & Characklis, G. W. (2021). California's food-energy-water system: An open source simulation model of adaptive surface and groundwater management in the Central Valley. *Environmental Modelling and Software*, *141*(April), 105052. https://doi.org/10.1016/j.envsoft.2021.105052

Chapter 5 Conclusions

This study examines the potential impacts of climate change on groundwater and proposes operational policies for managing irrigation districts to ensure farmers' profits while safeguarding aquifers. We developed an emulator for an existing groundwater model, namely C2VSimFG. The model can integrate climate, hydrological, and water distribution components. The emulator reduces computational time and allows exploring a wide range of scenarios. Due to the lower hydrological uncertainties in C2VSim compared to climatic uncertainties and its extended computational time, employing emulators proved to be an efficient strategy. We tested three emulators (MLR, MLP, LSTM) incorporating static and dynamic variables to address spatial and temporal effects. The selected emulator, LSTM, performed best based on the results of the metrics Root Mean Squared Error (RMSE), Nash–Sutcliffe Efficiency coefficient (NSE), and the Kling-Gupta Efficiency coefficient (KGE). Findings using the LSTM emulator supported the hypothesis that climate change would significantly impact groundwater levels in the region compared to a historical climate (1995-2015). However, by implementing appropriate measures (such as reducing crop consumptive use), we demonstrated that achieving sweet spots for both financial and groundwater sustainability is feasible.

In the face of forthcoming challenges, including elevated temperatures and increased variability in precipitation, scientific progress plays a crucial role. Advancements in climatic, hydrological, statistical, and optimization models empower us to forecast and proactively implement effective adaptation strategies. By integrating climate and groundwater monitoring networks, enhancing model accuracy, and utilizing optimization techniques, there is potential to identify practical and economically viable solutions for managing water in irrigation districts. The research presented here is a compelling example of such feasibility in examining operational policies for an irrigation district based on crop areas, groundwater, and climate change projections (Chapter 4). To identify such policies, we had to use advanced optimization techniques (Chapter 4), quantify potential climate change effects on groundwater (Chapter 3), and use reliable and agile models that allowed the simulation of thousands of scenarios (Chapter 2).

On the other hand, while California enjoys a privileged position in terms of information and model availability compared to other regions worldwide, it grapples with unique challenges, as discussed in Chapter 2. This challenge involves identifying optimal ways to couple existing models, reconciling diverse databases and programming languages, and navigating different time and space scales. We overcome those challenges by implementing an emulator for the widely accepted C2VsimFG model.

This work underscores the need for connecting elements within a framework to unveil comprehensive images at a larger scale. Without integrated research efforts, valuable knowledge would remain disjointed, limiting our understanding of the world. In this study, our focus wasn't solely on generating new fragments of knowledge but rather on interconnecting existing elements to attain a more comprehensive and reliable perspective on sustained water resource management. Furthermore, this research demonstrated that coupling these knowledge pieces is not feasible for individuals; it requires collaboration and interdisciplinary expertise.

Some significant findings arise from this work on several fronts.

Our analyses show that the emulators can adequately replicate the change in depth to groundwater as a function of static and dynamic variables to consider space and time interactions. On the one hand, static variables include the geometry of the districts and soil and water characteristics. In

contrast, the dynamic variables include water inflows (precipitation and surface water deliveries), water outflows (agricultural water demand), and changes in groundwater storage. The latter is highly related to the depth to groundwater of the uppermost confined aquifer.

The three emulators consider the effect of previous precipitation, surface water deliveries, and agricultural water demand in estimating the change in depth to groundwater. For this reason, fragments of these time series known as fragment lengths (FL) were shown to the emulators during training. Instead of using an optimization method for the FL definition, FL was estimated by examining a graph termed the Multiple Squared Correlation Function (MSCF), akin to the autocorrelation function utilized in time series analysis. Based on the MSCF analysis encompassing all water districts (as depicted in Figure 2-8 and detailed in Appendix A.4), it was observed that the relevance of the relationship between dynamic variables and change in depth to groundwater extends up to 12 months.

The performance of the analyzed emulators considered credibility, efficacy, and efficiency, facilitating groundwater integration in broader modeling frameworks. Hence, decision-makers will be able to evaluate multiple scenarios relatively simply and accurately without compromising the quality of the results. Besides, our findings indicate that the LSTM is the best emulation alternative because it meets the desired attributes, such as the quality of the outcomes, compared to the other two emulators (MLR and MLP).

In Chapter 3, three scenario groups (BU, IC2D, and IC3D) were proposed to test the hypothesis that climate change may increase aquifer drawdown rates. Such scenarios incept climate change gradually; thus, the BU scenario assumes climate conditions similar to those from 1974 to 2015. In the IC2D scenario, climate change impacts are incorporated into *P* and *SWD*. In contrast, in the IC3D scenario, climate change influences all three variables (*P*, *SWD*, and *AWD*). Also, under a six-GCM ensemble of climate change scenarios, groundwater levels will mainly continue to decline unless agricultural water demand is reduced or recharge augmented. Moreover, results show that groundwater levels would experience a more rapid decline under climate change scenarios compared to historical conditions (1995-2015).

In Chapter 4, we defined an operational policy as maximizing profits and minimizing the depth to groundwater based on the areas of annual and perennial crops and the expected climatic conditions from 2020 to 2040. Therefore, we formulated an optimization problem with two objectives, two decision variables, and four constraints to determine the optimal policies. The two decision variables, fractions of annual and perennial crops, represent the proportions of annual and perennial crops. The four constraints limit the fractions of annual and perennial crops and groundwater levels to meet SGMA requirements. Through Bayesian Optimization Programming (BOP), simulation and optimization were combined to determine the best policies for the Shafter-Wasco Irrigation District. BOP uses perfect foresight by simultaneously optimizing all variables for all periods, evaluating their performance collectively, and guiding the decision search process using Bayesian Optimization. The BOP approach highlights the importance of adapting annual crop management to accommodate changes in climatic conditions. The strategies developed through this approach consistently align with the Sustainable Groundwater Management Act (SGMA) requirements, ensuring that the Depth to groundwater (GWD) in the Shafter-Wasco Irrigation District is maintained above the designated minimum threshold of 160 meters.

The Pareto front highlights tradeoffs between farming profits and aquifer recovery. Shifting from a scenario where economic gains are prioritized (point 7 in Figure 4-7) to one that prioritizes aquifer preservation (point 1) leads to a $20.7 million profit reduction, resulting in a 23.6 m aquifer recovery. However, for those who find the profit reduction from point 7 to point 1 too extreme, point 3 in Figure 4-7 presents an appealing option. It boasts a net revenue of $59.2 million and a depth to groundwater of 96.7 m. Transitioning from point 7 to point 3 involves a profit decrease of $11.4 million while simultaneously achieving a 19.9 m aquifer recovery. Hence, point 3 represents a balanced approach between profit and aquifer restoration.

Despite the limitations of the BOP approach, it effectively captures the dynamics of depth to groundwater and net revenue in response to changing climatic conditions. The model responds to high surface water deliveries and precipitation by projecting aquifer recharge, while it turns to groundwater use when surface water supply diminishes.

5.1 Recommendations and future work

It is crucial to evaluate the LSTM performance in districts within the Central Valley that are distinct from those included in the GKCR to estimate the LSTM's generalization capacity, or what it is the same, the ability to infer behavioral patterns beyond those encountered during training, validation, and testing. Therefore, feeding the LSTM emulator with data from different water districts in the Central Valley spanning from 1974 to 2015 will be necessary. The goal is to compare the emulator's results with those obtained from C2VSimFG, aiming to determine how much the LSTM can replicate C2VSimFG results across diverse districts.

In Chapter 3, we utilized an ensemble of six GCMs and two RCPs to study projected climate impacts on groundwater. However, we only used a hydrological model (C2VSimFG) and a water allocation model (CALFEWS). For future research, we recommend a more comprehensive approach employing ensembles of hydrological models, such as HydroGeoSphere (HGS), the Penn State Integrated Hydrologic Model (PIHM), Modular Groundwater Flow (MODFLOW), and ensembles of water allocation models like CALVIN or CALSIM. This broader approach will provide a more holistic perspective on future groundwater levels because there is uncertainty associated with the climatic data and the results the models can offer regarding the same input values.

During optimal operating policy identification, we employed the Global Climate Model called CanESM2 under the intermediate greenhouse gas and aerosol emissions scenario, RCP 4.5, to simulate future average climate conditions. It is recommended to analyze other Global Climate Models and RCPs to better understand possible policies under different climate scenarios.

Certain crucial aspects must be considered to improve the BOP methodology and validity of its results. Firstly, the research does not simulate how farmers make decisions regarding economic or climate factors. Additionally, the categorization of crops at the Shafter-Wasco Irrigation District was relatively broad, and it is suggested that more specific categories be included in future research. Also, it is recommended that surface water and groundwater costs be differentiated in future research. Furthermore, it would be worthwhile to use alternative global climate models (GCMs) and representative concentration pathways (RCPs) to identify additional optimal policies. Lastly, our model could not capture the growth trend of perennial crops and the decline of annual crops over the last decades. Therefore, additional efforts must be undertaken to solve this critical situation

Appendix A Change in depths to groundwater through deep learning models in agricultural regions, additional information

Appendix A.1 Comparison of standardized water volumes

Wheeler Ridge-Maricopa Water Storage District

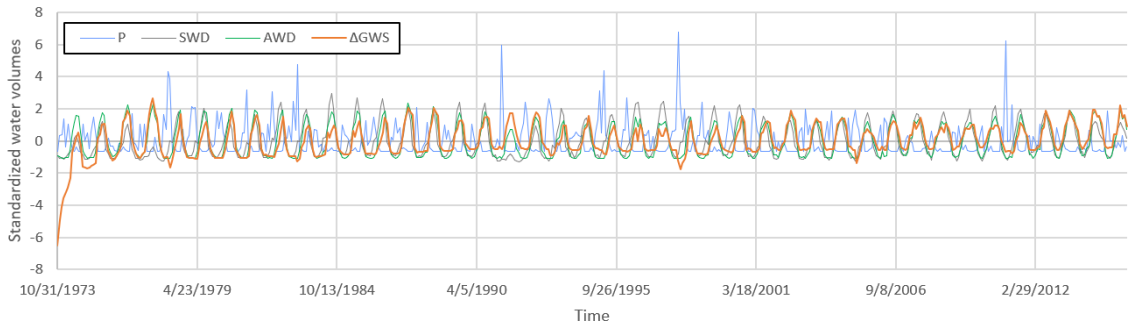

Rosedale-Rio Bravo Water Storage District

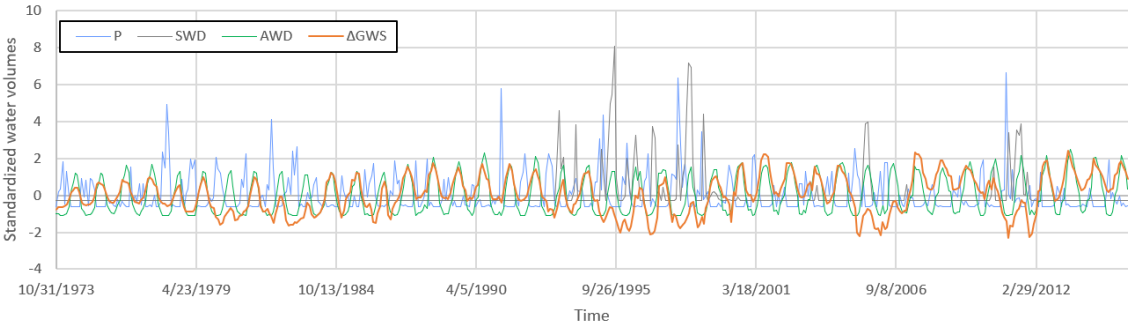

Southern San Joaquin Municipal Utility District

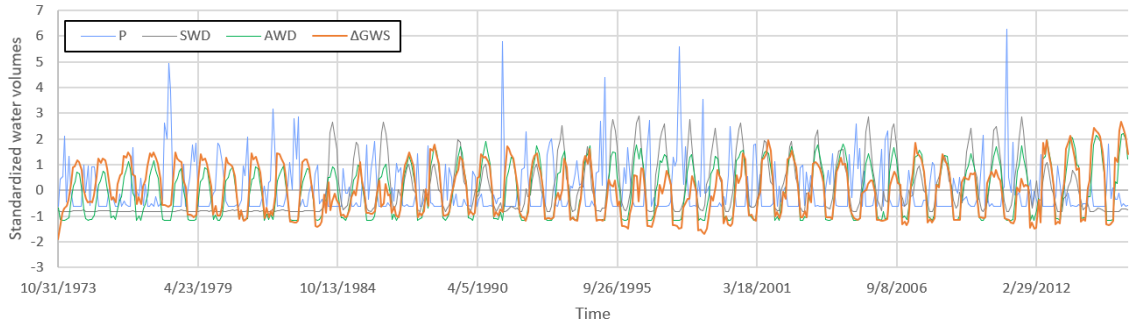

Arvin-Edison Water Storage District

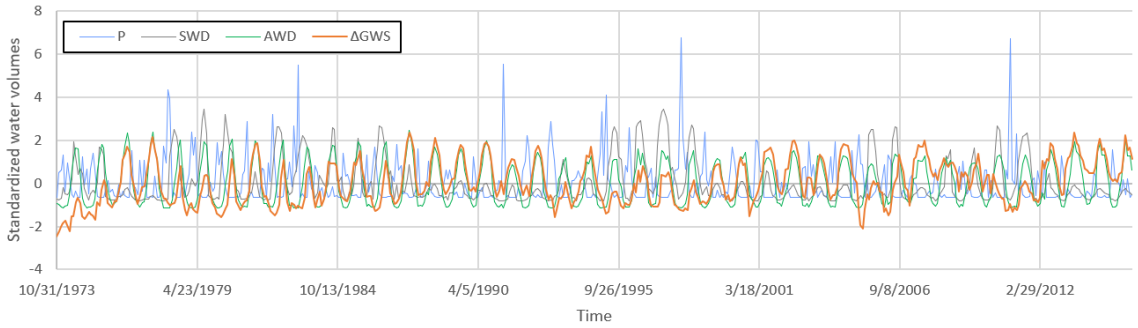

Kern Delta Water District

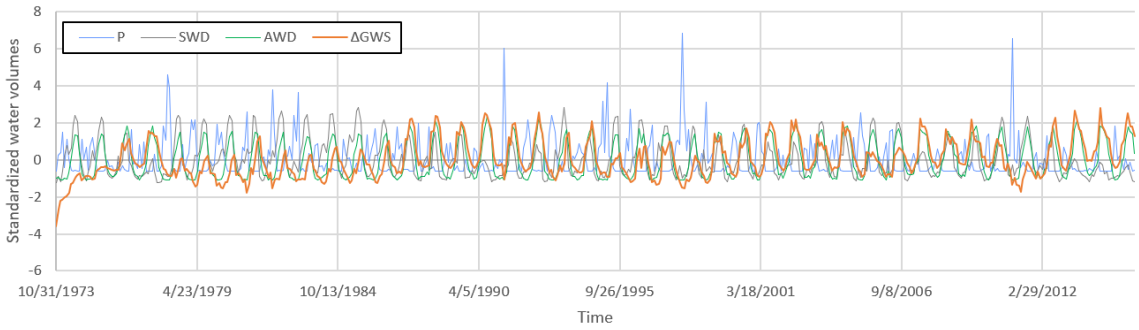

Cawelo Water District

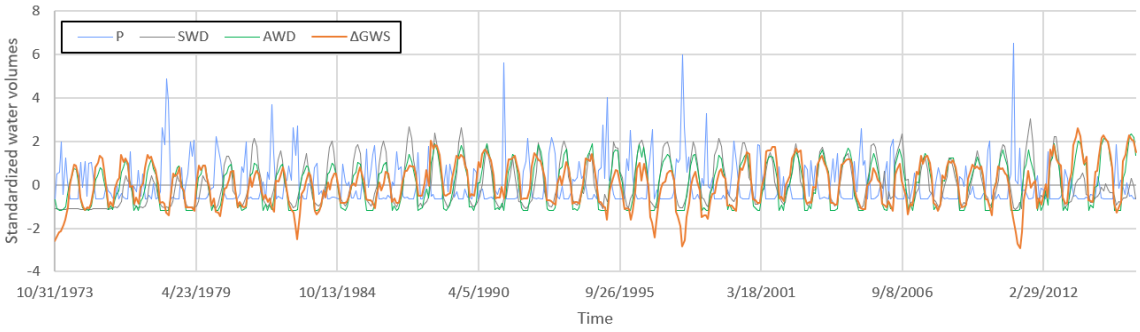

Shafter-Wasco Irrigation District

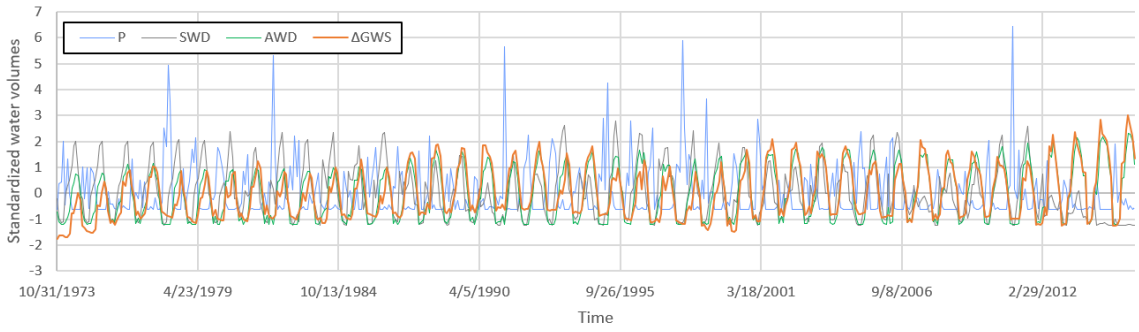

Buena Vista Water Storage District

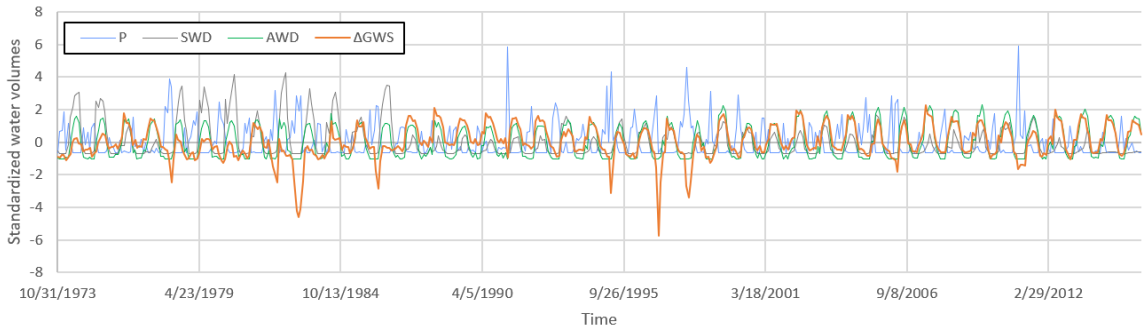

Henry Miller Water District

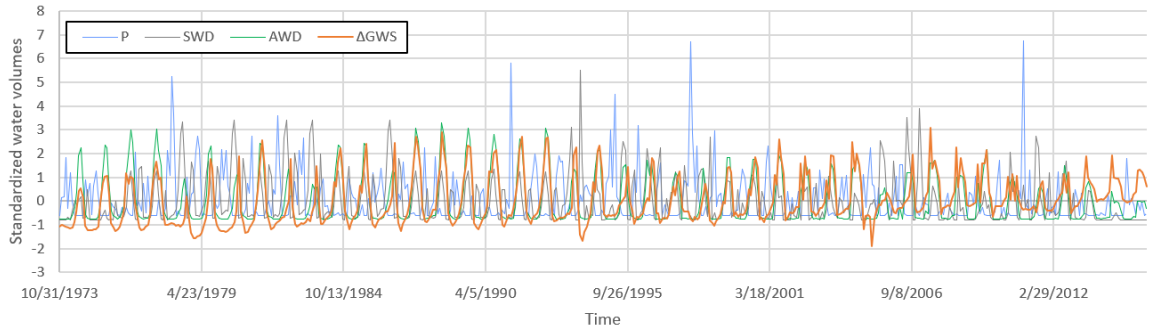

North Kern Water Storage District

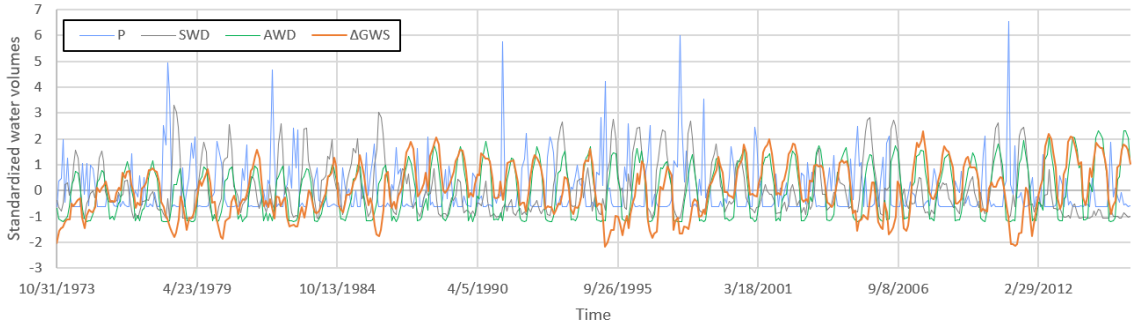

Tulare Irrigation District

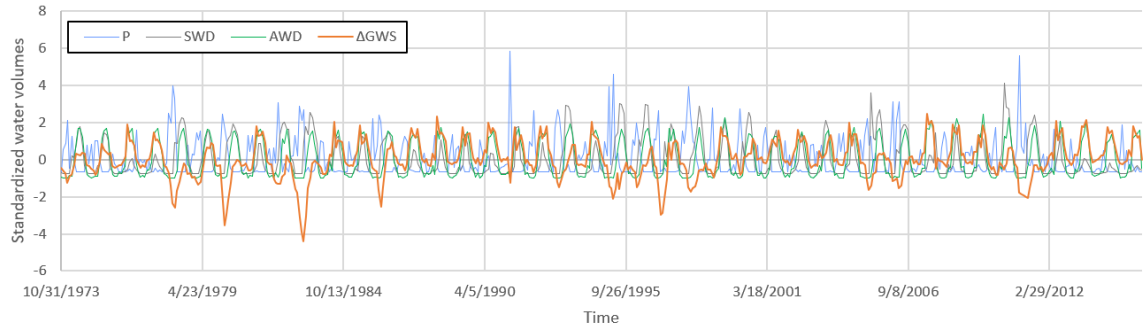

Saucelito Irrigation District

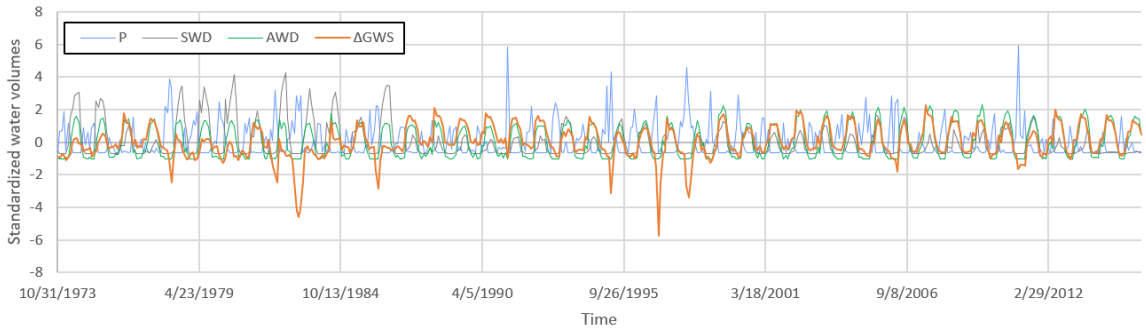

Delano Earlimart Irrigation District

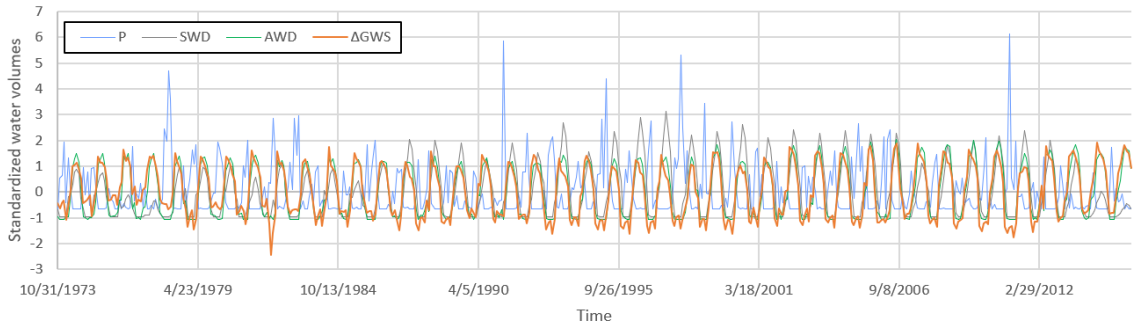

Kern Tulare Water District

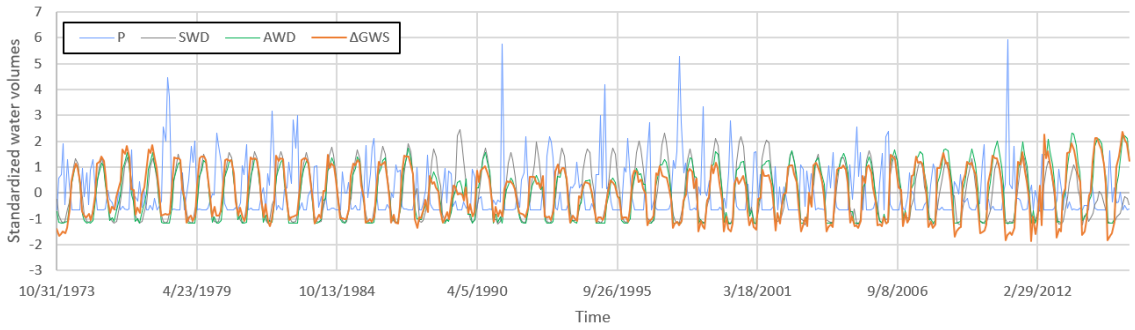

Appendix A.2 Comparison of standardized and de-seasonalized water volumes

Wheeler Ridge-Maricopa Water Storage District

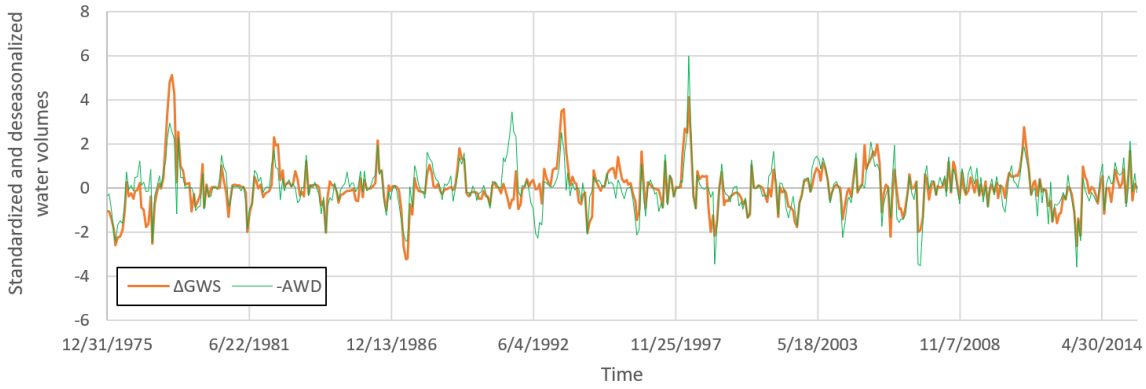

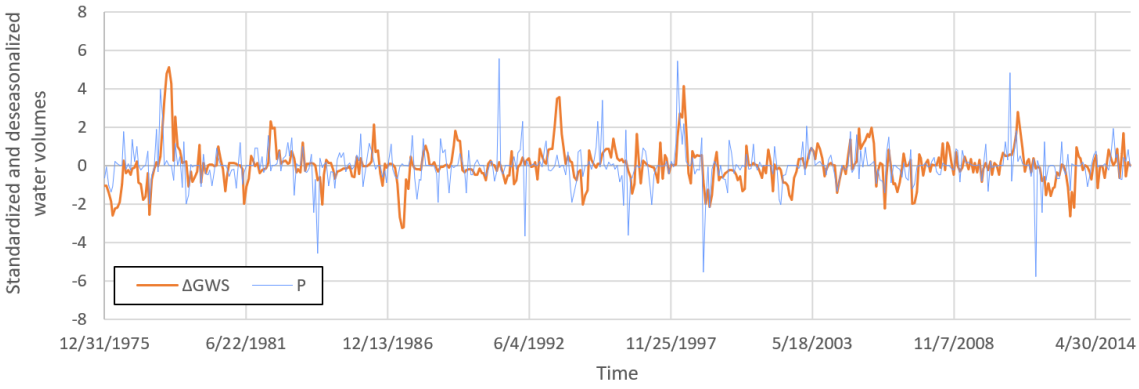

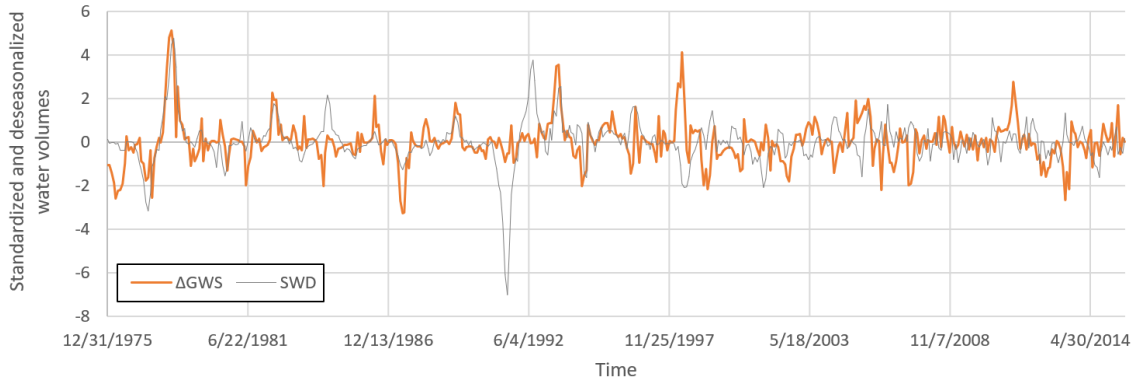

Rosedale-Rio Bravo Water Storage District

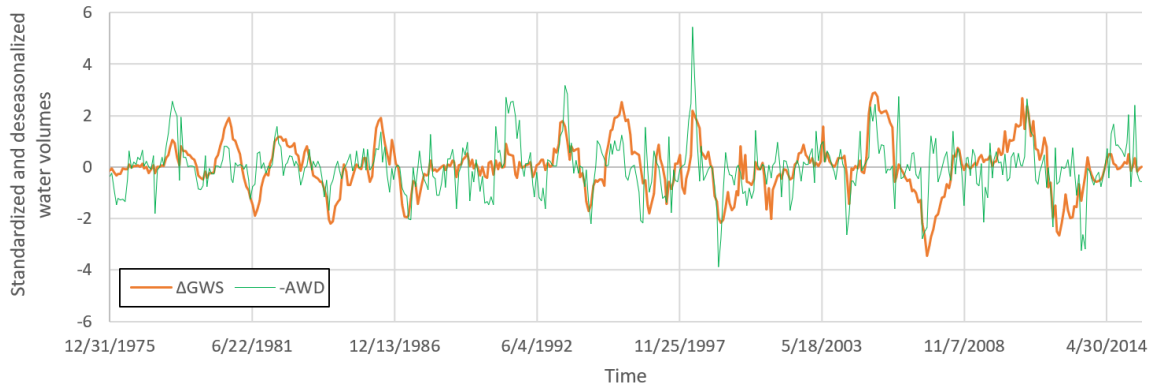

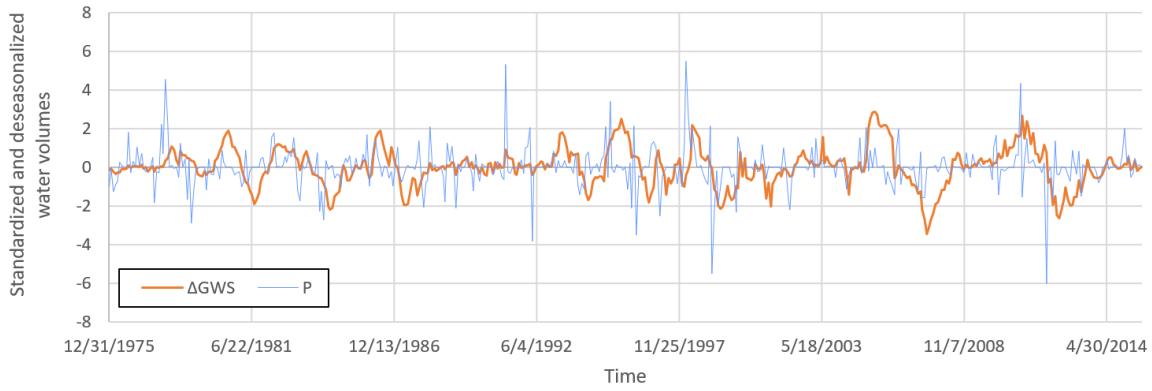

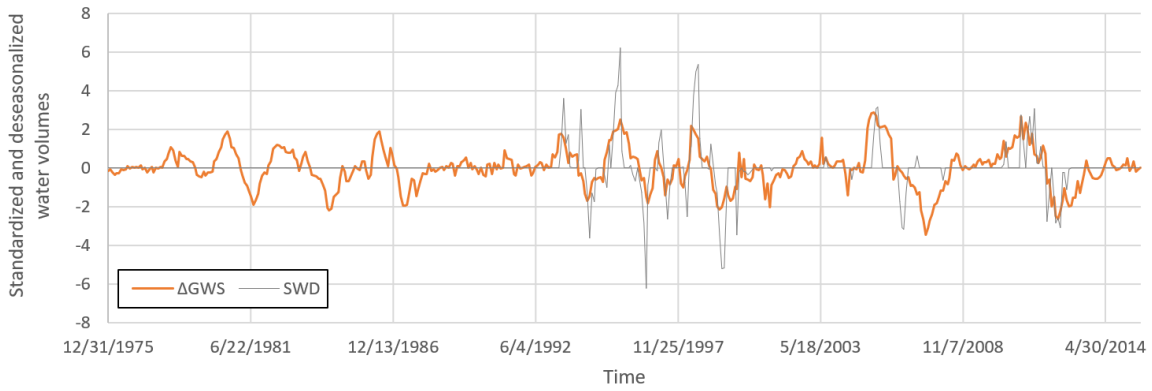

Southern San Joaquin Municipal Utility District

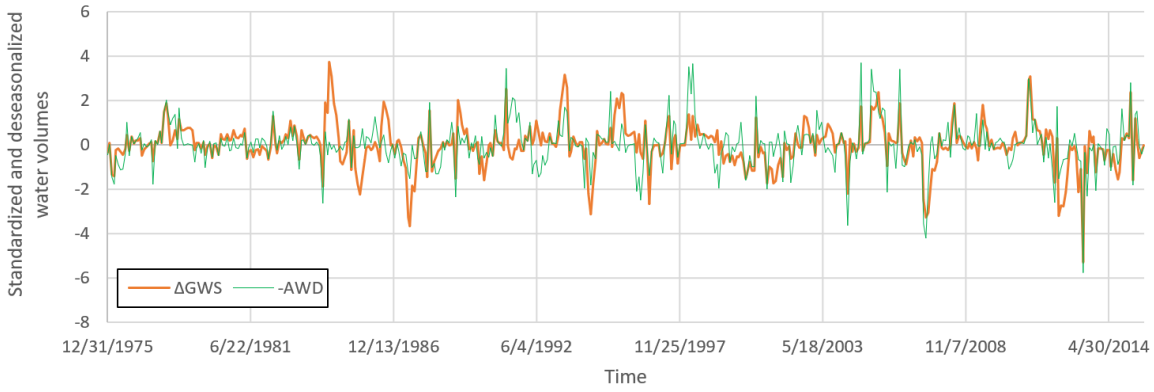

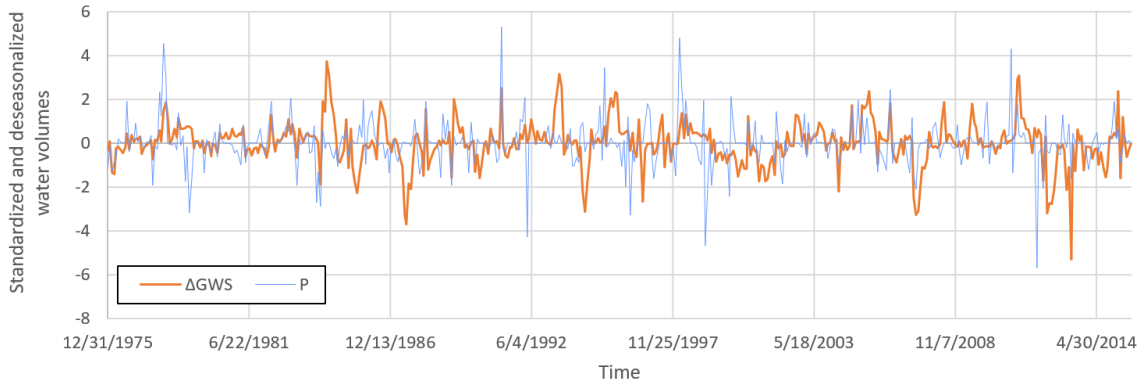

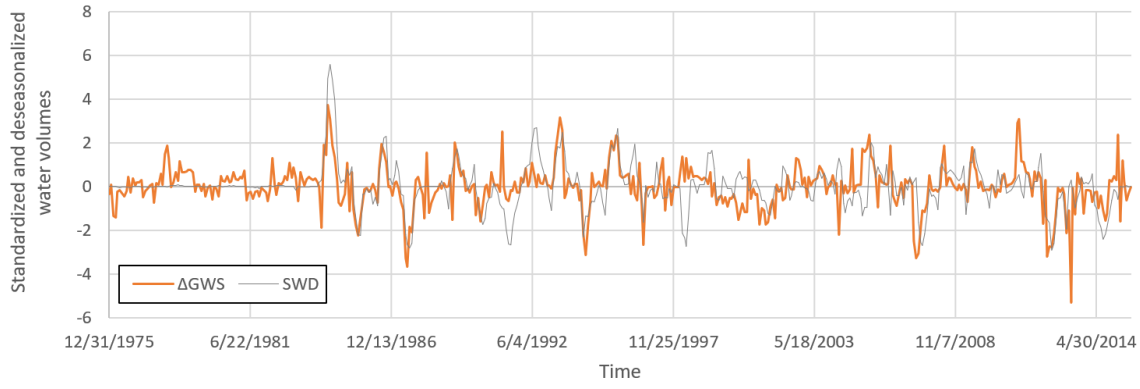

Arvin-Edison Water Storage District

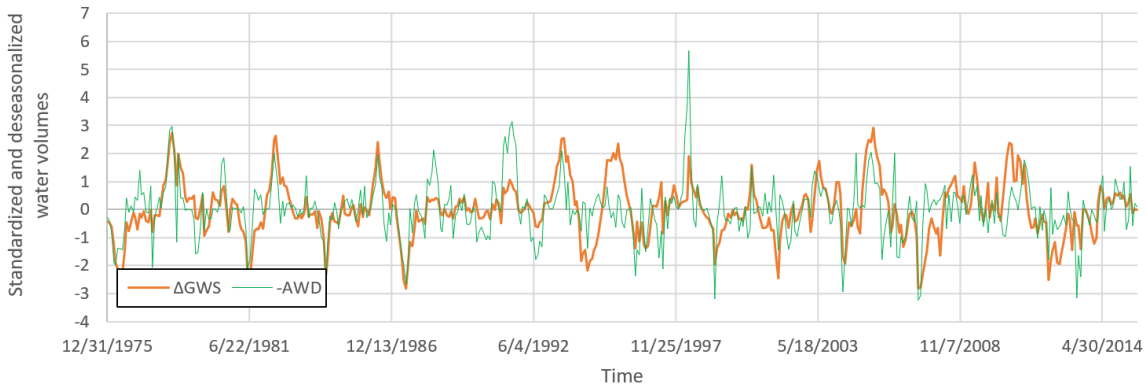

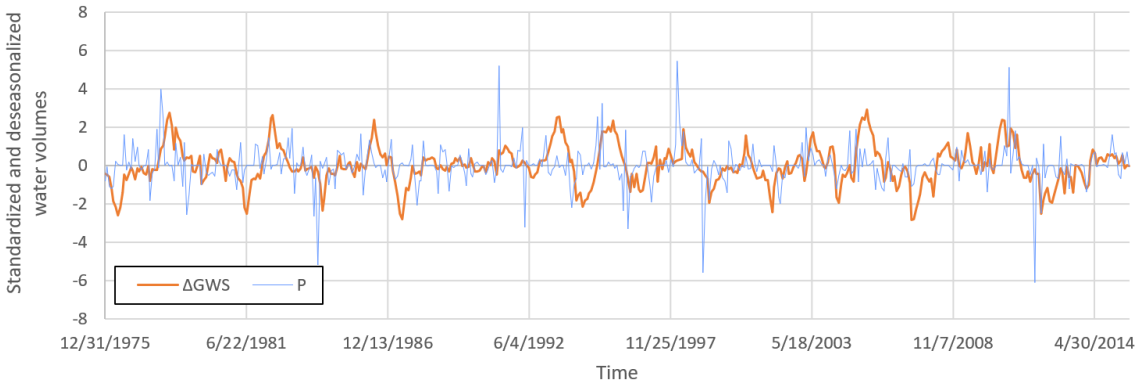

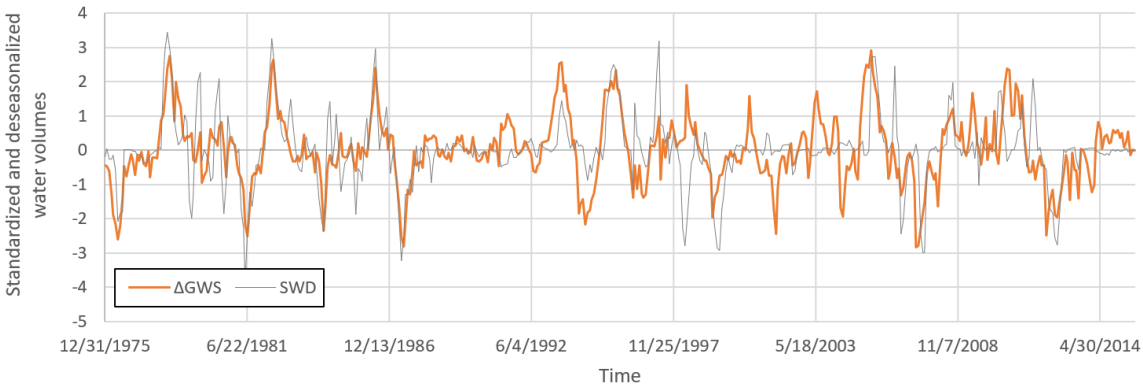

Kern Delta Water District

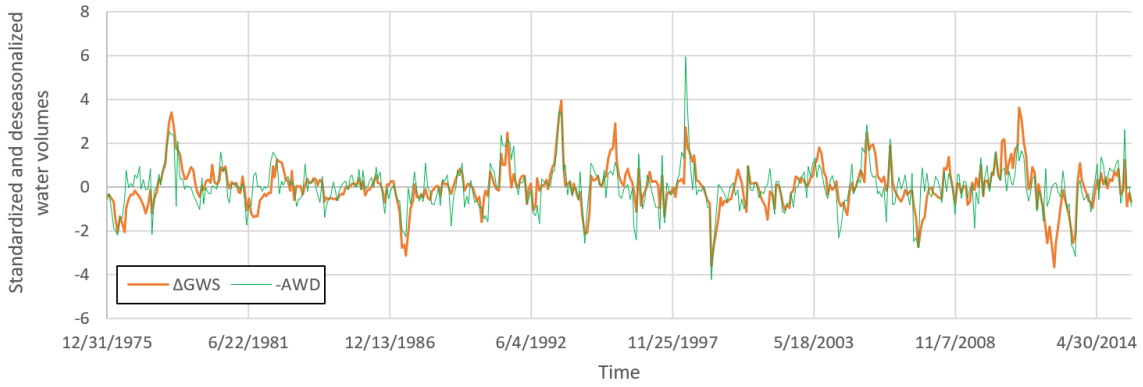

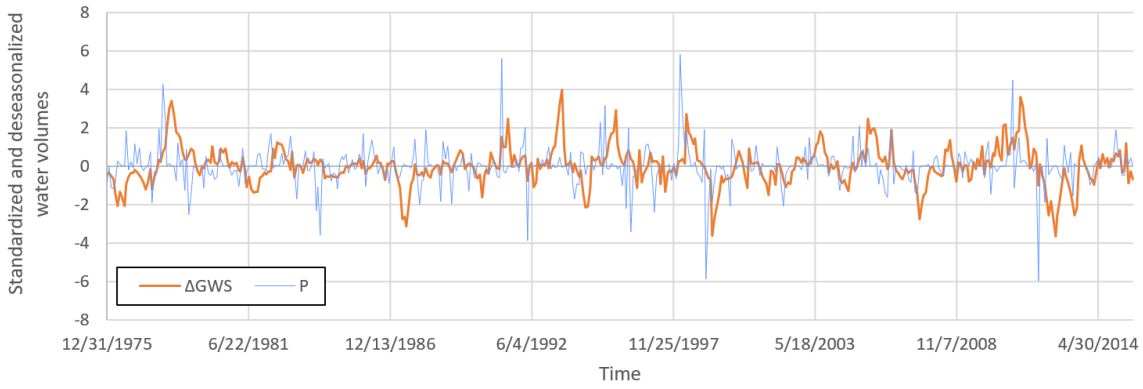

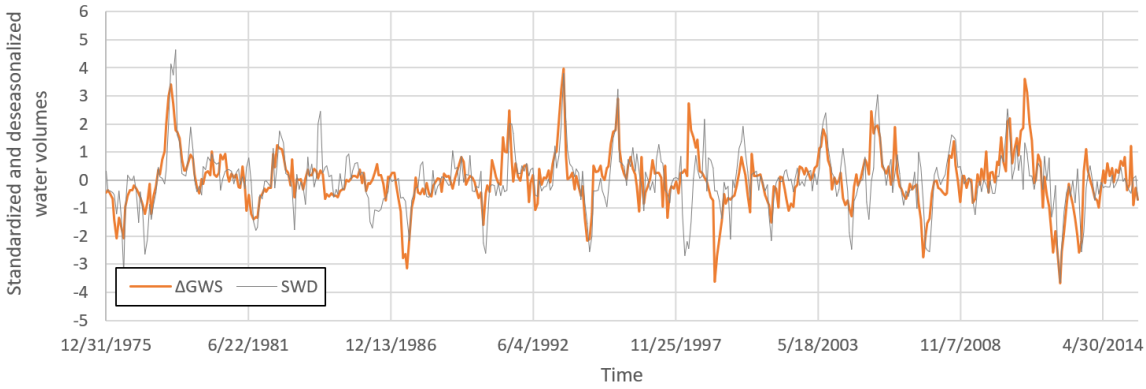

Cawelo Water District

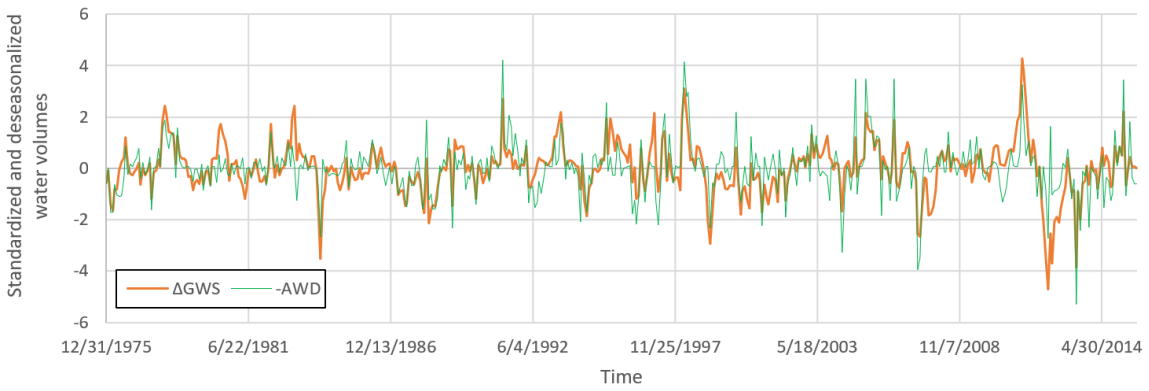

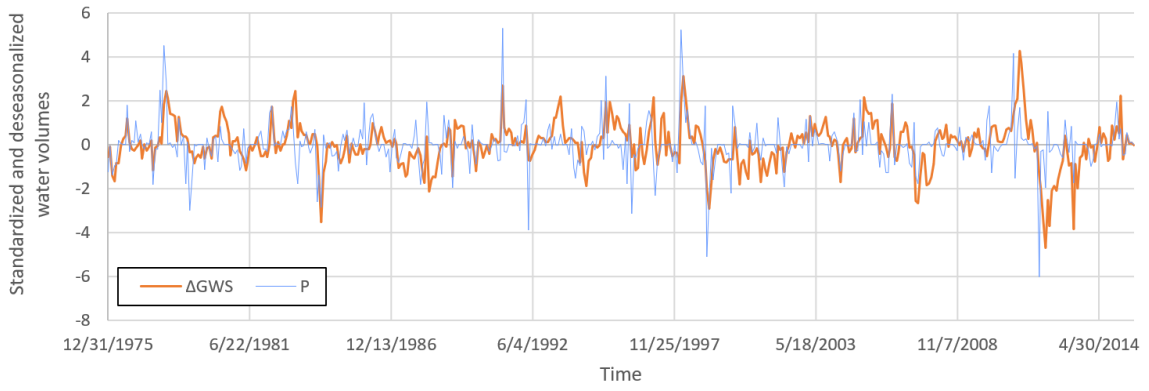

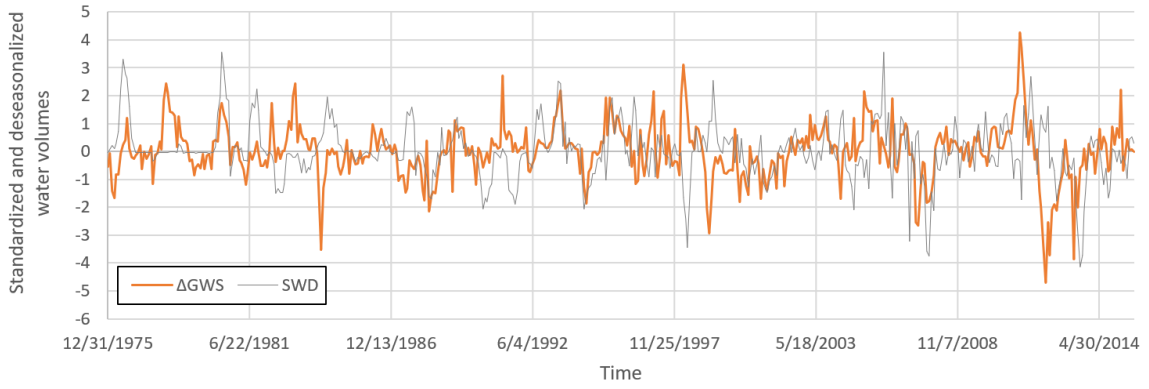

Shafter-Wasco Irrigation District

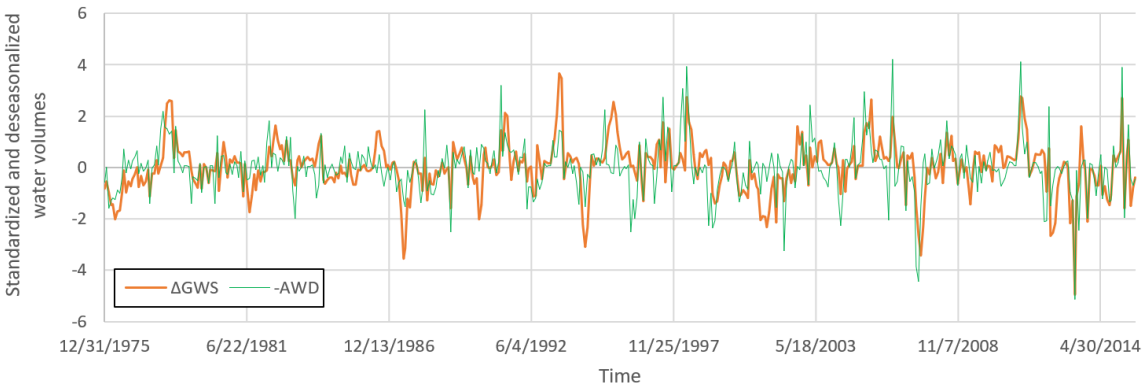

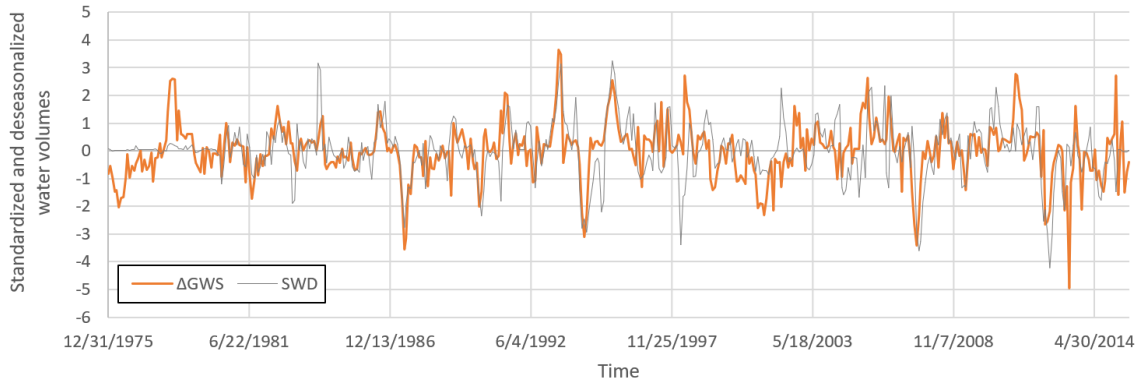

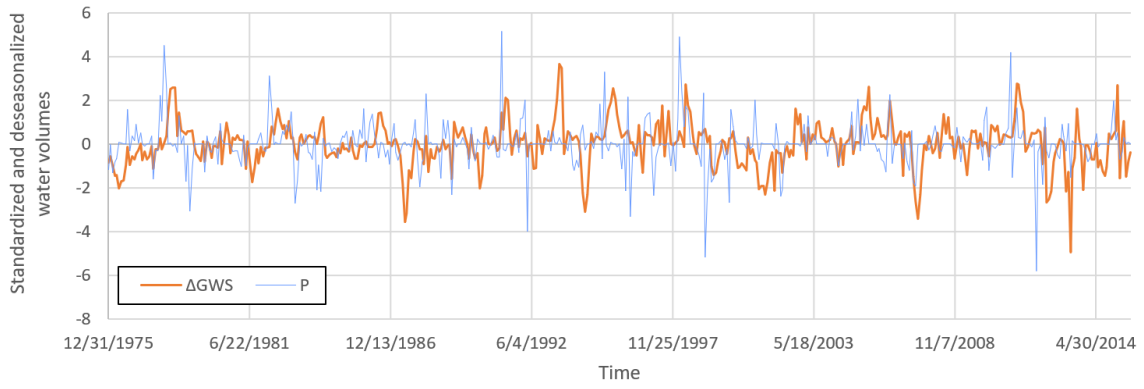

Buena Vista Water Storage District

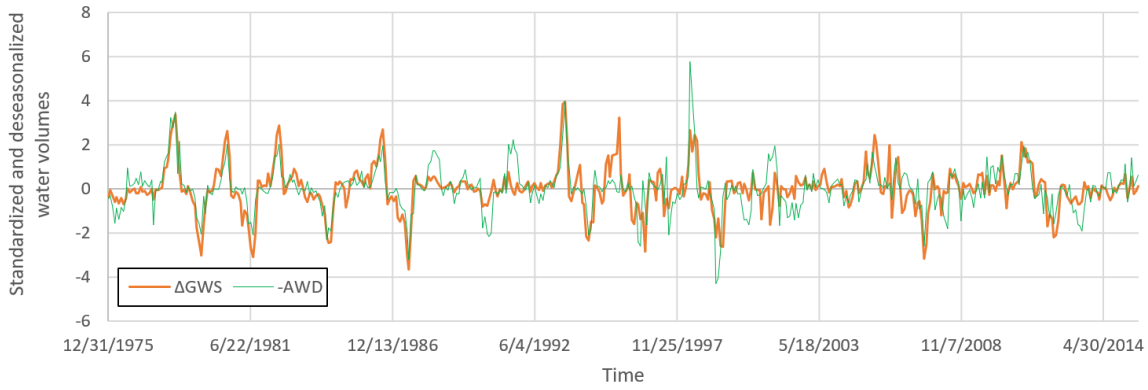

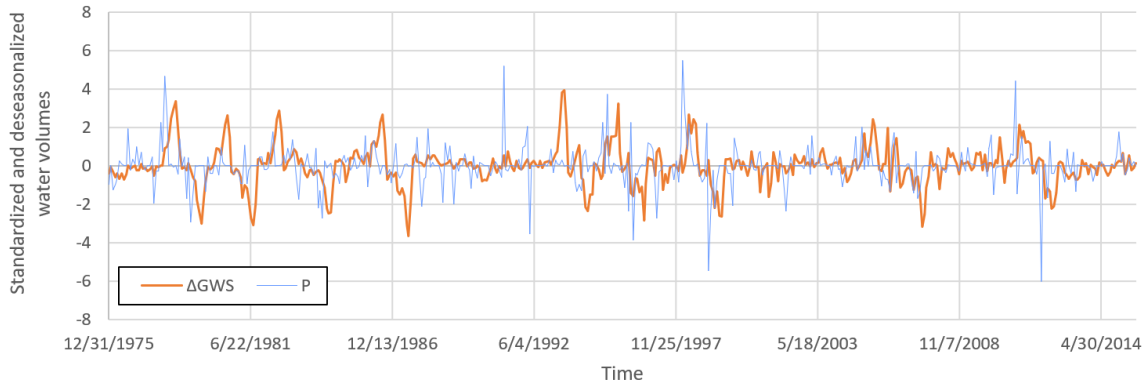

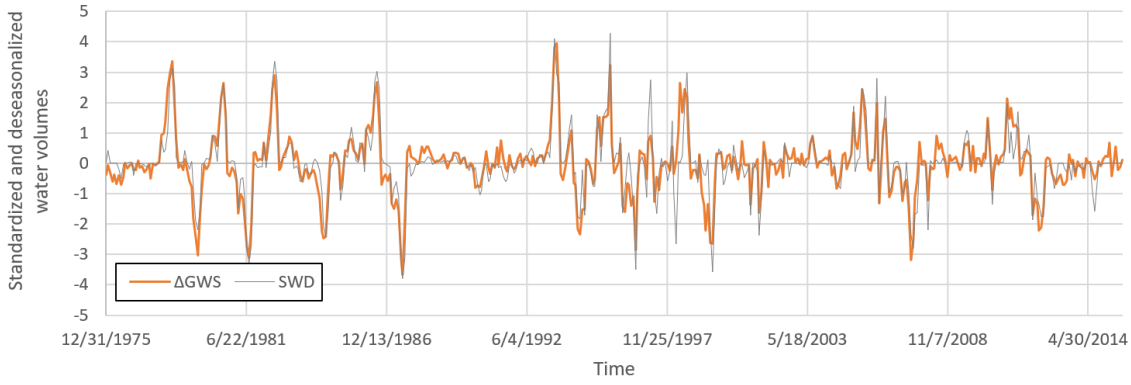

Henry Miller Water District

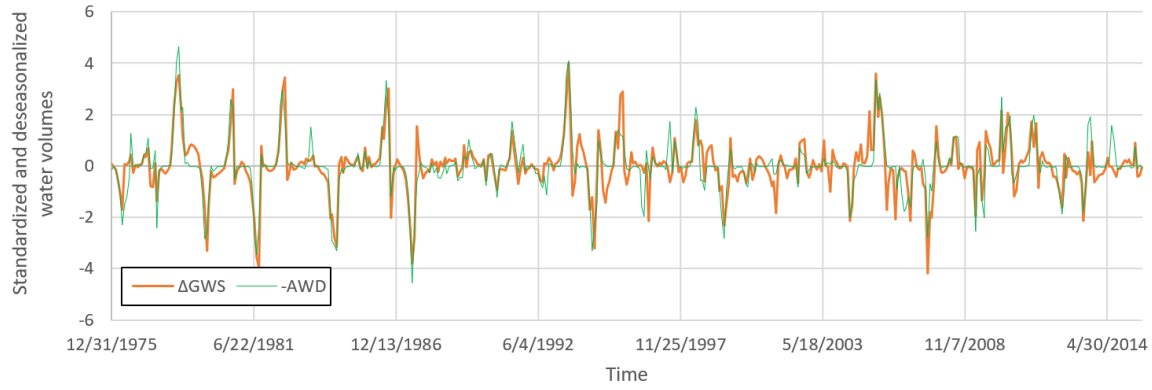

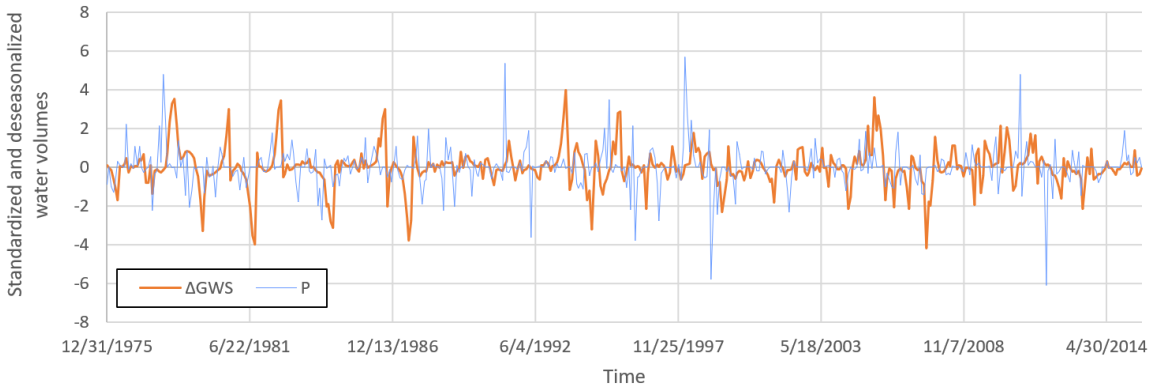

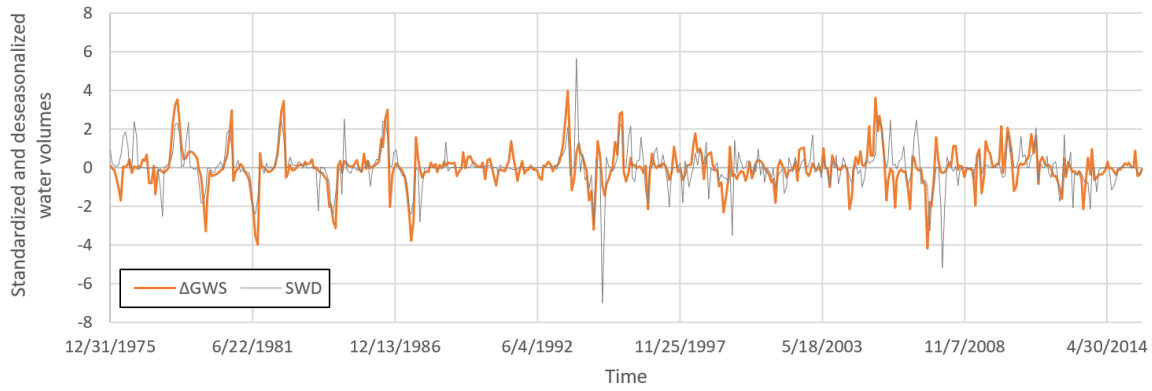

North Kern Water Storage District

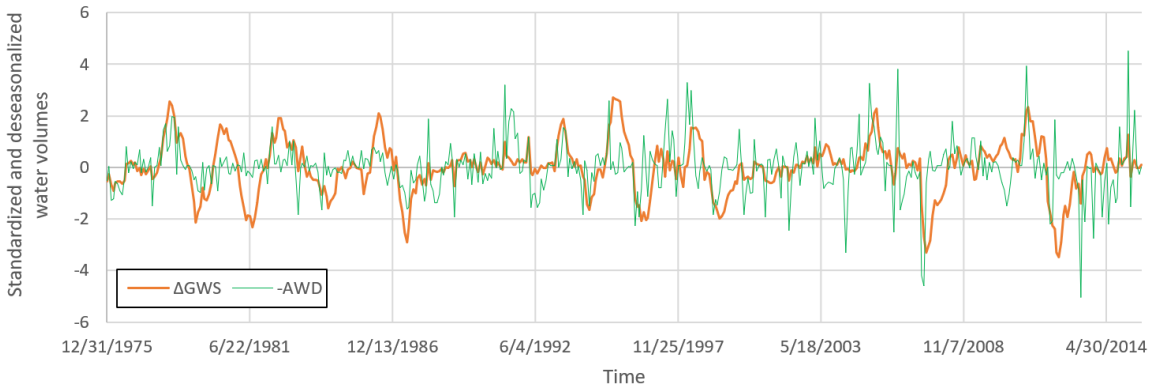

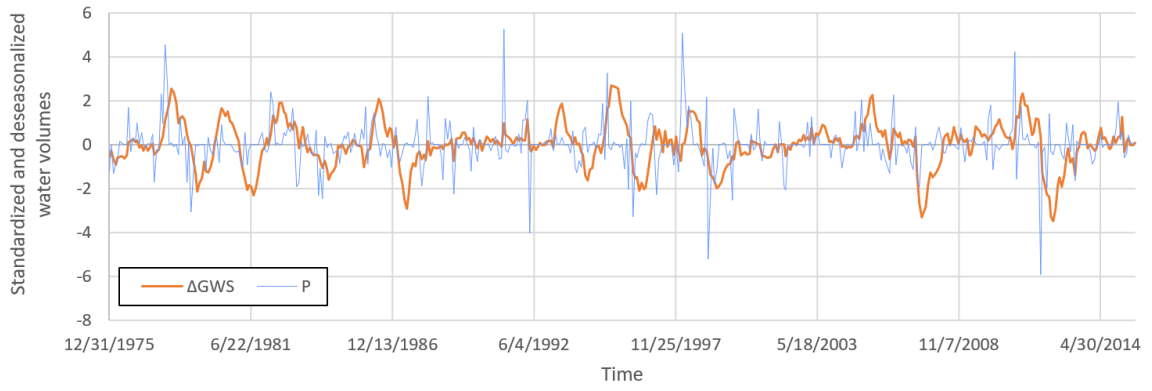

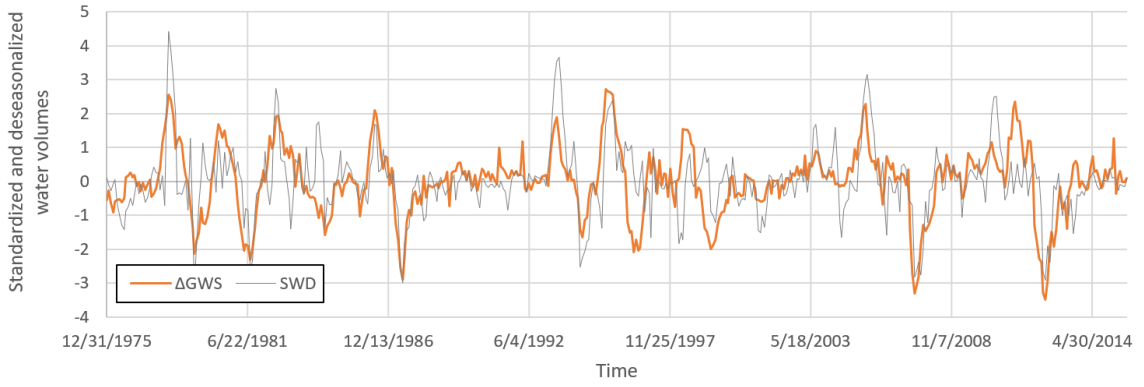

Tulare Irrigation District

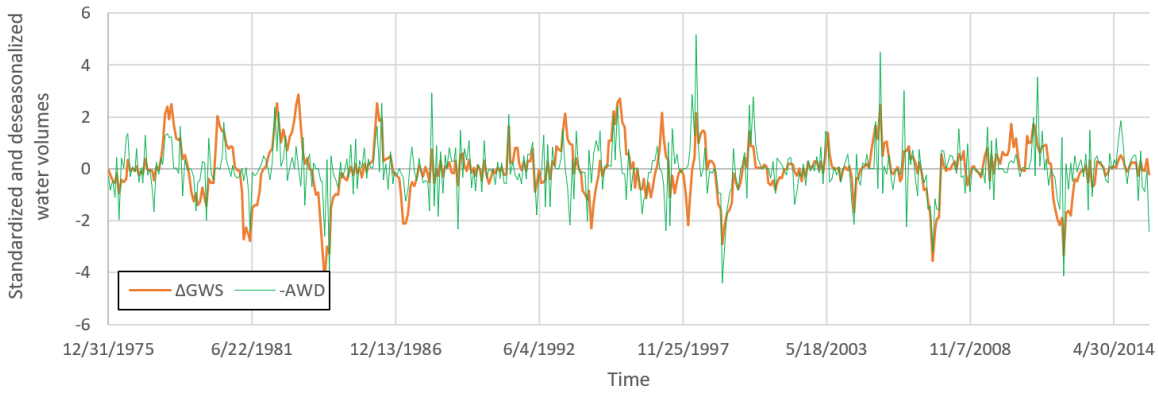

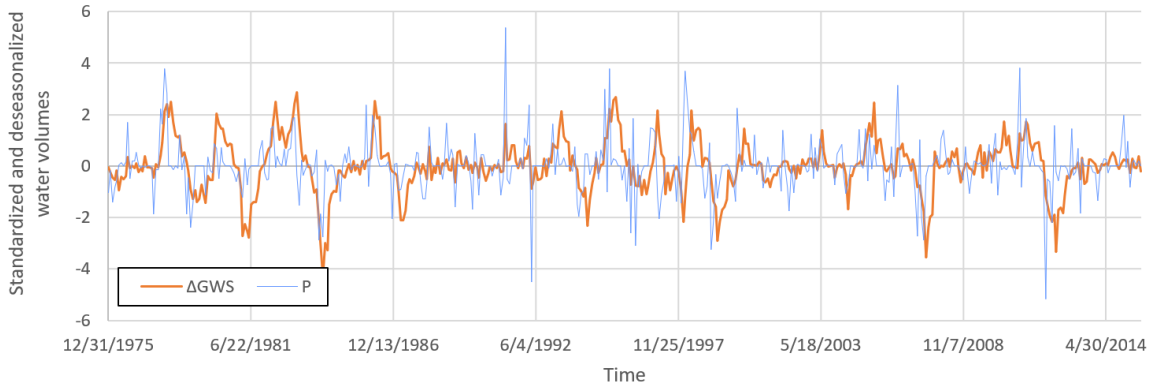

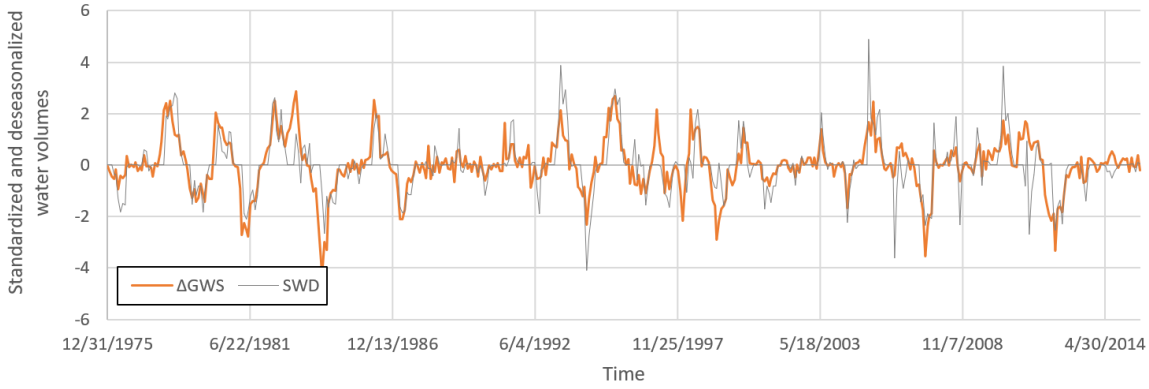

Saucelito Irrigation District

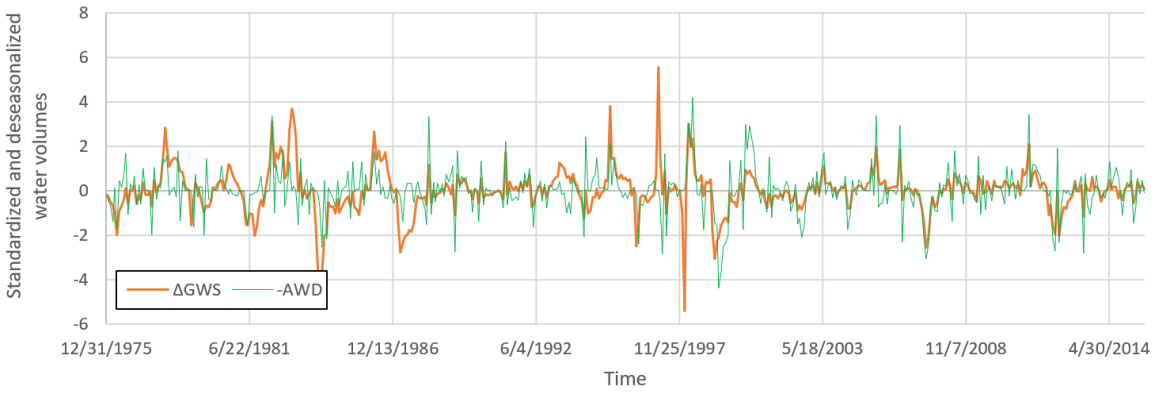

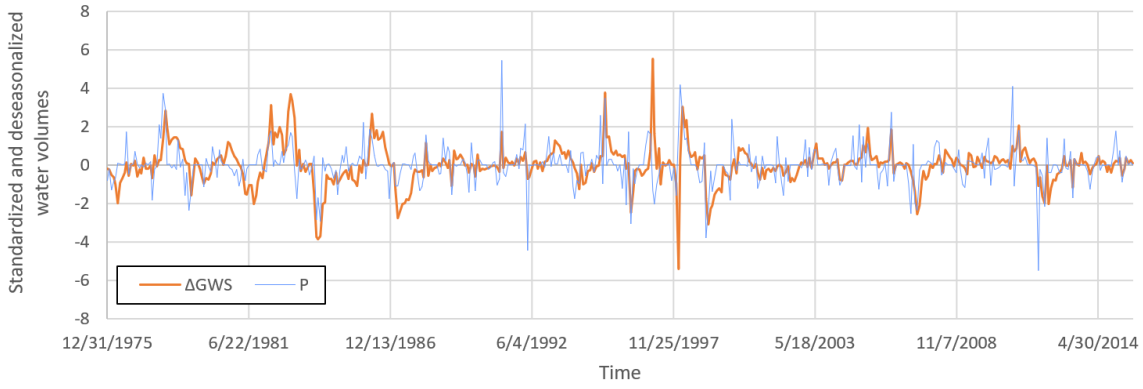

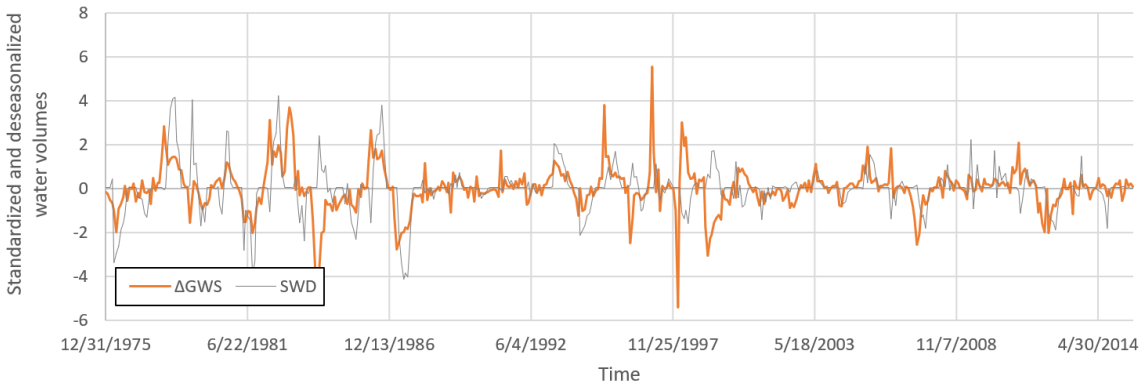

Delano Earlimart Irrigation District

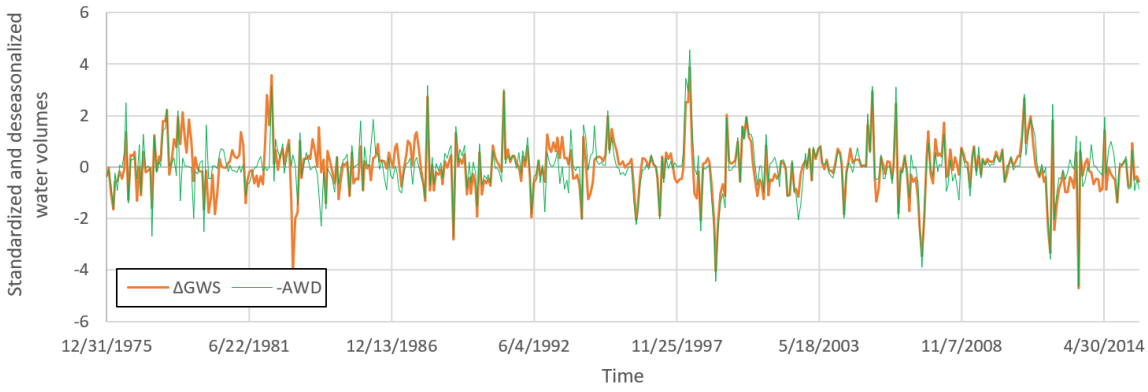

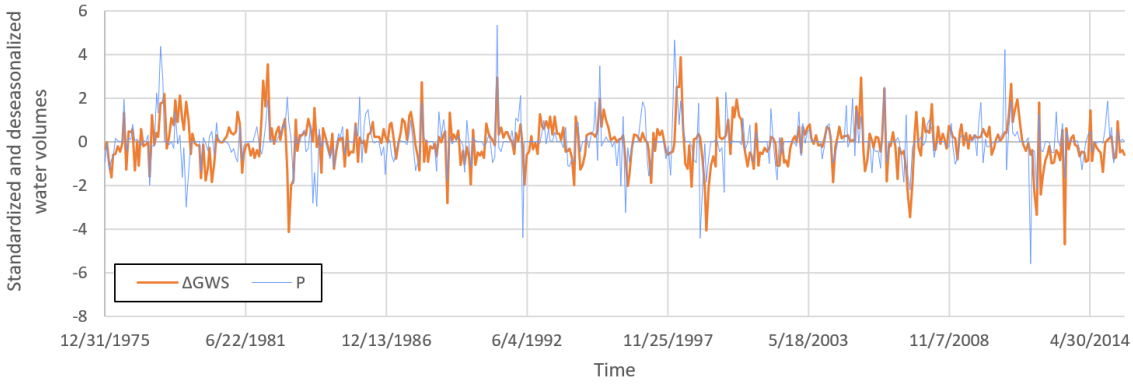

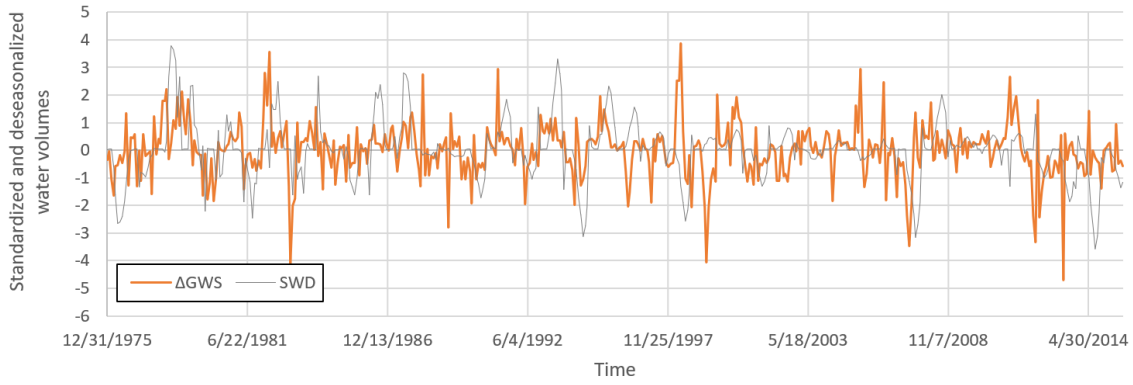

Kern Tulare Water District

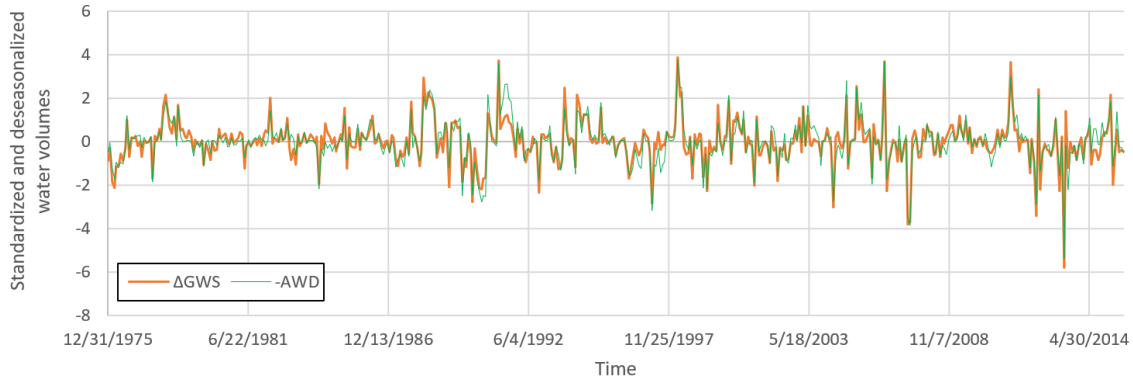

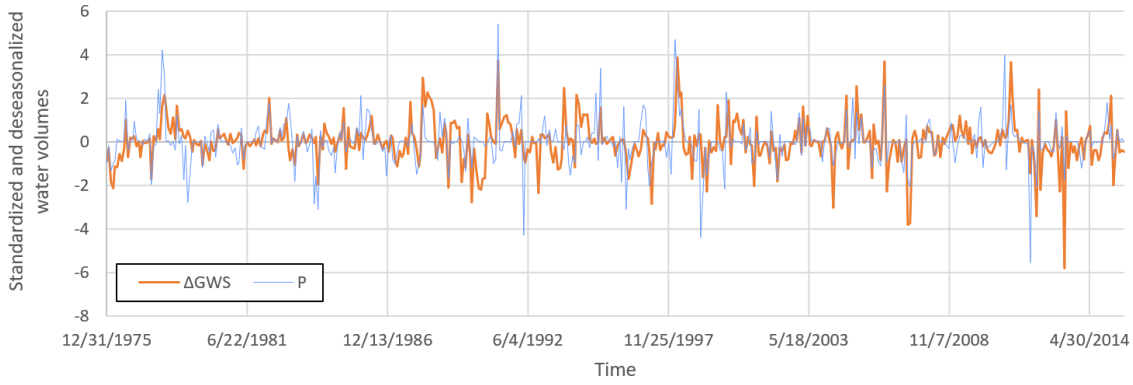

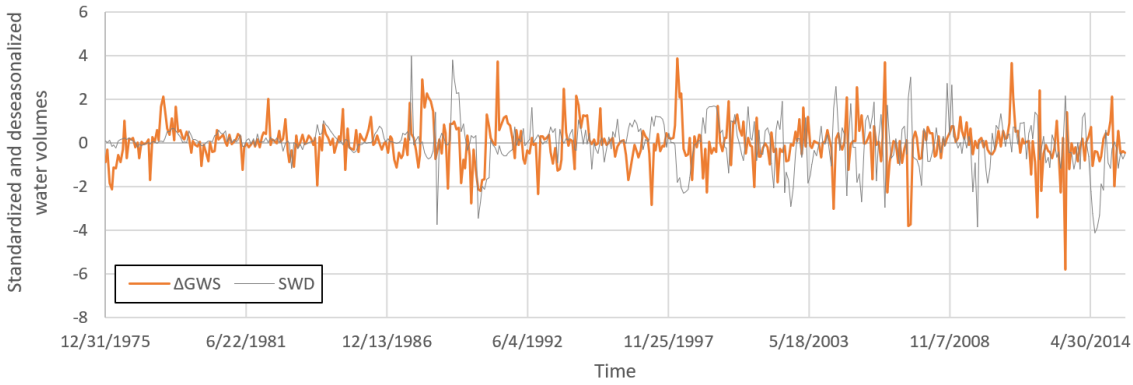

Appendix A.3 Standardized moving average values for depth to groundwater (GWD) and groundwater storage (GWS)

The vertical axis was reversed to facilitate interpretation. The decrease in the brown and black lines represents the increase in depth and the decrease in storage, respectively.

Wheeler Ridge-Maricopa Water Storage District

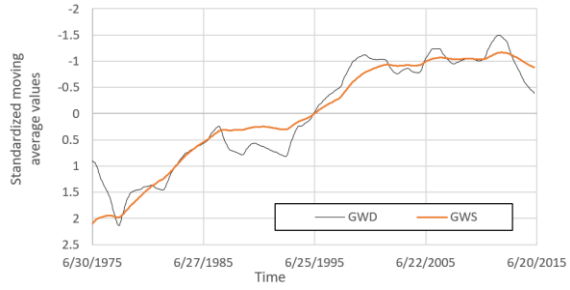

Rosedale-Rio Bravo Water Storage District

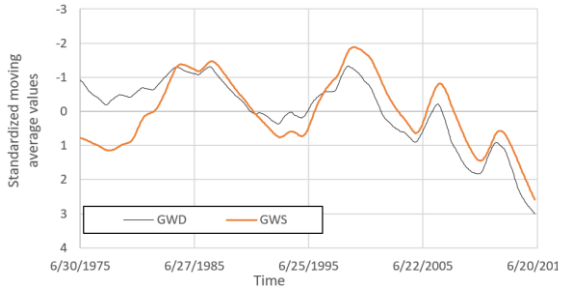

Southern San Joaquin Municipal Utility District

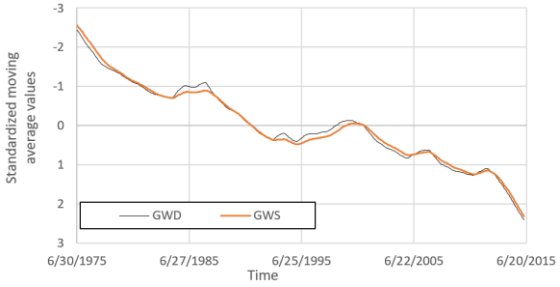

Arvin-Edison Water Storage District

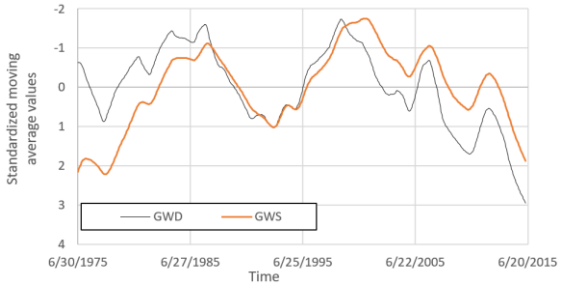

Kern Delta Water District

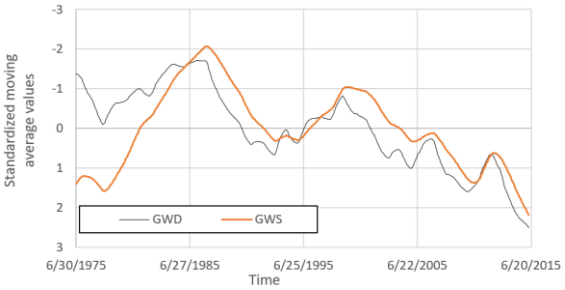

Cawelo Water District

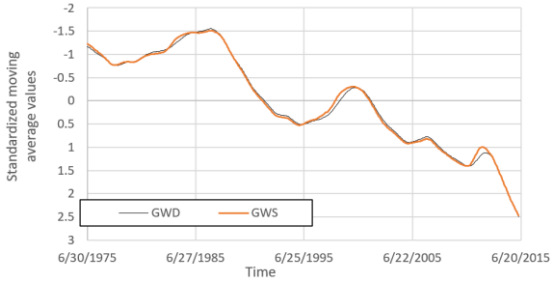

Shafter-Wasco Irrigation District

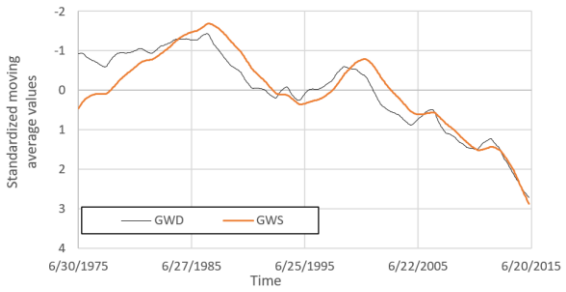

Buena Vista Water Storage District

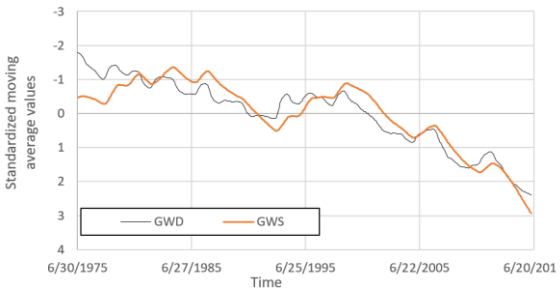

Henry Miller Water District

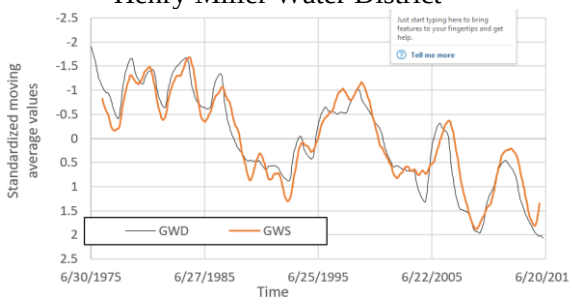

North Kern Water Storage District

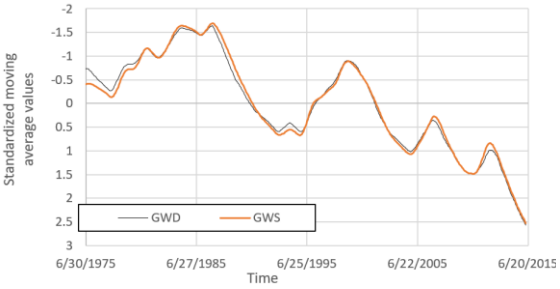

Tulare Irrigation District

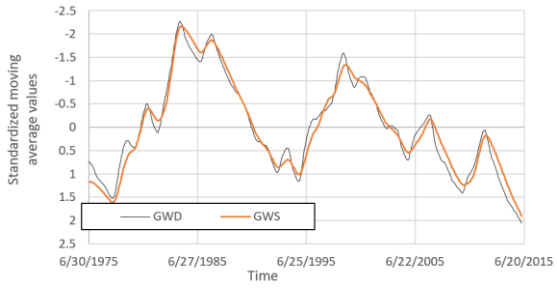

Saucelito Irrigation District

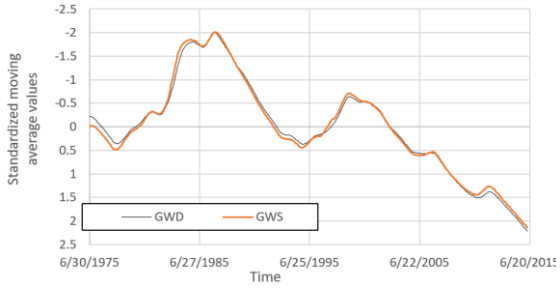

Delano Earlimart Irrigation District

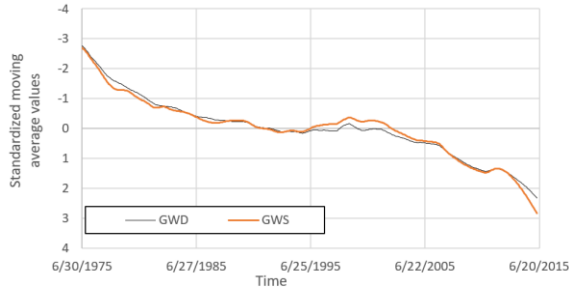

Kern Tulare Water District

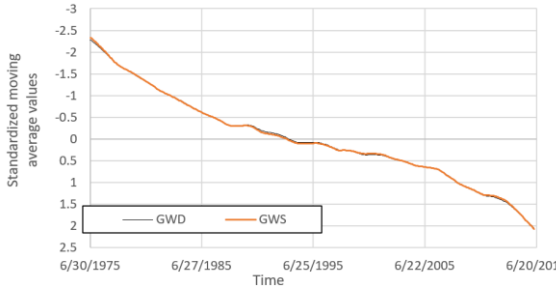

Appendix A.4 Multiple Squared Correlation Function (MSCF) between the dynamic variables and change in depth to groundwater (ΔGWD) after removing seasonal effects.

Wheeler Ridge-Maricopa Water Storage District

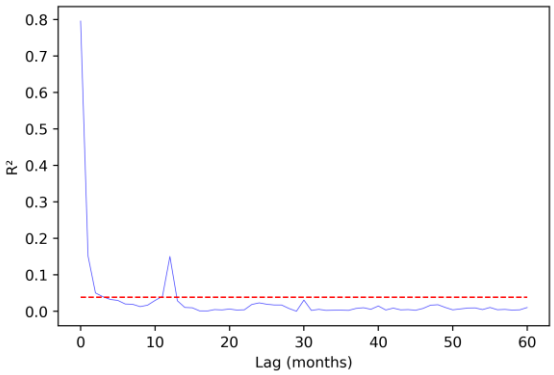

Rosedale-Rio Bravo Water Storage District

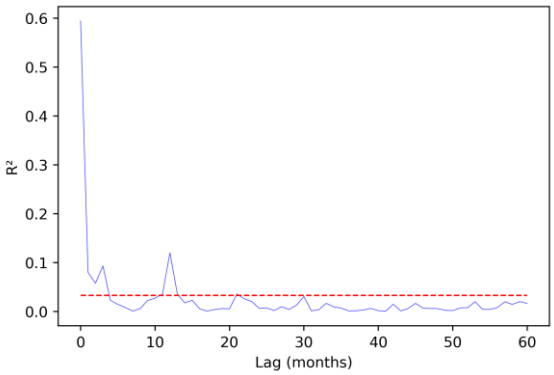

Southern San Joaquin Municipal Utility District

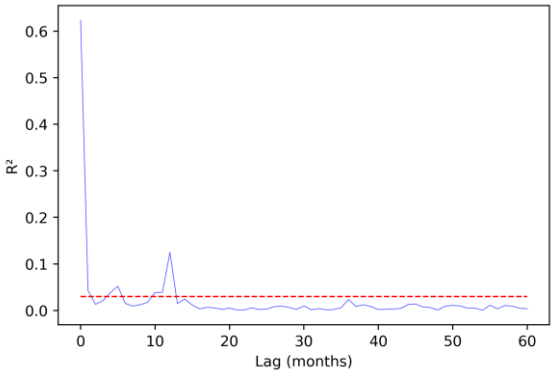

Arvin-Edison Water Storage District

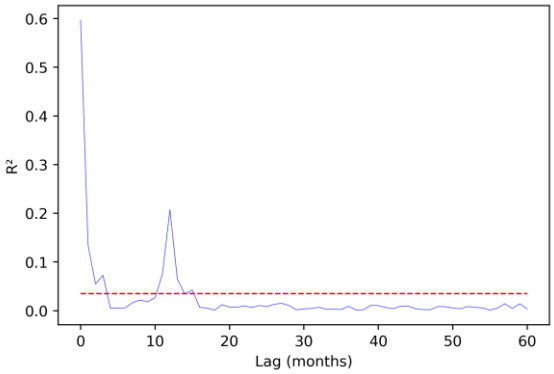

Kern Delta Water District

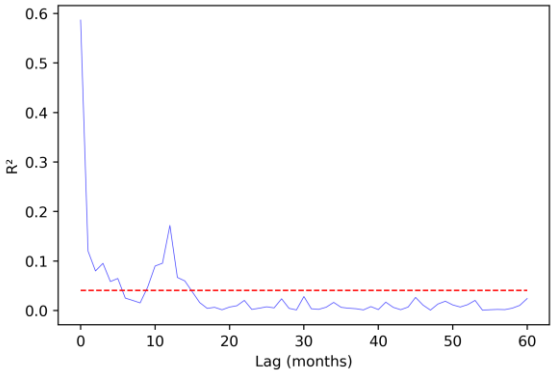

Cawelo Water District

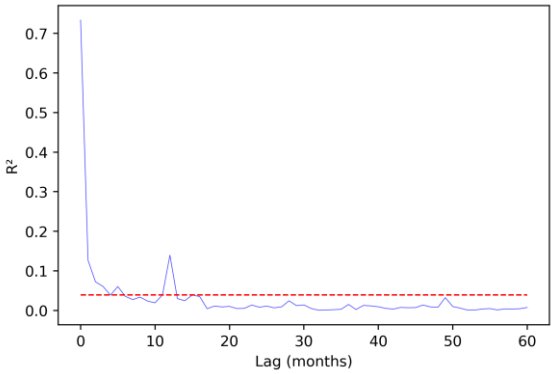

Shafter-Wasco Irrigation District

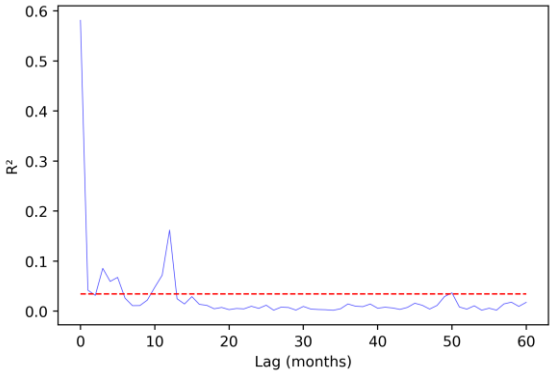

Buena Vista Water Storage District

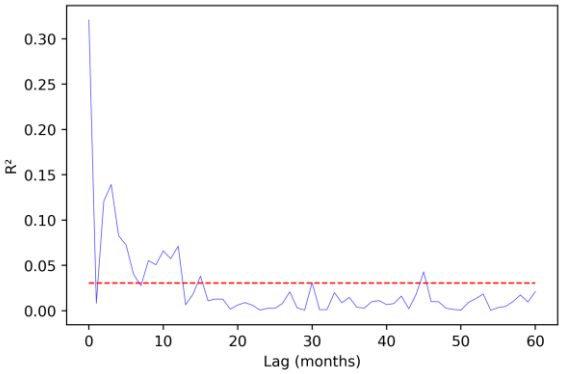

Henry Miller Water District

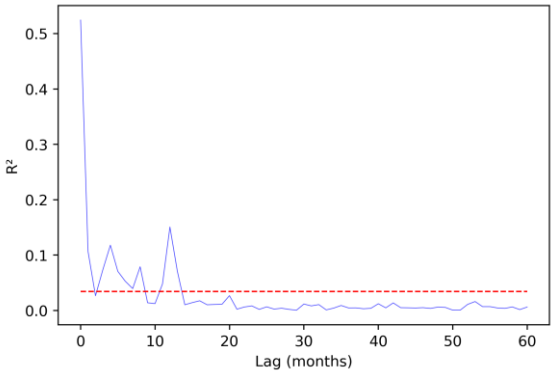

North Kern Water Storage District

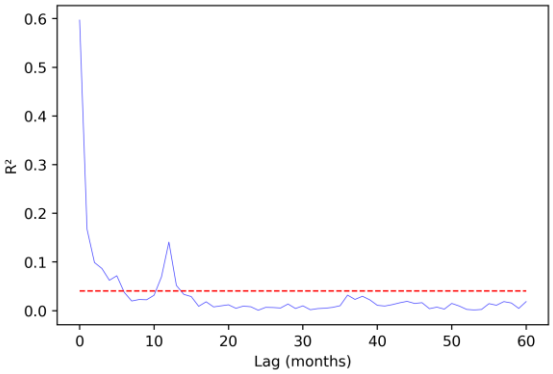

Tulare Irrigation District

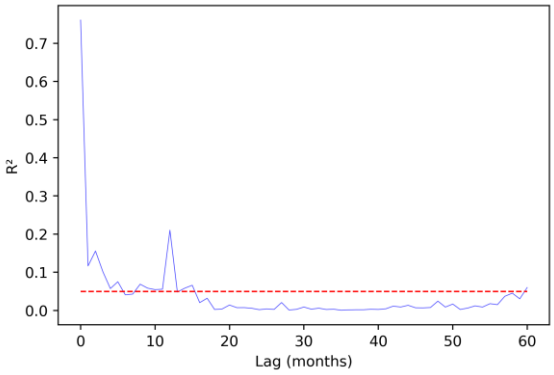

Saucelito Irrigation District

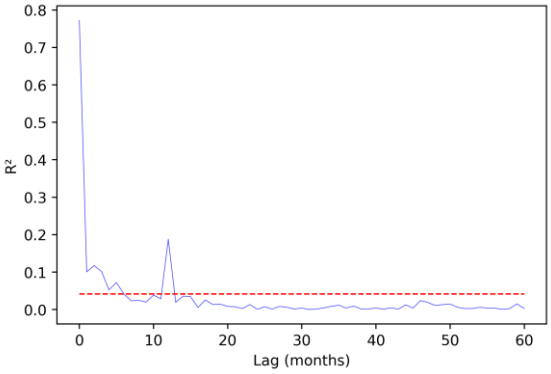

Delano Earlimart Irrigation District

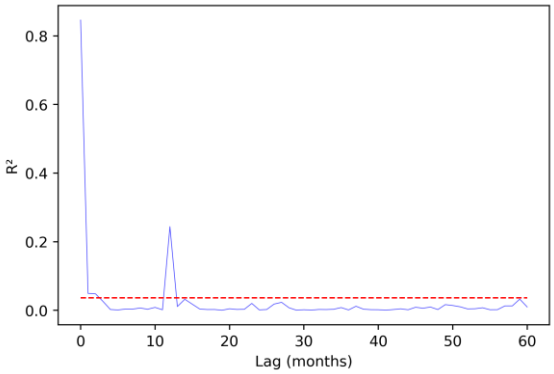

Kern Tulare Water District

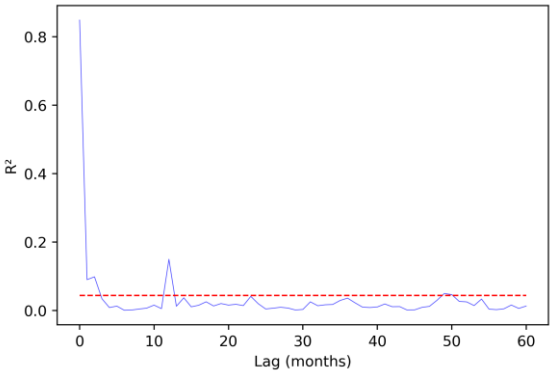

Appendix A.5 Changes in depths to groundwater (ΔGWD) using emulators
Left column: Multiple Linear Regression (MLR). Middle column: Multilayer Perceptron (MLP). Right column: Long Short-Term Memory (LSTM)

Wheeler Ridge-Maricopa Water Storage District

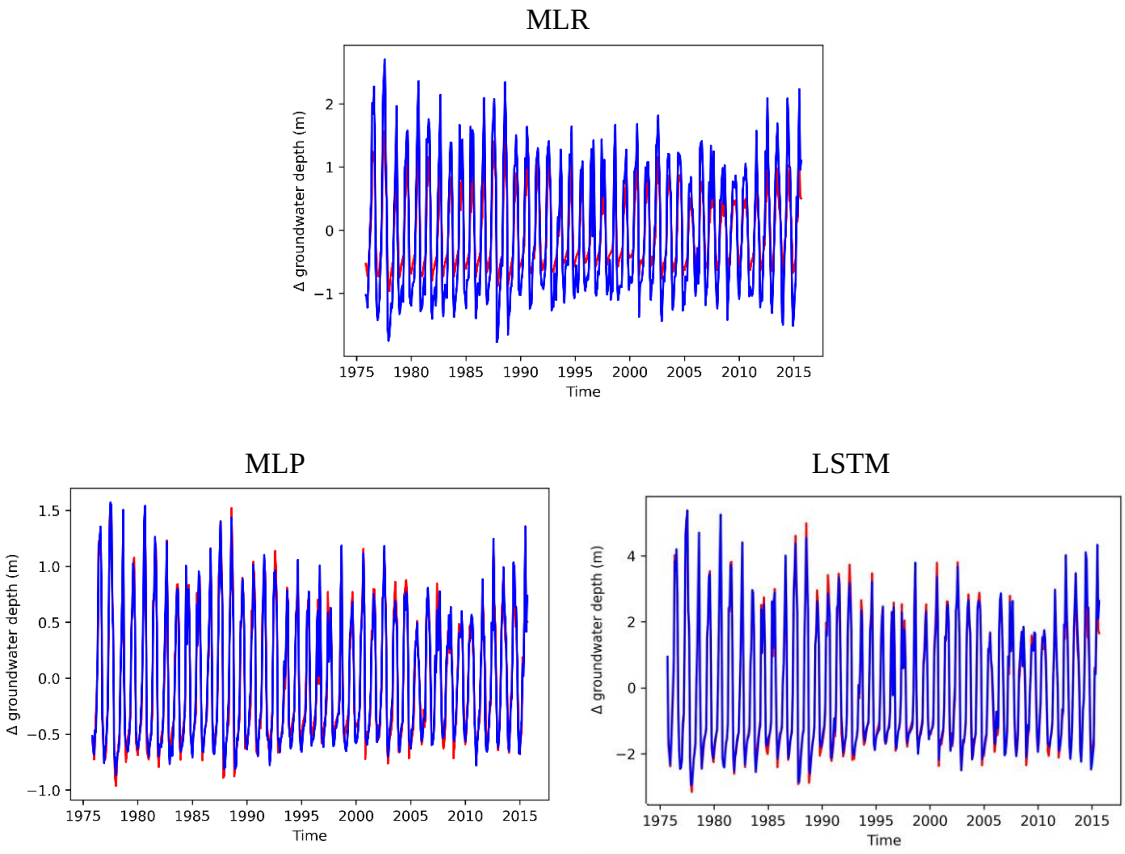

Rosedale-Rio Bravo Water Storage District

MLR

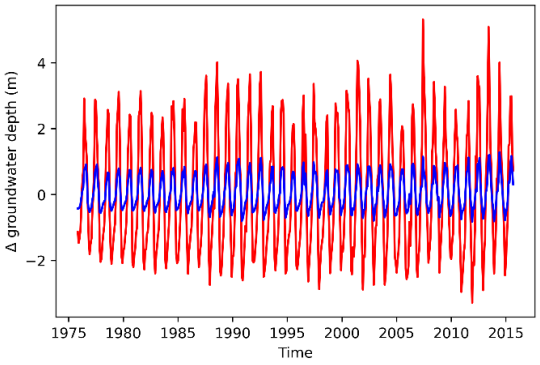

MLP

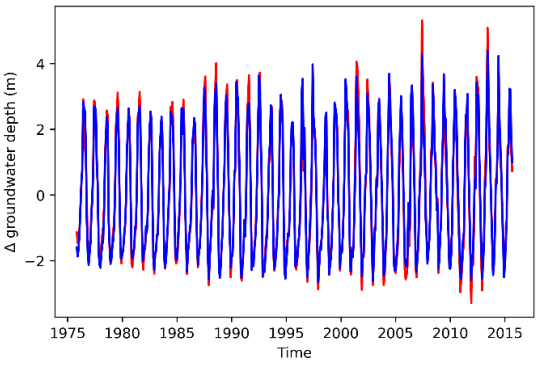

LSTM

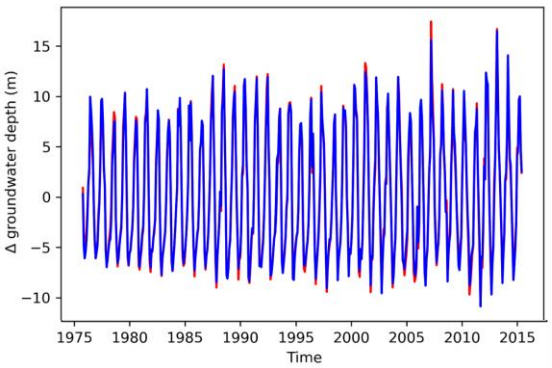

Southern San Joaquin Municipal Utility District

MLR

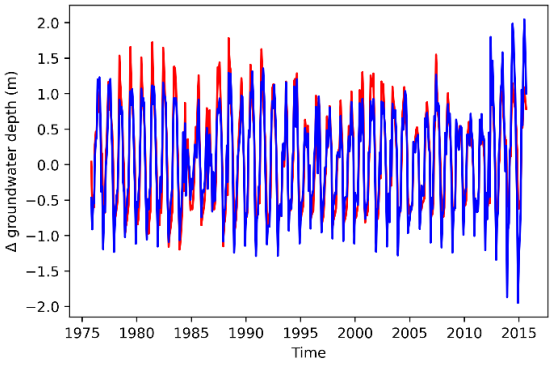

MLP

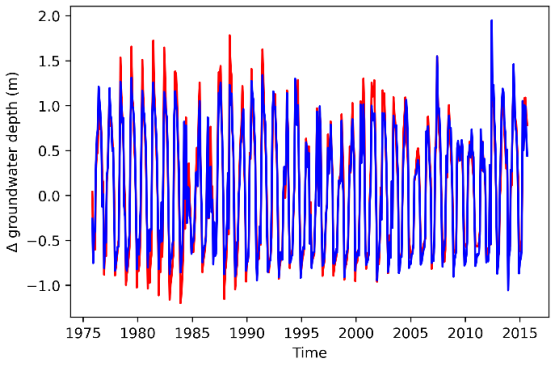

LSTM

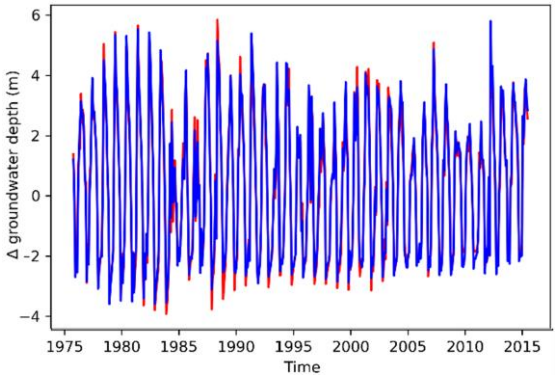

Arvin-Edison Water Storage District

MLR

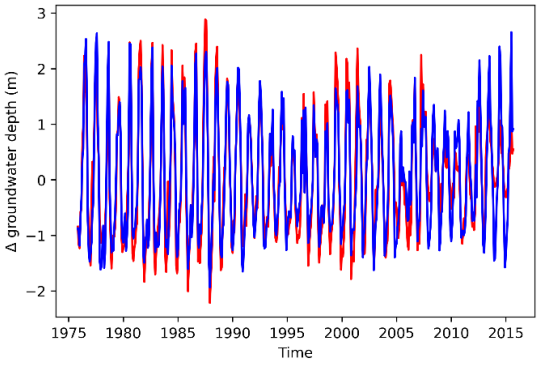

MLP

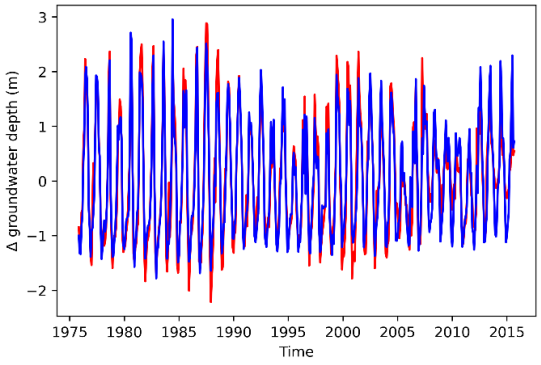

LSTM

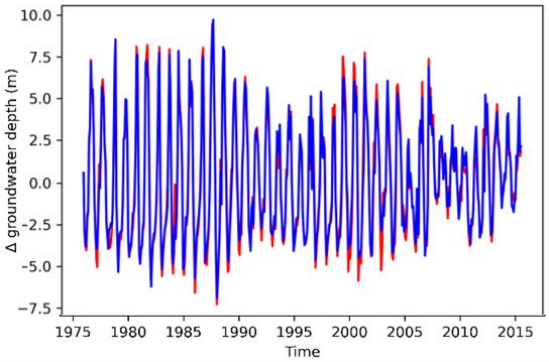

Kern Delta Water District

MLR

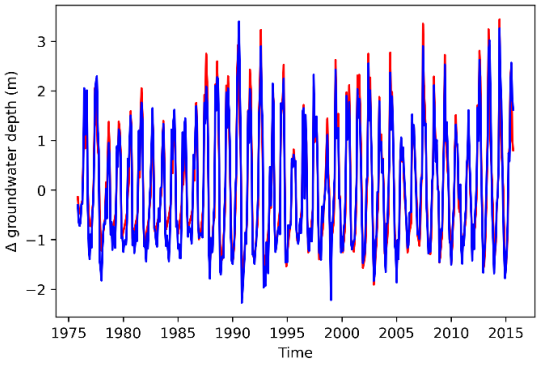

MLP

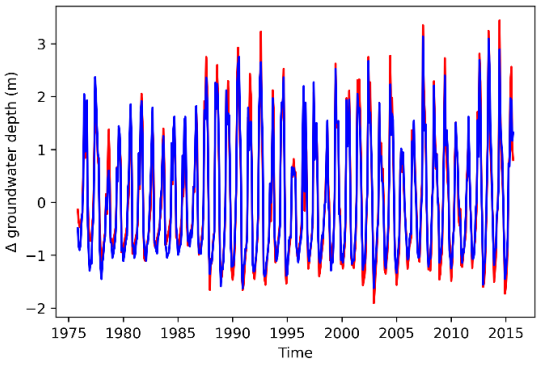

LSTM

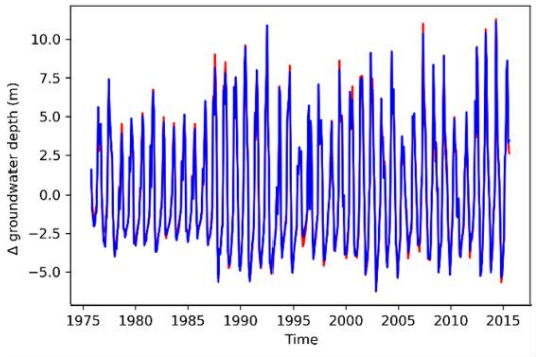

Cawelo Water District

MLR

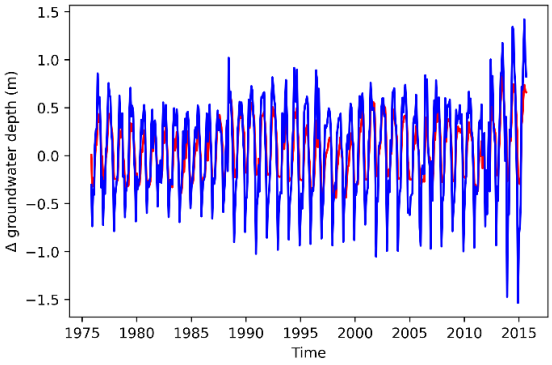

MLP

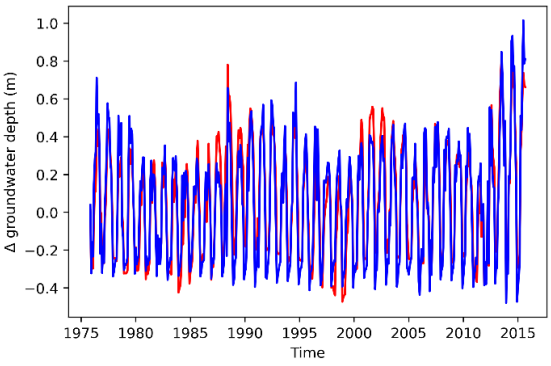

LSTM

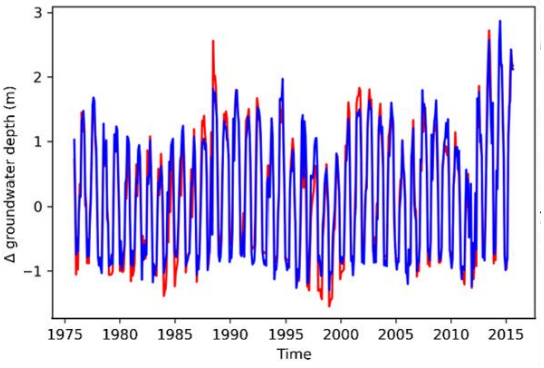

Shafter-Wasco Irrigation District

MLR

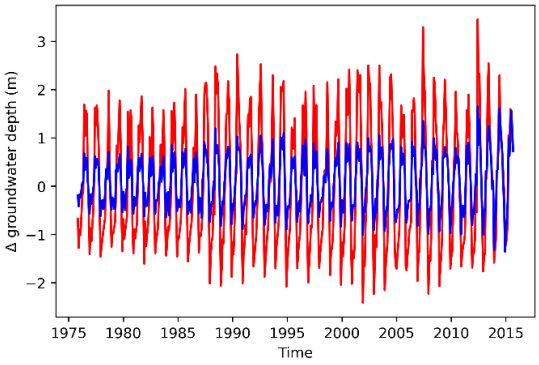

MLP

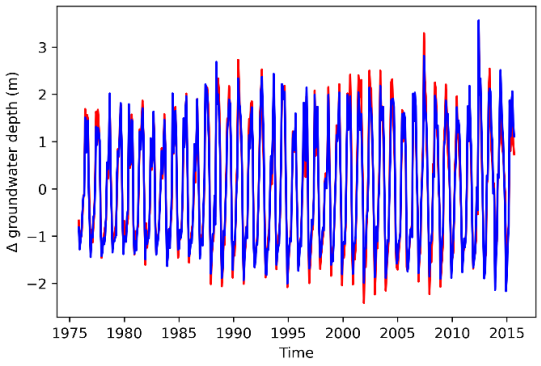

LSTM

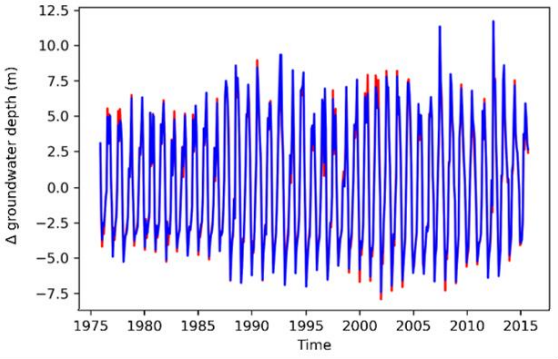

Buena Vista Water Storage District

MLR

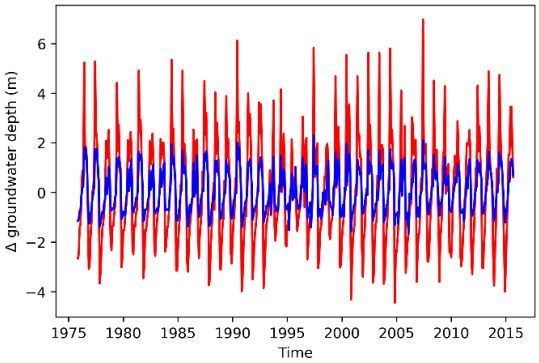

MLP

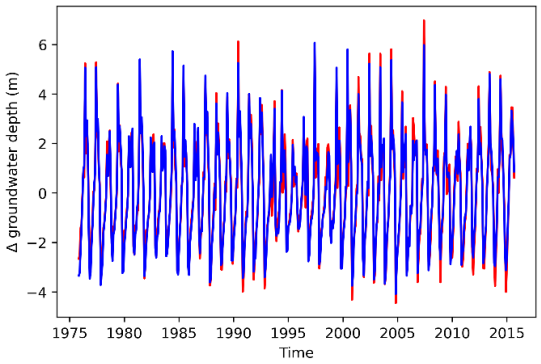

LSTM

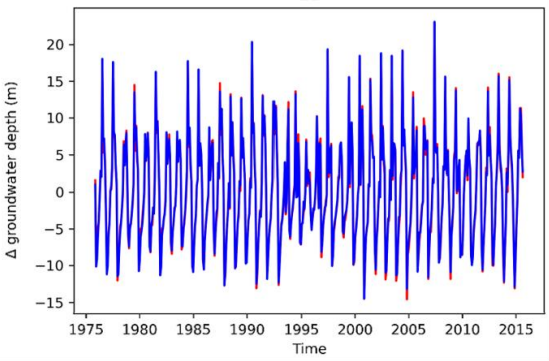

Henry Miller Water District

MLR

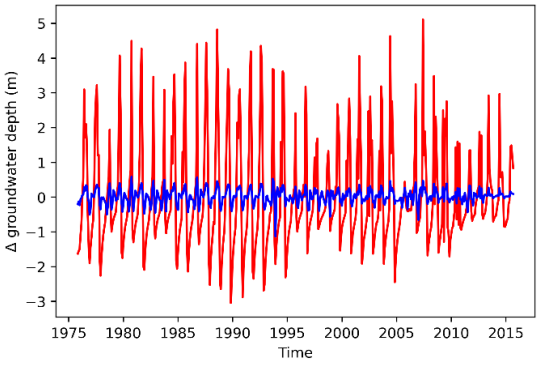

MLP

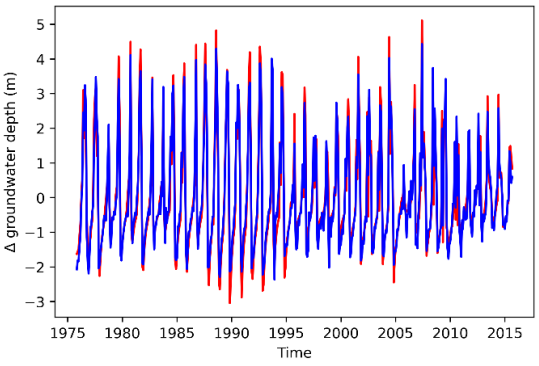

LSTM

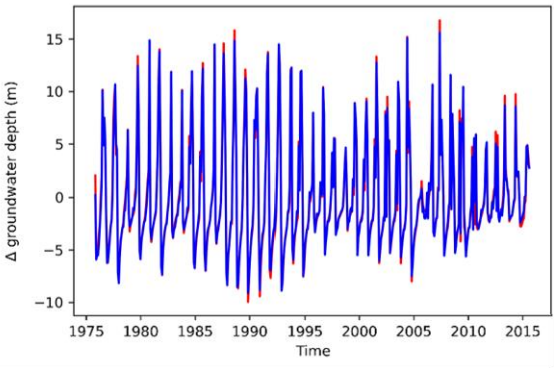

North Kern Water Storage District

MLR

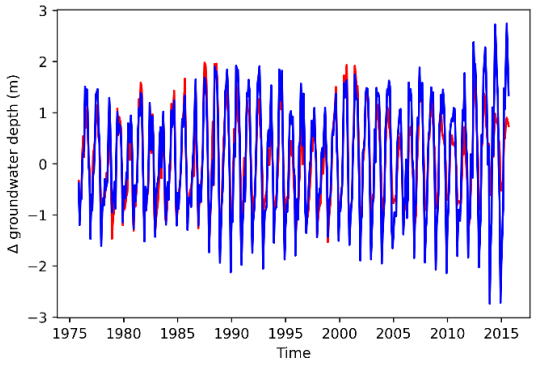

MLP

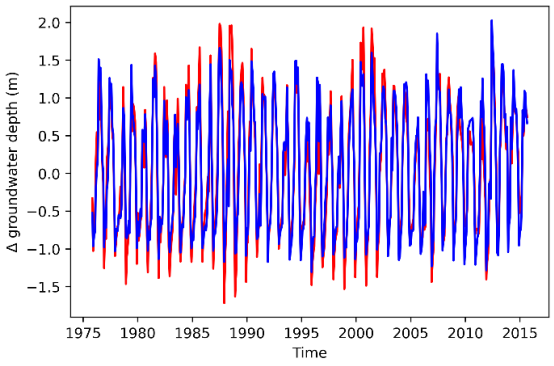

LSTM

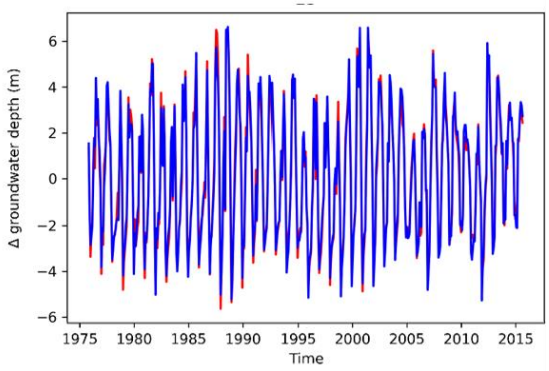

Tulare Irrigation District

MLR

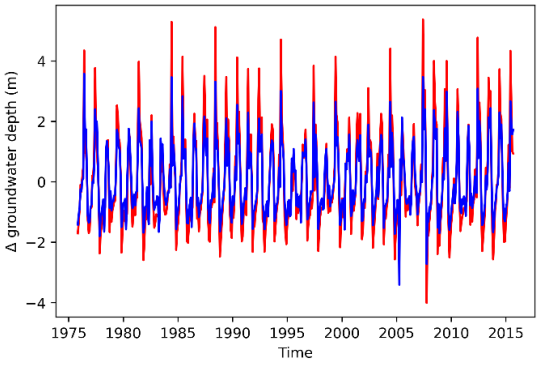

MLP

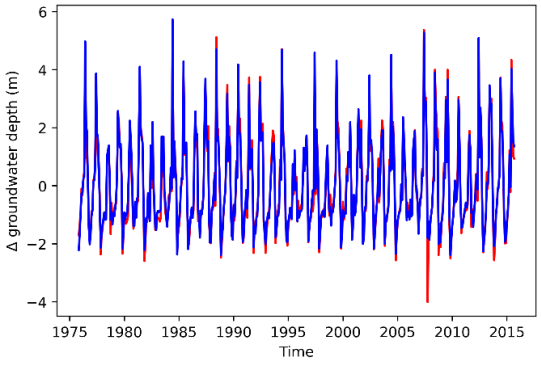

LSTM

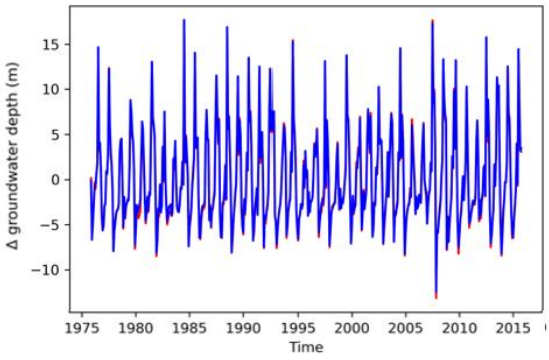

Saucelito Irrigation District

MLR

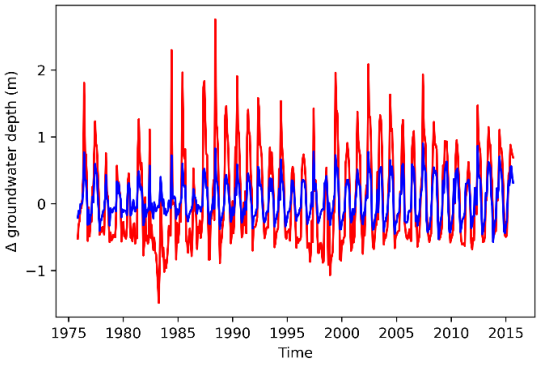

MLP

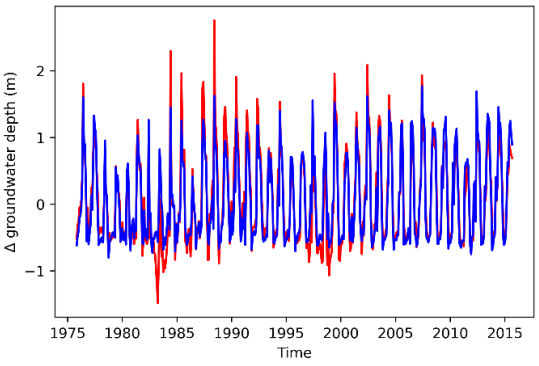

LSTM

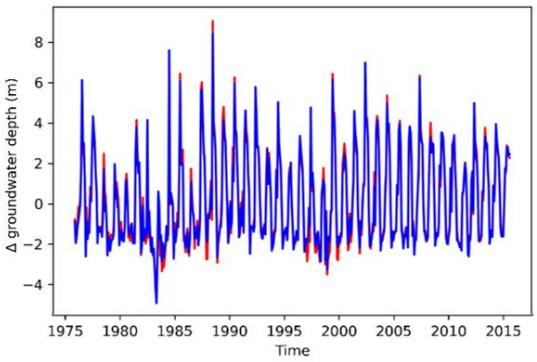

Delano Earlimart Irrigation District

MLR

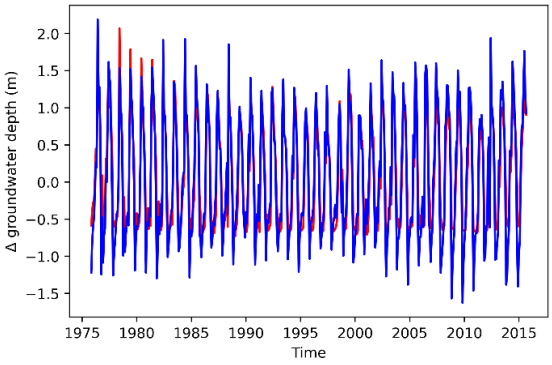

MLP

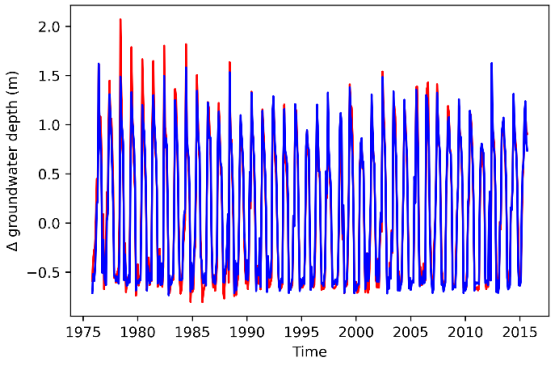

LSTM

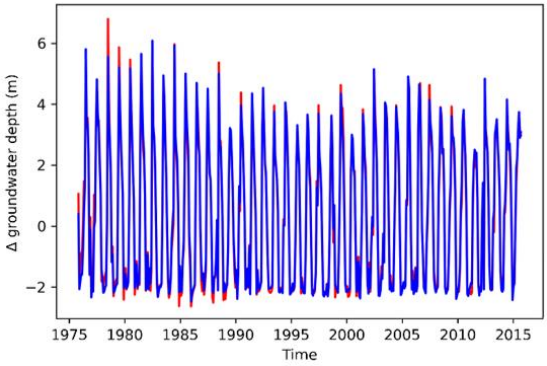

Kern Tulare Water District

MLR

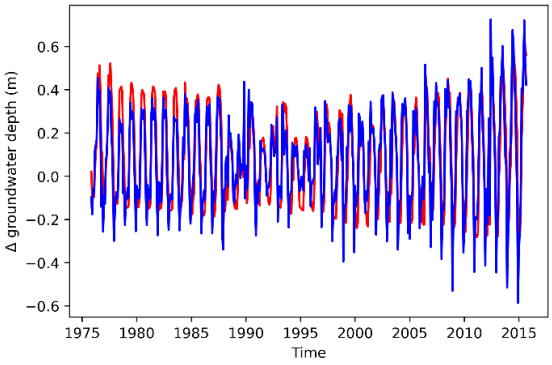

MLP

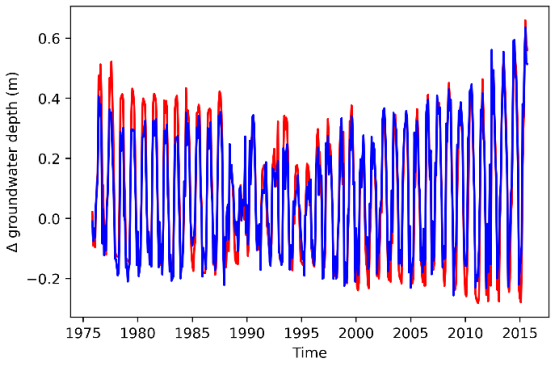

LSTM

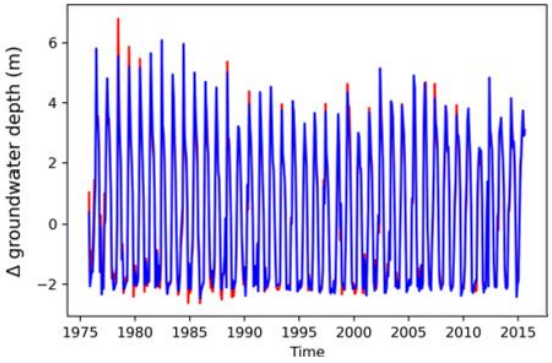

Appendix B Climate change impacts on groundwater levels for irrigated agriculture in the greater Kern County region, additional information

Appendix B.1 Seasonal distribution of precipitation, surface water deliveries, and agricultural water demand for historical and projected climate

Historical data is presented in green, while the future climate projections for each Global Climate Model (GCM) are depicted in blue for RCP 4.5 and orange for RCP 8.5. The horizontal axis displays four temporal intervals: Historical (HIST, 1974-2015), beginning of the century (BOC, 2016-2040); middle of the century (MOC, 2041-2070), end of the century (EOC, 2071-2099). The irrigation period runs from March 1 to September 30.

Semitropic WSD, CanESM2

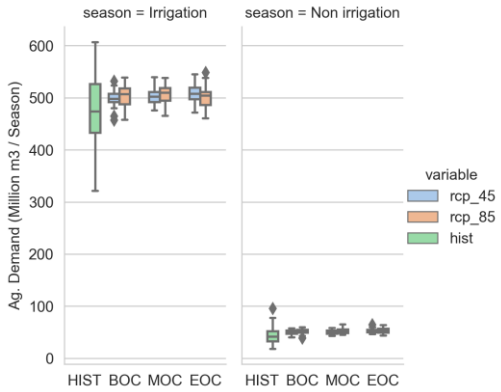

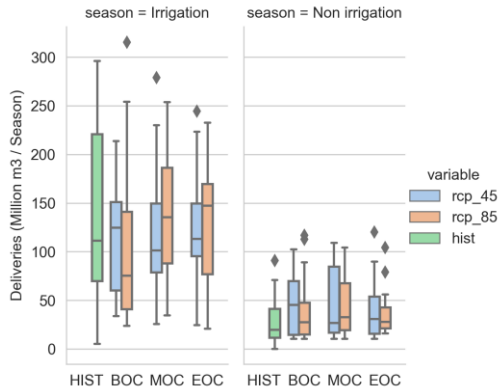

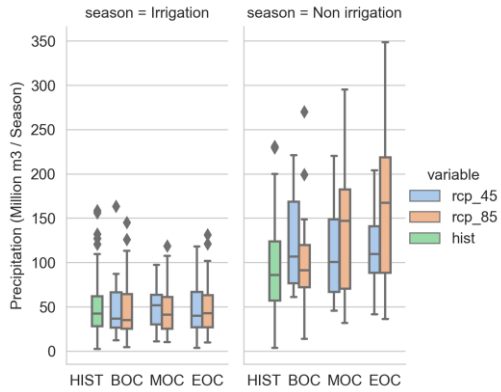

Semitropic WSD, CCSM4

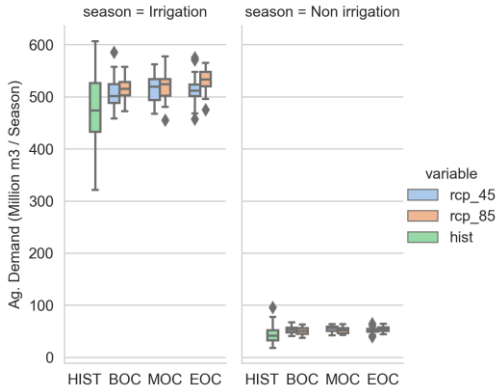

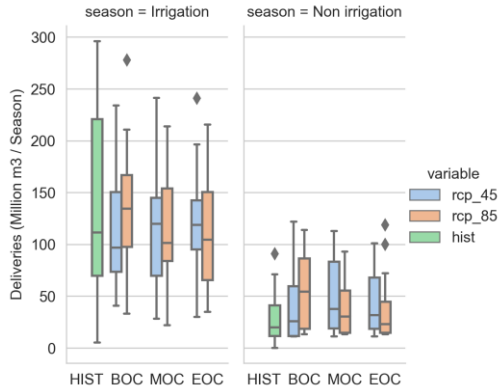

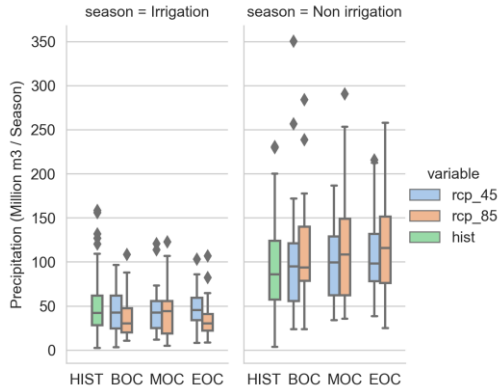

Semitropic WSD, CNRM-CM5

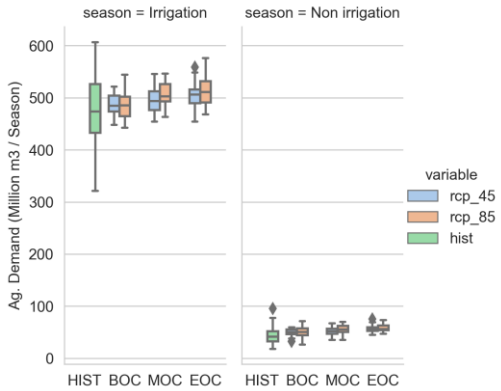

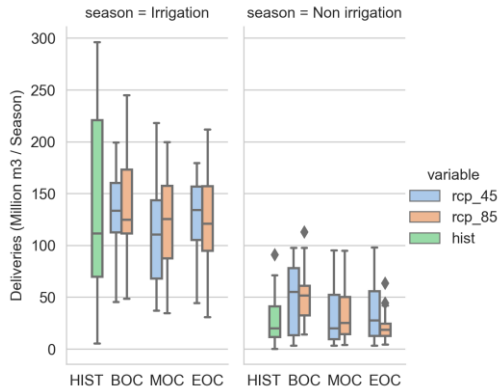

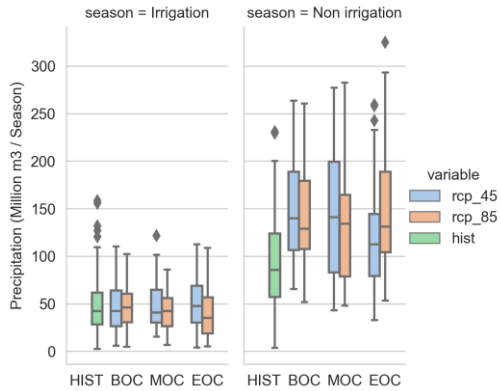

Semitropic WSD, HadGEM2-CC

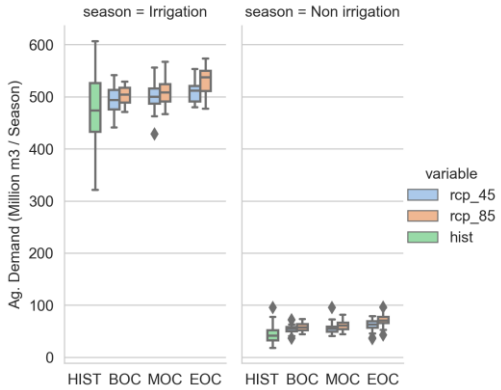

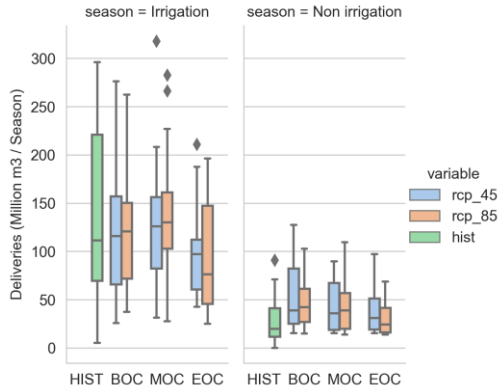

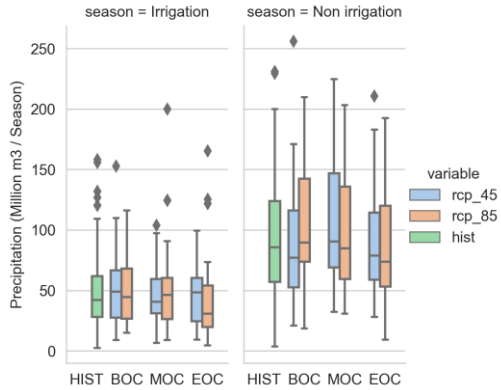

Semitropic WSD, HadGEM2-ES

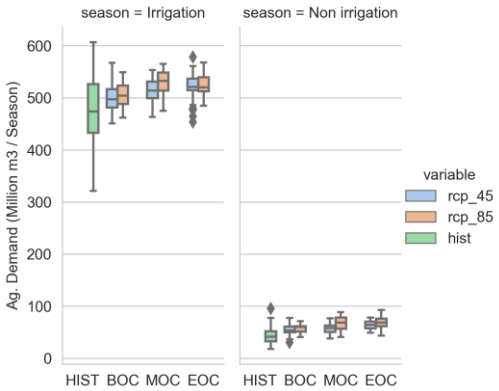

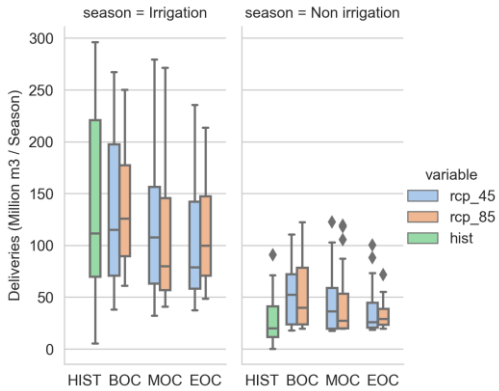

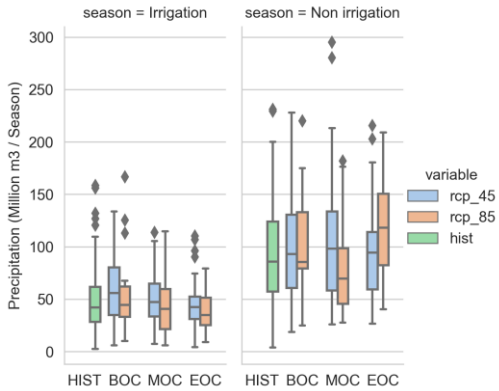

Semitropic WSD, MIROC5

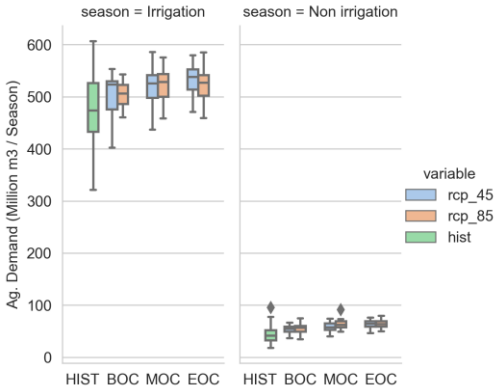

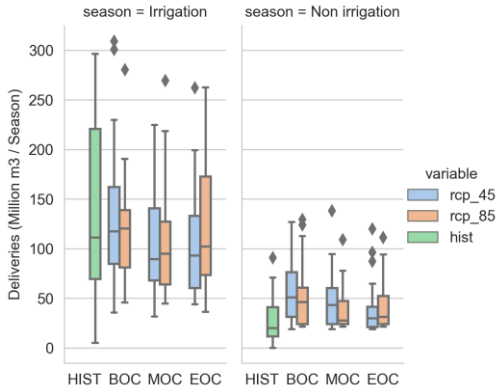

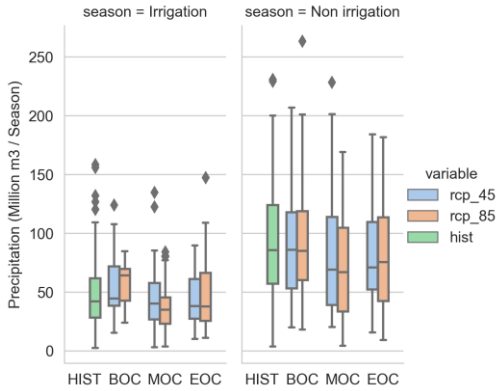

Wheeler Ridge-Maricopa WSD, CanESM2

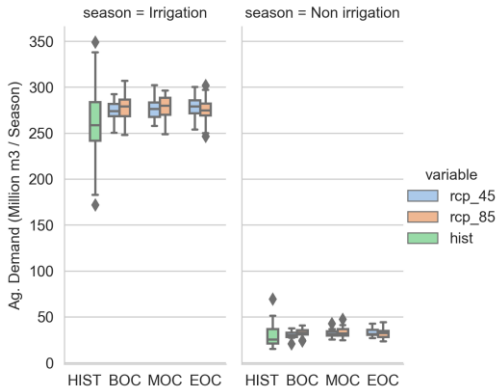

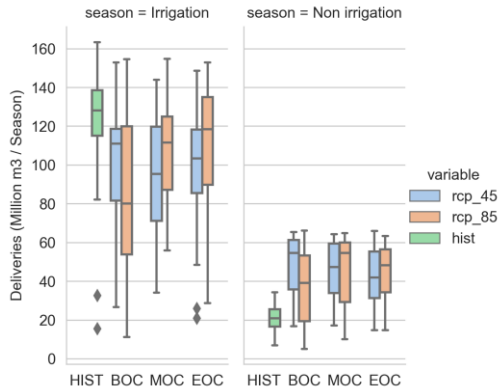

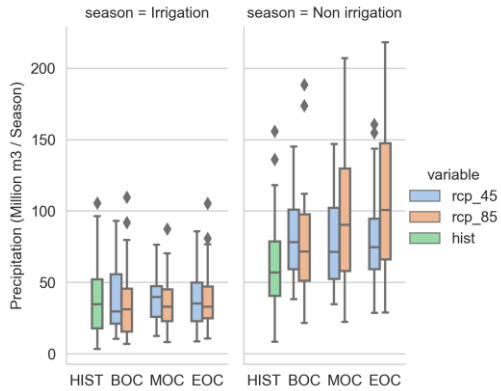

Wheeler Ridge-Maricopa WSD, CCSM4

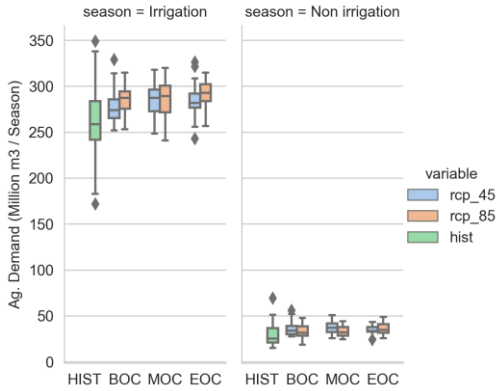

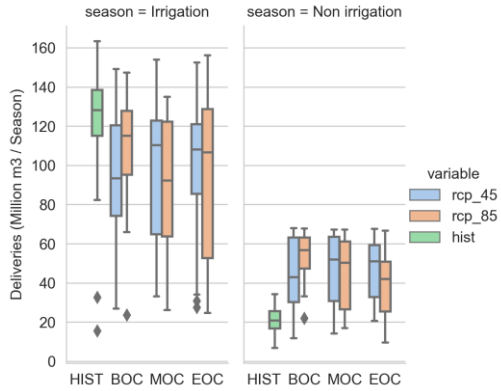

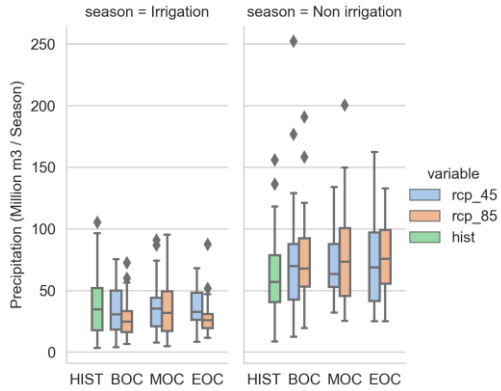

Wheeler Ridge-Maricopa WSD, CNRM-CM5

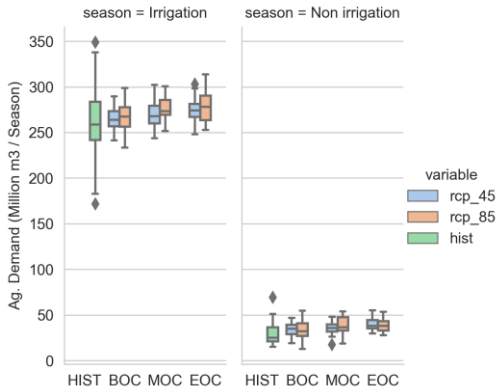

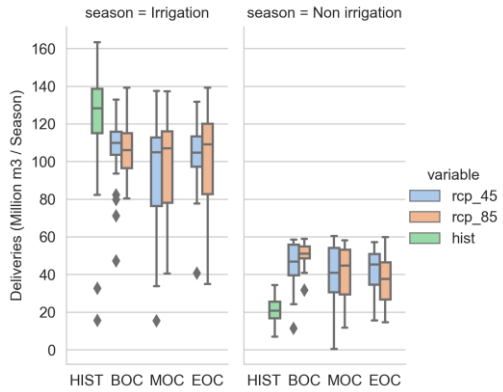

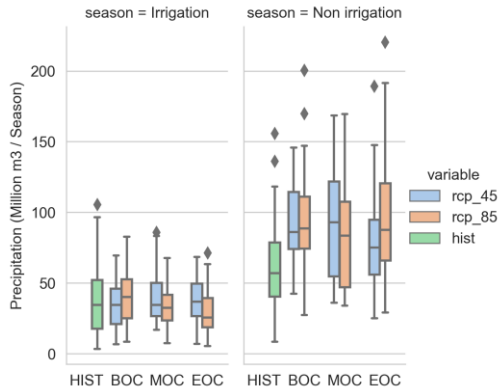

Wheeler Ridge-Maricopa WSD, HadGEM2-CC

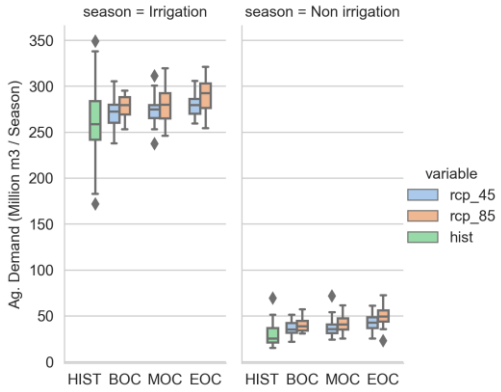

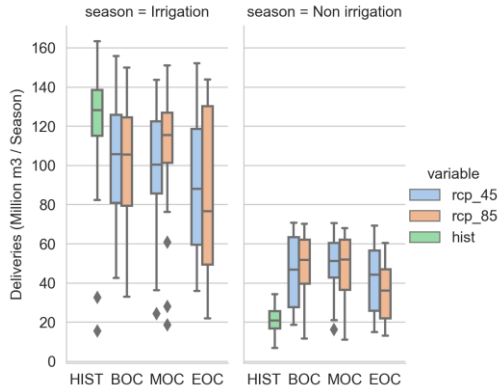

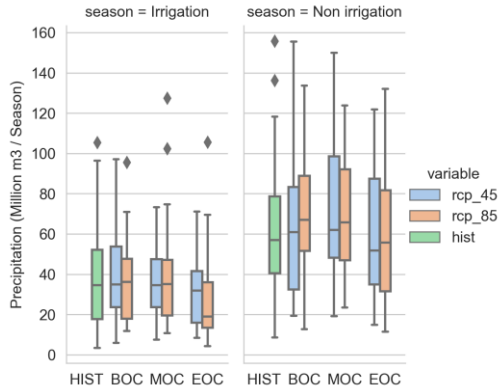

Wheeler Ridge-Maricopa WSD, HadGEM2-ES

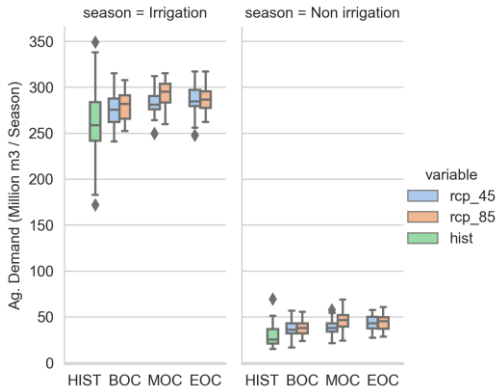

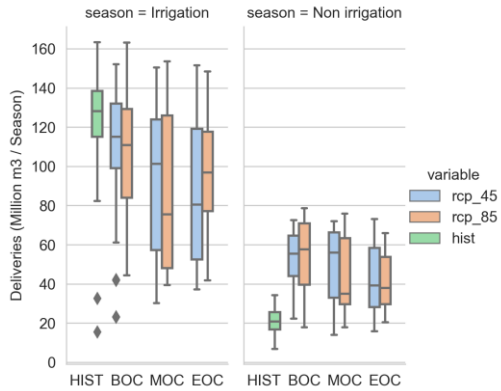

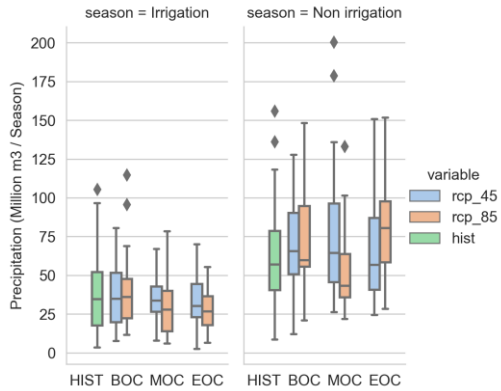

Wheeler Ridge-Maricopa WSD, MIROC5

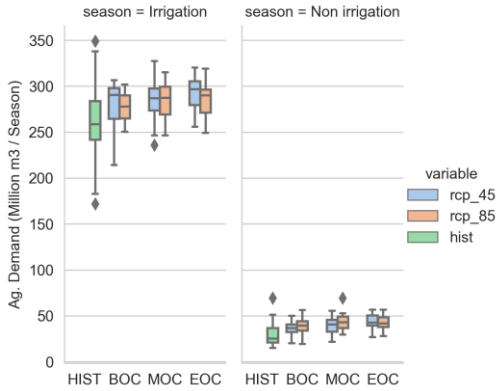

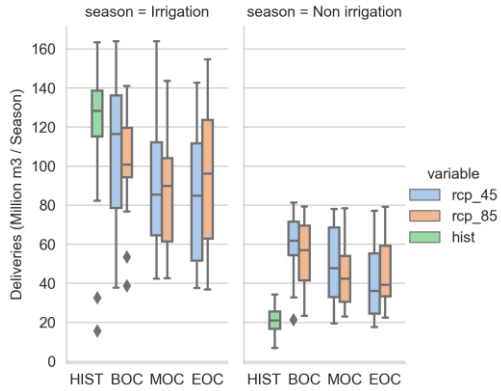

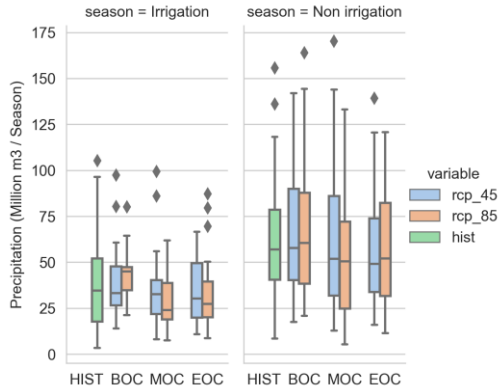

Kern Delta WD, CanESM2

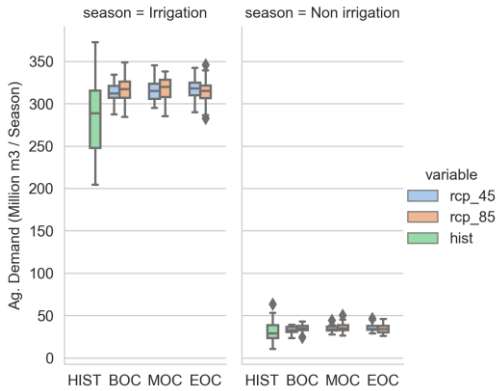

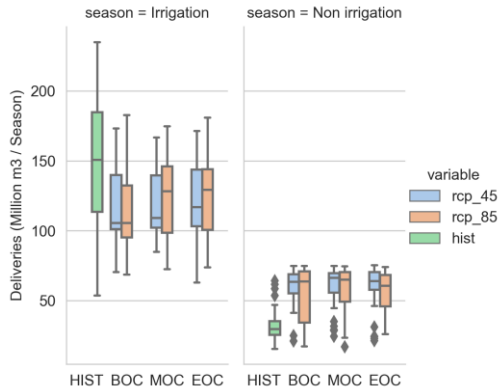

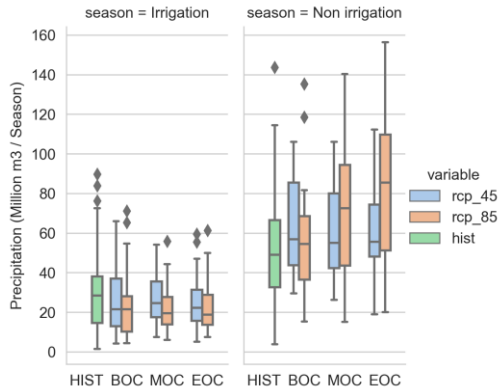

Kern Delta WD, CCSM4

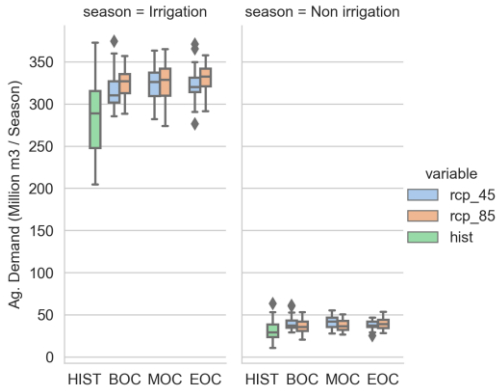

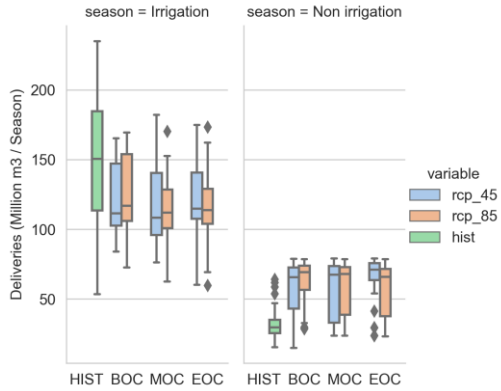

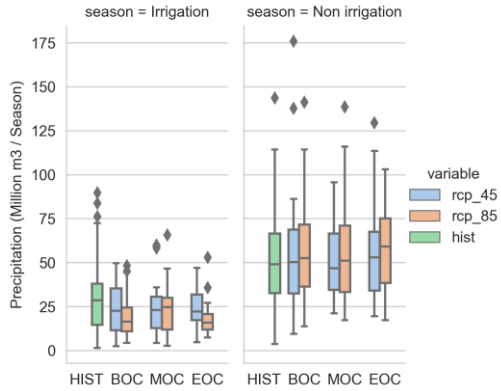

Kern Delta WD, CNRM-CM5

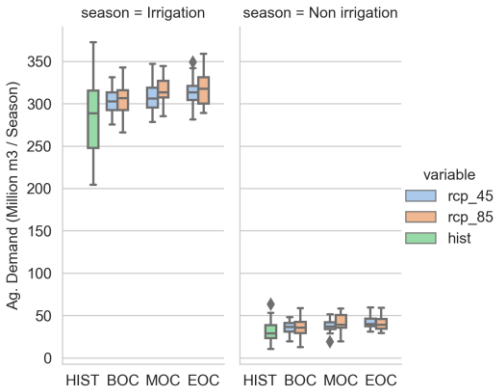

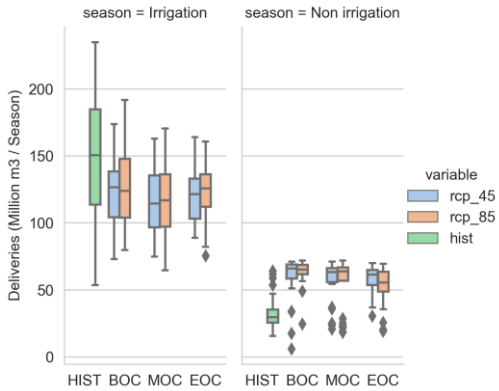

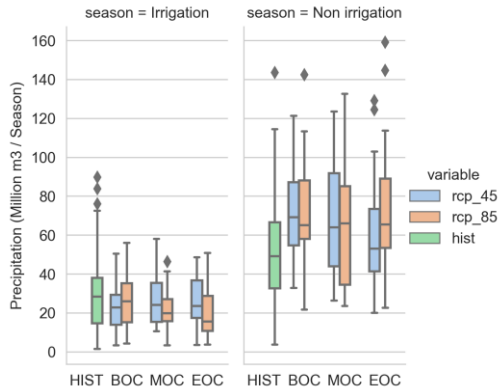

Kern Delta WD, HadGEM2-CC

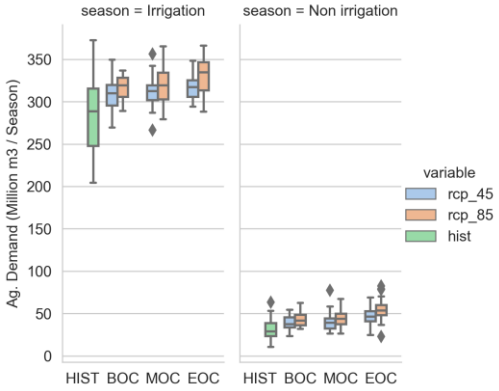

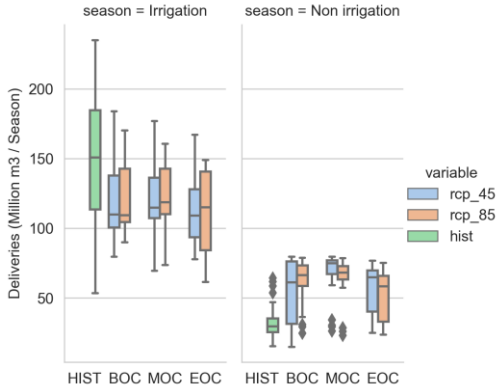

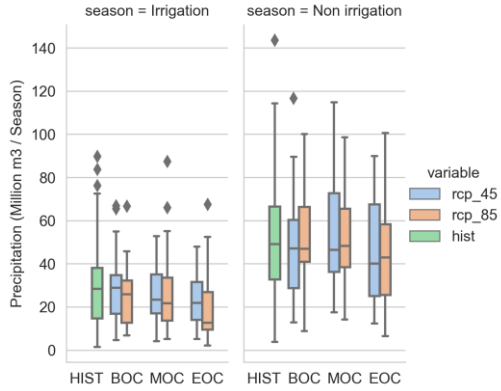

Kern Delta WD, HadGEM2-ES

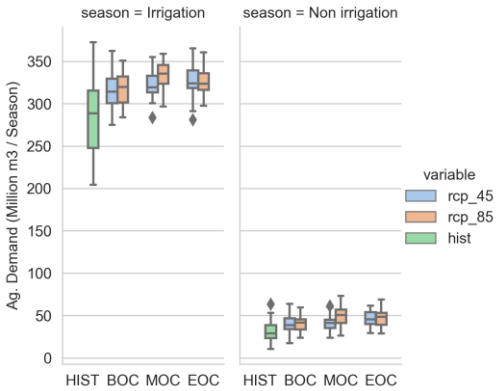

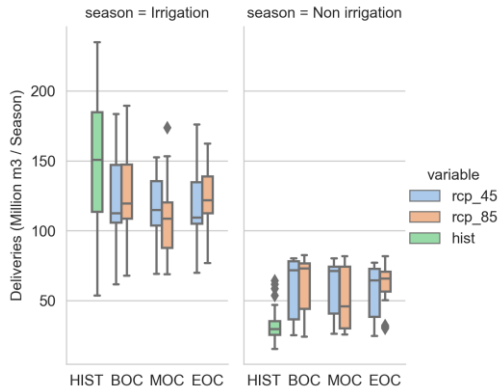

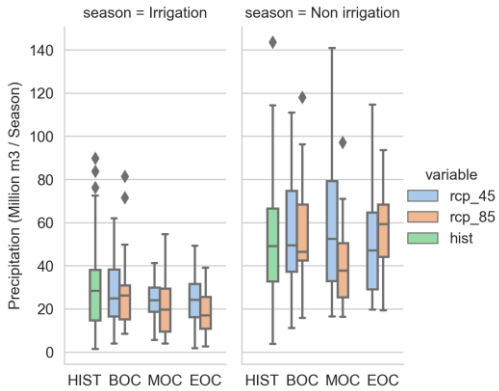

Kern Delta WD, MIROC5

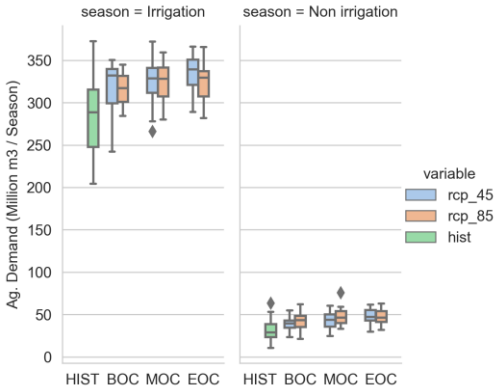

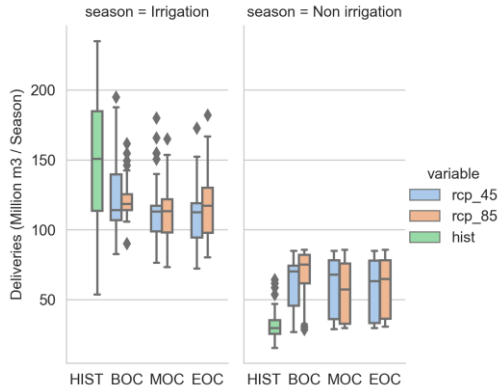

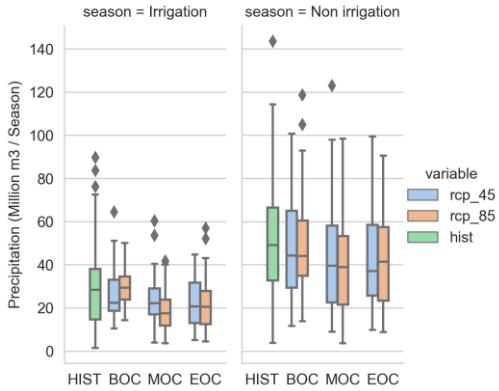

Cawelo WD, CanESM2

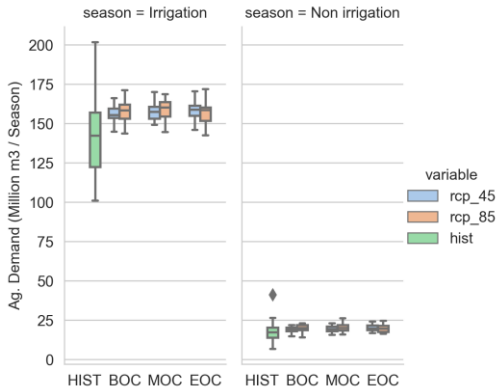

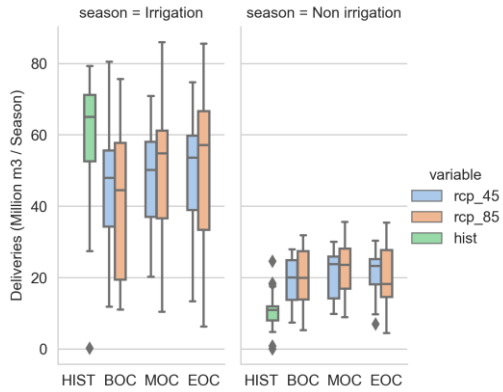

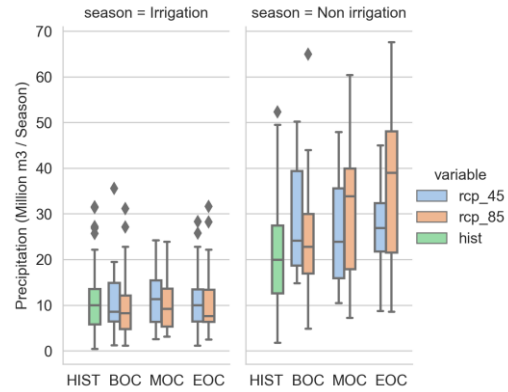

Cawelo WD, CCSM4

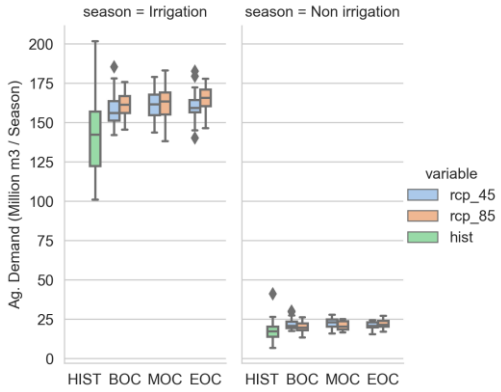

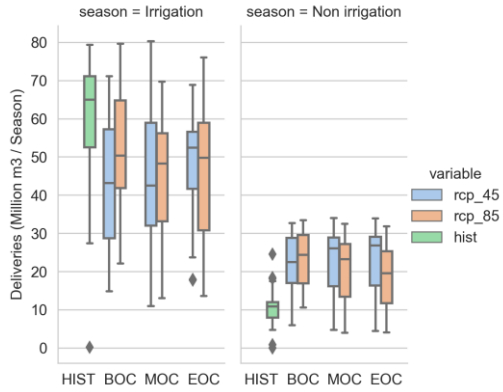

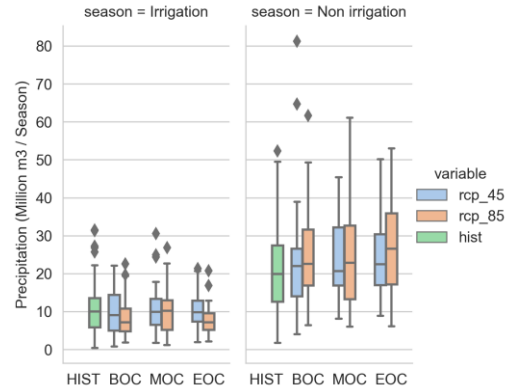

Cawelo WD, CNRM-CM5

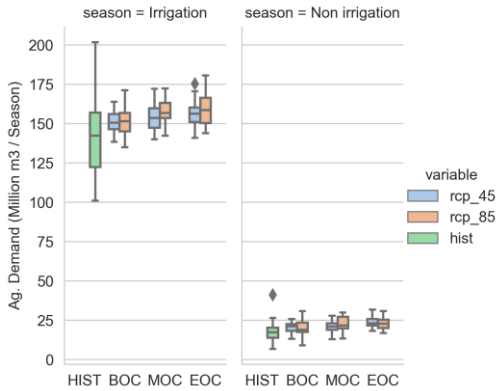

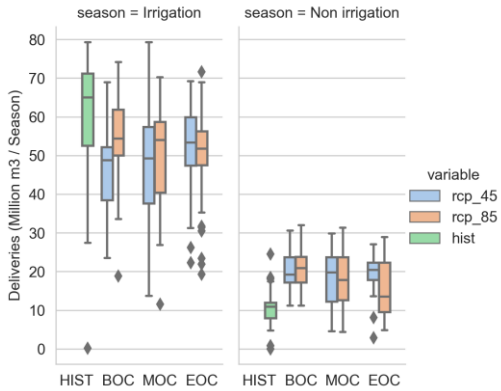

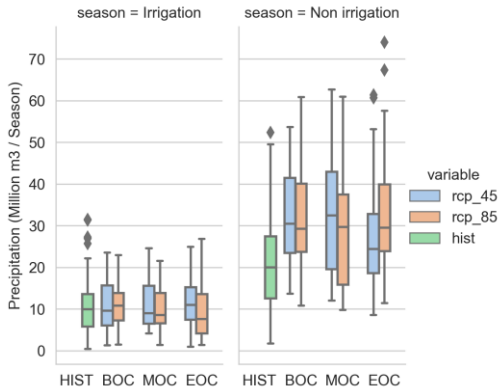

Cawelo WD, HadGEM2-CC

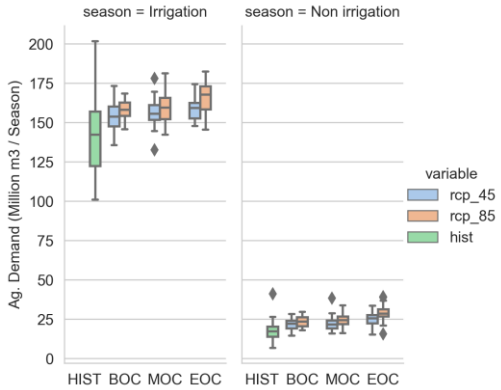

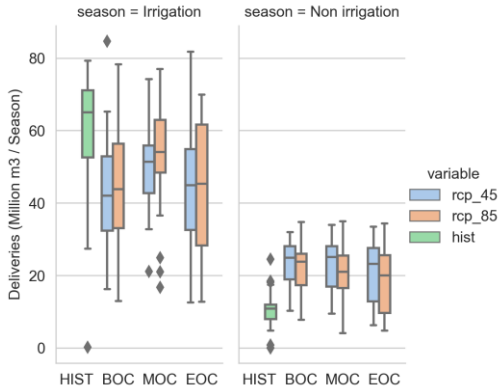

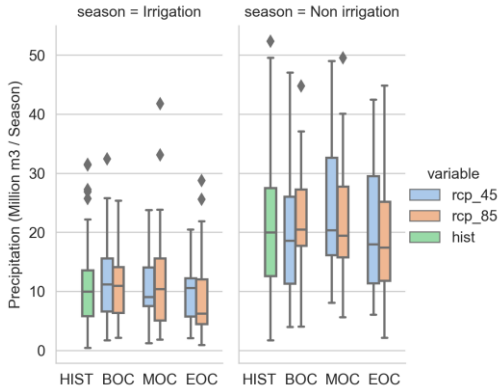

Cawelo WD, HadGEM2-ES

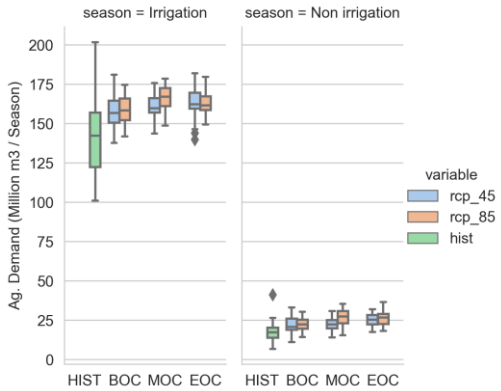

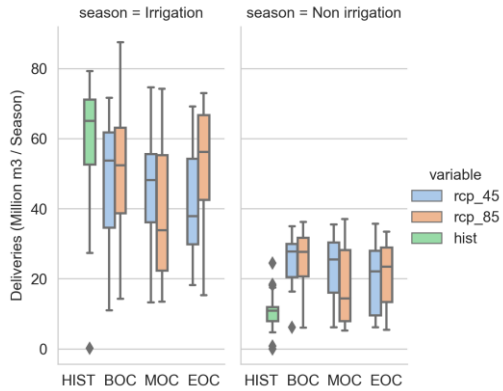

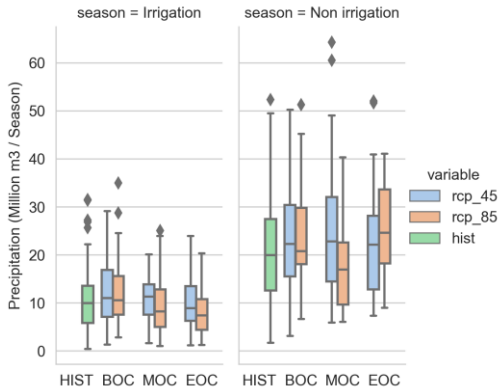

Cawelo WD, MIROC5

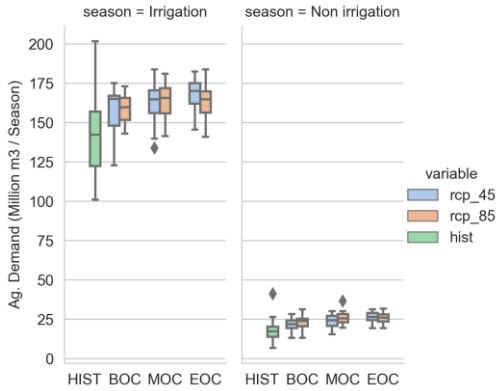

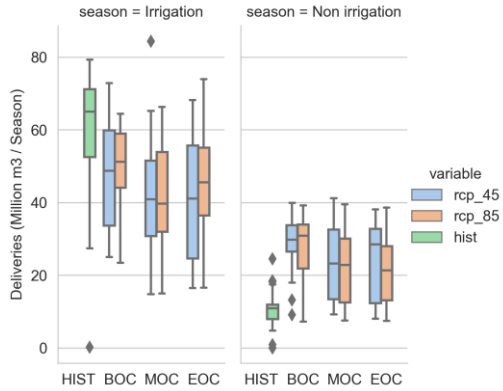

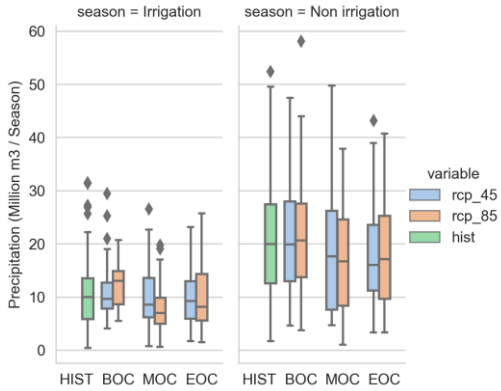

Shafter Wasco ID, CanESM2

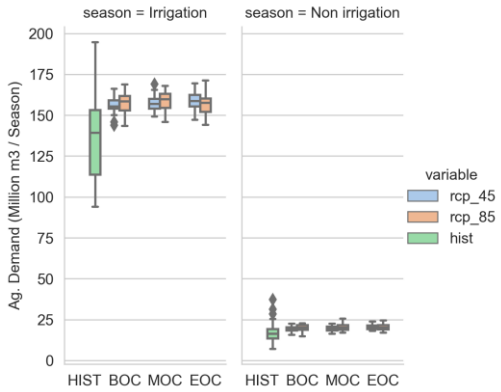

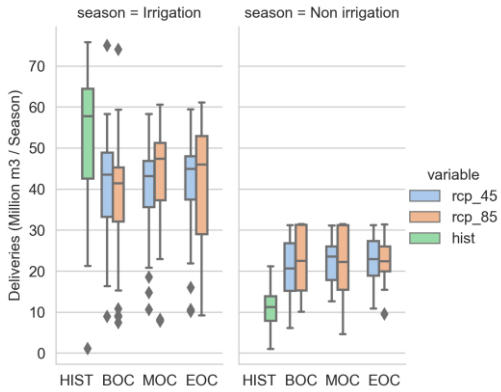

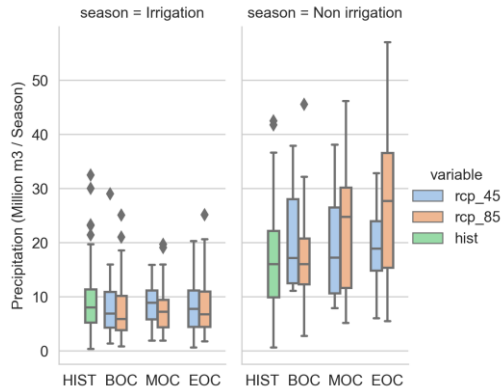

Shafter Wasco ID, CCSM4

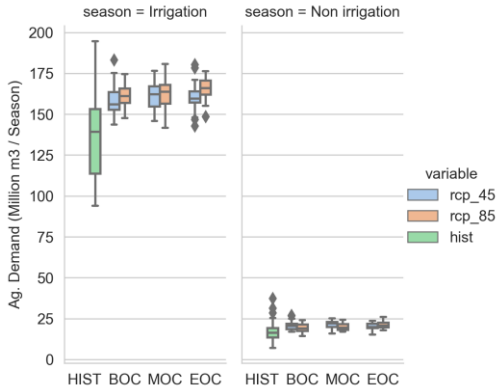

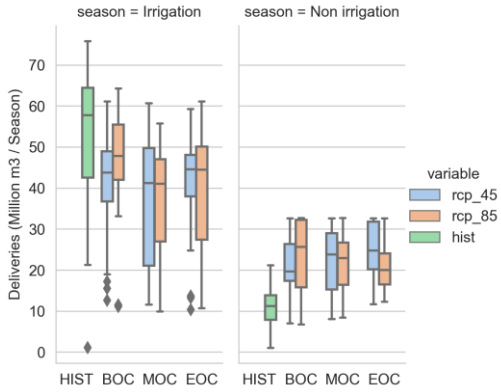

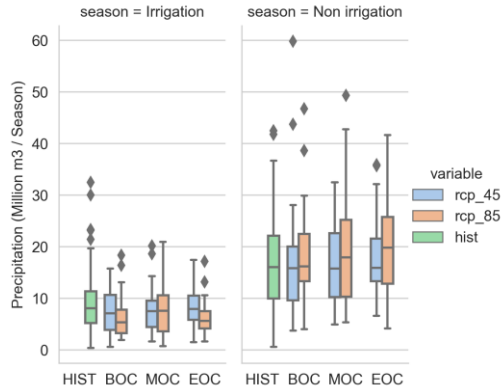

Shafter Wasco ID, CNRM-CM5

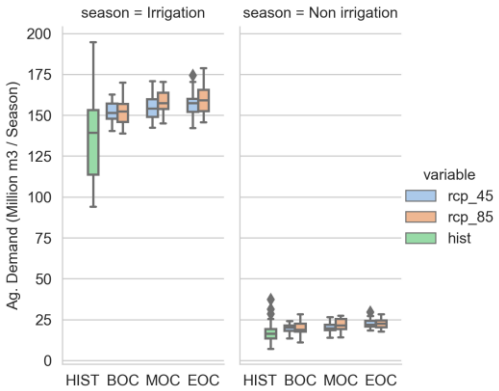

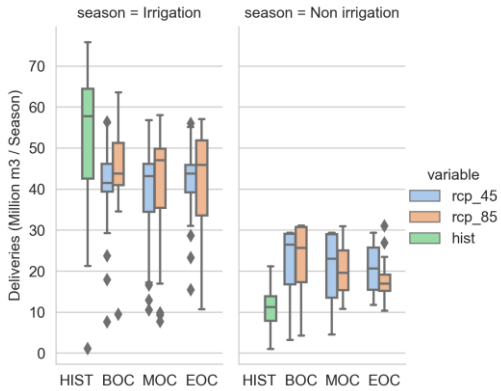

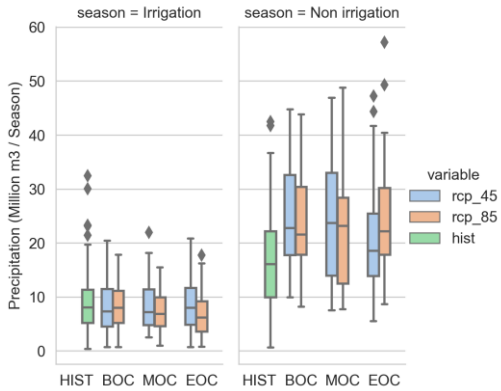

Shafter Wasco ID, HadGEM2-CC

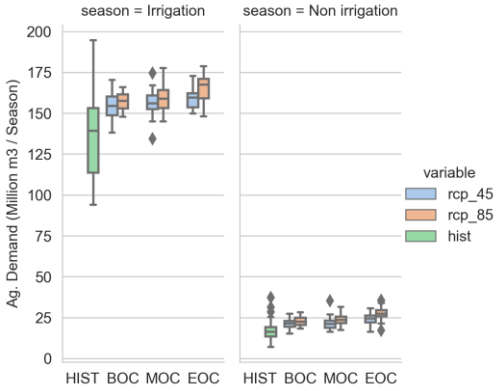

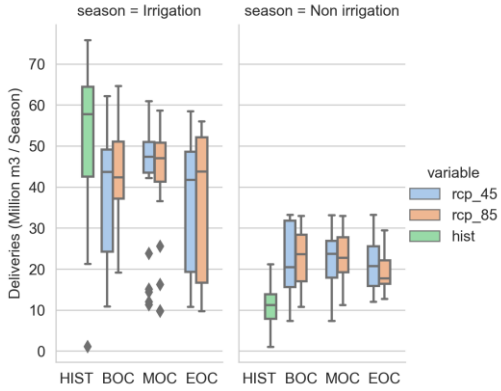

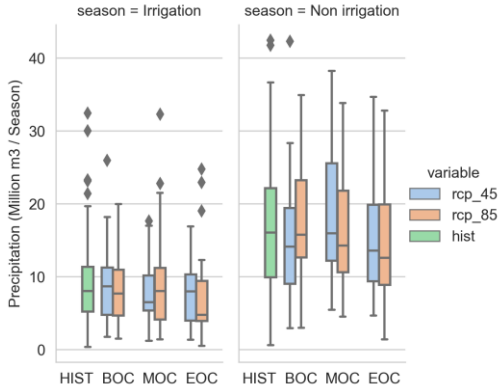

Shafter Wasco ID,HadGEM2-ES

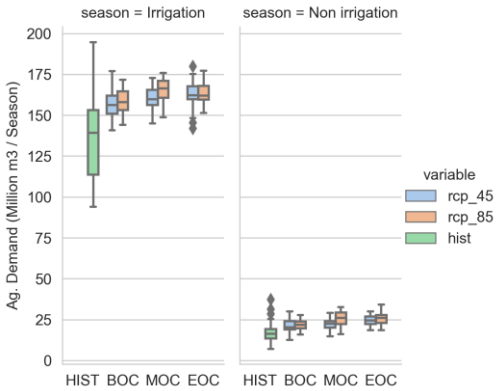

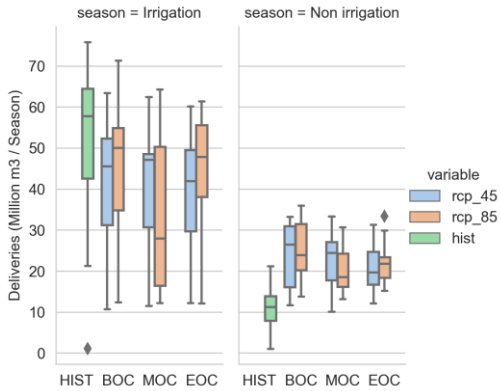

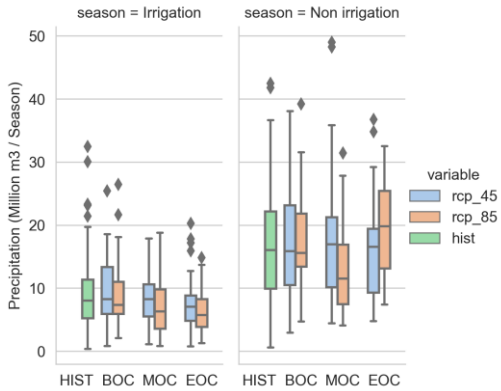

Shafter Wasco ID, MIROC5

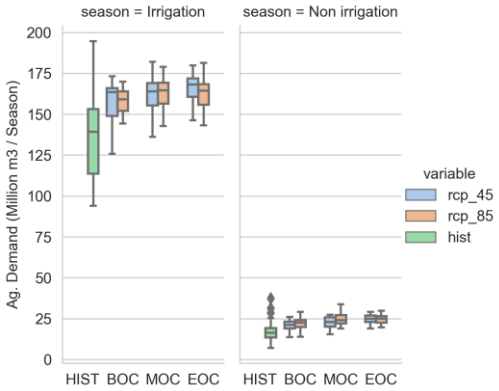

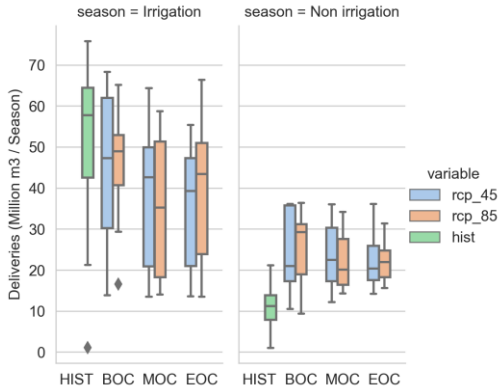

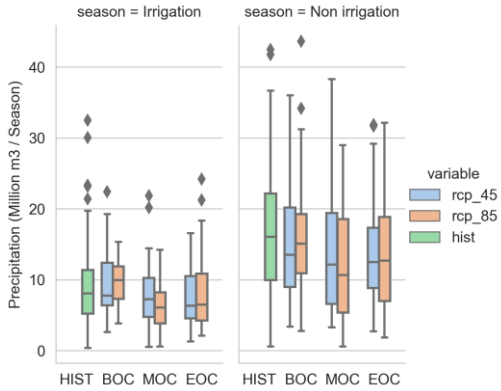

Buena Vista WSD, CanESM2

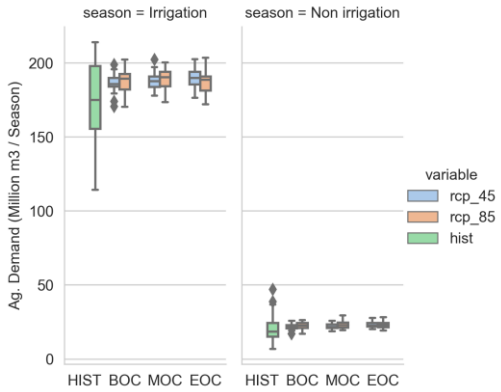

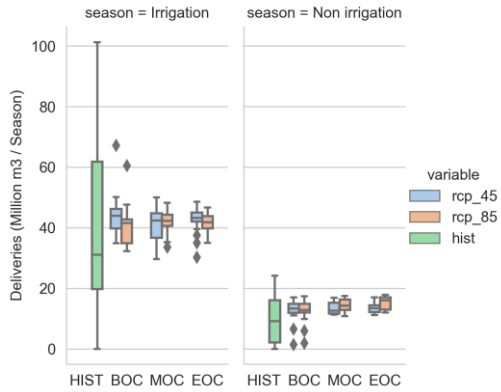

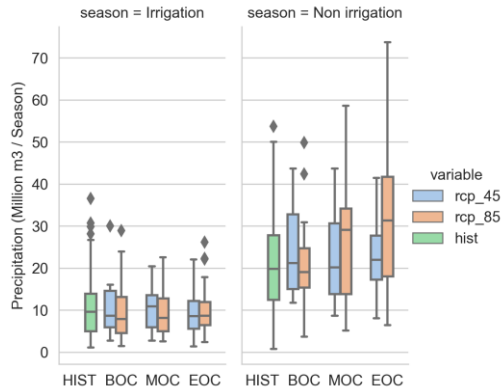

Buena Vista WSD, CCSM4

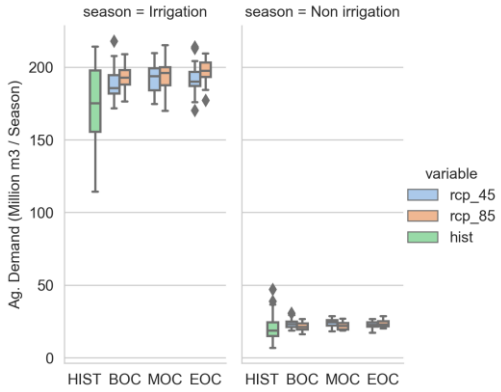

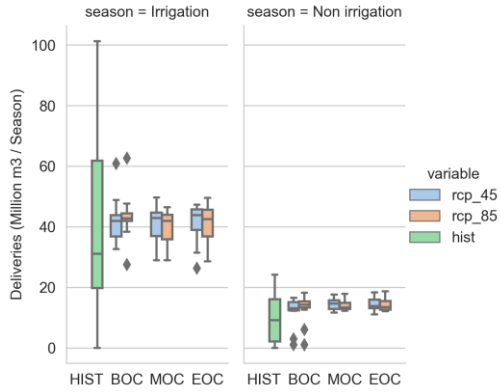

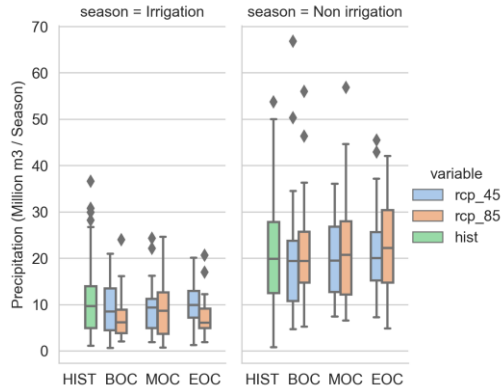

Buena Vista WSD, CNRM-CM5

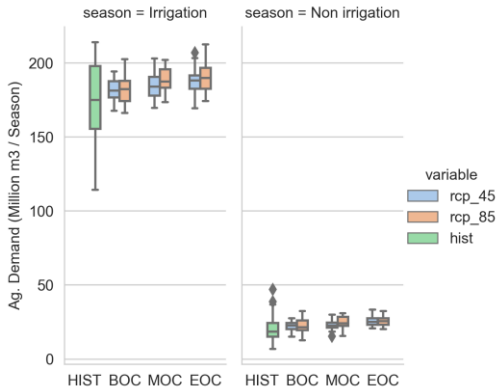

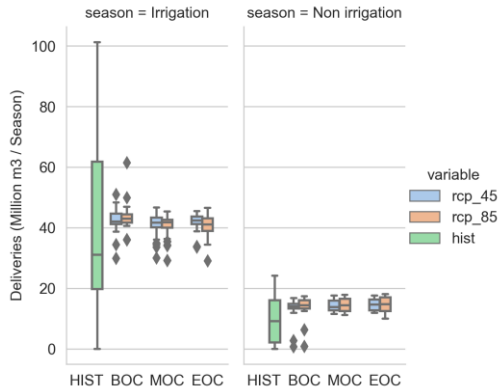

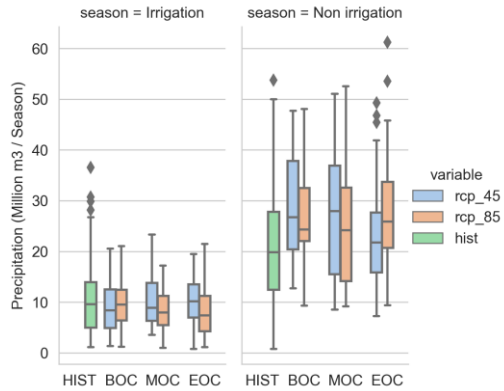

Buena Vista WSD, HadGEM2-CC

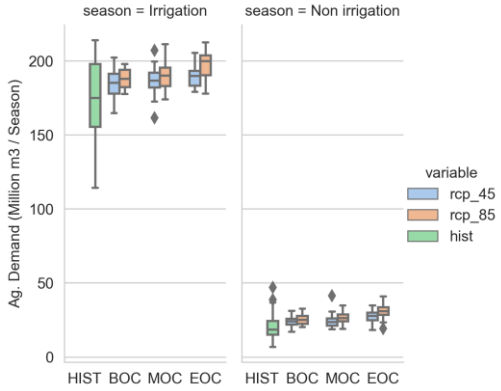

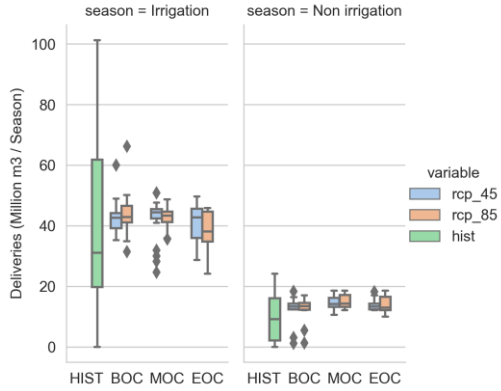

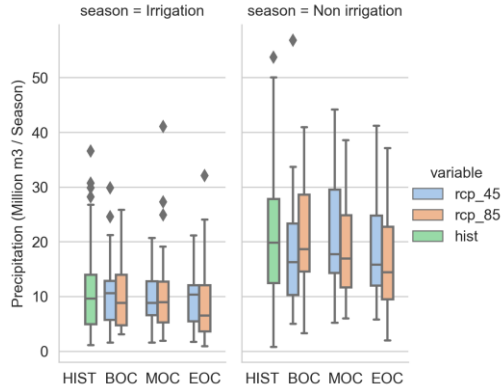

Buena Vista WSD, HadGEM2-ES

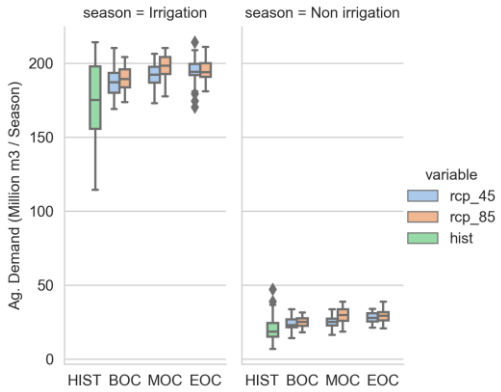

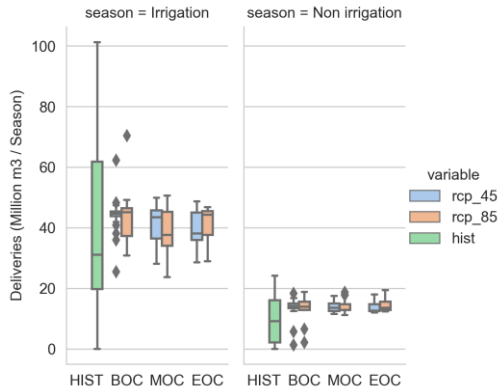

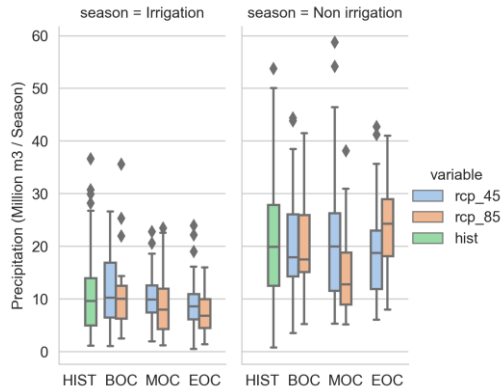

Buena Vista WSD, MIROC5

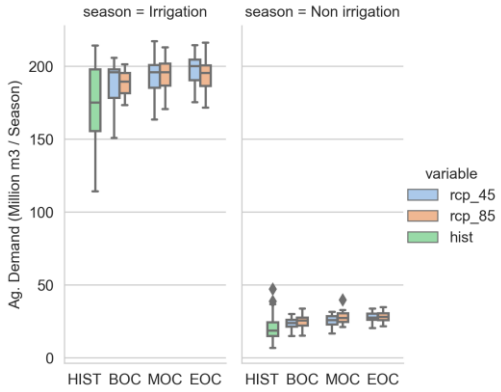

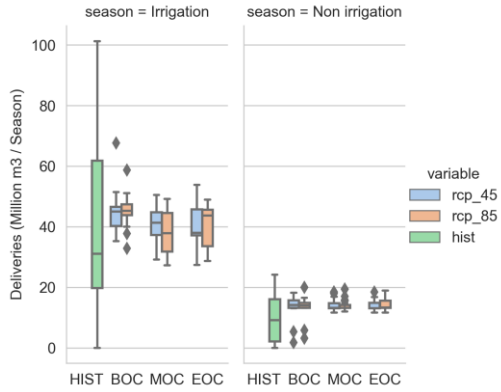

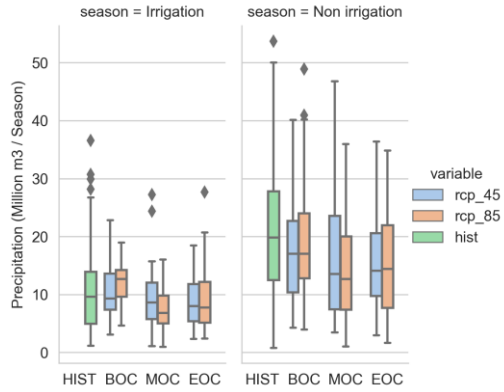

North Kern WSD, CanESM2

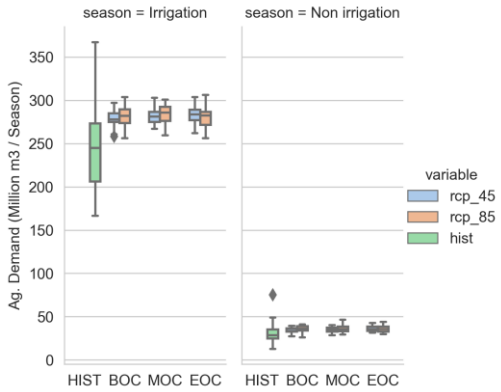

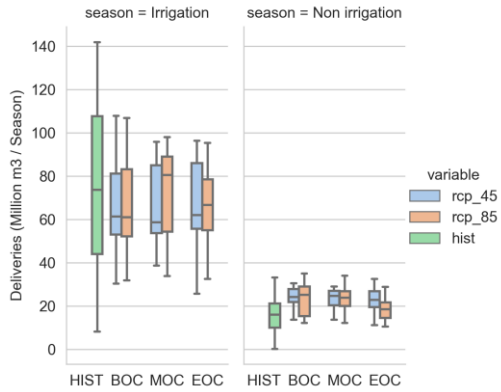

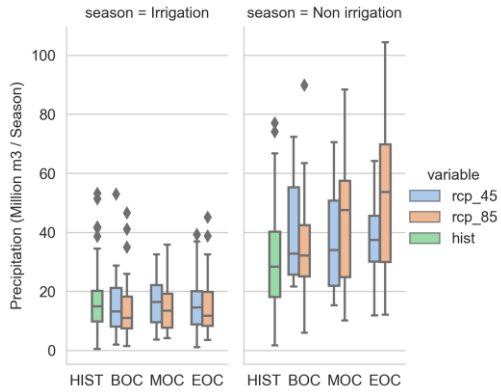

North Kern WSD, CCSM4

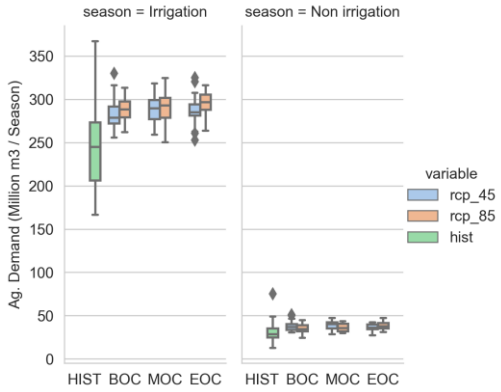

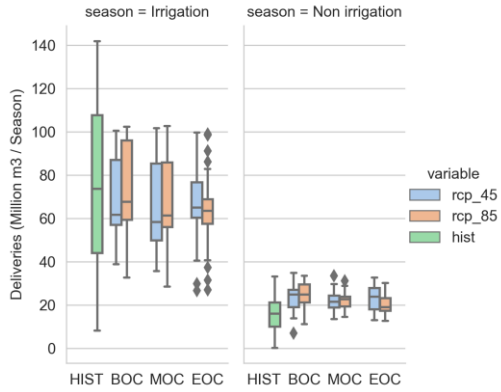

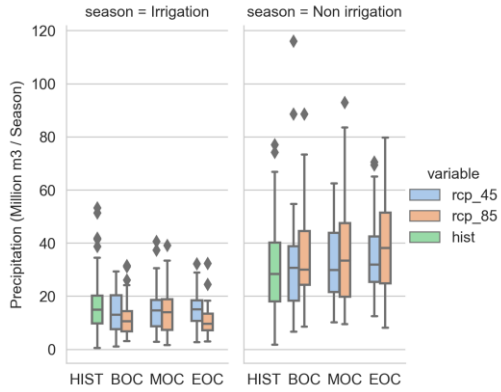

North Kern WSD, CNRM-CM5

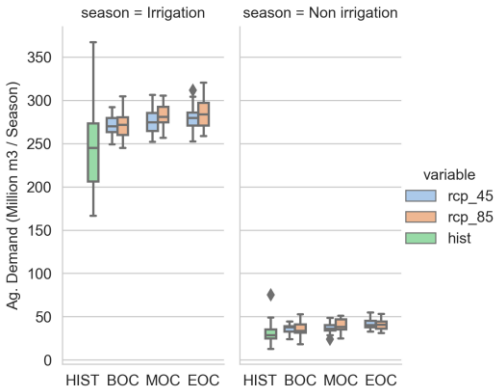

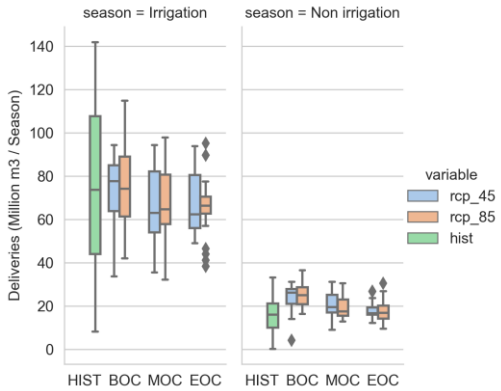

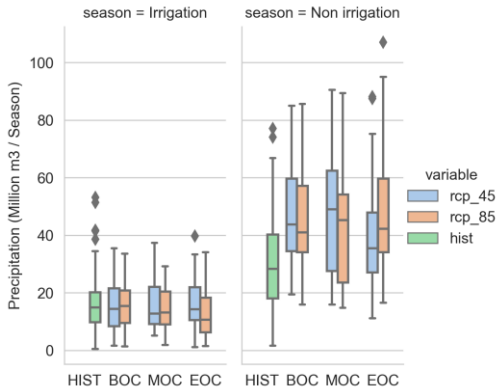

North Kern WSD, HadGEM2-CC

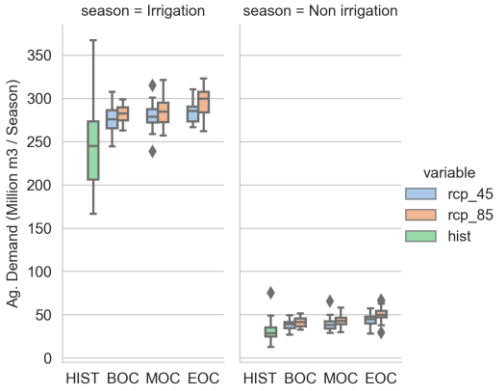

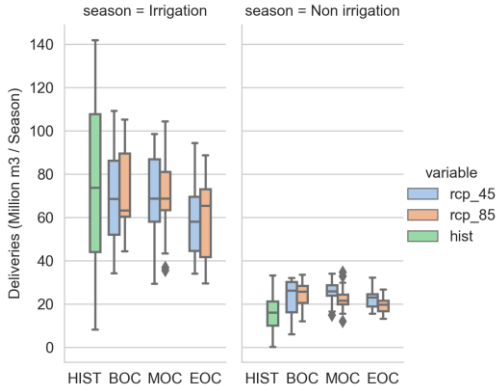

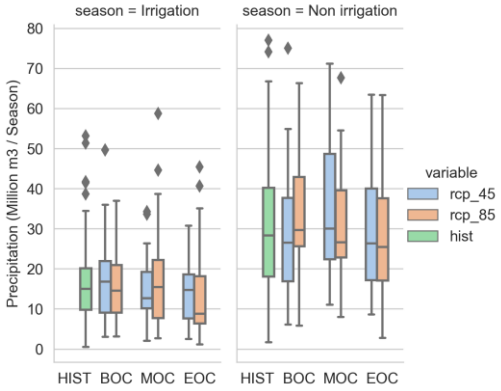

North Kern WSD, HadGEM2-ES

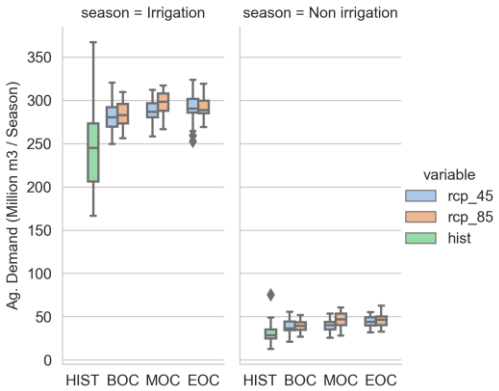

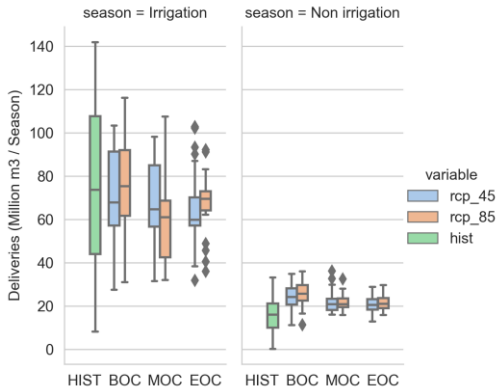

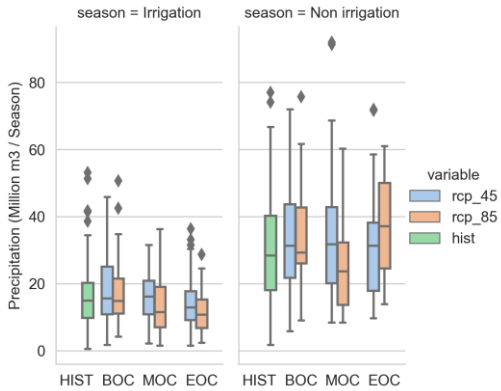

North Kern WSD, MIROC5

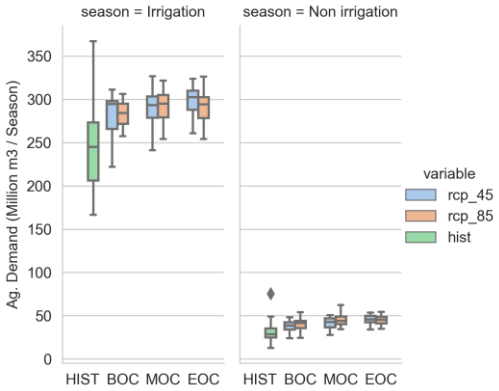

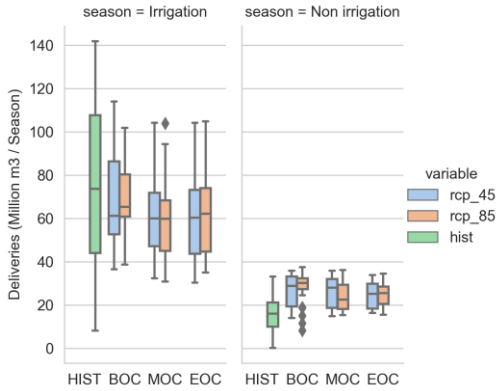

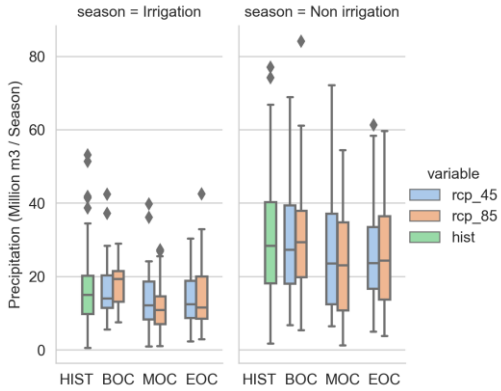

Delano - Earlimart ID, CanESM2

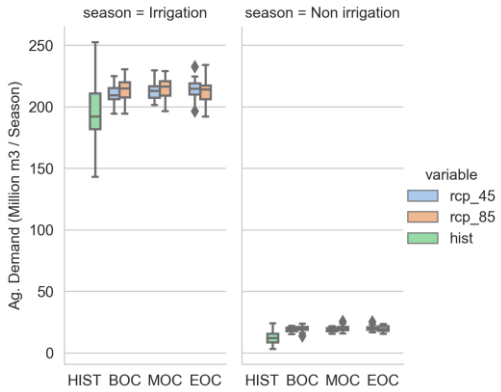

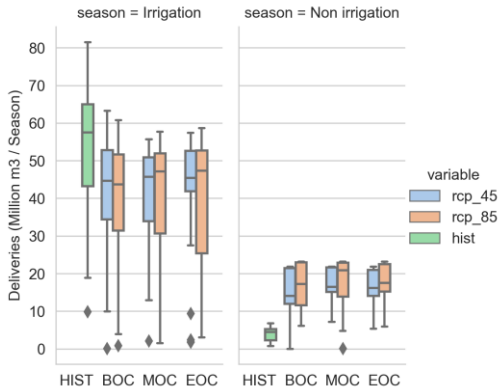

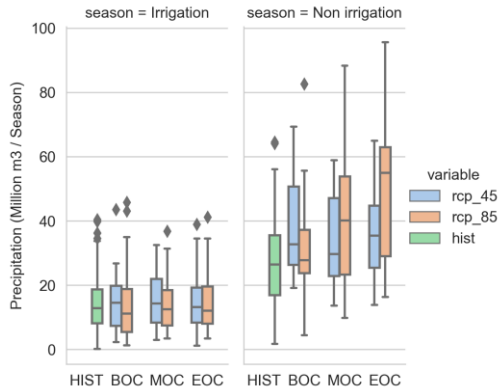

Delano - Earlimart ID, CCSM4

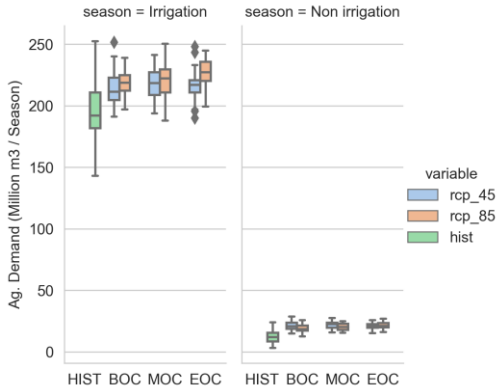

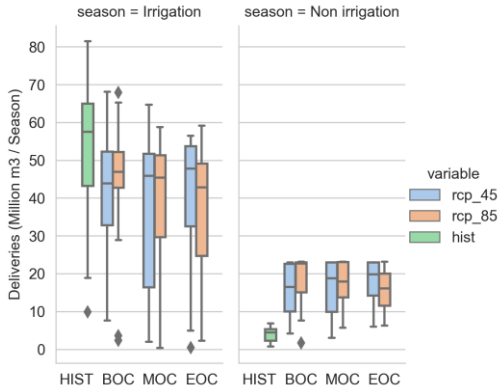

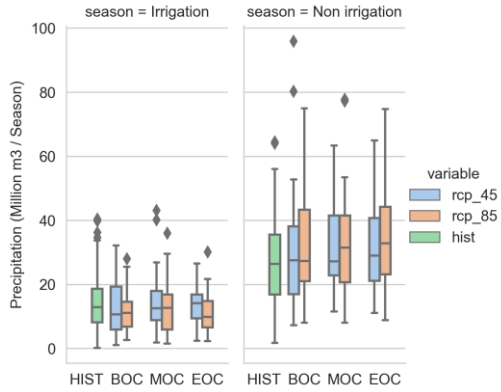

Delano - Earlimart ID, CNRM-CM5

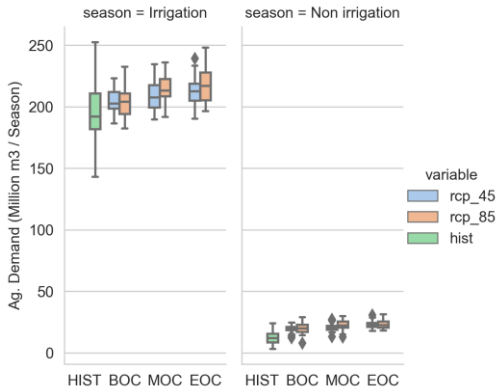

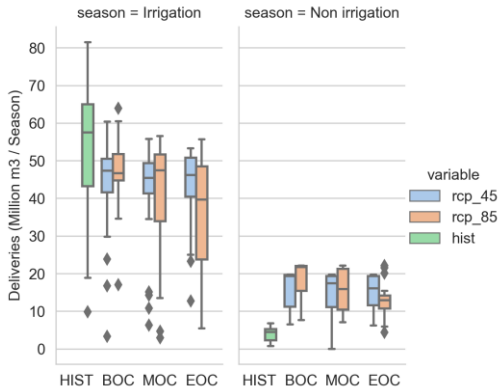

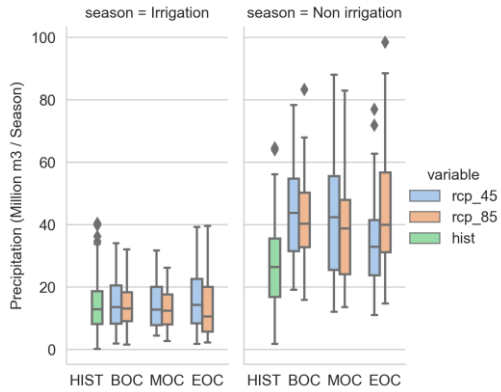

Delano - Earlimart ID, HadGEM2-CC

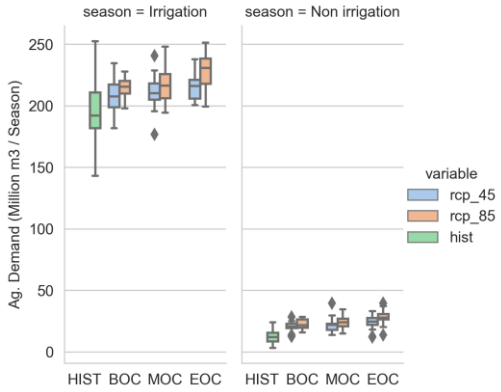

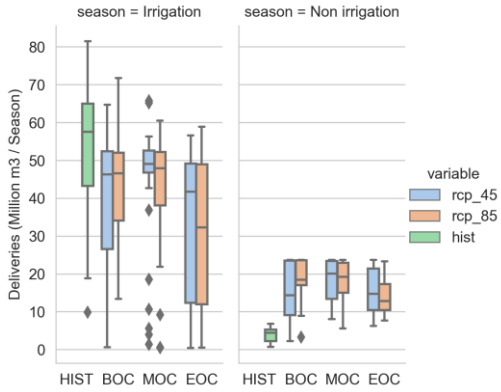

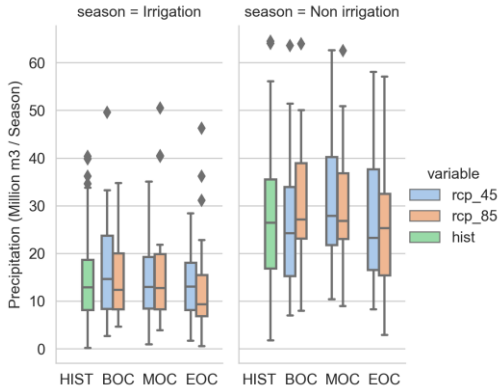

Delano - Earlimart ID, HadGEM2-ES

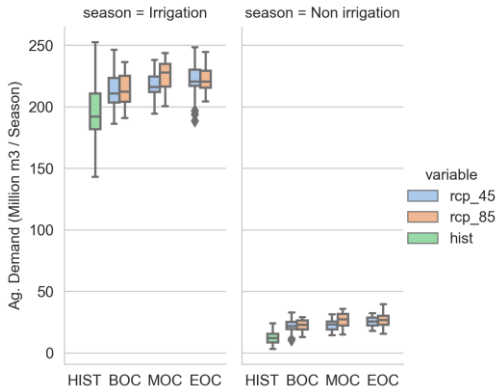

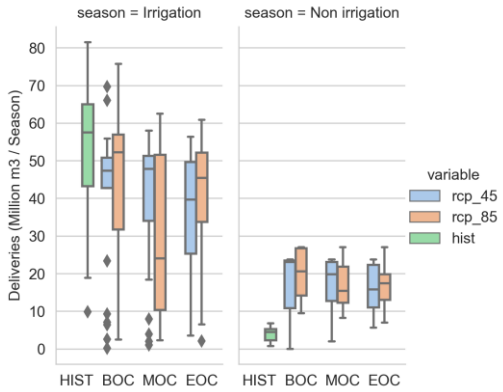

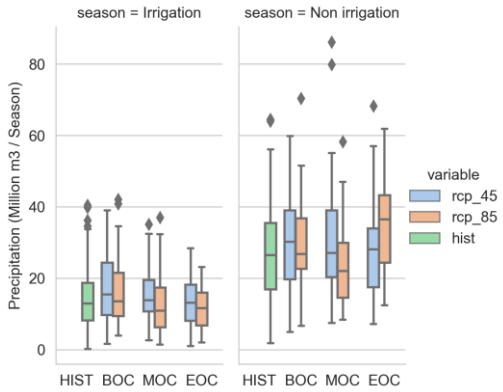

Delano - Earlimart ID, MIROC5

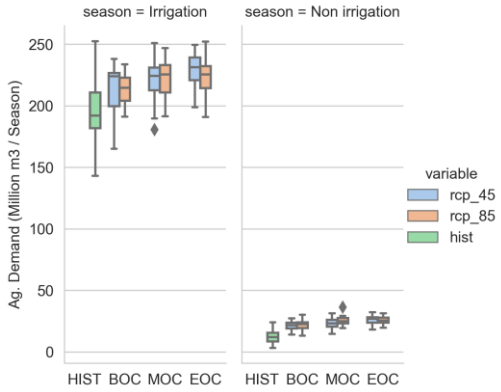

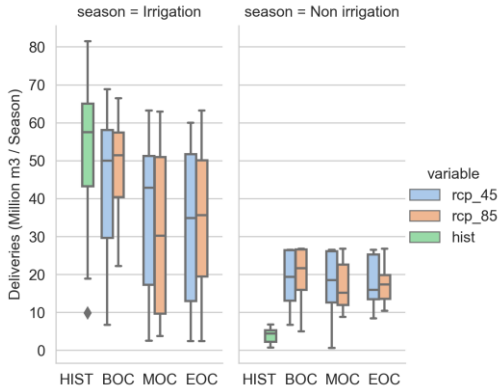

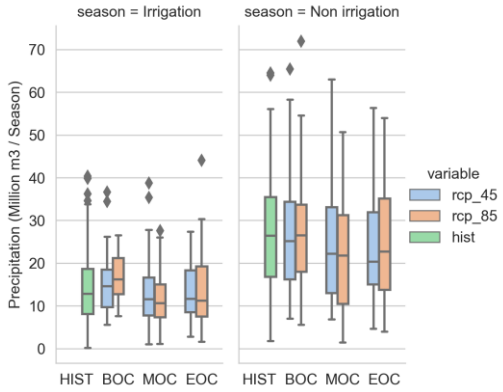

Kern - Tulare WD, CanESM2

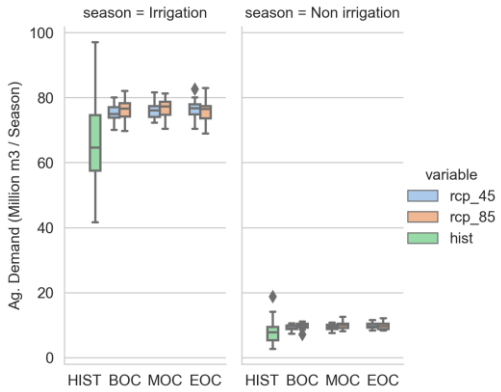

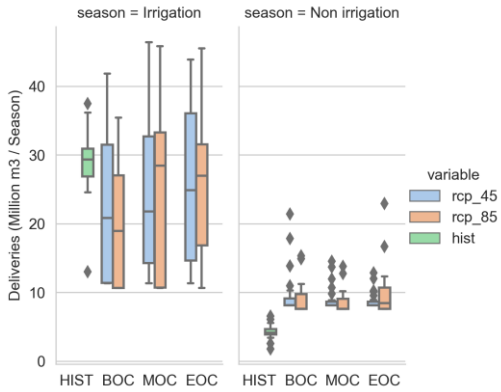

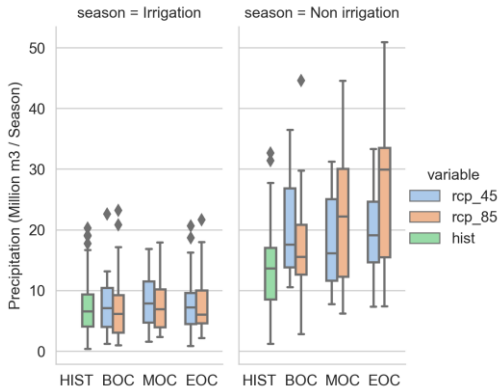

Kern - Tulare WD, CCSM4

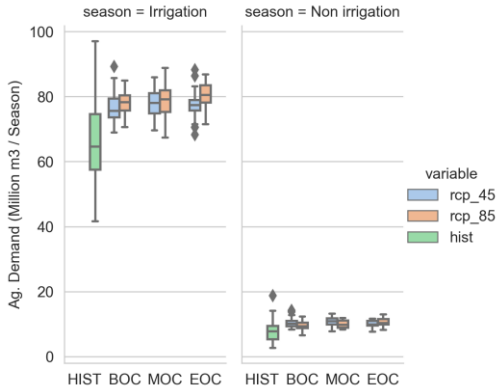

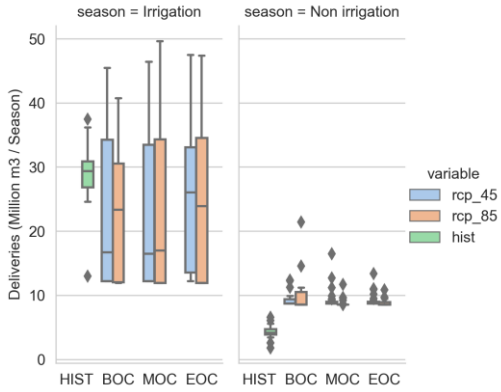

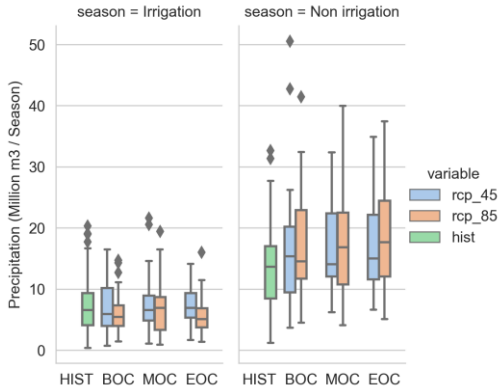

Kern - Tulare WD, CNRM-CM5

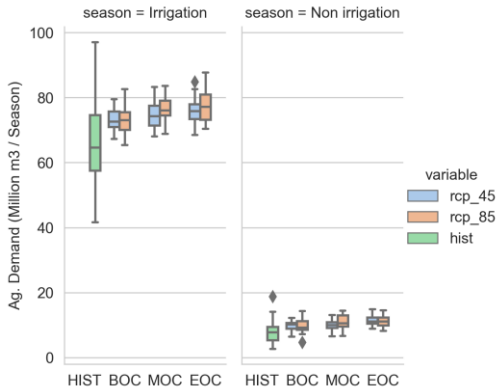

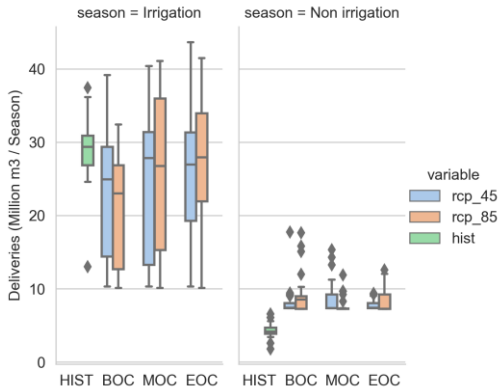

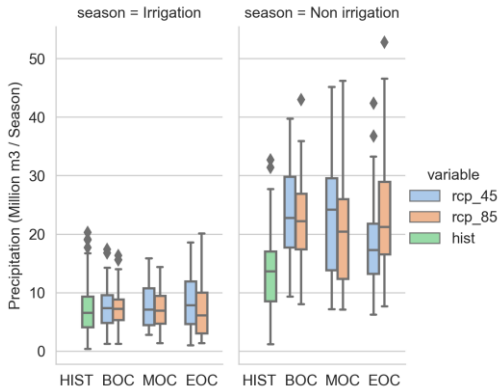

Kern - Tulare WD, HadGEM2-CC

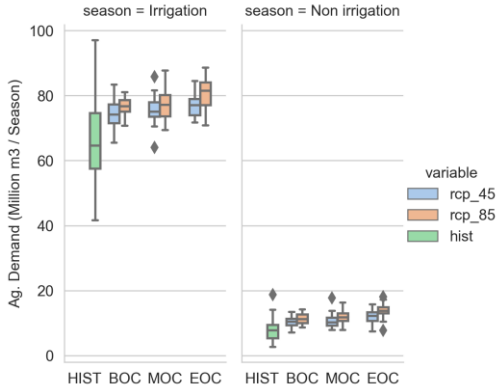

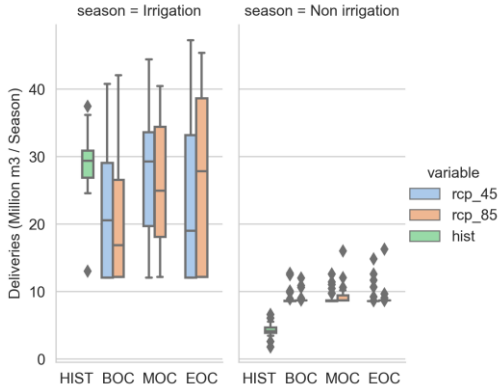

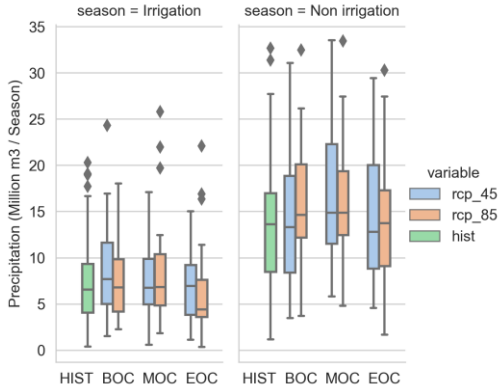

Kern - Tulare WD, HadGEM2-ES

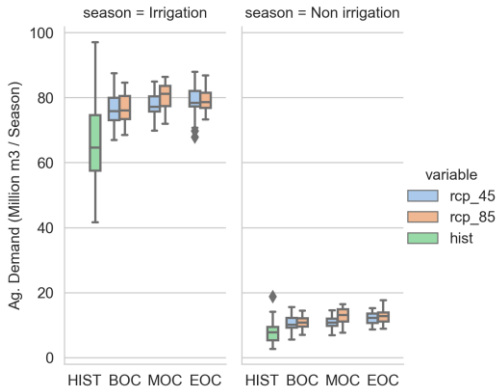

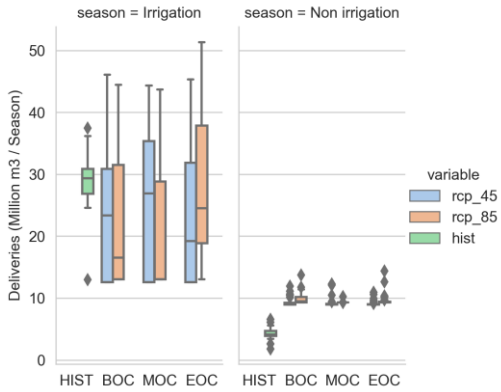

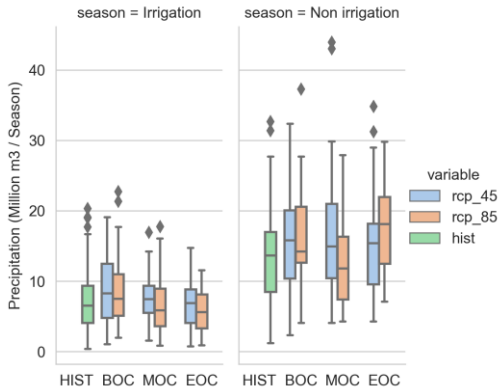

Kern - Tulare WD, MIROC5

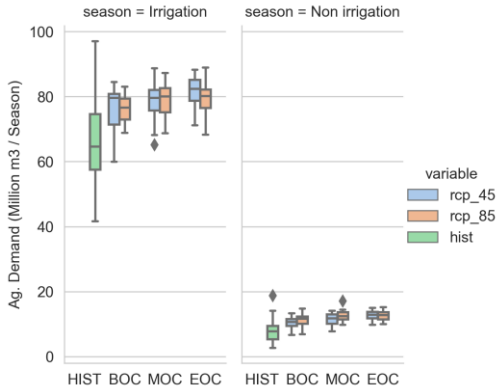

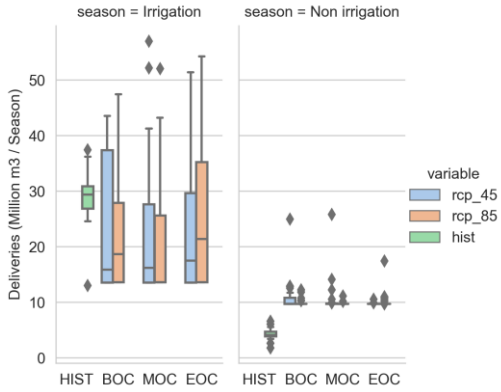

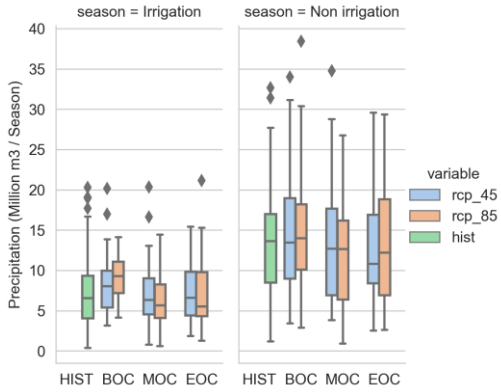

Appendix B.2 Depths to groundwater for different scenario groups of Precipitation, Agricultural Water Demand, and Surface Water Deliveries

The analyzed scenario groups are Business as Usual (BU, blue area), Influence of Climate Change in Two Dynamic Variables (IC2D, green area), and Influence of Climate Change in Three Dynamic Variables (IC3D, orange area). The thick lines in the middle of the shaded regions symbolize the median of the scenario group. The vertical axis has been inverted to facilitate interpretation.

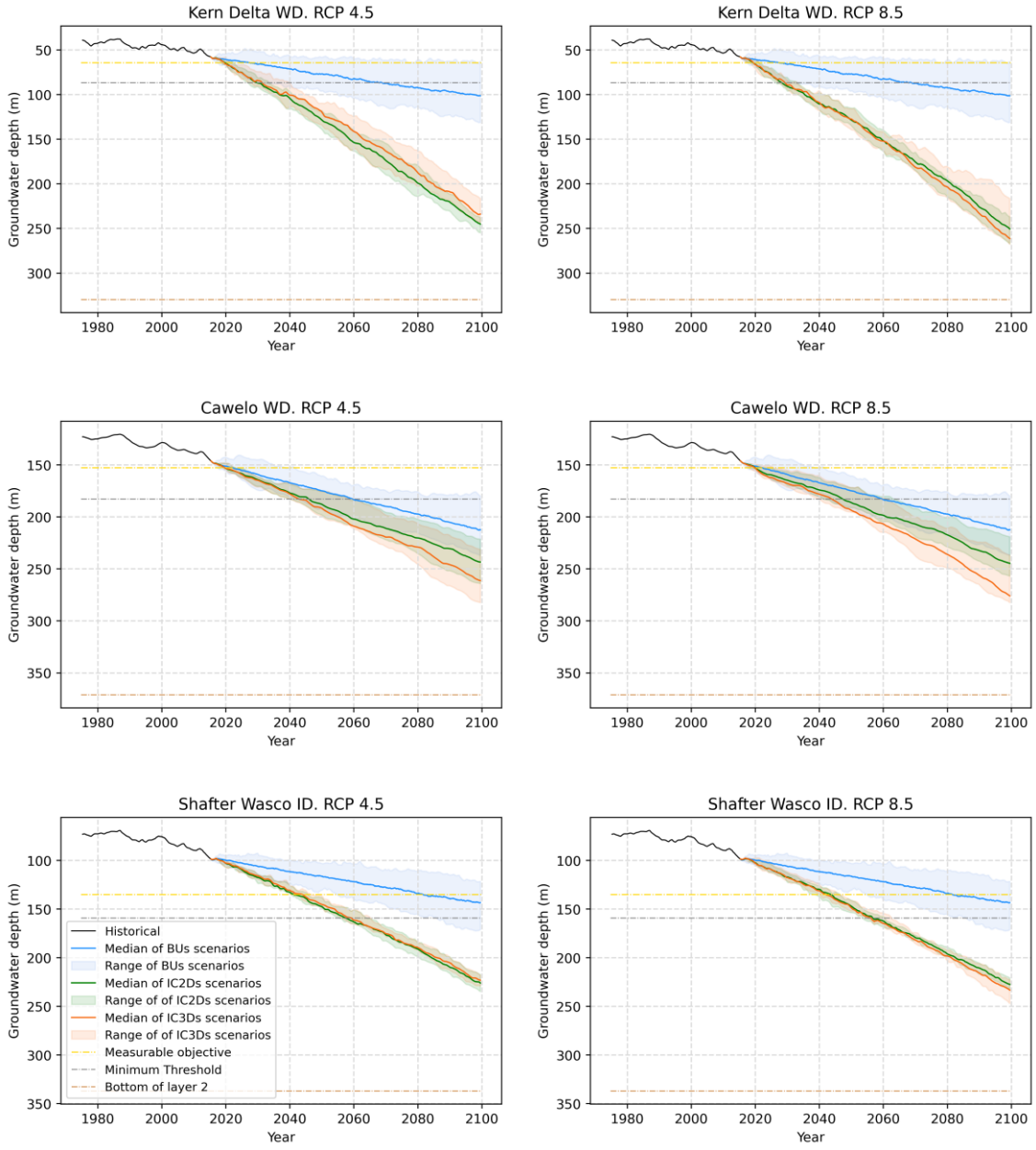

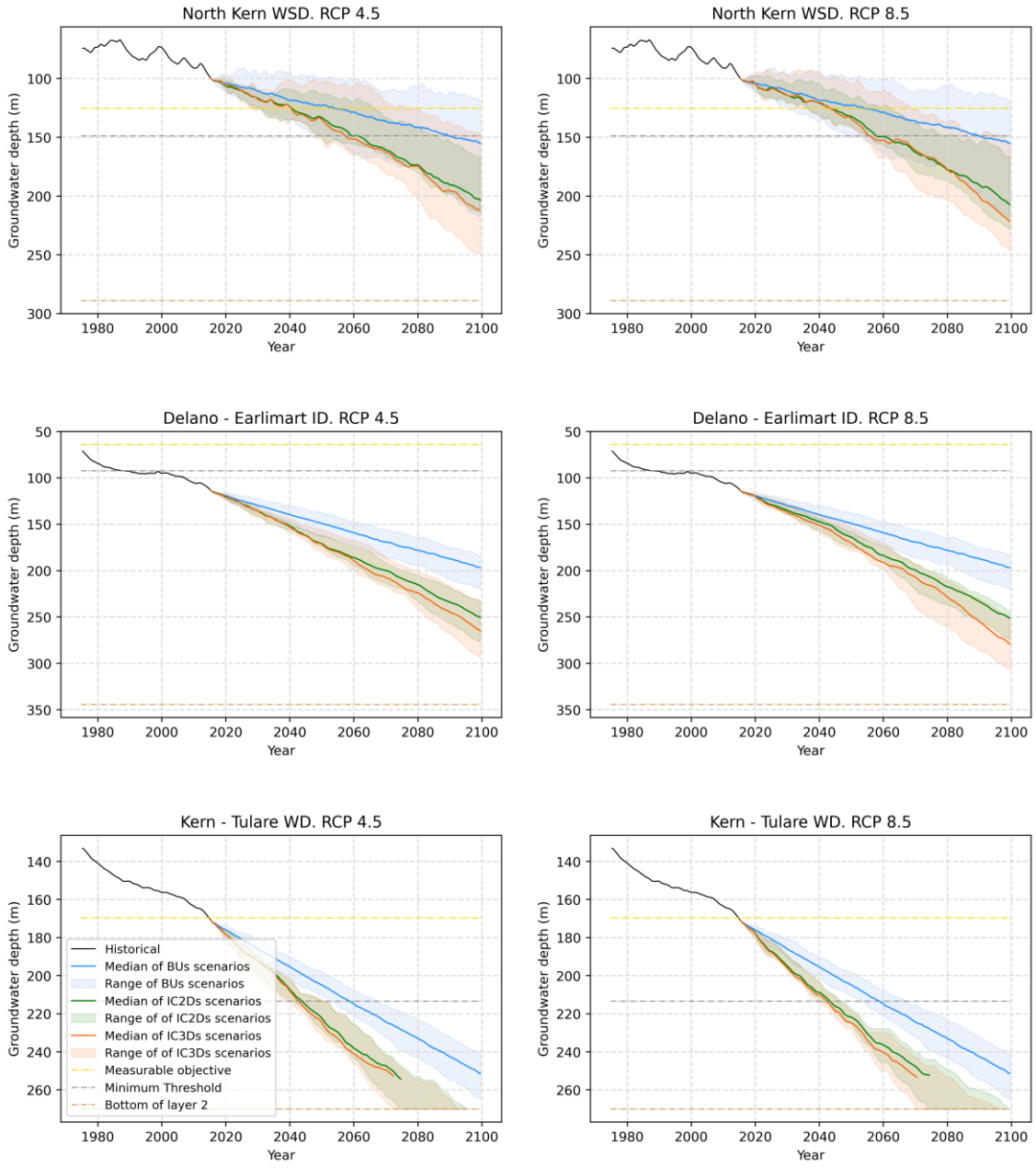
North Kern WSD. RCP 4.5
North Kern WSD. RCP 8.5
Delano - Earlimart ID. RCP 4.5
Delano - Earlimart ID. RCP 8.5
Kern - Tulare WD. RCP 4.5
Kern - Tulare WD. RCP 8.5
Groundwater depth (m)
Year
Historical
Median of BUs scenarios
Range of BUs scenarios
Median of IC2Ds scenarios
Range of of IC2Ds scenarios
Median of IC3Ds scenarios
Range of of IC3Ds scenarios
Measurable objective
Minimum Threshold
Bottom of layer 2

Appendix B.3 Groundwater depletion or recharge rates

Groundwater depletion or recharge rate (DRR) by timeframe (columns) and scenario group (rows). Different colors represent different RCPs: Historical (green), 4.5 (blue), and 8.5 (orange). The circle's border color indicates whether the depth increases (red) or decreases (black) over time. The number inside the circles on the right shows the yearly DRR magnitude in meters.